



# **Development and Evaluation of Therapeutic PSMA-Binding Radiopharmaceuticals with Optimized Pharmacokinetics**

Jan-Philip Kunert

Vollständiger Abdruck der von der TUM School of Natural Sciences der Technischen Universität  
München zur Erlangung des akademischen Grades eines

**Doktors der Naturwissenschaften (Dr. rer. nat.)**

genehmigten Dissertation.

Vorsitz: Prof. Dr. Angela Casini  
Prüfer\*innen: 1. Prof. Dr. Susanne Kossatz  
2. apl. Prof. Dr. Matthias Eiber

Die Dissertation wurde am 28.03.2023 bei der Technischen Universität München eingereicht und  
durch die TUM School of Natural Sciences am 23.06.2023 angenommen.





## Danksagung - Acknowledgements

Allen voran möchte ich mich herzlich bei **Prof. Dr. Hans-Jürgen Wester** bedanken, der mir diese Promotion und die Arbeit an seinem Lehrstuhl ermöglicht hat. Das spannende Forschungsprojekt, mit dem die Arbeit begann, aber ebenso die Projekte, die „unterwegs“ entstanden sind, haben mir große Freude gemacht und mich viel gelehrt! Ebenso bin ich Ihnen dankbar für die exzellente Betreuung, all Ihre Ideen und detailliertes Feedback, angeregte wissenschaftliche Diskussionen beim Schreiben der Paper und nicht zuletzt auch für die wunderbaren Feiern an und mit dem Lehrstuhl!

Meiner Mentorin der Promotion, **Prof. Dr. Margret Schottelius**, gilt ebenso besonderer Dank. Nicht nur für vielfache Ermutigung und Rat während der Promotion, sondern auch für die Bachelor- und Masterarbeit zuvor, während der Sie meine Begeisterung für die Radiopharmazie angestoßen und durch Ihre optimistische, positive Art immer wieder neue Motivation geweckt haben! Ganz besonders danke ich Ihnen für die Ermutigung, kumulativ zu promovieren – ich bin froh, es gewagt zu haben!

I furthermore want to thank **Prof. Dr. Angela Casini** for her kind support in the last administrative steps of this thesis.

Herzlicher Dank gilt außerdem all meinen wunderbaren Kollegen am Lehrstuhl: **Christine Winkler** möchte ich danken für ihre Hilfe in allen großen und kleinen organisatorischen Dingen. Ich bewundere deine große Geduld und tiefenentspannte Freundlichkeit, mit denen du den Lehrstuhl bereicherst! **Dr. Roswitha Beck** und **Dr. Nicole Urtz-Urban** haben mir mit ihrer Arbeit die *in vivo* Studien als einen großen (und den mitunter wichtigsten) Teil meiner Arbeit erst möglich gemacht – vielen, vielen Dank für alles, was ihr mir beigebracht habt, alle Unterstützung und die Gespräche zwischen Tür und Angel. Ihr seid echte „Möglich-Macherinnen“! Eine besondere Freude war mir außerdem das tägliche Im-Labor-Stehen mit **Dr. Alexander Wurzer**, **Dr. Thomas Günther**, **Dr. Veronika Felber**, **Dr. Matthias Konrad**, **Mara Parzinger**, **Daniel Di Carlo**, **Stefanie Färber**, **Dr. Markus Fahnauer**, **Sebastian Fischer**, **León Stopper**, **Nadine Holzleitner**, **Sebastian Fenzl**, **Sandra Deiser**, **Franziska Schuderer**, **Jana Schulz** und **Tanja Reichhart** – ihr seid eine geniale Truppe und habt mit all eurer Unterstützung im Labor, der schönen Gemeinschaft und den Erlebnissen in und außerhalb der Arbeit dazu beigetragen, dass ich mich am Lehrstuhl richtig wohl gefühlt habe und sich glücklicherweise nicht alles nur um Chemie gedreht hat. Besonders danke ich dir, Alex, für deinen so hilfsbereiten Support bei allen möglichen Fragen, und dass ich durch deine Vorarbeit an so einem genialen Thema arbeiten durfte! Thomas, danke für all die kleinen Tipps und Tricks und unsere entspannten Tea-Times! Danke, Markus, für deine große Gastfreundschaft, Rennradtouren und deine ansteckende Begeisterung für alles Mögliche – ich feier's! Basti, PSMA-Bruder und genialer Teamplayer nicht nur beim Kickern, sondern

auch im Labor, danke für alle Unterstützung, Mithilfe und gegenseitiges Ermutigen während diesem Marathon-Projekt – und natürlich für unsere entspannten Espresso-Pausen!

Kurzum: es war ein Geschenk und eine Freude mit euch allen zu arbeiten – vielen Dank!

Ebenso möchte ich mich bei meinen Studenten bedanken, die ich betreuen durfte: **Lisa Richter, Johannes Heipke, Mirza Grebo, Ilias Asimakopoulos, Daniel Werner** und allen voran **Max Müller** - Danke für euren Einsatz und all eure Hilfe!

Unter den Kollegen der Radiochemie München möchte ich mich herzlich bei **Dr. Christoph Lierse von Gostomski, Dr. Stefan Hifinger, Dr. Catalin Alecu, Dr. Thomas Bücherl, Stefanie Schlücking, Andreas Cziasto, Gerhard Matheis, Herbert Größlhuber** und **Alijah Bory** für all die Arbeit im Bereich Strahlenschutz und Räumlichkeiten bedanken, die uns ausgezeichnete Arbeitsbedingungen ermöglicht haben. Besonderer Dank gilt außerdem **Marie von Landenberg** und **Doris Pufitsch** für die täglich herzlichen Begrüßungen und alle Hilfe mit Besuchern, Studenten und Paket-Fluten!

Unglaublich dankbar bin ich außerdem für meine wunderbare **Familie!** Danke für eure Ermutigung und Unterstützung, vor allem wenn mir alles zu viel war! Besonders ehren möchte ich meine Eltern, **Susanne** und **Andreas:** für eure bedingungslose Liebe und Versorgung, alles Zuhören, euer Gebet, alles Mitfeiern, Mitfeiern und von euch bekocht werden – Danke!

Und zu guter Letzt gilt mein ganzer Dank Gott, meinem Herrn **Jesus Christus** – meine Freude, Kraft und Hoffnung kommen von ihm und seine Liebe, Treue und Leben sind mir das größte Geschenk!

## List of Publications

The presented work was carried out at the Chair of Pharmaceutical Radiochemistry of the Technical University of Munich from August 2018 to March 2022. The PhD thesis was supervised by Prof. Dr. Hans-Jürgen Wester.

### Work on the presented PhD thesis resulted in the following peer-reviewed publications:

Wurzer, A.\*; **Kunert, J.-P.\***; Fischer, S.; Felber, V.; Beck, R.; de Rose, F.; d'Alessandria, C.; Weber, W.; Wester, H.-J. Synthesis and Preclinical Evaluation of  $^{177}\text{Lu}$ -labeled Radiohybrid PSMA Ligands for Endoradiotherapy of Prostate Cancer. *J Nucl Med* **2022**, *63* (10), 1489-1495, doi: 10.2967/jnumed.121.263371.

**Kunert, J.-P.\***; Fischer, S.; Wurzer, A.; Wester, H.-J. Albumin-Mediated Size Exclusion Chromatography: The Apparent Molecular Weight of PSMA Radioligands as Novel Parameter to Estimate Their Blood Clearance Kinetics. *Pharmaceuticals* **2022**, *15* (9), 1161, doi: 10.3390/ph15091161.

**Kunert, J.-P.\***; Müller, M.; Günther, T.; Stopper, L.; Urtz-Urban, N.; Beck, R.; Wester, H.-J. Synthesis and Preclinical Evaluation of Novel  $^{99\text{m}}\text{Tc}$ -labeled PSMA Ligands for Radioguided Surgery of Prostate Cancer. *EJNMMI Res* **2023**, *13* (2), doi: 10.1186/s13550-022-00942-7.

*First authors are indicated with an asterisk (\*).*

### Further work contributed to the following publication:

Günther, T.\*; Konrad, M.; Stopper, L.; **Kunert, J.-P.**; Fischer, S.; Beck, R.; Casini, A.; Wester, H.-J. Optimization of the Pharmacokinetic Profile of [ $^{99\text{m}}\text{Tc}$ ]Tc-N4-Bombesin Derivatives by Modification of the Pharmacophoric Gln-Trp Sequence. *Pharmaceuticals* **2022**, *15* (9), 1133, doi: 10.3390/ph15091133.

*First authors are indicated with an asterisk (\*).*

**Work on the presented PhD thesis resulted in the following patent applications:**

Wester, H.-J.; Fischer, S.; Wurzer, A.; **Kunert, J.-P.** Dual-mode radiotracer and -therapeutics. *EP 21 157 154.2, 2021.*

Wurzer, A.; Wester, H.-J.; Fischer, S.; **Kunert, J.-P.** Silicon-containing ligand compounds. *WO2022018264A1, 2022.*

Wester, H.-J.; Günther, T.; Holzleitner, N.; **Kunert, J.-P.**; Beck, R.; Fahnauer, M.; Fenzl, S.; Deiser, S.; Stopper, L.; Urtz-Urban, N.; Fischer, S. Silicon based-fluoride acceptor groups for radiopharmaceuticals. *Patent application pending, 2022.*

Wester, H.-J.; **Kunert, J.-P.** Radiolabeled PSMA ligand compounds and precursors thereof. *Patent application pending, 2022.*

## Abstract

Prostate cancer (PCa) continues to be a major global health problem and the second most frequent cancer in men worldwide. In advanced stages of the disease, like metastatic castration-resistant prostate cancer (mCRPC), acquired resistance against conventional therapeutic interventions like chemotherapy or androgen deprivation therapy (ADT) represents a serious clinical challenge and demands for alternative treatment options for PCa patients. Its consistently high expression in PCa lesions has rendered the prostate-specific membrane antigen (PSMA) an attractive molecular target and object of intense research throughout the past three decades. As a result, several highly specific inhibitors of PSMA, based on the urea-glutamate binding motive, were developed. After first-generation PSMA-targeted radiopharmaceuticals for diagnostic and therapeutic purposes have been established in clinical application and, in part, received regulatory approval, optimized next-generation radiopharmaceuticals are needed to further improve response and survival of PCa patients beyond the current scope. Therefore, the aim of this work was the development of PSMA-targeted radioligands with optimized pharmacokinetics (PK) for therapeutic applications such as radioligand therapy (RLT) and radioguided surgery (RGS).  $^{177}\text{Lu}$ -labeled PSMA ligands for RLT were based on the recently developed radiohybrid concept (rhPSMA), while a lead structure derived from these rhPSMA ligands was combined with a tetraamine (N4) chelator to create  $^{99\text{m}}\text{Tc}$ -labeled compounds suitable for RGS ( $^{99\text{m}}\text{Tc}$ ]Tc-N4-PSMA). Furthermore, as a major challenge in radioligand development lies in the accurate preclinical assessment of pharmacokinetic parameters, the development of a methodology was envisioned that might allow to estimate the blood clearance kinetics of various PSMA radioligands *in vitro*.

Chelator-based PSMA ligands were synthesized using a mixed solution phase / solid phase synthetic approach and ligands were radiolabeled with lutetium-177 or technetium-99m. Lipophilicity of the radioligands was assessed via the shake flask method in octanol and phosphate buffered saline. PSMA affinity and PSMA-mediated internalization were determined in *in vitro* cell assays using PSMA-positive LNCaP cells and [ $^{125}\text{I}^{\text{mat}}$ ]IBA-KuE as reference compound. Binding to fresh human plasma or human serum albumin (HSA) was analyzed in ultrafiltration experiments or with the newly developed method ‘albumin-mediated size exclusion chromatography’ (AMSEC), respectively. The latter was developed applying size exclusion chromatography with HSA dissolved in the mobile phase and injections of PSMA radioligands. Biodistribution experiments and  $\mu\text{SPECT/CT}$ -imaging were executed in LNCaP tumor-bearing CB17-SCID mice.

Isomers of the radiohybrid ligands rhPSMA-7 and rhPSMA-10 were obtained in high chemical purities of > 97% and labeling with lutetium-177 resulted in radiochemical purities (RCP) of > 95%. All ligands showed low lipophilicity comparable to the references [ $^{177}\text{Lu}$ ]Lu-PSMA-617 and [ $^{177}\text{Lu}$ ]Lu-PSMA-I&T.  $^{177}\text{Lu}$ -labeled rhPSMA ligands exhibited potent PSMA affinity in the nanomolar range and high but slightly varying internalization. Pronounced differences even among stereoisomers were observed for the apparent molecular weight ( $\text{MW}_{\text{app}}$ ) determined in AMSEC experiments.

Biodistribution studies revealed high tumor uptake, varying kidney retention and efficient clearance from blood and background organs. After initial application in the evaluation of rhPSMA ligands, AMSEC was developed further by means of a normalization procedure that accounts for unspecific interactions of PSMA radioligands with the column matrix. Data acquisition was extended to additional rhPSMA ligands with diverse chemical structures and obtained normalized  $MW_{app, norm.}$  ranged from 1.9 – 39.9 kDa resulting in calculated glomerular sieving coefficients ( $GSC_{calc}$ ) of 0.992 – 0.003. N4-PSMA ligands for RGS application were synthesized with high chemical purities > 98% and RCP of > 95% were obtained for the  $^{99m}Tc$ -labeled compounds. Comparative *in vitro* characterization revealed varying internalization, comparable PSMA affinity and significantly decreased lipophilicity and plasma protein binding for the [ $^{99m}Tc$ ]Tc-N4-PSMA ligands as compared to [ $^{99m}Tc$ ]Tc-PSMA-I&S. Comparable tumor uptake but accelerated clearance from most background organs was observed for the novel N4-PSMA ligands and [ $^{99m}Tc$ ]Tc-N4-PSMA-12 showed higher tumor-to-background ratios than [ $^{99m}Tc$ ]Tc-PSMA-I&S in blood and every evaluated organ.

Regarding the  $^{177}Lu$ -labeled rhPSMA isomers, remarkable differences in preclinical tracer performance were found. In summary, [ $^{177}Lu$ ]Lu-rhPSMA-10.1 was identified as most promising therapeutic candidate owing to its moderate  $MW_{app}$ , as determined by the newly developed AMSEC method, its high tumor uptake and low kidney retention. A clinical trial (NCT05413850) currently investigates the therapeutic efficacy of [ $^{177}Lu$ ]Lu-rhPSMA-10.1 for RLT of mCRPC patients. It is expected that the study will shed light on whether this novel therapeutic drug could outperform currently established radiotherapeutics for RLT of mCRPC. Furthermore, the newly developed AMSEC method represents an intriguing tool that might allow for the preclinical comparison of human blood clearance kinetics of PSMA-radioligands. If clinical data confirm the expected significance of  $MW_{app, norm.}$  and  $GSC_{calc}$ , a broader application of AMSEC might facilitate the development of next-generation radiopharmaceuticals with improved therapeutic efficacy. Regarding novel tracers for RGS, promising  $^{99m}Tc$ -labeled N4-PSMA ligands were developed and the superior pharmacokinetic profile of [ $^{99m}Tc$ ]Tc-N4-PSMA-12 renders this novel radioligand an attractive candidate for PSMA-targeted RGS. Clinical studies will be needed to elucidate whether [ $^{99m}Tc$ ]Tc-N4-PSMA-12 has the potential to overcome current limitations of RGS with [ $^{99m}Tc$ ]Tc-PSMA-I&S.

## Kurzzusammenfassung

Prostatakrebs (PCa) stellt weltweit ein großes Gesundheitsproblem dar und ist die zweithäufigste Krebserkrankung bei Männern. In fortgeschrittenen Krankheitsstadien wie dem metastasierten kastrationsresistenten Prostatakrebs (mCRPC) stellt die erworbene Resistenz gegen konventionelle therapeutische Maßnahmen wie Chemotherapie oder Androgendeprivationstherapie (ADT) eine ernsthafte klinische Herausforderung dar und erfordert alternative Behandlungsmöglichkeiten für PCa-Patienten. Aufgrund seiner konstant hohen Expression in PCa-Läsionen entwickelte sich das prostataspezifische Membranantigen (PSMA) in den letzten drei Jahrzehnten zu einer attraktiven molekularen Zielstruktur und zum Gegenstand intensiver Forschung. Infolgedessen wurden mehrere hochspezifische, auf dem Urea-Glutamat-Bindemotiv basierende PSMA-Inhibitoren entwickelt. Nachdem sich PSMA-gerichtete Radiopharmaka der ersten Generation für diagnostische und therapeutische Zwecke in der klinischen Anwendung etabliert und zum Teil die Zulassung erhalten haben, bedarf es optimierter Radiopharmaka der nächsten Generation, um das Ansprechen und die Überlebenschancen von PCa-Patienten über den derzeitigen Rahmen hinaus weiter zu verbessern. Ziel dieser Arbeit war daher die Entwicklung von PSMA-gerichteten Radioliganden mit optimierter Pharmakokinetik für therapeutische Anwendungen wie die Radioligandentherapie (RLT) und ‚radioguided surgery‘ (RGS). Hierbei basierten  $^{177}\text{Lu}$ -markierte PSMA-Liganden für RLT auf dem vor Kurzem entwickelten Radiohybrid-Konzept (rhPSMA), während eine von rhPSMA-Liganden abgeleitete Leitstruktur mit einem Tetraamin (N4)-Chelator kombiniert wurde, um  $^{99\text{m}}\text{Tc}$ -markierte Verbindungen für RGS zu kreieren ( $[\text{}^{99\text{m}}\text{Tc}]\text{Tc-N4-PSMA}$ ). Da eine der größten Herausforderungen bei der Entwicklung von Radioliganden in der genauen präklinischen Bewertung pharmakokinetischer Eigenschaften liegt, wurde die Entwicklung einer Methode zur *in vitro* Einschätzung der relativen Blut-Clearance-Kinetik diverser PSMA-Radioliganden ins Auge gefasst.

Chelator-basierte PSMA-Liganden wurden in einem Lösungs-/Festphasen-Syntheseverfahren synthetisiert und mit Lutetium-177 bzw. Technetium-99m markiert. Die Lipophilie der Radioliganden wurde mit der Schüttelmethode in Octanol und phosphatgepufferter Kochsalzlösung untersucht. Die PSMA-Affinität und die PSMA-vermittelte Internalisierung wurden in *in vitro* Zelltests mit PSMA-positiven LNCaP-Zellen und  $[\text{}^{125}\text{I}^{\text{nat}}]\text{IBA-KuE}$  als Referenzverbindung bestimmt. Die Bindung an frisches humanes Plasma oder Humanalbumin (HSA) wurde in Ultrafiltrationsexperimenten bzw. mit der neu entwickelten Methode ‚albumin-mediated size exclusion chromatography‘ (AMSEC) analysiert. Letztere wurde basierend auf Größenausschlusschromatographie mit in der mobilen Phase gelöstem HSA und Injektionen von PSMA-Radioliganden entwickelt. Biodistributionsexperimente und  $\mu\text{SPECT/CT}$ -Bildgebung wurden in LNCaP Tumor-tragenden CB17-SCID-Mäusen durchgeführt.

Die Isomere der radiohybriden Liganden rhPSMA-7 und rhPSMA-10 wurden in hoher chemischer Reinheit (> 97%) erhalten und die Markierung mit Lutetium-177 führte zu radiochemischen Reinheiten (RCP) von > 95%. Alle Liganden wiesen eine geringe, mit den Referenzen  $[\text{}^{177}\text{Lu}]\text{Lu-PSMA-617}$  und

[<sup>177</sup>Lu]Lu-PSMA-I&T vergleichbare Lipophilie auf. <sup>177</sup>Lu-markierte rhPSMA-Liganden zeigten eine hohe PSMA-Affinität im nanomolaren Bereich und eine ausgeprägte, leicht variierende Internalisierung. Hinsichtlich des mittels AMSEC-Experimenten bestimmten apparenten Molekulargewichts ( $MW_{app}$ ) wurden selbst zwischen Stereoisomeren deutliche Unterschiede festgestellt. Biodistributionsstudien zeigten hohe Tumoraufnahme, unterschiedliche Nierenretention und effiziente Clearance aus Blut und Hintergrundorganen. Die AMSEC-Methode wurde nach anfänglicher Anwendung zur Evaluierung von rhPSMA-Liganden mit Hilfe eines Normalisierungsverfahrens weiterentwickelt, das unspezifische Wechselwirkungen von PSMA-Radioliganden mit der Säulenmatrix berücksichtigt. Die Datenerfassung wurde auf zusätzliche rhPSMA-Liganden mit unterschiedlichen chemischen Strukturen ausgeweitet wobei die erhaltenen normalisierten  $MW_{app,norm.}$  von 1.9 – 39.9 kDa reichten, was zu berechneten glomerulären Siebkoeffizienten ( $GSC_{calc}$ ) von 0.992 – 0.003 führte. N4-PSMA-Liganden für die RGS-Anwendung wurden mit hoher chemischer Reinheit (> 98%) synthetisiert. Für die <sup>99m</sup>Tc-markierten Verbindungen wurden radiochemische Reinheiten (RCP) von > 95% erzielt. Eine vergleichende *in vitro* Charakterisierung ergab unterschiedliche Internalisierung, vergleichbare PSMA-Affinität sowie deutlich reduzierte Lipophilie und Plasmaproteinbindung der [<sup>99m</sup>Tc]Tc-N4-PSMA-Liganden im Vergleich zu [<sup>99m</sup>Tc]Tc-PSMA-I&S. Neben vergleichbarer Tumoraufnahme wurde für die neuartigen N4-PSMA-Liganden eine beschleunigte Clearance beobachtet und [<sup>99m</sup>Tc]Tc-N4-PSMA-12 wies im Blut sowie in jedem untersuchten Organ ein höheres Tumor-zu-Hintergrund-Verhältnis auf als [<sup>99m</sup>Tc]Tc-PSMA-I&S.

Bezüglich <sup>177</sup>Lu-markierter rhPSMA-Isomere konnten bemerkenswerte Unterschiede der präklinischen Eigenschaften festgestellt werden, wobei [<sup>177</sup>Lu]Lu-rhPSMA-10.1 aufgrund des moderaten, mittels AMSEC ermittelten  $MW_{app}$ , der hohen Tumoraufnahme und der geringen Nierenretention als vielversprechendster therapeutischer Kandidat identifiziert wurde. Klinische Studien (NCT05413850) untersuchen gegenwärtig die therapeutische Effizienz von [<sup>177</sup>Lu]Lu-rhPSMA-10.1 für RLT von mCRPC-Patienten und die Studienergebnisse werden Aufschluss darüber geben, ob dieses neuartige Verbindung den derzeit etablierten Radiotherapeutika für RLT von mCRPC überlegen ist. Darüber hinaus stellt die neu entwickelte Methode AMSEC ein interessantes Instrument dar, welches einen präklinischen Vergleich der humanen Blut-Clearance-Kinetik ermöglichen könnte. Falls klinische Daten die erwartete Signifikanz von  $MW_{app,norm.}$  und  $GSC_{calc}$  bestätigen, könnte eine breitere Anwendung von AMSEC die Entwicklung von Radiopharmaka der nächsten Generation mit verbesserter therapeutischer Wirksamkeit erleichtern. Hinsichtlich neuer Tracer für RGS wurden vielversprechende <sup>99m</sup>Tc-markierte N4-PSMA-Liganden entwickelt und das überlegene pharmakokinetische Profil von [<sup>99m</sup>Tc]Tc-N4-PSMA-12 macht diesen neuartigen Radioliganden zu einem attraktiven Kandidaten für PSMA-gerichtete RGS. Klinische Studien werden erforderlich sein, um zu evaluieren, ob [<sup>99m</sup>Tc]Tc-N4-PSMA-12 das Potenzial birgt, die derzeitigen Limitationen von RGS mit [<sup>99m</sup>Tc]Tc-PSMA-I&S zu überwinden.

## List of Abbreviations

### A

AA	amino acid
ADME	absorption, distribution, metabolism and excretion of a drug
ADT	androgen deprivation therapy
AMSEC	albumin-mediated size exclusion chromatography

### B

BSOC	best standard of care
BT	brachytherapy

### C

CT	computed tomography
----	---------------------

### D

DOTA	1,4,7,10-tetraazacyclododecan-N,N',N'',N'''-tetraacetic acid
DOTAGA	1,4,7,10-tetraazacyclododecane-N-(glutaric acid)-N',N'',N'''-triacetic acid

### E

EuE	glutamate-ureido-glutamate binding motive
-----	-------------------------------------------

### F

FA	fatty acid binding site
----	-------------------------

FDA	Food and Drug Administration
FOLH1	folate hydrolase 1
FPG	folyl-poly- $\gamma$ -glutamate
<b>G</b>	
GCPII	glutamate carboxypeptidase II
GSC	glomerular sieving coefficient
GSC <sub>calc</sub>	calculated glomerular sieving coefficient
<b>H</b>	
HBED-CC	<i>N,N'</i> -bis-[2-hydroxy-5-(carboxyethyl)benzyl]ethylenediamine- <i>N,N'</i> -diacetic acid
HSA	human serum albumin
<b>I</b>	
IPA	<i>p</i> -iodo-4-phenylbutanoic acid
<b>K</b>	
KuE	glutamate-ureido-lysine binding motive
<b>L</b>	
LET	linear energy transfer
LNCaP	'lymph node carcinoma of the prostate' human cell line
<b>M</b>	
mAb	monoclonal antibody
mCRPC	metastatic castration-resistant prostate cancer
mHSPC	metastatic hormone-sensitive prostate cancer

mpMRI	multi-parametric magnetic resonance imaging
$\mu$ SPECT	micro single photon emission computed tomography
MW	molecular weight
MW <sub>app</sub>	apparent molecular weight
MW <sub>app,norm.</sub>	normalized apparent molecular weight
MW <sub>app,raw</sub>	raw apparent molecular weight

### **N**

N4	tetraamine chelator (6-(carboxy)-1,4,8,11-tetrazaundecane)
NAA	<i>N</i> -acetyl aspartate
NAAG	<i>N</i> -acetyl-aspartyl-glutamate
NAALADase	<i>N</i> -acetyl- $\alpha$ -linked acidic dipeptidase

### **P**

PBS	phosphate buffered saline
PCa	prostate cancer
PEG	polyethylene glycol
PET	positron emission tomography
PK	pharmacokinetics
PLND	pelvic lymph node dissection
PSA	prostate-specific antigen
PSM'	cytosolic splice variant of PSMA
PSMA	prostate-specific membrane antigen

**R**

RCP	radiochemical purity
RGS	radioguided surgery
rhPSMA	radiohybrid PSMA ligand
RLT	radioligand therapy
RMBLR	red marrow-to-blood activity concentration ratio
RP	radical prostatectomy
RT	radiation therapy

**S**

SEC	size exclusion chromatography
SiFA	silicon fluoride acceptor
SiOH	hydrolyzed SiFA moiety (OH-for-F-substitution)
sLND	sentinel lymph node dissection
SPECT	single photon emission computed tomography

**T**

TAT	targeted $\alpha$ -therapy
-----	----------------------------

# Table of Contents

<b>Danksagung - Acknowledgements</b>	<b>i</b>
<b>List of Publications</b>	<b>iii</b>
<b>Abstract</b>	<b>v</b>
<b>Kurzzusammenfassung</b>	<b>vii</b>
<b>List of Abbreviations</b>	<b>ix</b>
<b>Table of Contents</b>	<b>xiii</b>
<b>1. Introduction</b>	<b>1</b>
1.1. Prostate Cancer	1
1.2. PSMA	3
1.3. Therapeutic Applications of PSMA-Targeted Radiopharmaceuticals	11
1.4. Optimization of Pharmacokinetics of PSMA Radioligands	25
<b>2. Objectives</b>	<b>32</b>
<b>3. Results - Publications</b>	<b>33</b>
3.1. Synthesis and Preclinical Evaluation of <sup>177</sup> Lu-labeled Radiohybrid PSMA Ligands for Endoradiotherapy of Prostate Cancer	33
3.2. Albumin-Mediated Size Exclusion Chromatography: The Apparent Molecular Weight of PSMA Radioligands as Novel Parameter to Estimate Their Blood Clearance Kinetics	35
3.3. Synthesis and Preclinical Evaluation of Novel <sup>99m</sup> Tc-labeled PSMA Ligands for Radioguided Surgery of Prostate Cancer	37
<b>4. Conclusion and Outlook</b>	<b>39</b>
<b>5. References</b>	<b>41</b>
<b>6. Appendix</b>	<b>60</b>
6.1. List of Figures	60
6.2. Reprint Permissions and Reprints of Original Publications	64
6.2.1. The Journal of Nuclear Medicine – Synthesis and Preclinical Evaluation of <sup>177</sup> Lu-labeled Radiohybrid PSMA Ligands for Endoradiotherapy of Prostate Cancer	64
6.2.2. Pharmaceuticals – Albumin-Mediated Size Exclusion Chromatography: The Apparent Molecular Weight of PSMA Radioligands as Novel Parameter to Estimate Their Blood Clearance Kinetics	82
6.2.3. EJNMMI Research – Synthesis and Preclinical Evaluation of Novel <sup>99m</sup> Tc-labeled PSMA Ligands for Radioguided Surgery of Prostate Cancer	112
6.3. Eidesstattliche Erklärung	136

# 1. Introduction

## 1.1. Prostate Cancer

### Epidemiology of Prostate Cancer

With an estimate of over 19 million new cases and nearly 10 million deaths in 2020 cancer continues to be one of the greatest medicinal challenges worldwide<sup>[1]</sup>. Among men, prostate cancer (PCa) is the second most frequent cancer with an estimate of over 1.4 million new cases in 2020 and, since 2008, constantly increasing numbers of both incidence and deaths have been reported throughout the latest four GLOBOCAN studies by the International Agency for Research on Cancer<sup>[1-4]</sup>. Besides the common risk factor of aging, several endogenous factors have been described to increase the risk to develop PCa, among them family history<sup>[5-7]</sup>, hormone-related processes<sup>[8-10]</sup> and genetic predispositions in certain populations like American males of African ancestry<sup>[11-13]</sup>. Furthermore, factors such as environmental or occupational exposure to carcinogens<sup>[14-15]</sup>, high-fat diets<sup>[16-17]</sup> and obesity<sup>[18-20]</sup>, as well as prostatic inflammations<sup>[21-23]</sup> constitute exogenous factors presumably increasing the risk for carcinogenesis and progression of PCa. However, the interplay between different risk factors, lifestyle and socioeconomic aspects is complex and thus complicates the unambiguous identification of pathological correlations<sup>[24-27]</sup>.

### Diagnosis and Treatment of Prostate Cancer

In the diagnosis of PCa, digital rectal examination of the lower rectum and pelvis or screening of serum levels of prostate-specific antigen (PSA) are established procedures for the early detection of PCa<sup>[28-29]</sup>. Furthermore, multi-parametric magnetic resonance imaging (mpMRI)<sup>[30-31]</sup> may be applied to ascertain the suspicion of PCa before sonography-guided needle biopsy and histopathology are used to verify the presence of PCa<sup>[31-33]</sup>. The treatment options of PCa are manifold, depend on the stage of the disease and are oftentimes applied as a combination of different approaches. For patients presenting with non-metastasized, localized PCa, the most established therapeutic interventions are brachytherapy (BT)<sup>[34-35]</sup>, radical prostatectomy (RP)<sup>[36-37]</sup> or radiation therapy (RT)<sup>[38-39]</sup>. *Kupelian et al.* reported comparable outcomes in terms of biochemical relapse-free survival for patients with localized PCa regardless of whether BT, RP or RT was applied, as long as the latter was conducted with sufficiently high doses ( $\geq 72$  Gy)<sup>[40]</sup>. Nevertheless, treatment-related side effects like urinary dysfunction, impotence or impaired bowel function vary among treatment options and need to be considered thoroughly in clinical decision-making<sup>[36, 41-42]</sup>. Alternatively, a strategy of active surveillance involving regular digital rectal examination and PSA-testing for disease control may be pursued in low-risk patients instead of an immediate treatment<sup>[43-44]</sup>. However, this approach seems to come with an increased risk of disease progression with metastatic spread<sup>[36, 44]</sup>. Thus, especially for patients with

higher baseline life expectancy, the short-term benefit of spared treatment should be carefully weighed against possible future complications.

In advanced stages of the disease, the pelvic lymph nodes are among the first sites of metastasis formation. If lymph node-positive PCa is assessed, a pelvic lymph node dissection (PLND) might be performed in addition to RP, aiming for the resection of cancer-infested tissue <sup>[45]</sup>. However, the extent of PLND and the therapeutic benefit of this surgical procedure are object of controversial debate and no evidence for a direct therapeutic effect based on prospective studies is given to date <sup>[45-47]</sup>. A combination of RT and androgen deprivation therapy (ADT) represents an alternative to the aforementioned surgical interventions and especially for high-risk patients prolonged adjuvant ADT of up to three years after RT has shown reduction in disease progression and increased overall survival <sup>[48-49]</sup>. In ADT, the physiological testosterone production is significantly reduced to serum levels below 20 ng/mL via different approaches, e.g. surgical orchiectomy, chemical castration or antiandrogen therapy, thus reducing androgen-promoted growth of PCa lesions <sup>[50-51]</sup>. ADT constitutes an important backbone of systemic treatment in advanced PCa and combinations with various complementary therapeutic options have been explored. As an example, combination of ADT with hormonal therapy using the synthetic steroid abiraterone plus prednisone or the nonsteroidal antiandrogen enzalutamide achieved increased overall survival or increased radiographic progression-free survival, respectively, as compared to ADT alone in patients with metastatic hormone-sensitive prostate cancer (mHSPC) <sup>[52-53]</sup>. However, despite the advances in patient care applying ADT and hormonal therapy, further disease progression in spite of castrate levels of testosterone is observed in a significant number of patients with advanced PCa leading to the manifestation of metastatic castration-resistant prostate cancer (mCRPC), the most advanced form of PCa. Treatment regimens against mCRPC are palliative in character, highly personalized depending on the treatment history of the individual patient and usually consist of hormonal therapy with abiraterone/prednisone or enzalutamide <sup>[54-55]</sup>, chemotherapy with docetaxel or cabazitaxel <sup>[56-57]</sup> and optionally [<sup>223</sup>Ra]radium dichloride against symptomatic bone metastases <sup>[58-59]</sup>, among others. However, resistances against hormonal and chemotherapeutic agents are commonly observed throughout the course of the treatment <sup>[60-62]</sup> and mCRPC is currently considered incurable <sup>[63]</sup>. Thus, despite the diverse repertoire of available treatment options, novel and complementary therapeutic concepts are urgently needed to further prolong or even save patients' lives in the fight against mCRPC.

## 1.2. PSMA

Besides the disciplines of urology, oncology and radiology as established key players in the clinical management of PCa, modern nuclear medicine has joined the fight against the disease and progressively enriched both the diagnostic and therapeutic arsenal against PCa for more than a decade. After early applications of radio immunoconjugates [64-65] and diagnostic procedures applying e.g. [<sup>11</sup>C]acetate or <sup>11</sup>C- and <sup>18</sup>F-labeled choline analogs for positron emission tomography (PET) imaging [66-68], the rise of nuclear medicine's impact on the management of PCa can be mainly attributed to radiolabeled small-molecule inhibitors of the molecular target prostate-specific membrane antigen (PSMA).

### Structure and Physiological Function of PSMA

PSMA, also called glutamate carboxypeptidase II (GCPII), is a type II transmembrane metallopeptidase and its amino acid (AA) sequence was first revealed by *Israeli et al.* who successfully cloned the protein in 1993 [69-72]. Full-length PSMA comprises 750 AAs and consists of a short N-terminal intracellular tail (AA 1-19), a helical transmembrane part (AA 20-43) and a large C-terminal extracellular domain (AA 44-750) [69, 73]. The extracellular domain of PSMA is further divided into three subdomains: a protease domain (AA 56-116 and 352-591), an apical domain (AA 117-351) and a helical domain (AA 592-750) [72, 74]. A large cavity of ~ 1100 Å<sup>2</sup> is formed at the interface of the three subdomains and contains a binuclear active site with two zinc ions (figure 1) [72, 74]. The helical domain is furthermore responsible for extracellular dimerization of PSMA and, even though each monomer contains a structurally independent active site, hydrolytic activity is apparently lost in membrane-bound monomeric PSMA indicating allosteric involvement of dimerization on the integrity of the active site [72, 75]. Furthermore, N-glycosylation at nine AA residues on the extracellular domain of PSMA were shown to be essential for secretion of the recombinant extracellular domain, proper folding and hydrolytic activity [76-77].

The peptidase activity of PSMA is selective for C-terminal glutamate residues and serves different physiological functions depending on its site of expression [72-73, 78]. According to its role in the nervous system PSMA is also termed N-acetyl- $\alpha$ -linked acidic dipeptidase (NAALADase) and it accounts for the hydrolysis of N-acetyl-aspartyl-glutamate (NAAG) to N-acetyl-L-aspartate (NAA) and L-glutamate [78]. NAAG represents the most abundant mammalian peptide neurotransmitter and activates metabotropic glutamate receptor 3 at presynaptic neurons and astrocytes which modulates neuronal excitability and synaptic transmission by inhibition of glutamate release [79-80]. Thus, NAALADase activity plays an important role in the regulation of the neurotransmitter function of NAAG in the nervous system. However, pathologically dysregulated peptidase activity might lead to increased amounts of glutamate in the synaptic cleft and cause glutamate excitotoxicity which is associated with neuronal disorders [81-82]. In accordance with this suggestion, inhibition of NAALADase showed neuroprotective effects in preclinical models of amyotrophic lateral sclerosis [82], epilepsy [83] and

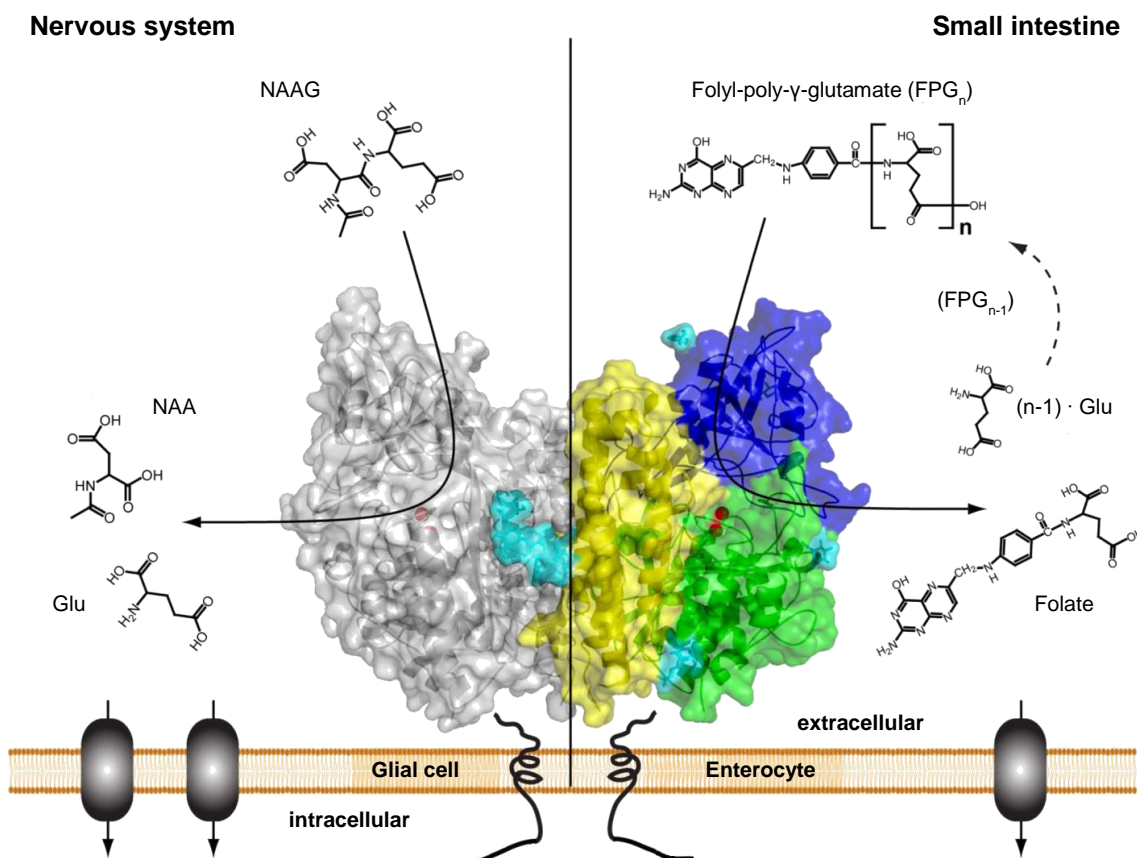


**Figure 1:** Crystal structure of the membrane-bound homo-dimer of prostate-specific membrane antigen (PSMA, left monomer depicted in grey, right monomer depicted in color). The extracellular domain consists of three subdomains: helical domain (yellow), apical domain (blue) and protease domain (green). The binuclear active site of PSMA is located at the interface of the three subdomains and bears two zinc ions (red spheres). N-glycosylations are depicted in cyan. **Left side:** in the nervous system PSMA catabolizes the neurotransmitter N-acetyl-aspartyl-glutamate (NAAG) and the hydrolysis products N-acetyl-aspartate (NAA) and glutamate (Glu) are transported to neuronal glial cells. **Right side:** in the membrane brush border of the small intestine mono-glutamylated folate (folic acid) is provided via iterative cleavage of C-terminal glutamates from foyl-poly- $\gamma$ -glutamate (FPG<sub>n</sub>) by PSMA. Folic acid can subsequently be selectively transported into the enterocytes (figure adapted from Barinka *et al.* Glutamate Carboxypeptidase II in Diagnosis and Treatment of Neurologic Disorders and Prostate Cancer. *Curr Med Chem.* 2012;19(6):856-870. Copyright © 2012, with permission from Bentham Science Publishers).

schizophrenia<sup>[84]</sup> underlining the potential of PSMA/NAALADase as therapeutic target in the treatment of these neuronal diseases.

Another physiological function of PSMA is related to folate uptake in the small intestine. Folate constitutes an essential vitamin and dietary folate is consumed in form of foyl-poly- $\gamma$ -glutamate (FPG)<sup>[85]</sup>. The proton-coupled folate transporter in the small intestine mediates the uptake of folates into the vascular system by selectively transporting foyl-mono-glutamate (folic acid)<sup>[85-86]</sup>. The necessary hydrolytic cleavage of C-terminal glutamates from FPG yielding mono-glutamylated folic acid is provided by folate hydrolase 1 (FOLH1), which is expressed in the membrane brush border of the proximal small intestine and was found to be identical with PSMA<sup>[73, 87]</sup>.

## Physiological and Pathological Expression of PSMA

Apart from its presence in the nervous and intestinal system, physiological expression of PSMA was also found in the prostatic epithelium, the proximal tubuli of the kidney and in salivary glands [88-90]. Low levels of PSMA expression have furthermore been reported for a variety of other healthy tissues, among them heart, liver, testis and pancreatic islets [90-91], however the function of PSMA in these organs is not understood yet nor has physiological expression in these organs gained relevance in clinical PSMA-targeting to date.

Compared to benign prostatic tissue significantly increased expression of PSMA in a staggering majority of PCa-samples of both primary tumors and metastases was reported by several studies [92-94]. On an mRNA expression level, different splice variants of PSMA were identified, among them two variants encoding for either full-length, membrane-bound PSMA or a cytosolic form lacking the transmembrane domain (PSM') [95-96]. *Su et al.* reported PSMA/PSM'-ratios in PCa to exceed ratios in normal prostate by more than 100-fold [95]. Thus, in contrast to healthy prostatic tissue, PSMA is not only overexpressed in PCa cells but is furthermore predominantly presented on the cell surface where it is accessible for diagnostic and therapeutic agents rendering PSMA a superb molecular target. In addition, PSMA expression was shown to correlate with tumor grade [89, 93] and recent studies described PSMA expression as an independent predictor of biochemical recurrence after radical prostatectomy [94, 97-98] thus allowing for early prognosis of disease outcome and facilitating clinical decision making.

The biological function of PSMA in PCa cells is not yet fully unveiled and different suggestions have been made concerning the role of PSMA towards the aggressiveness of PCa. *Gosh et al.* described increased invasion of PSMA-negative or PSMA-inhibited cells compared to PSMA-positive cells *in vitro* suggesting PSMA as possible suppressor of PCa invasiveness [99]. In contrast, *Yao et al.* found increased proliferation of PSMA-positive cells in the presence of physiological levels of folate and consequently suggested that folate hydrolase activity of PSMA might confer a growth advantage to PSMA-positive PCa cells over PSMA-negative ones [100-101]. While these findings apparently seem contradicting, they also emphasize that further research is needed to gain a more accurate understanding of how PSMA-related factors (e.g. invasive behaviour, proliferation, availability of substrates) influence the aggressiveness of PCa.

Besides its involvement in PCa, presence of PSMA has been confirmed in the endothelial cells of the neovasculature of various solid tumors such as e.g. renal cell carcinoma [102], gastric and colorectal cancers [103], breast cancer [104] and thyroid tumors [105]. PSMA-targeted molecular imaging was successfully performed for a variety of these malignancies and first experiences with PSMA-targeted therapy foreshadow future applications in non-prostate cancers, thus adding to the already outstanding value of PSMA as a target in PCa [106-108].

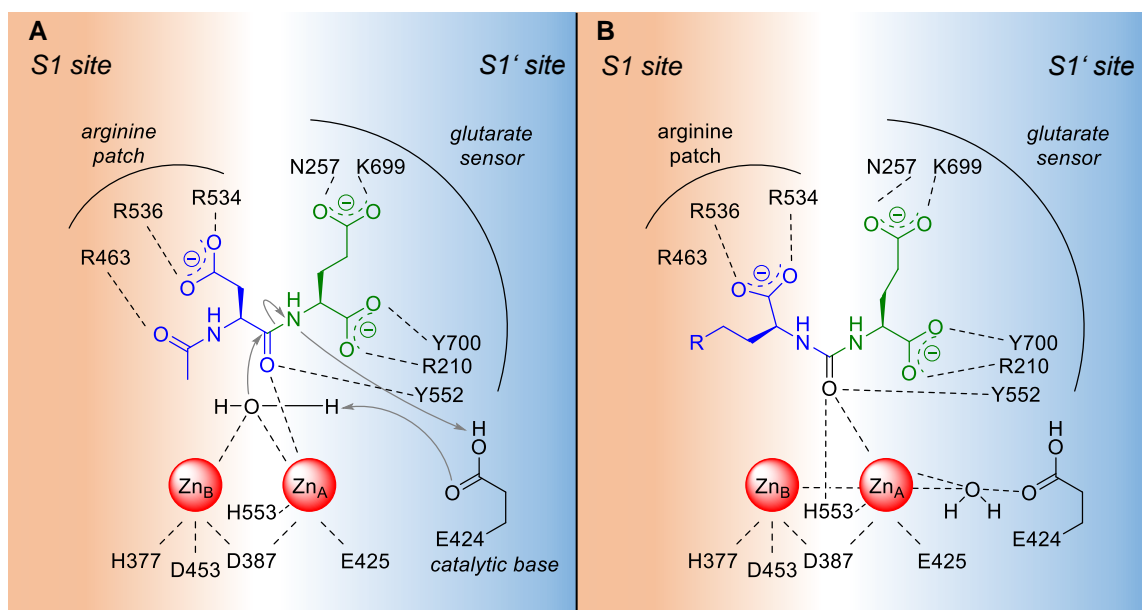


**Figure 2:** Schematic representation of the natural substrate NAAG and urea-based inhibitors within the active site of PSMA. The S1' pharmacophore pocket and S1 pocket are indicated in pale blue and pale orange, respectively. Zinc ions are depicted as red spheres, the P1' side and P1 side of substrate and inhibitors are colored green and blue, respectively. **A)** Orientation of NAAG within the active site of PSMA. Glutamate is coordinated by the glutarate sensor, the amide bond oxygen coordinates to zinc-ion A and a water molecule (polarized by Zn-ions A and B and the catalytic base E424) acts as hydrolytic nucleophile (mechanism indicated by grey arrows). The aspartyl carboxylate is coordinated by guanidinium groups of the arginine patch (interactions between substrate and binding pocket according to crystal structures reported by *Klusak et al.* Reaction mechanism of glutamate carboxypeptidase II revealed by mutagenesis, X-ray crystallography, and computational methods. *Biochemistry* 2009;48(19):4126–38). **B)** Orientation of a urea-based PSMA-inhibitors within the active site of PSMA. Glutamate recognition resembles NAAG, the hydrolysis-resistant urea group coordinates to zinc-ion A and H553, and the P1 carboxylate interacts with guanidinium groups of the arginine patch (interactions between substrate and binding pocket according to *Barinka et al.* Interactions between Human Glutamate Carboxypeptidase II and Urea-Based Inhibitors: Structural Characterization. *J Med Chem.* 2008;51(24):7737–7743).

### Structural Design of PSMA-Targeted Ligands

The discovery of PSMA is closely interwoven with the first PSMA-targeted ligand, the murine monoclonal antibody (mAb) 7E11-C5.3, which was generated by *Horoszewicz et al.* via immunization of Balb/c mice with the human PCa cell line LNCaP<sup>[109]</sup>. Several years later, identification and sequence elucidation of this antibody's target, PSMA, was achieved<sup>[69]</sup>. In the following, the <sup>111</sup>In-labeled murine IgG1 mAb 7E11-C5.3 (<sup>111</sup>In-Capromab Pendetide, ProstaCint®) was developed and approved as first diagnostic radio-immunoconjugate for imaging of PCa<sup>[64, 110]</sup>. A restricting property of 7E11-C5.3, namely targeting an intracellular epitope of PSMA exposed only upon cell death<sup>[109, 111]</sup>, prompted the subsequent development of de-immunized mAbs such as J591<sup>[111]</sup> that bind to the extracellular domain of PSMA and numerous studies emphasize this mAb's persisting clinical significance<sup>[65, 112-113]</sup>.

Development of small-molecule inhibitors of PSMA was initially driven by the aim to inhibit NAALADase activity in the brain to potentially treat neuronal disorders. Based on the known structure of NAAG, the endogenous substrate of NAALADase, first inhibitor generations mimicked the

acetylated dipeptide but affinities didn't exceed the micromolar range<sup>[114-115]</sup> until in 1996 *Jackson et al.* reported the development of 2-PMPA, an  $\alpha$ -methylene glutarate-substituted phosphonate with sub-nanomolar affinity and still one of the most potent inhibitors of PSMA to date<sup>[116]</sup>. Since then, a plethora of PSMA-targeted small-molecule inhibitors has been developed in mostly ligand- and structure-based rational drug design approaches. In the following, the rational structural design of PSMA-targeted small-molecule inhibitors will be discussed in the context of the active site and several secondary binding sites in PSMA.

The active site of PSMA is divided into the S1' pharmacophore pocket that accepts the C-terminal part of substrates/inhibitors (figure 2, highlighted in blue) and the adjacent S1 pocket located towards the entrance funnel (highlighted in orange). Structural subunits of substrates/inhibitors are correspondingly termed P1' and P1 (green and blue structures, respectively, in figure 2). Both natural substrates of PSMA, NAAG and FPG, bear a C-terminal L-glutamate that is coordinated by a 'glutarate sensor' consisting of residues K699 and Y700 in the S1' pharmacophore pocket<sup>[70, 74, 117]</sup>. Glutamate position is highly conserved in crystal structures of a variety of glutamate-containing inhibitors complexed to PSMA (figure 3A)<sup>[118-119]</sup> and substitution of the glutarate moiety generally lead to significantly decreased affinity<sup>[114, 116, 120]</sup>. Therefore, a P1' glutarate moiety is generally considered crucial for high PSMA affinity. Within the binuclear active site of PSMA, two zinc-ions are stably complexed by residues H377, D453, D387, H553 and E425<sup>[72]</sup>. A highly polarized water molecule serves as nucleophile in the hydrolysis of natural substrate NAAG and the carboxylate residue of E424 functions as catalytic base<sup>[117]</sup>. Potent inhibitors either mimic the planar peptide bond in NAAG via a urea functionality (an amide-bioisostere resistant against hydrolysis)<sup>[121]</sup> or the sp<sup>3</sup>-hybridized transition state via phosphonates (e.g. in 2-PMPA)<sup>[116, 120]</sup> or phosphoramidates<sup>[119]</sup>. Both urea and phosphonates coordinate to one or two zinc-ions, respectively<sup>[118, 122]</sup>, thus further strengthening the interaction between inhibitor and PSMA. Due to their broad synthetic accessibility, high affinity and stability urea-based inhibitors comprising a XuE-motive (E: L-glutamate; u: bridging urea function; X: L- $\alpha$ -amino acid, mostly L-glutamate (EuE) or L-lysine (KuE)) are the most relevant and widespread inhibitors of PSMA in today's clinical practice and research<sup>[123]</sup>. Another common and affinity-enhancing structural signature in these urea-based inhibitors is a P1 carboxylate that was shown to interact with the guanidinium groups of arginines R436, R534 and R536<sup>[118]</sup>. This so-called 'arginine patch' constitutes a characterizing feature of the S1 pocket and is associated with a preference for negatively charged substrates<sup>[70, 74, 122]</sup>. In contrast to the S1' pocket, however, the S1 pocket is more flexible and accommodates substrates/inhibitors with versatile structural features<sup>[118, 120, 123]</sup>. In that context, *Barinka et al.* discovered a unique interplay between the arginine patch and the accessibility of a secondary binding site, the 'S1 accessory pocket' (figure 3B-D)<sup>[118]</sup>. While the position of R534 is essentially invariant, R536 can adopt a 'stacking' (R536s) or a 'binding' (R536b) conformation. The latter, induced by interaction with a suitable inhibitor, facilitates the shift of R463 from a 'down' position (R463d) to an 'up' position (R463u) which opens up the S1 accessory pocket, a hydrophobic cavity with

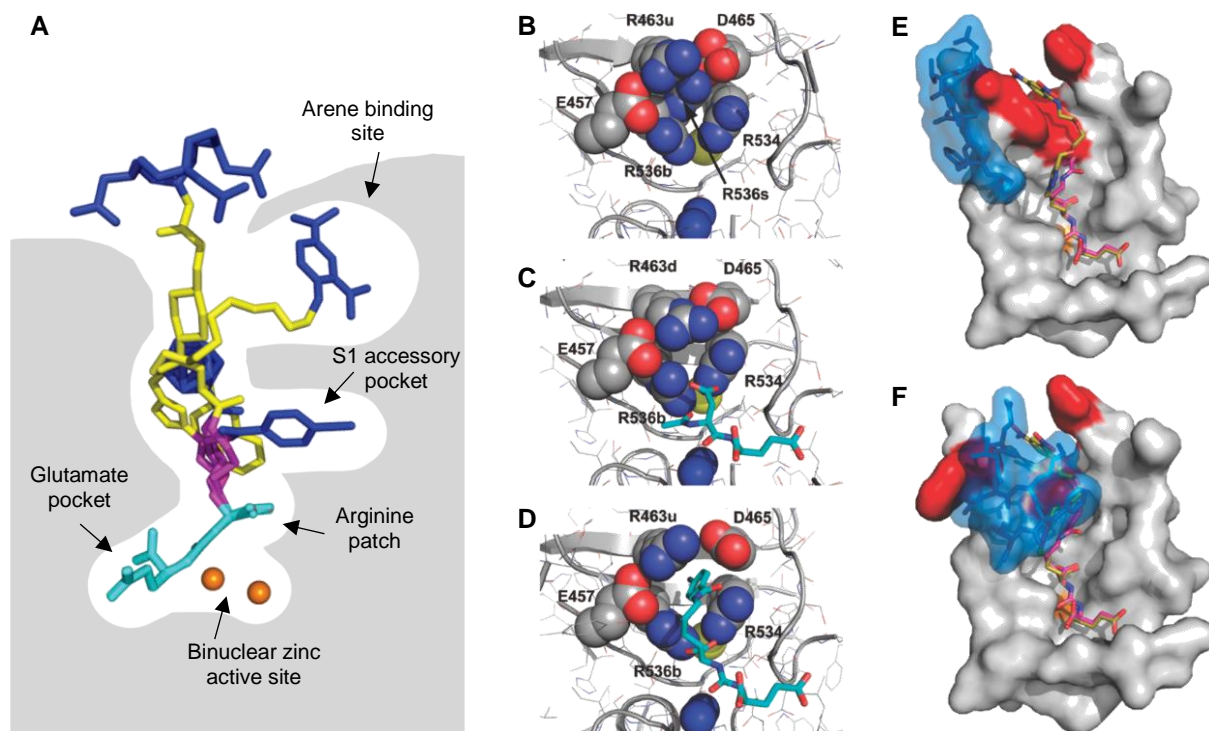


**Figure 3:** **A)** PSMA binding pocket with superimposed structures of different PSMA-inhibitors. Active site and secondary binding sites are indicated with arrows. **B)** Arginine patch in uncomplexed PSMA. Residue R536 is flexible and adopts either ‘stacking’ (R536s) or ‘binding’ (R536b) position. Residue R463 adopts ‘up’ (R463u) position. The S1 accessory pocket is not accessible. **C)** In NAAG-complexed PSMA the conformation R536b and R463d (‘down’ position) occlude the S1 accessory pocket. **D)** Upon complexation with IBA-KuE, R536b and R463u conformation of the arginine patch opens the S1 accessory pocket for interaction with the 4-iodobenzyl moiety of the inhibitor. **E)** Complexation of PSMA with inhibitor ARM-P4 promotes an open conformation of the entrance lid (blue) and residues forming the arene binding site (red) can interact with the dinitroarene in ARM-P4. **F)** When complexed with IBA-KuE the entrance lid of PSMA (blue) remains in a closed conformation and residues forming the arene binding site are relatively dislocated. Ligand structures of ARM-P4 and IBA-KuE are superimposed in panels E and F (figure A modified from *Kopka et al.* Glu-Ureido-Based Inhibitors of Prostate-Specific Membrane Antigen: Lessons Learned During the Development of a Novel Class of Low-Molecular-Weight Theranostic Radiotracers. *J Nucl Med.* 2017;58(S2):17S-26S. Copyright © 2017 SNMMI; figures B-D reproduced from *Barinka et al.* Interactions between Human Glutamate Carboxypeptidase II and Urea-Based Inhibitors: Structural Characterization. *J Med Chem.* 2008;51(24):7737–7743. Copyright © 2008 American Chemical Society; figures E and F reproduced from *Zhang et al.* A Remote Arene-Binding Site on Prostate Specific Membrane Antigen Revealed by Antibody-Recruiting Small Molecules. *J Am Chem Soc.* 2010;132(36):12711–12716. Copyright © 2010 American Chemical Society).

approximate dimensions of  $8.5 \text{ \AA} \times 7 \text{ \AA} \times 9 \text{ \AA}$  <sup>[118]</sup>. Inhibitors like IBA-KuE <sup>[124]</sup> or DCFBC <sup>[125]</sup> bearing a P1 aromatic moiety in a defined intramolecular distance to the urea-motive can access the S1 accessory pocket and thereby benefit from enhanced affinity. Ultimately, a further secondary binding site was characterized by *Zhang et al.* in 2010 <sup>[126]</sup>. KuE-based inhibitors functionalized with dinitroarenes via polyethylene glycol (PEG) chains of varying length had shown staggering PSMA-affinities in the picomolar range and lead to the assumption of a bidentate interaction with PSMA. Indeed, a remote arene binding site was identified within the entrance funnel of the binding pocket where aromatic structures can interact with the indole residue of W541 and the guanidinium group of R511 via  $\pi$ -stacking and  $\pi$ -cationic interactions, respectively (figure 3E+F) <sup>[126]</sup>. Interestingly,

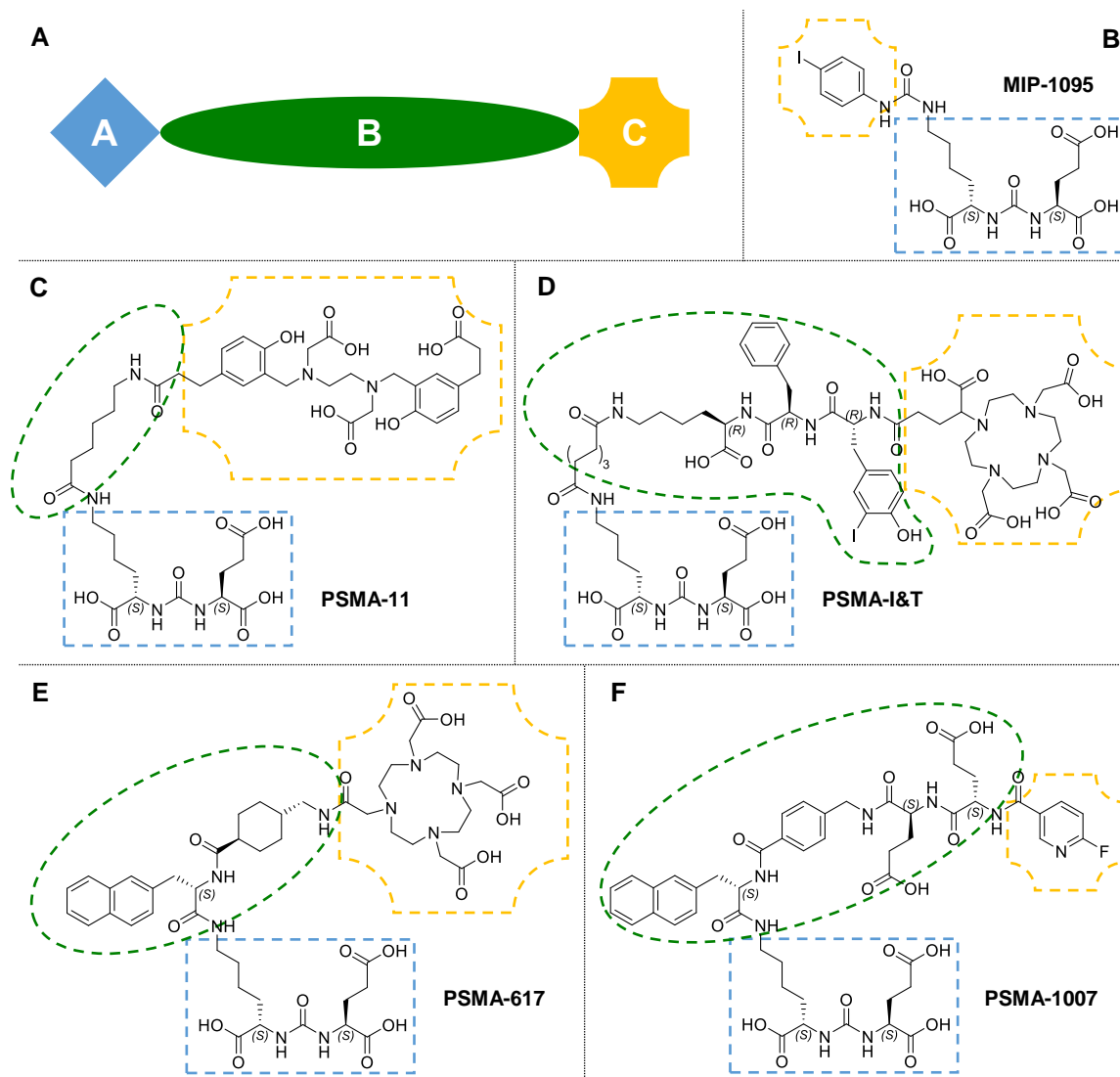


**Figure 4:** Structures of some important small-molecule, urea-based PSMA-inhibitors. **A)** Schematic structure of PSMA-targeted ligands consisting of a urea-based targeting vector (A, blue), an optional linker moiety (B, green) and a site for either covalent radiolabeling or radiometal complexation (C, yellow). In panels B-F, urea binding motives are indicated with blue dotted squares, linker regions displayed by green dotted ellipsoids and sites of radiolabeling are highlighted by yellow dotted edging. **B)** MIP-1095 comprises the common KuE binding motive, a 4-iodo-phenyl group enhances affinity via interaction with the S1 accessory pocket and furthermore serves for radiolabeling with isotopes of iodine. **C)** PSMA-11 comprises a HBED-CC chelator for labeling with gallium-68. A linear linker provides optimal distance between the KuE binding motive and the chelator. **D)** PSMA-I&T comprises a DOTAGA chelator for labeling with diagnostic and therapeutic radionuclides. The linker region is composed of D-amino acids for enhanced metabolic stability and lipophilic interactions with the arene binding site in PSMA. **E)** The linker region in PSMA-617 was specifically optimized for enhanced internalization. A DOTA chelator allows for use in theranostic applications. **F)** PSMA-1007 was developed for  $^{18}\text{F}$ -based PET-imaging. The linker moiety is derived from PSMA-617 and comprises two glutamates to counteract the compound's high lipophilicity. Labeling with fluorine-18 is facilitated by a nicotinic acid prosthetic group.

the length of the linker between the urea binding motive and the aryl group proved decisive for optimal affinity and the arene binding site is only accessible for an open entrance lid conformation of PSMA. The latter seems to be prevalent for ligands with an extended linker region which might be exploited in the structural design of extended ligand constructs with tailored effector-moieties distal to the actual glutamate-bearing pharmacophore.

Apart from the target-binding aspects discussed so far, the structural design of PSMA-targeted ligands is fundamentally characterized by the intended field of application. In some radioligands such as MIP-1095<sup>[127]</sup>, BAY 1075553<sup>[128]</sup> or DCFPyL<sup>[129]</sup>, the radiohalogen was introduced as an integral part of the PSMA-targeting scaffold. However, a broad variety of diagnostic or therapeutic approaches involve the attachment of sterically demanding effector-moieties such as radiometal complexes<sup>[123]</sup>, IR-dyes<sup>[130]</sup>, cytotoxic drugs<sup>[131]</sup> or photosensitizers<sup>[132]</sup>. Therefore, to prevent steric clashes of these bulky substituents with relevant binding sites, PSMA-targeted ligands oftentimes show a three-compartmented structure (figure 4) consisting of A) a urea-based binding motive (e.g. EuE or KuE), B) a variable linker region and C) an effector-moiety (e.g. a radiometal complex). After potent targeting-scaffolds had been established and reliable metal chelators such as DOTA (1,4,7,10-tetraazacyclododecan-N,N',N'',N'''-tetraacetic acid) are commercially available building blocks, a large portion of structural development in novel PSMA-targeted radioligands in recent years focused on the optimal design of the linker region and modifications directed towards modulated pharmacokinetics (PK), optimized target binding or enhanced internalization have been explored in an extensive manner. Several of the most established PSMA-targeted radioligands are depicted in figure 4.

### 1.3. Therapeutic Applications of PSMA-Targeted Radiopharmaceuticals

The progression of PCa to a castration-resistant state is a common course of development for the disease and is observed in 10 – 20% of patients within 5 years after initial diagnosis [133]. Among patients with castration-resistance, over 84% present with osseous metastases already at the time of diagnosis [134-135]. In a significant fraction of the remaining patient population, metastatic spread was reported within only two years [136]. As mCRPC is correlated with poor survival and regularly challenges clinicians with acquired resistance against conventional therapeutic interventions like chemotherapy, steroids and antiandrogens, the complementary use of radioligand therapy (RLT) with PSMA-targeted radiopharmaceuticals represents a promising systemic treatment approach and an important enrichment of the previously available therapeutic armamentarium. First experiences with therapeutic applications of PSMA-targeted radioligands in mCRPC were made with  $^{90}\text{Y}$ - and  $^{177}\text{Lu}$ -labeled mAbs at the beginning of the millennium [65, 137-138]. However, the slow clearance kinetics and limited tumor penetration of these radio-immunoconjugates hamper both their diagnostic performance and therapeutic efficacy [139-140]. As discussed in the preceding chapter, urea-based small molecule inhibitors of PSMA have attracted widespread attention for the use as diagnostic and therapeutic radioligands because of their broad synthetic accessibility, excellent target-affinity and favorable clearance kinetics. In this section, the current state of therapeutic interventions in mCRPC using radio-labeled, urea-based small molecule inhibitors of PSMA will be discussed.

#### The Theranostic Principle

After early encouraging results with PSMA-targeted radioligands for single photon emission computed tomography- (SPECT) and PET-imaging, the concept of theranostics has entered the spotlight of PSMA tracer development. The term *theranostics* (a portmanteau derived from *therapy* and *diagnostics*) describes the inseparability of diagnostics and therapy in modern precision oncology [141]. In the context of nuclear medicine, the theranostic principle implies that patient management is built upon a theranostic pair of radioligands: a diagnostic companion for molecular imaging serves the purpose of diagnosis, dosimetry calculation and therapy response control; a therapeutic companion is used as endoradiotherapeutic drug to systemically irradiate primary tumors and metastases [142-144]. These theranostic companions are radioligands sharing highly similar (or in cases even identical) targeting and pharmacokinetic properties that allow for the unique possibility to “see what you treat and treat what you see”. Herein, pre- and post-therapeutic imaging is used to determine optimal dosage, to rapidly assess response to RLT and to continuously adjust the therapy protocol on behalf of the individual patient (figure 5) [142-144]. Clinical practice oftentimes employs different radiochelates (e.g. [ $^{68}\text{Ga}$ ]Ga-complex and [ $^{177}\text{Lu}$ ]Lu-complex) of the same ligand or even two different ligands with matching targeting and pharmacokinetic properties as theranostic companions. Technically, however, chemically identical companions varying only in the diagnostic/therapeutic radioisotope would optimally exploit the potential of the theranostic principle.

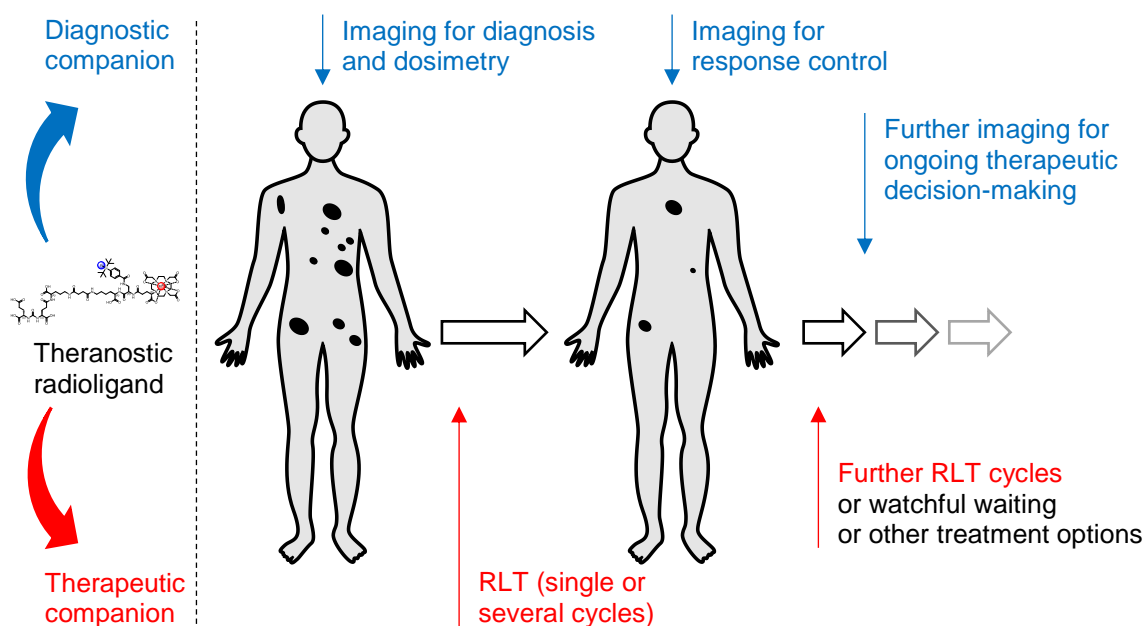


**Figure 5:** Schematic overview of clinical patient management using theranostic radioligands. The diagnostic companion of the theranostic pair (related procedures are indicated in blue) is used for initial diagnosis via molecular imaging. Dosage of subsequent radioligand therapy (RLT) with the therapeutic companion (indicated in red) is based on dosimetry calculations derived from quantitative imaging with the diagnostic companion. Response to RLT can be controlled via post-therapeutic imaging which contributes to subsequent decision-making towards further RLT cycles or alternative treatment options.

Consequently, chemical elements with multiple radioisotopes eligible for both diagnostic and therapeutic purposes are predestined for theranostic applications. As an example,  $^{123}\text{I}$ - and  $^{131}\text{I}$ -based SPECT-imaging<sup>[145-147]</sup> is executed to select thyroid cancer patients for endoradiotherapy with radioiodine ( $[^{131}\text{I}]\text{I}^-$ ,  $\beta^-$ -emitter, 606 keV)<sup>[148-149]</sup>. The latter has been used since the 1940s for the therapy of thyroid carcinoma metastases and emphasizes the long history of theranostics with radioactive compounds in oncologic disease<sup>[150-151]</sup>. In the context of PCa,  $^{123}\text{I}$ -labeled compounds MIP-1072 and MIP-1095 were among the first PSMA-targeted radioligands evaluated in patients<sup>[140]</sup> and opened up the way for a first theranostic application of MIP-1095 comprising  $^{124}\text{I}$ -based PET-imaging and RLT with the  $^{131}\text{I}$ -labeled compound in 2014<sup>[152]</sup>. Apart from iodine, the copper isotope copper-64 has gained increased attention in the development of theranostic radioligands<sup>[153-155]</sup>. The isotope itself combines theranostic properties, namely partial  $\beta^+$ -decay ( $E_{\beta^+} = 655$  keV positron energy, 18%)<sup>[156]</sup> qualifying  $^{64}\text{Cu}$ -labeled ligands for PET-imaging and  $\beta^-$ -emissions ( $E_{\beta^-} = 573$  keV, 38%)<sup>[156]</sup> that can be exploited for RLT. Especially its comparatively long half-life of 12.7 h makes  $^{64}\text{Cu}$ -labeled ligands attractive tools for PET-studies at late imaging time points aiming for superior contrast due to enhanced clearance of the tracer from non-target tissue<sup>[153]</sup>. Furthermore, the existence of the purely therapeutic isotope copper-67 ( $\beta^-$ -emitter,  $t_{1/2} = 61.8$  h,  $E_{\beta^-} = 141$  keV)<sup>[157]</sup> has rendered theranostic pairs of  $^{64}\text{Cu}/^{67}\text{Cu}$ -labeled radiopharmaceuticals subjects of intensive research<sup>[158-160]</sup>. A potential for an even wider theranostic utility is found in the lanthanide terbium. A unique quadruplet of terbium radioisotopes with clinically suitable decay properties technically allows for the execution of PET (with terbium-152), SPECT (with terbium-155),  $\beta^-$ -therapy (with terbium-161) and  $\alpha$ -therapy (with terbium-149) using

Tb-labeled radioligands [161-162]. Besides extensive basic and preclinical research [161, 163-165] a first-in-man study by *Baum et al.* using  $^{152}\text{Tb}$ -labeled DOTATOC for PET-imaging in a patient with metastatic neuroendocrine neoplasms revealed high imaging contrast at late time points and visualization of even small metastases was found to be feasible [166]. Subsequently, PET-imaging was also reported in a patient with mCRPC using  $^{152}\text{Tb}$ -labeled PSMA-617 [167] before the feasibility of  $^{161}\text{Tb}$ -based RLT was exemplified in patients with metastatic paraganglioma and metastatic neuroendocrine neoplasms for the first time [168]. To date, however, a broader application of Tb-labeled radioligands is still impeded by scarce availability due to technological aspects in the production and purification of these radionuclides [162].

Thus, from a practical perspective,  $\beta^-$ -RLT procedures are predominantly executed with  $^{177}\text{Lu}$ -labeled compounds, mainly because of the favorable dosimetric and radiation properties, excellent availability and established chelating systems for this radiometal [169-171], while targeted alpha therapy (TAT) procedures increasingly make use of actinium-225 [172-174]. At least in the case of lutetium-177, its  $\gamma$ -emissions may be exploited for SPECT-imaging, however, due to the lack of suitable isotopes for high resolution pre-therapeutic PET-imaging,  $^{68}\text{Ga}$ -labeled PET-tracers are conventionally applied to accompany  $^{177}\text{Lu}$ - or  $^{225}\text{Ac}$ -based RLT. Two successful examples from clinical practice are the radioligand pairs of [ $^{68}\text{Ga}$ ]Ga-/[ $^{177}\text{Lu}$ ]Lu-DOTATATE against neuroendocrine tumors [175-176] and [ $^{68}\text{Ga}$ ]Ga-PSMA-11 in combination with [ $^{177}\text{Lu}$ ]Lu- or [ $^{225}\text{Ac}$ ]Ac-PSMA-617 for the treatment of mCRPC [172, 177]. However, the intrinsic advantage of the theranostic principle is not fully exploited with these pairs of radioligands, as diagnostic and therapeutic compounds differ in their chemical and/or radio-chelate structure which can result in diverging targeting properties and pharmacokinetic behaviour [178-179]. Furthermore, the conservative structural concept of interchanging a given radionuclide to generate the respective theranostic companion of a radioligand holds the drawback that the lighthouse diagnostic nuclide fluorine-18 cannot be integrated into a true theranostic pair of radioligands.

### The Concept of Theranostic Radiohybrid Ligands

A recent development, however, successfully faced the latter limitations and made the combined introduction of the established radionuclides lutetium-177 and fluorine-18 to the true theranostic world possible. So-called radiohybrid ligands contain two independent structural motives for radiolabeling: a silicon-fluoride acceptor (SiFA) for the optional  $^{18}\text{F}$ -labeling by isotopic exchange with fluorine-19 and a chelating unit for the complexation of a (radio)metal [180-182]. Based on this structural concept true theranostic companions, also referred to as theranostic twins due to their identity in chemical structure, are either  $^{18}\text{F}$ -labeled for diagnostic use while complexed with a non-radioactive metal or they contain non-radioactive fluorine-19 combined with the therapeutic radiometal complex for therapy (figure 6). In 2020, the radiohybrid concept was described by *Wurzer et al.* [182] exemplified by radiohybrid PSMA (rhPSMA) ligands for solely imaging purposes that combined the [ $^{18}\text{F}/^{19}\text{F}$ ]SiFA moiety with a

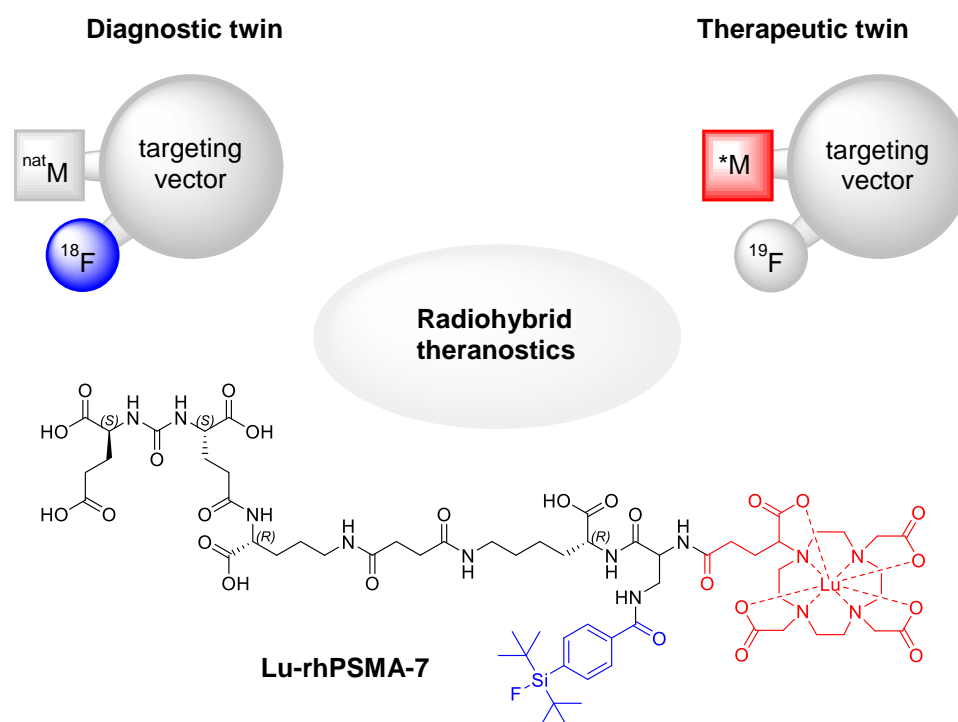


**Figure 6:** Radiohybrid theranostic ligands contain a chelating unit (square in schematic depiction, red in chemical structure) for the complexation of either the natural isotope ( $^{nat}M$ ) or the therapeutic radionuclide ( $^{*}M$ ) of a metal such as lutetium and a silicon-fluoride acceptor (SiFA) moiety (small circle in schematic depiction, blue in chemical structure) that can be labeled with fluorine-18 for PET-imaging. The diagnostic twin is labeled with fluorine-18 (blue) and complexed with a non-radioactive metal ion (e.g.  $^{nat}Lu^{3+}$ ), while the therapeutic twin contains non-radioactive fluorine-19 and a therapeutic radiometal (red, e.g.  $^{177}Lu^{3+}$ ) complexed to the chelating unit. Examples for diagnostic and therapeutic twins are  $[^{18}F][^{nat}Lu]Lu$ -rhPSMA-7 and  $[^{19}F][^{177}Lu]Lu$ -rhPSMA-7, respectively.

$^{nat}Ga/^{68}Ga$ -complex. This innovation bridges the gap between  $^{18}F$ - and  $^{68}Ga$ -based PSMA PET-imaging in PCa by offering chemically identical PET-tracers to clinics and nuclear medicine centers irrespective of whether the local infrastructure allows radiosynthesis with either cyclotron-generated fluorine-18 or generator-based gallium-68. The racemic tracer  $[^{18}F]Ga$ -rhPSMA-7 and its single isomer  $[^{18}F]Ga$ -rhPSMA-7.3<sup>[183]</sup> have since been investigated for PET-imaging of both primary and recurrent PCa and high detection rates comparable to the FDA-approved ligand  $[^{68}Ga]Ga$ -PSMA-11 as well as superior sensitivity, specificity and accuracy compared to conventional morphological imaging were reported<sup>[184-187]</sup>. The current evaluation of the diagnostic lead compound  $[^{18}F]Ga$ -rhPSMA-7.3 in the prospective phase 3 clinical trials ‘LIGHTHOUSE’ (ClinicalTrials.gov identifier NCT04186819) for imaging of newly diagnosed PCa and ‘SPOTLIGHT’ (NCT04186845) in recurrent disease may possibly lead to the regulatory approval of this innovative diagnostic radiopharmaceutical in the near future.

The paramount clinical potential of rhPSMA ligands, however, more than anything lies in their theranostic application. The advantages of  $^{18}F$ -labeled radiopharmaceuticals over their  $^{68}Ga$ -labeled counterparts, namely large-scale cyclotron-based production for high numbers of patients, a longer physical half-life (110 min vs 68 min, respectively) allowing shipment to nuclear medicine centers without own production facility<sup>[188]</sup>, and improved spatial resolution owing to reduced positron energy

(0.65 MeV vs 1.90 MeV, respectively) <sup>[189]</sup>, render <sup>18</sup>F-labeled, Lu-complexed rhPSMA ligands highly promising and broadly available diagnostic tools for pre-therapeutic imaging. Dosimetry calculations would be quantitatively transferable to the corresponding therapeutic twin [<sup>177</sup>Lu]Lu-rhPSMA due to chemically identical structures enabling the execution of accurate personalized RLT in mCRPC patients. The radiohybrid concept therefore constitutes a remarkable approach to harness the full potential of the theranostic principle while simultaneously exploiting the specific advantages of fluorine-18 for diagnostics and lutetium-177 for RLT in the treatment of oncological diseases.

### Endoradiotherapy of PCa

The first clinical application of endoradiotherapy in mCRPC based on small-molecule PSMA inhibitors was executed in 2014 by *Zechmann* and colleagues using MIP-1095 labeled with the  $\beta^-$ -emitter iodine-131 <sup>[152]</sup>. High uptake and impressive retention in metastatic lesions was observed and the dosimetry of the small-molecule radioligand was found to be superior to <sup>90</sup>Y-labeled mAb J591 and comparable to [<sup>177</sup>Lu]Lu-J591. A decline in serum PSA levels of  $\geq 50\%$  in 61% of the patients, radiographic reduction in disease burden and reported pain relieve from bone metastases represented encouraging results. At the same time, however, significant doses to salivary glands ( $4.62 \pm 3.10$  Sv/GBq, mean value) caused xerostomia in several patients and raised concerns about long-term salivary gland toxicity for repeated RLT cycles <sup>[152]</sup>. Currently, there are two active clinical phase 2 trials evaluating [<sup>131</sup>I]MIP-1095 alone or in combination with enzalutamide in mCRPC patients (NCT04085991 and NCT03939689, respectively, as of 08.03.2023).

Since this radioiodinated compound had opened up the therapeutic stage for small-molecule PSMA-inhibitors, two chelator-based ligands have established themselves as the mainstay of RLT in mCRPC: PSMA-617 <sup>[190]</sup> and PSMA-I&T <sup>[191]</sup>. Both theranostic radioligands represent prime examples for the iterative molecular structure development in preclinical radiopharmaceutical research. PSMA-617 was developed with the aim to create a DOTA-based PSMA-targeted radioligand that could possibly be used for theranostic purposes, after [<sup>68</sup>Ga]Ga-PSMA-11 had shown promising results as a PET-imaging agent <sup>[192-193]</sup>. In contrast to the HBED-CC chelator incorporated in PSMA-11, DOTA not only allows for the radiolabeling of gallium-68 for PET-imaging but also affords stable complexes with therapeutic isotopes like yttrium-90, lutetium-177 or actinium-225. Mere substitution of HBED-CC by DOTA, however, resulted in reduced PSMA-affinity of DOTA-Ahx-KuE and, correspondingly, low tumor uptake in LNCaP-bearing xenografts <sup>[192]</sup>. Therefore, in a second step, PSMA-617 was developed by means of linker modifications aiming to increase the lipophilic interactions of the radioligand with the PSMA binding pocket to promote high PSMA affinity and PSMA-mediated internalization (figure 7) <sup>[190, 194]</sup>. In a similar fashion, PSMA-I&T was developed by iterative structure modifications based on DOTA-FFK-Sub-KuE, one of the first DOTA-based PSMA ligands reported by *Banerjee at al.* in 2010 <sup>[195]</sup>. In a first step, the substitution of DOTA by the DOTAGA chelator (1,4,7,10-tetraazacyclododecane-N-(glutaric acid)-N',N'',N'''-triacetic acid) resulted in PSMA-TUM1, the first

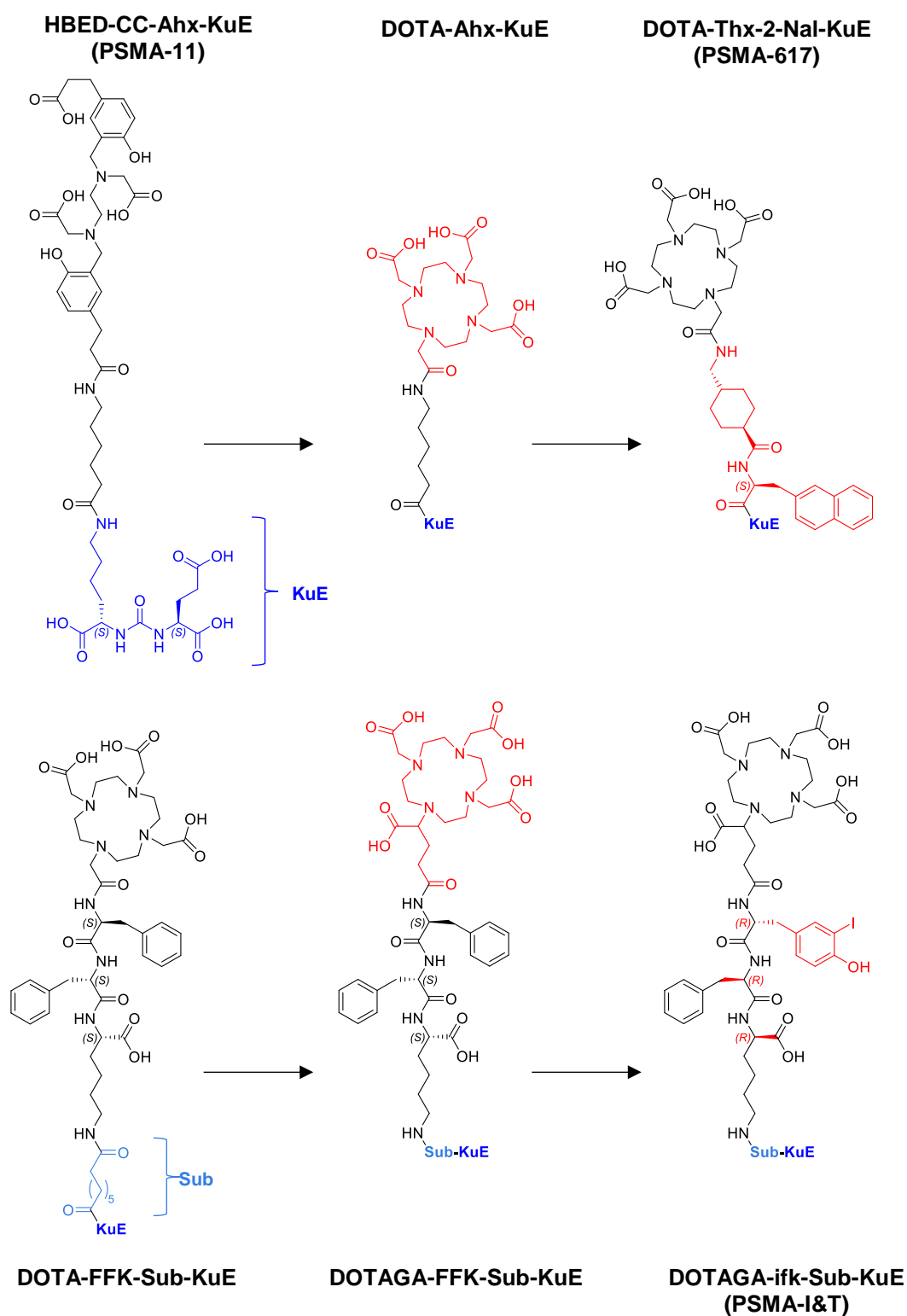


**Figure 7:** The molecular structure of PSMA-617 (upper row) was developed by introduction of a DOTA chelator into a PSMA-11-derived compound (DOTA-Ahx-KuE) and subsequent optimization of the linker unit focusing on lipophilic interaction with the PSMA binding pocket. The structure of DOTA-FFK-Sub-KuE (bottom row) was in a first step optimized by replacement of DOTA by DOTAGA. Subsequent introduction of D-configured amino acids in the linker for enhanced metabolic stability and substitution of N-terminal phenylalanine by 3-iodo-tyrosine for ameliorated interaction with the arene binding site led to the development of PSMA-I&T. Iterative chemical modifications are indicated in red.

<sup>177</sup>Lu-labeled urea-based PSMA-ligand clinically applied in RLT of mCRPC [196-197]. Subsequent optimizations, namely a D-configured linker for increased metabolic stability and the introduction of lipophilic 3-iodo-tyrosine for enhanced interaction with the remote arene binding site [126], resulted in the molecular structure of PSMA-I&T (figure 7) [191].

To date, PSMA-617 has been labeled with several different  $\beta^-$ -emitting radioisotopes. While [<sup>161</sup>Tb]Tb-PSMA-617 and its <sup>47</sup>Sc- and <sup>67</sup>Cu-labeled analogs have currently not proceeded beyond the preclinical setting [198-200], <sup>64</sup>Cu- and <sup>90</sup>Y-labeled PSMA-617 have found their way into initial clinical evaluation besides the established [<sup>177</sup>Lu]Lu-PSMA-617 [201-202]. The high energy of  $\beta^-$ -particles emitted by yttrium-90 (2.28 MeV [202]) results in high tissue penetration of up to 11 mm and metastatic lesions of 28 – 42 mm in diameter should benefit most from this increased cross-fire effect [203-204]. Accordingly, [<sup>90</sup>Y]Y-PSMA-617 has only been suggested in carefully selected patients with oligometastatic PCa and bulky lesions [202]. In contrast, optimal therapeutic efficacy of lutetium-177 (497 keV [202]) was proposed for rather small metastases of 1.2 – 3.0 mm [203] rendering <sup>177</sup>Lu-labeled PSMA inhibitors optimally suited radioligands for RLT of mCRPC, an oftentimes disseminated disease including bone and visceral metastases. Promising first patient applications of [<sup>177</sup>Lu]Lu-PSMA-617 revealed high and persistent tumor uptake while fast and efficient renal clearance occurred from off-target tissue. *Kratochwil et al.* reported biochemical response in terms of decline in serum PSA levels for 21 (70%) of 30 patients and PSA decline was  $\geq 50\%$  in 13 patients (43%). Out of 11 patients that received three RLT cycles even 73% (8 patients) presented with  $\geq 50\%$  decline in serum PSA at 24 weeks after initial treatment. After these encouraging results clinical trials were rapidly prompted and reported similar or even higher response rates (defined as  $\geq 50\%$  decline in serum PSA) of 45% [205] and 57% [206], although differences might in part be due to variations in treatment protocols. Furthermore, significant pain relief was reported by symptomatic patients and clinically meaningful improvements in quality of life were assessed [206-207]. Besides high mean tumor absorbed doses (2.80 – 4.80 Gy/GBq) [<sup>177</sup>Lu]Lu-PSMA-617 showed a favorable safety profile with highest absorbed doses to salivary glands followed by kidneys and lacrimal glands [208-211]. As a consequence of salivary gland uptake, xerostomia was among the most common adverse events, however, mild and reversible in most cases [205-206, 208]. While the kidneys as excretory organs generally represent organs at risk in RLT procedures, no acute nephrotoxicity grade 3 or higher was observed for [<sup>177</sup>Lu]Lu-PSMA-617 [205-206, 212-213]. Dosimetry studies determined mean absorbed doses of 0.39 – 0.61 Gy/GBq [209-210, 213] for the kidneys, which would, in a scenario of 4 cycles á 7.4 GBq [<sup>177</sup>Lu]Lu-PSMA-617, result in a cumulative dose between 11.5 – 18.1 Gy which is still below the generally accepted renal dose limit of 23 Gy derived from external beam radiation therapy [214]. Although clinical experience suggests that cumulative renal doses of up to 37 Gy might be tolerated in PSMA RLT [152], large inter-individual variations in kidney uptake need to be considered and underline the necessity for personalized dosimetry. In addition, as ongoing efforts in the treatment and care of PCa patients will hopefully result in prolonged survival, possible long-term side effects need to be considered and reduction of renal absorbed doses should remain a priority in clinical application

and preclinical development of PSMA radiotherapeutics. Besides salivary glands and kidneys, the red bone marrow represents an organ at risk in PSMA-targeted RLT and varying hematologic toxicity was repeatedly reported by several studies with [<sup>177</sup>Lu]Lu-PSMA-617 [205-206, 208, 215]. Besides perfusion-induced self-dose, spill-in radiation from the remainder of the body and especially nearby bone metastases can contribute with up to 50% to the effective bone marrow dose [208]. Consequently, the red bone marrow might be dose-limiting for RLT in patients with diffuse bone marrow infiltration.

[<sup>177</sup>Lu]Lu-PSMA-I&T constitutes the most important therapeutic PSMA ligand besides [<sup>177</sup>Lu]Lu-PSMA-617 and is currently evaluated in two phase 3 clinical studies ('SPLASH'-study: NCT04647526; 'ECLIPSE'-study: NCT05204927). Clinical dosimetry studies revealed widely similar tissue distribution and absorbed doses compared to [<sup>177</sup>Lu]Lu-PSMA-617 [197, 216] and *Baum et al.* reported a high biochemical response rate of 59% (defined as  $\geq 50\%$  decline in serum PSA) in a cohort of 56 patients resulting in a long progression-free survival of 13.7 months and overall survival of 79% after 28 months, indicating a potential survival benefit of RLT with [<sup>177</sup>Lu]Lu-PSMA-I&T [217]. In a recent study by *Karimzadeh* and colleagues including 301 patients, a median overall survival of 13.8 months was assessed while serum PSA levels decreased by  $\geq 50\%$  in only 34% of the patients [218]. Considering prior chemotherapy in two thirds of the patient population this apparently lower response rate is, however, well in line with previous results for [<sup>177</sup>Lu]Lu-PSMA-617 in a comparable cohort (response rate of 33%, 13 months median overall survival) which underlines the similar therapeutic efficacy of both radioligands [219].

In early 2022, a milestone in modern nuclear medicine was achieved by the regulatory approval of [<sup>177</sup>Lu]Lu-PSMA-617 (Pluvicto™) for RLT of mCRPC [220]. The approval by the Food and Drug Administration (FDA) was based on the positive results of VISION, a large international, randomized, open-label phase 3 clinical trial (NCT03511664) enrolled in 2018 [221-222]. Patients with mCRPC and PSMA-positive [<sup>68</sup>Ga]Ga-PSMA-11 PET/CT scan that had been treated with at least one androgen-receptor-pathway inhibitor and one or two taxane regimens received four to six cycles of [<sup>177</sup>Lu]Lu-PSMA-617 in addition to the best standard of care (BSOC) or BSOC alone. Image-based progression-free survival and overall survival were significantly prolonged by RLT with [<sup>177</sup>Lu]Lu-PSMA-617 (8.7 and 15.3 months, respectively) compared to the BSOC control group (3.4 and 11.3 months, respectively), thus meeting both primary endpoints of the study [221]. While the approval of [<sup>177</sup>Lu]Lu-PSMA-617 will not only lead to a broader application and improved availability of RLT for PCa patients, it might also pave the way for PSMA-targeted RLT in earlier stages of the disease and respective clinical trials are already underway (e.g. NCT04430192, NCT04343885, NCT04443062).

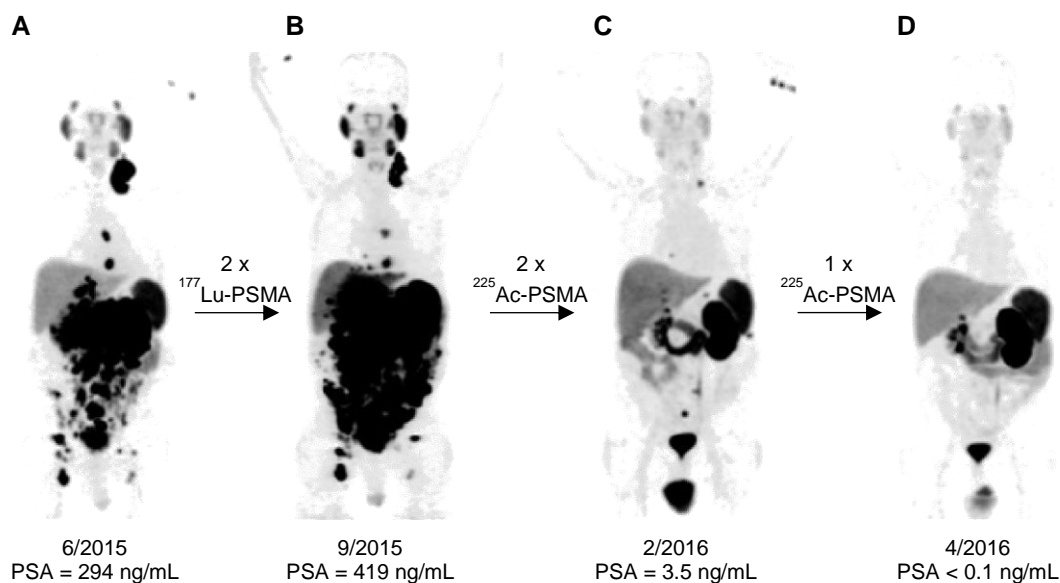


**Figure 8:** Pre-, intra- and post-therapeutic [ $^{68}\text{Ga}$ ]Ga-PSMA-11 PET scans of a mCRPC patient presenting with peritoneal carcinomatosis and liver metastases (A). After disease progression under RLT with [ $^{177}\text{Lu}$ ]Lu-PSMA-617 (B), complete biochemical and radiographic response to targeted  $\alpha$ -therapy was achieved using [ $^{225}\text{Ac}$ ]Ac-PSMA-617 (C, D). Severe radiotoxicity to the salivary glands was reported and is reflected by reduced uptake of the diagnostic tracer in the respective organs observed in scans C and D (figure adapted from Kratochwil *et al.*  $^{225}\text{Ac}$ -PSMA-617 for PSMA-Targeted  $\alpha$ -Radiation Therapy of Metastatic Castration-Resistant Prostate Cancer. *J Nucl Med.* 2016;57(12):1941-44. Copyright © 2016 SNMMI).

Despite these groundbreaking advancements in the treatment of mCRPC,  $^{177}\text{Lu}$ -based endoradiotherapy in PCa faces the severe limitation that approximately 30% of patients do not respond to the treatment [205, 208]. In that regard, targeted  $\alpha$ -therapy (TAT) has been suggested as a promising alternative. The emission energy (5 – 9 MeV) as well as the linear energy transfer (LET, ~80 – 100 keV/ $\mu\text{m}$ ) of  $\alpha$ -particles is very high which results in a dramatically increased ionization density compared to  $\beta^-$ -particles [223]. Thus, the higher number of DNA double-strand breaks induced by  $\alpha$ -particles offer the opportunity to damage much more cancer cells irreversibly already at low activity levels and mostly independent of the cell cycle state and hypoxic conditions [223-225]. Another distinct advantage constitutes the limited tissue penetration of  $\alpha$ -particles (50 – 100  $\mu\text{m}$ , 2 – 3 cell diameters), which might be a decisive factor in sparing the red bone marrow in patients with severe bone marrow infiltration [172, 226]. In line with these theoretic foundations, dramatic radiographic response in a patient that had progressed under  $^{177}\text{Lu}$ -based PSMA-targeted RLT was reported in an early clinical study with  $^{225}\text{Ac}$ -labeled PSMA-617 (figure 8) while another patient with severe bone marrow infiltration showed complete radiographic and biochemical response with remarkably low hematologic toxicity [172]. Further studies have since drawn a similar promising picture for PSMA-TAT in mCRPC [174, 227-230] and, besides [ $^{225}\text{Ac}$ ]Ac-PSMA-617 that entered a clinical phase 1 study in PSMA-positive PCa patients (NCT04597411), also  $^{225}\text{Ac}$ -labeled PSMA-I&T is currently evaluated for TAT of mCRPC in a phase 2 clinical trial (NCT05219500). In terms of toxicity, however, in contrast to efficiently spared bone marrow, a drawback of PSMA-TAT is constituted in severe xerostomia that arises from salivary gland uptake of  $\alpha$ -labeled PSMA-ligands.

While only mild and reversible in  $^{177}\text{Lu}$ -based RLT [205-206, 208], severe and persistent xerostomia was reported in several studies with [ $^{225}\text{Ac}$ ]Ac-PSMA-617 [172, 227, 231]. Furthermore, *Kratochwil et al.* and *Feuerecker et al.* reported 10% and even 23% of patients, respectively, that discontinued treatment due to xerostomia-related impairment in quality of life like dry mouth, loss of taste or problems with sleep and mastication [227, 231-232]. Several approaches to reduce salivary gland uptake have only shown moderate clinical efficacy to date [232] which emphasizes that intense preclinical and clinical research is mandatory to solve this eminent drawback of current PSMA radioligands. Although the exact uptake mechanism of PSMA radioligands into the salivary glands is currently unknown, the presence of L-glutamate in the urea-based PSMA binding motive seems to be a pivotal structural feature. While most efforts to circumvent salivary gland uptake by modification of the PSMA inhibitor motive were unsuccessful so far [233-235], a recent study by *Kuo et al.* showed the preclinical feasibility to efficiently target PSMA-positive tumors with thoroughly designed ligands based on L-2-aminoadipic acid instead of L-glutamate [236]. Clinical data still need to confirm these findings, however, the successful development of high affinity PSMA-ligands without L-glutamate might play an important future role in sparing the salivary glands in PSMA-TAT.

Fueled by the clinical success of PSMA-617 and PSMA-I&T, a plethora of novel urea-based small-molecule inhibitors of PSMA has been developed for therapeutic purposes throughout the last years. Preclinically, research has covered a wide range of approaches reaching from the introduction of novel chelating moieties [237-239] and innovative radionuclides [198, 240-241] to alternative binding motives [233-234, 242-243] and structural modifications altering the radioligands' pharmacokinetic profile [244-247]. The latter has mainly focused on exploiting enhanced plasma protein binding for increased therapeutic efficacy and three  $^{177}\text{Lu}$ -labeled representatives of this class of albumin-binding PSMA ligands, namely CTT1403 (NCT03822871), EB-PSMA-617 [248] and PSMA-ALB-56 [211], have been evaluated in the clinical setting. Furthermore, [ $^{177}\text{Lu}$ ]Lu-PSMA-R2 [249] was developed aiming for minimal kidney dose and a first clinical trial has recently been terminated (NCT03490838). Among the novel class of radiohybrid PSMA ligands, [ $^{177}\text{Lu}$ ]Lu-rhPSMA-7.3 was the first candidate to be clinically evaluated in an intra-patient comparative dosimetry study in 2021 by *Feuerecker et al.* and revealed similar therapeutic efficacy as established [ $^{177}\text{Lu}$ ]Lu-PSMA-I&T [250]. Finally, as a result of ongoing preclinical development, clinical studies with the optimized radiohybrid lead candidate [ $^{177}\text{Lu}$ ]Lu-rhPSMA-10.1 have recently been initiated (NCT05413850) which represents an important next step to realize the theranostic potential of the radiohybrid concept within the clinical setting.

In conclusion, within only a few years PSMA-targeted RLT has developed into a forerunner of clinically impactful developments in modern radiopharmacy and has certainly not come to an end yet. Not least, the huge dynamics in the development of PSMA-targeted radiopharmaceuticals is an impressive example on how medicinal demand and economic potential can promote collaborations between (radio)pharmaceutical companies and academia and finally foster innovation to make new therapeutic options available to PCa patients in unprecedented speed.

## Radioguided Surgery

Radioguided surgery (RGS) constitutes another therapeutic intervention in oncologic malignancies and its origins date back to the late 1940s, when *Selverstone et al.* were the first to make use of a radioactive probe ( $[^{32}\text{P}]$ phosphate) and a Geiger-Müller counter to detect and resect brain tumors during surgery <sup>[251]</sup>. This concept of radioactivity guiding the surgeon towards the precise excision of cancer-infested tissue has since been developed further and was adopted to intratumorally and systemically injected radiopharmaceuticals for various tumor entities <sup>[252-256]</sup>. With surgery still being among the most established procedures to treat localized tumors, radioguidance can provide significant benefits for surgeons and patients, such as real-time information regarding the localization of the disease, assistance in the assessment of surgical resection margins and minimized invasiveness during surgery <sup>[257]</sup>. In PCa, the concept of RGS has been experimentally introduced only a few years ago and is used at a locoregional stage of the disease in patients with primary PCa or biochemical recurrence with a few metastases limited to the pelvic lymph nodes <sup>[258-259]</sup>. After patient selection based on PSMA-PET, a  $\gamma$ -ray emitting PSMA ligand for RGS is injected, SPECT-imaging is executed to validate uptake of the tracer in PSMA-positive lesions, and surgery is performed approximately 20 – 24 h after injection <sup>[258-259]</sup>. With the help of a hand-held  $\gamma$ -probe, the surgeon can locate radioactive lesions intraoperatively within the surgical field and resect respective metastases and surrounding tissue. Successful removal can instantly be validated by *ex vivo* radioactivity measurements outside the surgical field, before immunohistochemistry is applied to cross-validate the presence of metastases in the resected specimens (figure 9). The first PSMA-targeted small-molecule inhibitor applied in RGS was  $^{111}\text{In}$ -labeled PSMA-I&T <sup>[258, 260]</sup>. Promising results were obtained in a small cohort of patients, however,  $^{111}\text{In}$ -labeled tracers suffer from logistical drawbacks for routine clinical application such as restricted availability of  $[^{111}\text{In}]\text{InCl}_3$  and considerable radiation exposure <sup>[259]</sup>. In contrast, technetium-99m represents an optimal radionuclide for RGS because of superior physical properties ( $t_{1/2} = 6.01$  h;  $E_\gamma = 141$  keV), ease of accessibility by  $^{99}\text{Mo}/^{99\text{m}}\text{Tc}$ -generators and the long history of established  $^{99\text{m}}\text{Tc}$ -based procedures in nuclear medicine <sup>[261-262]</sup>. Therefore, the development of a  $^{99\text{m}}\text{Tc}$ -labeled probe for PSMA-targeted RGS was envisioned by the radiopharmaceutical research group at the Technical University of Munich and resulted in the introduction of  $[^{99\text{m}}\text{Tc}]\text{Tc-PSMA-I\&S}$  (figure 10) to clinical application in 2015 <sup>[263]</sup>. Positive results in terms of high sensitivity (84%), accuracy (93%) and specificity (100%) were presented by *Maurer et al.* for a cohort of 31 patients with biochemical recurrence after primary RP and the authors reported promising short-term outcomes like complete biochemical response in 67% of the study population which was persisting in 43% after a median follow-up of 13.8 months <sup>[259]</sup>. Interestingly, even additional metastases as small as 3 mm that had not been observed on prior PET scans were successfully removed in RGS with  $[^{99\text{m}}\text{Tc}]\text{Tc-PSMA-I\&S}$  <sup>[259]</sup>. This observation is in line with earlier experiences with  $[^{111}\text{In}]\text{In-PSMA-I\&T}$  and highlights the potential of PSMA-targeted RGS for the treatment of locoregional PCa <sup>[258]</sup>. In a similar fashion, *Horn et al.* reported the successful removal of lesions in 120 of 121 patients using  $[^{99\text{m}}\text{Tc}]\text{Tc-PSMA-I\&S}$  and a complete biochemical

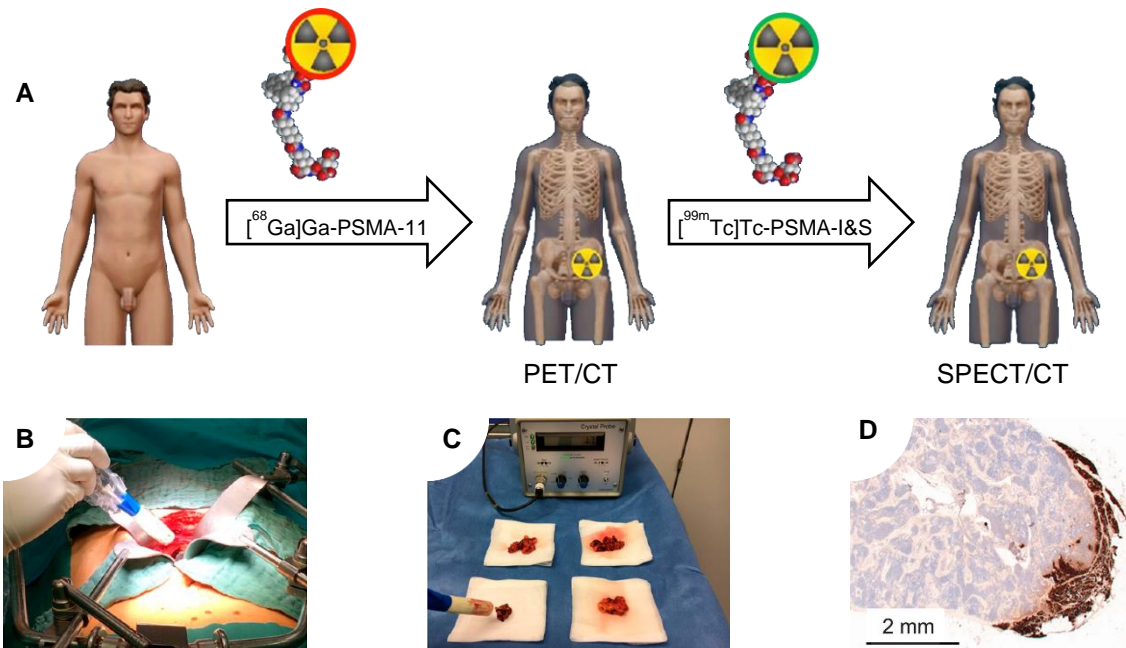


**Figure 9:** Principle of radioguided surgery (RGS). **A)** Patients are initially stratified by PET/CT-imaging using  $[^{68}\text{Ga}]\text{Ga-PSMA-11}$ . Patients eligible for RGS receive an injection of  $[^{99\text{m}}\text{Tc}]\text{Tc-PSMA-I\&S}$  approximately 20-24h prior to RGS and uptake in metastatic lesions is verified using SPECT/CT-imaging. **B)** A handheld  $\gamma$ -probe is applied to localize metastatic lesions intraoperatively. **C)** Outside the surgical field, PSMA-positivity in resected tissue samples can instantly be verified by *ex vivo* activity measurements. **D)** Histopathology of resected tissue specimens is used for final identification of metastatic lesions (figure A adapted from Maurer *et al.*  $^{99\text{m}}\text{Tc}$ -based Prostate-specific Membrane Antigen–radioguided Surgery in Recurrent Prostate Cancer. *Eur Urol.* 2019;75(4):659-666. Copyright © 2018 European Association of Urology. Figures B and C reproduced from Eiber *et al.* Prostate-Specific Membrane Antigen Ligands for Imaging and Therapy. *J Nucl Med.* 2017;58(S2):67S-76S. Copyright © 2017 SNMMI. Figure D reproduced from Maurer *et al.* Prostate-specific Membrane Antigen–radioguided Surgery for Metastatic Lymph Nodes in Prostate Cancer. *Eur Urol.* 2015;68(3):530-534. Copyright © 2015 European Association of Urology).

response was observed in 66% of the study population <sup>[264]</sup>. The authors concluded that RGS delays disease progression in patients with recurrent PCa after RP and best response was observed for patients that presented with low preoperative PSA levels and a single lesion on PSMA-PET. Furthermore, a first prospective clinical study reported by Knipper *et al.* compared conventional sentinel lymph node dissection (sLND) with PSMA radioguided sLND in a small cohort of 42 PCa patients with limited lymph node only recurrence <sup>[265]</sup>. The study assessed significantly improved metastases-yield and biochemical response six weeks after surgery for the radioguided approach, however larger studies such as TRACE (NCT03857113) are needed to reliably determine the added value of PSMA-targeted radioguidance to sLND in recurrent PCa.

The main limitation of PSMA-targeted RGS currently lies in the insufficient sensitivity for micrometastatic disease as small subcentimeter lesions that are missed during surgery can lead to early disease progression and further metastatic spread. Several technological advancements in the field of (radioguided) surgery such as robot-assisted laparoscopic procedures <sup>[266-267]</sup> as well as laparoscopy-compatible drop-in or click-on  $\gamma$ -probes <sup>[268-270]</sup> can certainly help to ameliorate lesion detection with minimal surgical invasiveness. However, the detection of micrometastatic lesions

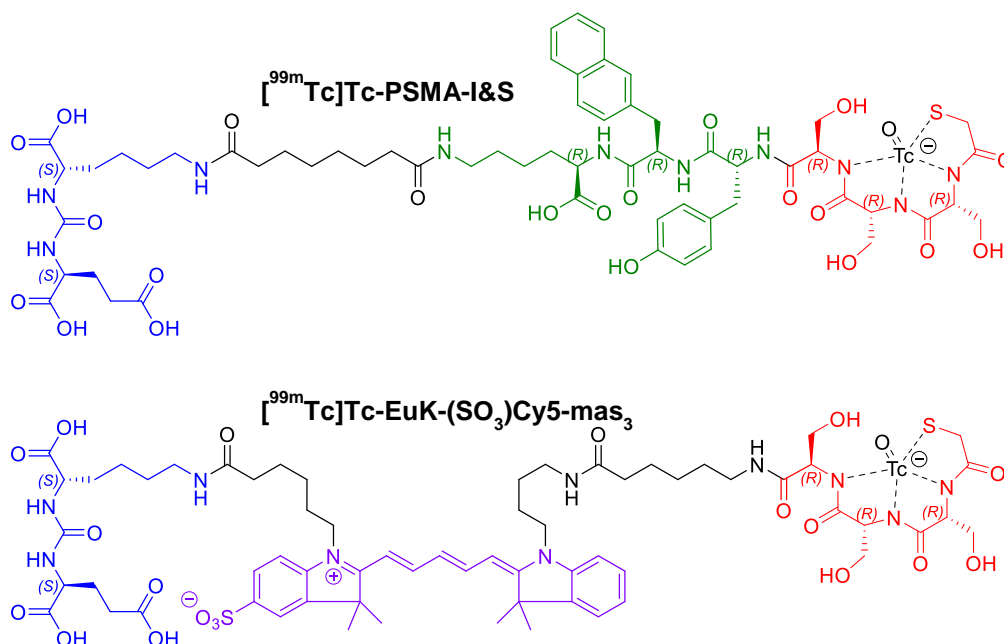


**Figure 10:** Structure of [ $^{99m}\text{Tc}$ ]Tc-PSMA-I&S (upper row) for RGS and hybrid tracer [ $^{99m}\text{Tc}$ ]Tc-EuK-(SO<sub>3</sub>)Cy5-mas<sub>3</sub> (bottom row) for radio- and fluorescence-guidance. Both tracers share the common glutamate-urea-based PSMA binding motive (blue) and a mas<sub>3</sub>-chelator (red). The linker of PSMA-I&S contains lipophilic amino acids (green) for optimal target interaction while a SO<sub>3</sub>-substituted Cy5 fluorescent dye (purple) is incorporated in EuK-(SO<sub>3</sub>)Cy5-mas<sub>3</sub> to facilitate fluorescence-guidance.

primarily requires sufficient signal-to-background contrast which, in term, is fundamentally governed by the PK of the applied radioligand. Generally applied [ $^{99m}\text{Tc}$ ]Tc-PSMA-I&S shows relatively slow whole body clearance with a significant hepatobiliary contribution, thus, incomplete clearance from background tissue at the time of surgery might be a highly relevant factor possibly concealing small metastatic lesions. As a potential alternative [ $^{99m}\text{Tc}$ ]Tc-MIP-1404, a tracer originally developed for SPECT-imaging, has recently been successfully applied for PSMA-targeted RGS in nine patients [271]. Valid comparison with [ $^{99m}\text{Tc}$ ]Tc-PSMA-I&S requires larger patient cohorts and well-defined study criteria, however, based on the reported results and data from literature it is highly questionable if [ $^{99m}\text{Tc}$ ]Tc-MIP-1404 can overcome the limited sensitivity of [ $^{99m}\text{Tc}$ ]Tc-PSMA-I&S in micrometastatic disease due to its similar dosimetry and likewise slow clearance kinetics [263, 272-273]. Next-generation  $^{99m}\text{Tc}$ -labeled PSMA ligands with a pharmacokinetic profile optimized for RGS application thus represent a meaningful task for radiopharmaceutical development, especially as no dedicated optimization of a  $^{99m}\text{Tc}$ -labeled PSMA ligand tailored specifically for RGS application has been reported since the introduction of [ $^{99m}\text{Tc}$ ]Tc-PSMA-I&S. Instead, research within the field of PSMA-guided surgery of PCa has lately concentrated on the development of hybrid tracers. Beyond radioactivity detection with a  $\gamma$ -probe, these radioligands enable fluorescence imaging as an additional intraoperative imaging method by means of a fluorescent dye incorporated into the molecular structure of the ligand. Fluorescence-guidance during open-field or robot-assisted surgery bears the distinct advantage that an instant visual feedback helps the surgeon to ensure negative surgical margins during the resection of malignant tissue. Fluorescence-guidance alone, however, comes with the inherent drawback of limited

tissue penetration which hampers the detection of obscure or atypically localized lesions <sup>[274-275]</sup>. In that regard, the combined advantages of hybrid radioligands providing  $\gamma$ -radiation with deep tissue penetration for sensitive lesion detection and fluorescence-based real-time visual information for thorough resection renders hybrid tracers a concept of great potential for the evolution of imaging-guided surgery <sup>[276]</sup>. Several hybrid PSMA-targeted tracers have been reported to date and combine fluorescent dyes like IRDye800CW, Cy5-derivatives or FITC with the radioisotopes fluorine-18, gallium-68 or technetium-99m <sup>[130, 277-280]</sup>. While most hybrid tracers have been only explored in the preclinical setting, first clinical experience was made with <sup>18</sup>F-labeled BF<sub>3</sub>-Cy3-ACUPA and <sup>68</sup>Ga-labeled PSMA-914 <sup>[279, 281]</sup>. Due to their radionuclides' short half-life, however, surgery of PCa patients was executed only supported by fluorescence-guidance and in case of PSMA-914 preoperative PET-imaging and intraoperative fluorescence-guidance required two separate tracer injections. Therefore, the theoretical potential to enable radio- and fluorescence-guidance by a single injection of a hybrid radioligand is currently still an unachieved goal. Another promising hybrid PSMA-ligand is <sup>99m</sup>Tc-labeled EuK-(SO<sub>3</sub>)Cy5-mas<sub>3</sub> (figure 10) <sup>[278]</sup>. Preclinical studies revealed favorable targeting characteristics and biodistribution in mice and *Dell'Oglio et al.* recently reported the feasibility of fluorescence-guidance with the unlabeled compound in a porcine model using a microdosing regimen <sup>[282]</sup>. Due to the suitable radioactive half-life of [<sup>99m</sup>Tc]Tc-EuK-(SO<sub>3</sub>)Cy5-mas<sub>3</sub> this tracer might possibly meet the criteria for simultaneous radio- and fluorescence-guidance in a surgical setting, however, future clinical studies in PCa patients are needed to corroborate this assumption and explore whether the promising preclinical results can be transferred to the human situation.

While RGS has already exerted remarkable impact on the clinical management of PCa patients, the application of hybrid tracers for PSMA-targeted surgery is currently still in its infancy. Nonetheless, from a radiopharmaceutical perspective both approaches share the same fate in terms of their future impact on patient care, namely that exploiting the whole potential of these surgical procedures for the benefit of PCa patients will depend to a great extent on the successful development of next-generation radiopharmaceuticals with thoroughly optimized PK.

## 1.4. Optimization of Pharmacokinetics of PSMA Radioligands

### Pharmacokinetic Considerations for Therapeutic Applications

Besides efficient target interaction and the therapeutic mode of action, the pharmacokinetic behavior represents a pivotal aspect for the therapeutic performance of systemically applied drugs such as radiopharmaceuticals. The PK of a drug is often described within the ADME concept which focusses on the pharmaceutical's absorption, distribution, metabolism and excretion [283-284]. Small-molecule peptidic radioligands are generally applied by intravenous injection, thus, instant absorption to the vascular system is inherently realized by this route of drug administration. In contrast, the distribution of radiopharmaceuticals can vary greatly, for example due to structure-specific plasma protein binding properties. Furthermore, the lipophilicity of a radioligand shapes its distribution profile (e.g. via the extent of hepatic uptake) and significantly influences whether excretion occurs via the preferred renal pathway or (in part) via the hepatobiliary route. Metabolism represents a critical aspect for both target binding and excretion of radiopharmaceuticals [285-286]. In contrast to linear polypeptidic ligands (targeting e.g. gastrin-releasing peptide receptor or cholecystokinin-2 receptor) that can be prone to endogenous peptidases [287-289], state-of-the-art PSMA-ligands are usually composed of a stable glutamate-urea binding motive, common radiometal complexes with established chelators and a linker region that oftentimes contains unnatural building blocks or D-configured amino acids. These structural features usually confer high metabolic stability to the entire ligand. Therefore, the main focus in optimizing the PK of PSMA-radioligands lies in structure-related fine-tuning of their distribution- and excretion-driven clearance kinetics as the latter substantially shapes the absorbed dose ratios between tumor and healthy tissue.

In that regard, specific requirements towards a radioligand are closely tied to the intended clinical application. PET- and SPECT-imaging rely on high contrast at early time points realized by preferably high initial lesion uptake followed by rapid systemic clearance via the renal pathway. Also in RLT efficient renal clearance from healthy tissue is paramount to ensure low radiotoxic side effects [213, 217, 290]. Simultaneously however, a slightly decelerated clearance as compared to diagnostic tracers is envisioned to prolong the tracer's availability for target binding and thus to maximize the therapeutic dose to cancerous lesions. Requirements for RGS application basically resemble those for diagnostic tracers, however, maximal contrast is to be achieved at a later time point suitable for the half-life of the applied radionuclide and complying with logistic considerations of the surgical procedure. While seeming only marginally different on a theoretical level, the aforementioned pharmacokinetic requirements need to be optimally met for each specific application to open up the full clinical potential of PSMA-targeted radiopharmaceuticals for PCa patients.

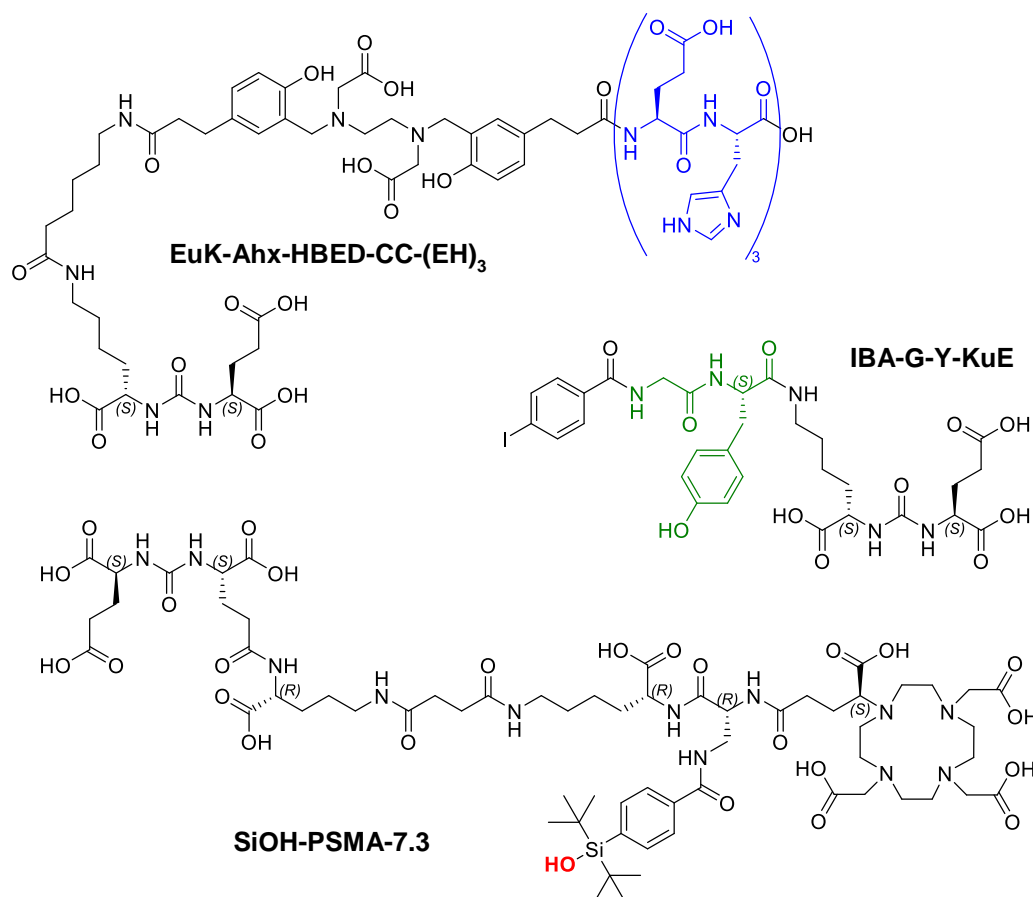


**Figure 11:** Examples of PSMA ligands incorporating distinct structural modifications to alter their pharmacokinetic profile. A repeat of glutamyl-histidine (blue) in EuK-Ahx-HBED-CC-(EH)<sub>3</sub> leads to reduced renal and hepatic uptake of the <sup>68</sup>Ga-labeled radioligand in mice. An enzyme-cleavable glycyl-tyrosine sequence (green) in IBA-G-Y-KuE aims for reduced kidney uptake by metabolic cleavage in the proximal tubule. The hydroxyl functionality (red) in SiOH-PSMA-7.3 replacing the corresponding fluoride in the analog radiohybrid compound leads to accelerated clearance and an increased tumor-to-kidney ratio of the <sup>177</sup>Lu-labeled radioligand in mice.

### PK-related Structural Developments in PSMA Radioligands

On the level of radiopharmaceutical structure development, different approaches have been explored to shape the PK of PSMA radioligands aiming for a distribution profile optimally tailored for the intended clinical application (selected structural examples are depicted in figure 11). For instance, a potentially nephroprotective approach was pursued by several groups by insertion of a peptidic sequence such as glycyl-lysine (GK) [291], glycyl-tyrosine (GY) [292] or methionyl-valyl-lysine (MVK) [293] which can be cleaved by brush border enzymes found on the membrane of proximal tubules in the kidney [294-295]. The cleavable sequence is either located in proximity to the PSMA-binding motive to create radiometabolites without PSMA affinity to lower PSMA-mediated kidney-uptake or adjacent to the radiochelate to create hydrophilic, fast-clearing radiometabolites. Preclinical studies of these kidney-cleavable PSMA ligands could in part show reduced kidney uptake, however, superiority over conventional ligands was not

achieved due to simultaneously reduced tumor uptake <sup>[292-293, 296]</sup> thus preventing this approach from clinical translation.

Besides this rather sophisticated concept of targeted metabolic instability, various ways of conventional structure modifications have been examined and exhibited similarly complex and delicate effects on the PK of PSMA-targeted radioligands. For instance, *Eder et al.* inserted a glutamyl-histidine repeat (EH<sub>3</sub>) into the structure of the imaging agent PSMA-11 and found unaltered high tumor uptake but significantly reduced renal and hepatic uptake in a murine xenograft model <sup>[297]</sup>. Such effects sparing excretory organs from excessive radiation exposure might be of particular interest for the design of therapeutic radioligands. Further studies on this amino acid based pharmacokinetic modifier led to the development of PSMA-914, a hybrid tracer that has recently entered the stage of early clinical evaluation <sup>[280-281, 298]</sup>. More subtle but likewise impactful structure modifications can be implemented by insertion or substitution of functional groups within the scaffold of a lead compound, as demonstrated with a series of Cy5-containing PSMA ligands by *Hensbergen et al.* Decoration of the linker-embedded fluorophore with either an aryl or sulphonate functionality lead to markedly altered blood clearance and excretion profiles depending on the type and localization of the functional group <sup>[278]</sup>. An even smaller functional modification implemented by *Wurzer et al.*, namely the substitution of fluoride in therapeutic rhPSMA ligands by a hydroxyl functionality (SiOH-PSMA), was reported to accelerate renal clearance by means of reduced plasma protein binding and increase tumor-to-kidney ratios of SiOH-PSMA ligands in preclinical studies <sup>[299]</sup>. As the kidney is still considered a major organ at risk in RLT of PCa these SiOH-PSMA ligands might represent valuable options for reducing the cumulative renal absorbed dose for multiple RLT cycles. A final example impressively depicting the immense influence of structural modifications on the PK of PSMA radioligands is the differential uptake analysis of [<sup>18</sup>F]Ga-rhPSMA-7 executed at the Technical University of Munich <sup>[183]</sup>. The radioligand, composed of four diastereomers differing in only two stereocenters, was injected in LNCaP tumor-bearing mice and a radio-HPLC-based organ analysis revealed significant differences in tracer uptake and excretion patterns between the single isomers. As compared to the isomers' abundance in the injected solution, uptake of D-Dap containing isomers [<sup>18</sup>F]Ga-rhPSMA-7.1 and [<sup>18</sup>F]Ga-rhPSMA-7.3 in blood, kidneys, liver and tumor were found to be consistently elevated by around 5-13%, while the remaining isomers showed correspondingly reduced differential uptake <sup>[183]</sup>. These reproducible differences originating only from an altered stereochemistry impressively underline how delicate and subtle the response of a radioligand's PK is even towards minuscule structure modifications. In consequence, a dedicated and meticulous structure optimization of PSMA radioligands for every therapeutic application is mandatory to ensure optimal clinical performance and benefit for PCa patients.

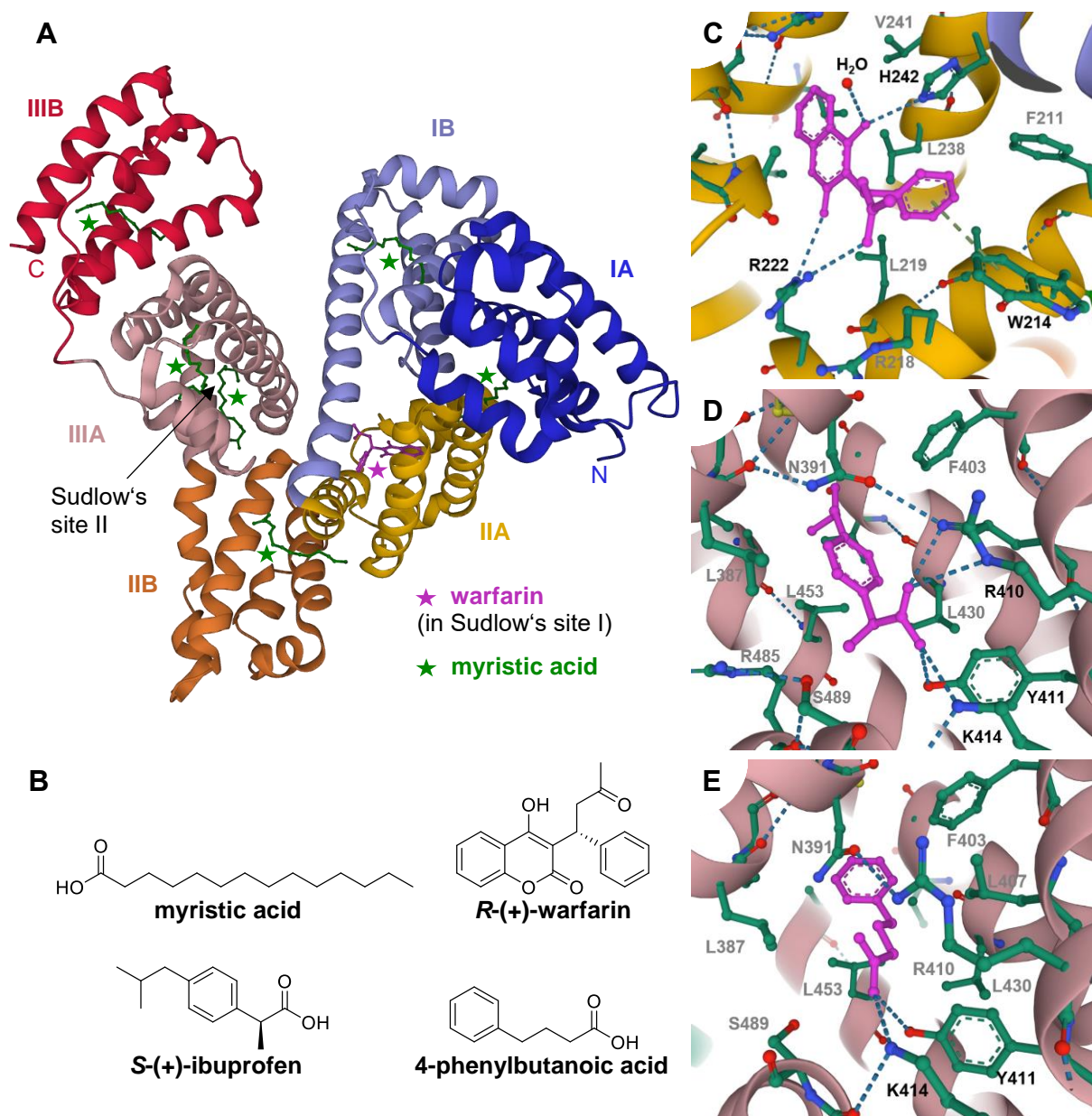


**Figure 12:** **A**) Crystal structure of human serum albumin (HSA) complexed with myristic acid and *R*-(+)-warfarin (Protein Data Base (PDB) ID: 1H9Z; doi: 10.2210/pdb1H9Z/pdb). Subdomains are indicated by color code: subdomain IA: dark blue; subdomain IB: pale blue; subdomain IIA: yellow; subdomain IIB: orange; subdomain IIIA: rose; subdomain IIIB: red. Green stars indicate the location of six myristic acid molecules in fatty acid binding sites (FA) 1-6 of HSA. The pink star indicates Sudlow's site I occupied by *R*-(+)-warfarin (pink stick representation) with the latter impeding the binding of another myristic acid molecule to FA7. Sudlow's site II is indicated with an arrow and overlaps with FA3 and FA4. **B**) Chemical structures of some HSA-binding compounds. Their site of binding is represented in panels A and C-E. **C**) Orientation of *R*-(+)-warfarin (pink stick representation) in Sudlow's site I (PDB ID: 1H9Z). Major interactions are H-bonds (blue dotted lines) of oxo-groups with arginine (R222) and histidine (H242) residues and a water molecule as well as  $\pi$ -interactions (green dotted lines) with a tryptophan (W214) residue. **D**) Orientation of *S*-(+)-ibuprofen (pink stick representation) in Sudlow's site II (PDB ID: 2BXG; doi: 10.2210/pdb2BXG/pdb). The aromatic portion is located in an apolar pocket and the carboxylate is oriented towards a polar patch formed by residues of arginine (R410), tyrosine (Y411) and lysine (K414). **E**) Orientation of 4-phenylbutanoic acid (pink stick representation) in Sudlow's site II (PDB ID: 5YOQ; doi: 10.2210/pdb5YOQ/pdb). In analogy to ibuprofen the molecule's aromatic portion covers a hydrophobic pocket while amino acid residues of the polar patch (predominantly Y411 and K414) coordinate the carboxylate.

### Albumin Binding of PSMA Radioligands

Besides the aforementioned concepts, binding to human serum albumin (HSA) represents another approach to modify the PK of therapeutic PSMA radioligands and has gained tremendous influence within the last decade. HSA is a non-glycosylated, 66.5 kDa monomeric, allosteric plasma protein composed of 585 AA [300-302]. With a concentration of about 700  $\mu\text{M}$  HSA represents the most abundant human plasma protein and accounts for approximately 60% of the total plasma protein amount [300-301]. Apart from its key role in regulating colloidal osmotic pressure and the plasma's antioxidant capacity, HSA acts as the most important carrier protein and depot for a wide variety of endogenous compounds such as fatty acids, heme or thyroxine and xenobiotics like drugs and contaminants [300-302]. Structure analysis revealed HSA to be composed of three homologous domains (I, II and III), each of them divided into two helical subdomains (A and B, see figure 12A) [303]. Apart from seven binding sites for fatty acids (FA1-7), two primary high-affinity binding sites that play a crucial role in the transport of a variety of drugs have been identified: Sudlow's site I in subdomain IIA overlaps with FA7 and binds bulky heterocyclic anions with warfarin as a stereotypical representative [300, 304-305]. Sudlow's site II that overlaps with FA3 and FA4 is located in subdomain IIIA and binds aromatic anionic structures such as ibuprofen or benzodiazepines like diazepam [300, 303]. It is of particular interest and of pharmacologic relevance that both binding sites show sufficient flexibility to bind a scope of structurally different small molecule drugs yet binding remains specific and of high affinity (exemplified for Sudlow's site II in figure 12 D+E) [303]. With the aim of enhancing the circulatory half-life and thus the availability of otherwise rapidly excreted drugs, many efforts have been made to structurally understand and exploit the binding capacity of the various binding sites of HSA [303, 305-307]. Recently, *Dumelin et al.* reported a series of 4-phenylbutanoic acid derivatives that potently bind HSA in Sudlow's site II [308]. After the utility of the most potent derivative *p*-iodo-4-phenylbutanoic acid (IPA) was initially explored in long-acting magnetic resonance imaging contrast agents, fluorescein derivatives and antibody fragments [308-309], it was later on also applied in radiopharmaceuticals against manifold targets to alter their pharmacokinetic profile towards enhanced tumor uptake or increased tumor-to-kidney ratios [310-313].

Regarding PSMA-targeted radiotherapeutics, multiple efforts have been made to raise the therapeutic efficacy of novel albumin-binding ligands above clinically established PSMA-617 and PSMA-I&T (selected ligands are depicted in figure 13). *Benesova et al.* were among the first to develop IPA-modified derivatives of PSMA-617 and reported reasonable hydrophilicity and promising targeting characteristics showing the feasibility to incorporate small albumin-binding moieties into the scaffold of theranostic PSMA ligands [314]. Impressive tumor uptake of the  $^{177}\text{Lu}$ -labeled compounds of up to 80% iD/g confirmed the hypothesized beneficial effect of enhanced albumin binding in a PC3-Pip xenograft model. However, simultaneously increased kidney retention and dramatically prolonged blood retention of the novel radioligands lead to an overall inferior estimated dose ratio between tumor and blood, kidneys and liver, respectively [314]. Especially in mCRPC patients with severe bone marrow infiltration, prolonged blood circulation can eventually render the radiation exposure of the red bone

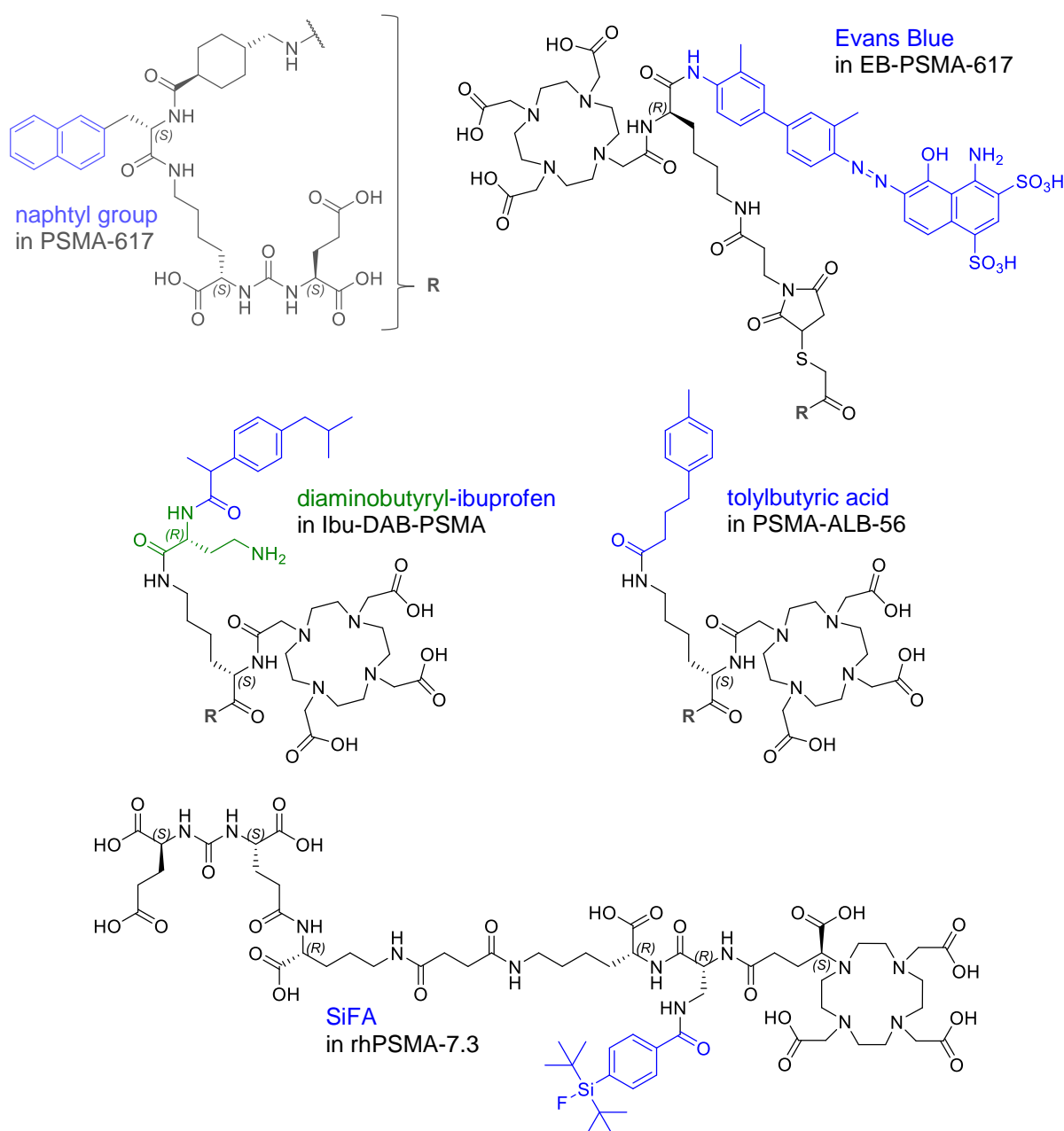


**Figure 13:** Chemical structures of selected HSA-binding PSMA-ligands with moieties conferring plasma protein binding properties highlighted in blue. Multiple compounds were derived from PSMA-617 by insertion of an albumin-binding motive between EuK-2-Nal-Thx (abbreviated as **R**) and the chelating moiety. EB-PSMA-617 and PSMA-ALB-56 contain the strong albumin-binding motives Evans Blue and 4-(*p*-tolyl)butanoic acid, respectively. Ibu-DAB-PSMA contains an altered linker structure (depicted in green) to modulate the effective albumin binding capacity of ibuprofen. The SiFA-group in rhPSMA-7.3 serves labeling with fluorine-18 and enhances PSMA affinity. Its lipophilic character, however, also endows significant plasma protein binding to the entire ligand. In a similar fashion, the naphthyl-group in PSMA-617 primarily serves enhanced target interactions but also confers moderate plasma protein binding to this rather fast clearing compound.

marrow dose-limiting. Therefore, in a next development step, the apparently excessive albumin-binding capacity of IPA was accounted for by the introduction of the less potent 4-(*p*-tolyl)butanoic acid moiety and the resulting compound [ $^{177}\text{Lu}$ ]Lu-PSMA-ALB-56 exhibited a superior pharmacokinetic profile with less pronounced blood retention compared to its IPA-derived analog [ $^{177}\text{Lu}$ ]Lu-PSMA-617 [247]. Encouraged by extraordinary tumor uptake even exceeding 100% iD/g after 24 h and promising results of a preclinical

therapy study, [<sup>177</sup>Lu]Lu-PSMA-ALB-56 was evaluated in a clinical study in mCRPC patients<sup>[211]</sup>. Despite approximately 2-fold increased tumor dose and similar uptake in salivary glands as compared to [<sup>177</sup>Lu]Lu-PSMA-617 and [<sup>177</sup>Lu]Lu-PSMA-I&T<sup>[210, 213, 217]</sup>, the therapeutic efficacy of [<sup>177</sup>Lu]Lu-PSMA-ALB-56 was hampered by unfavorably slow clearance kinetics and increased kidney retention. The latter was increased around 3- to 6-fold<sup>[209, 217]</sup> and an up to 8-fold increased dose to the red bone marrow was determined (comparison with *Delker et al.*<sup>[210]</sup> and *Baum et al.*<sup>[217]</sup> based on a red marrow-to-blood activity concentration ratio (RMBLR) of 1.0). Consequently, the authors identified the red bone marrow as dose limiting organ and the tumor dose at maximum injectable activity was calculated to be significantly lower than for [<sup>177</sup>Lu]Lu-PSMA-617 or [<sup>177</sup>Lu]Lu-PSMA-I&T<sup>[211]</sup>. In a similar fashion, hopes arisen upon promising preclinical data were also disappointed in the case of [<sup>177</sup>Lu]Lu-EB-PSMA-617, a PSMA ligand decorated with the strong albumin-binding motive Evans Blue<sup>[246]</sup>. A clinical study in mCRPC patients revealed even 3.0-fold increased tumor dose as compared to [<sup>177</sup>Lu]Lu-PSMA-617, however, the radiation dose to critical organs such as kidneys, liver, red marrow and salivary glands were elevated by a factor of 6.0, 5.7, 6.5 and 5.1, respectively<sup>[248]</sup>. In conclusion of the aforementioned clinical data and taken together with the fact that even state-of-the-art PSMA ligands without dedicated HSA-binding motives in part show considerable amount of plasma protein binding that shapes their overall PK<sup>[314-316]</sup>, it can be questioned if the incorporation of a strong albumin-binding entity such as IPA or Evans Blue is actually beneficial at all. The current state of preclinical and clinical research rather indicates that it is not an explicitly high but a well-balanced sweet spot of albumin binding that might confer the desired PK to a PSMA ligand to improve its therapeutic efficacy. Accordingly, the approach of albumin binding shares a common fate with the diverse chemical modifications described earlier, namely that detailed and thorough structure optimizations are necessary to yield a therapeutic PSMA ligand with a pharmacokinetic profile optimally tailored for RLT application. Appropriately, several groups are already experimenting with albumin-binders of differential potency or modifications in structural vicinity of the albumin binding motive<sup>[317-321]</sup>.

In conclusion, the optimization of the PK of PSMA radioligands is of great significance due to the increasing clinical demand and potential benefit for PCa patients. Future development will need to combine current knowledge and expertise together with diligence, novel (radio)chemical approaches and innovative methodologies to dig deeper into structure optimization hopefully yielding ever improved diagnostic, therapeutic and theranostic PSMA-targeted radiopharmaceuticals against PCa.

## 2. Objectives

The work presented in this thesis aimed to develop and evaluate novel and improved PSMA-binding radiopharmaceuticals with optimized PK for various therapeutic purposes in PCa by means of dedicated chemical structure optimization, thorough preclinical evaluation and development of methodological tools.

Within the discipline of nuclear medicine, PSMA-targeted RLT with  $^{177}\text{Lu}$ -labeled peptidic radioligands constitutes the most established therapeutic intervention in mCRPC [217, 221, 322]. Recently, *Wurzer et al.* introduced a novel class of radiolabeled PSMA-inhibitors, named radiohybrid PSMA or rhPSMA [182, 184]. While the diagnostic radioligand [ $^{18}\text{F}$ ]Ga-rhPSMA-7.3 is currently evaluated in phase 3 clinical trials for the PET-imaging of PCa (NCT04186819 and NCT04186845), the radiohybrid concept bears the potential to use the  $^{177}\text{Lu}$ -complexed tracers as radiotherapeutics. Therefore, one major objective of this thesis was the thorough preclinical evaluation of novel,  $^{177}\text{Lu}$ -labeled therapeutic rhPSMA compounds and the selection of a lead candidate for further clinical development.

Within the preclinical development process, assessment of plasma protein binding and, in particular, binding to HSA has recently gained increased attention as it constitutes a crucial molecular property that shapes the PK and therefore the therapeutic efficacy of PSMA radioligands. The preclinical selection of a therapeutic PSMA ligand that should bear optimal pharmacokinetic properties in humans, however, does not only require the knowledge of the quantitative extent of plasma protein binding (e.g. percent plasma bound ligand/free ligand) as conventionally determined via ultrafiltration experiments or chromatography-based studies [323-325]. A more effective way to preclinically select an optimal candidate should include the comparison of the expected blood clearance kinetics of tracers based on the ligands' HSA-binding. Such an approach could effectively bridge the gap between the current preclinical selection process and the corresponding PK subsequently assessed in clinical studies. The development of a novel methodology that might allow a more accurate selection of a promising next generation candidate already at the preclinical stage constituted another core objective of this thesis.

Furthermore, RGS represents a promising therapeutic intervention already at an early stage of primary or recurrent PCa that can significantly delay disease progression and metastatic spread [264]. However, despite promising results obtained in several studies [259, 264-265], increasing the sensitivity towards micrometastatic lesions remains a challenge in the execution of RGS with  $^{99\text{m}}\text{Tc}$ -labeled PSMA-I&S, a radioligand with rather slow whole-body clearance. Increased tumor-to-background ratios by means of optimized PK of the applied radioligand might help to detect even small metastatic lesions with higher sensitivity. Therefore next-generation  $^{99\text{m}}\text{Tc}$ -labeled PSMA ligands were developed in the course of this thesis with the goal to provide optimized radiolabeled probes for RGS of PCa.

### 3. Results - Publications

In this chapter the published work incorporated into this thesis is briefly summarized. The original articles and reprint permissions are attached in chapter 6. Appendix.

#### 3.1. Synthesis and Preclinical Evaluation of $^{177}\text{Lu}$ -labeled Radiohybrid PSMA Ligands for Endoradiotherapy of Prostate Cancer

Alexander Wurzer<sup>#1</sup>, **Jan-Philip Kunert<sup>#1</sup>**, Sebastian Fischer<sup>1</sup>, Veronika Felber<sup>1</sup>, Roswitha Beck<sup>1</sup>, Francesco de Rose<sup>2</sup>, Calogero d'Alessandria<sup>2</sup>, Wolfgang Weber<sup>2</sup> and Hans-Jürgen Wester<sup>1</sup>

<sup>1</sup> Chair of Pharmaceutical Radiochemistry, Technical University of Munich, Garching, Germany.

<sup>2</sup> Department of Nuclear Medicine, Klinikum Rechts der Isar, Technical University of Munich, Munich, Germany.

# contributed equally

*The Journal of Nuclear Medicine* **2022**, 63 (10), 1489-1495, doi: 10.2967/jnumed.121.263371.

Hyperlink: <https://jnm.snmjournals.org/content/63/10/1489>

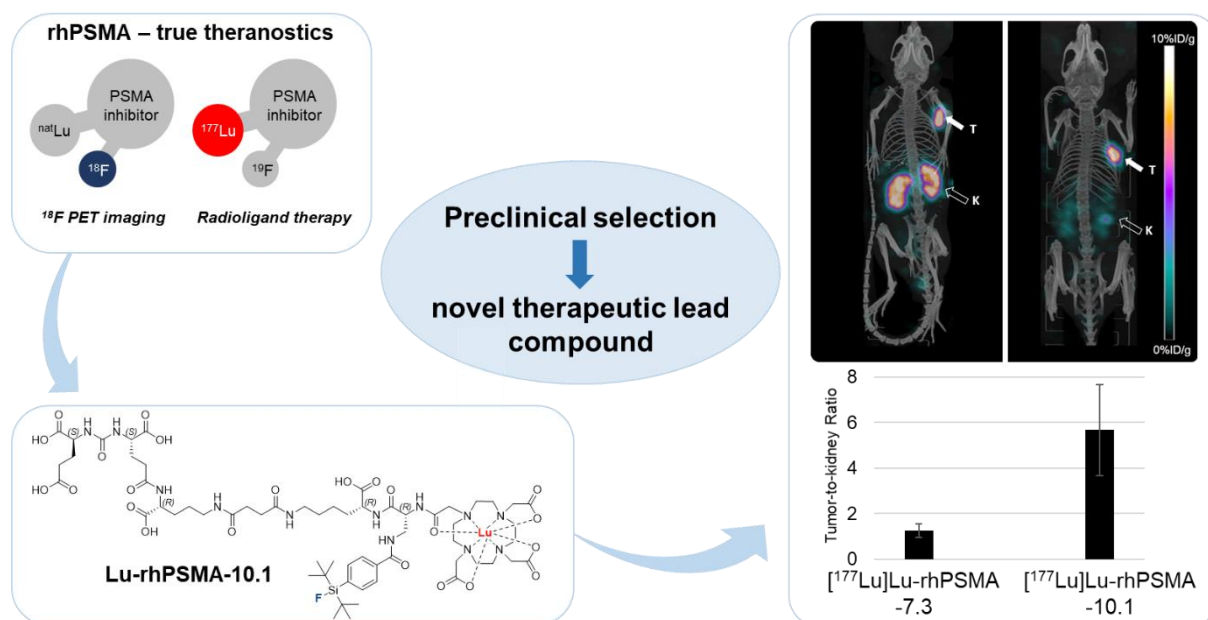


**Figure 14:** In a comparative preclinical selection process including thorough *in vitro* evaluation and *in vivo* biodistribution studies at 24 h p.i. among a group of six theranostic  $^{177}\text{Lu}$ -labeled rhPSMA ligands,  $^{177}\text{Lu}$ Lu-rhPSMA-10.1 was identified as therapeutic lead compound.  $^{177}\text{Lu}$ Lu-rhPSMA-10.1 exhibits an improved pharmacokinetic profile compared to  $^{177}\text{Lu}$ Lu-rhPSMA-7.3, e.g. low blood retention and increased tumor-to-kidney ratio. Figure reproduced with the permission of the publisher. © 2022 by the Society of Nuclear Medicine and Molecular Imaging, Inc.

In a recent preclinical study the diagnostic radioligand [ $^{18}\text{F}$ ]Ga-rhPSMA-7.3, an isomer of racemic [ $^{18}\text{F}$ ]Ga-rhPSMA-7, has been identified as the isomer with most favorable pharmacokinetics for PET-imaging<sup>[183]</sup>. In addition, when compared to racemic [ $^{18}\text{F}$ ]Ga-rhPSMA-7, a superior biodistribution profile in PET-imaging of mCRPC patients was reported for [ $^{18}\text{F}$ ]Ga-rhPSMA-7.3<sup>[326]</sup>. In a pretherapeutic comparative dosimetry study, its therapeutic equivalent, [ $^{177}\text{Lu}$ ]Lu-rhPSMA-7.3, has shown comparable therapeutic efficacy as the established radioligand [ $^{177}\text{Lu}$ ]Lu-PSMA-I&T<sup>[250]</sup>. As opposed to diagnostic radioligands, distinct pharmacokinetic characteristics, like slightly decelerated clearance kinetics and low kidney retention are required for therapeutic radioligands. Thus, rhPSMA-7.3 might not necessarily be the most favorable rhPSMA compound for RLT. The aim of the present study was to identify the most promising compound for therapeutic application among the four isomers of [ $^{177}\text{Lu}$ ]Lu-rhPSMA-7 (-7.1, -7.2, -7.3 and -7.4) and the two isomers of [ $^{177}\text{Lu}$ ]Lu-rhPSMA-10 (-10.1 and -10.2).

The six therapeutic radioligands were preclinically evaluated along with the established reference compounds [ $^{177}\text{Lu}$ ]Lu-PSMA-617 and [ $^{177}\text{Lu}$ ]Lu-PSMA-I&T. The radiohybrid ligands commonly exhibited potent PSMA-affinity in the low nM range, high internalization and low lipophilicity. Significant differences were observed in the apparent molecular weights ( $MW_{\text{app}}$ ) of rhPSMA radioligands that were persistently higher than for the references but differed considerably among the radiohybrid isomers indicating differential albumin-binding properties. *In vivo* biodistribution studies in LNCaP xenograft-bearing mice at 24 h p.i. revealed similar distribution patterns of rhPSMA compounds with high tumor uptake (12.7 – 9.8 %iD/g), efficient clearance from background tissue and variable kidney uptake ranging from  $19.7 \pm 4.5$  %iD/g for [ $^{177}\text{Lu}$ ]Lu-rhPSMA-7.2 to only  $2.0 \pm 0.8$  %iD/g for [ $^{177}\text{Lu}$ ]Lu-rhPSMA-10.1. The latter showed a similar tumor-to-kidney ratio ( $5.7 \pm 2.0$  vs  $5.9 \pm 3.0$ ) and even higher tumor uptake ( $9.8 \pm 0.3$  vs  $7.5 \pm 0.9$  %iD/g) as compared to state-of-the-art therapeutic radioligand [ $^{177}\text{Lu}$ ]Lu-PSMA-617. Furthermore, [ $^{177}\text{Lu}$ ]Lu-rhPSMA-10.1 exhibited a favorably low retention in blood ( $0.0009 \pm 0.0001$  %iD/g) resulting in the highest tumor-to-blood ratio ( $11498 \pm 1953$ ) among all evaluated radioligands.

These superior pharmacokinetic properties render [ $^{177}\text{Lu}$ ]Lu-rhPSMA-10.1 a promising candidate for therapeutic application and it was therefore selected as novel lead compound for further clinical studies (clinical phase I and II started, NCT05413850).

### **Author contribution**

The author of this thesis, Jan-Philip Kunert, shares the first authorship with Dr. Alexander Wurzer and participated in the planning and management of the study, performed radiolabelings of the evaluated compounds, determined albumin-binding properties and jointly carried out *in vivo* biodistribution studies and  $\mu\text{SPECT/CT}$ -imaging studies. He furthermore acquired and analyzed data and participated in writing and revision of the manuscript.

### 3.2. Albumin-Mediated Size Exclusion Chromatography: The Apparent Molecular Weight of PSMA Radioligands as Novel Parameter to Estimate Their Blood Clearance Kinetics

Jan-Philip Kunert<sup>1</sup>, Sebastian Fischer<sup>1</sup>, Alexander Wurzer<sup>1</sup> and Hans-Jürgen Wester<sup>1</sup>

<sup>1</sup> Chair of Pharmaceutical Radiochemistry, TUM Department of Chemistry, Technical University of Munich (TUM), 85748 Garching, Germany.

*Pharmaceuticals* **2022**, *15* (9), 1161, doi: 10.3390/ph15091161.

Hyperlink: <https://www.mdpi.com/1424-8247/15/9/1161>

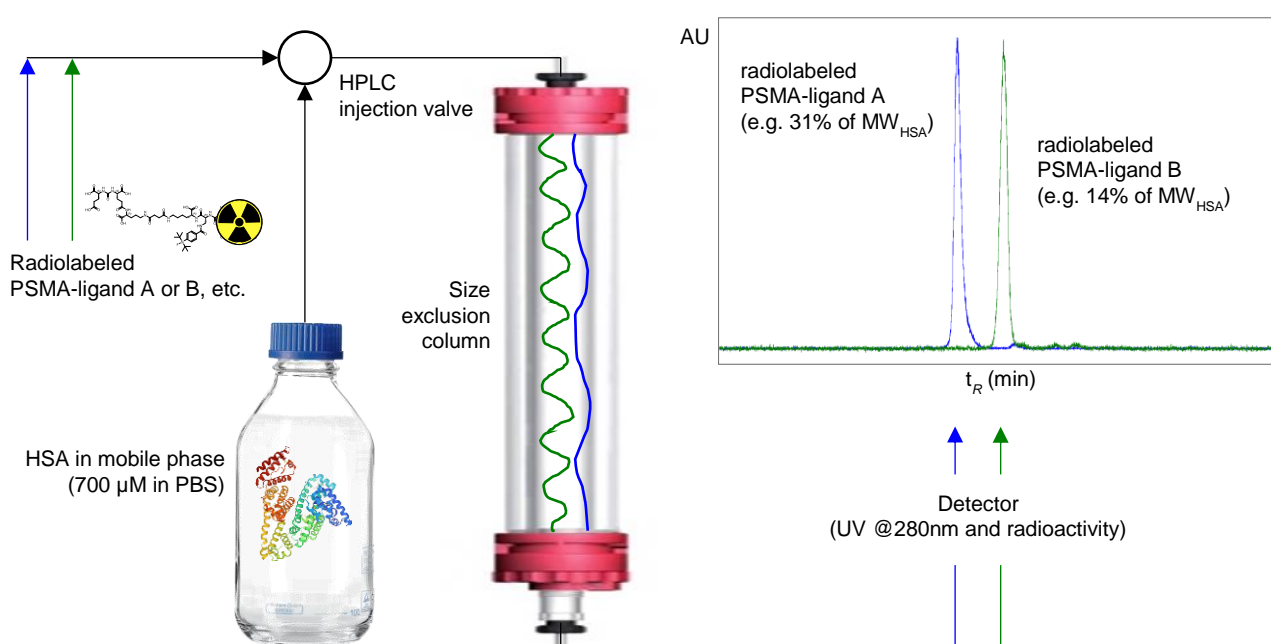


**Figure 15:** Conceptual design of ‘albumin-mediated size exclusion chromatography’ (AMSEC). A size exclusion column is equilibrated with 700  $\mu\text{M}$  HSA in phosphate buffered saline (PBS) and radioligands with a molecular mass below the column fractionation range are injected. A ligand-specific, HSA-mediated retention time is observed according to the strength of interaction between radioligand and HSA during the chromatographic run. Based on the acquired retention time an apparent molecular weight  $\text{MW}_{\text{app}}$  can be determined which can be used to calculate glomerular sieving coefficients of the radioligands. Figure reproduced with the permission of the publisher. © 2022 by the authors.

An optimally tailored pharmacokinetic profile represents a crucial prerequisite for improved therapeutic efficacy in the development of next-generation therapeutic radiopharmaceuticals. Preclinical methods like ultrafiltration and different chromatographic procedures [323–325] have been routinely applied in the development of PSMA radioligands to assess their binding to plasma proteins such as HSA [182, 314, 317, 319], a parameter that dramatically shapes the overall PK due to its impact on the ligand’s blood clearance kinetics. However, while the aforementioned methodologies only facilitate the quantification of protein-bound fractions or the radioligand’s affinity towards a certain plasma protein, an *in vitro* method that might allow to draw conclusions on a radioligand’s blood clearance kinetics in patients is needed

to enable the accurate identification of therapeutic lead compounds for clinical translation. In this work a novel methodology named ‘albumin-mediated size exclusion chromatography’ (AMSEC) has been developed to confront this pending need in the preclinical evaluation of therapeutic radiopharmaceuticals.

$^{177}\text{Lu}$ -labeled PSMA ligands were injected onto a size exclusion chromatography (SEC) column with HSA in the mobile phase and individual HSA-mediated retention times were observed due to transient HSA-ligand complexation. Retention times were used to calculate ligand-specific raw apparent molecular weights ( $\text{MW}_{\text{app,raw}}$ ) as a means to describe the ligands’ strength of HSA-binding. A normalization procedure based on blank runs and mathematical transformations was implemented to account for unspecific interactions between radioligands and the column matrix resulting in normalized  $\text{MW}_{\text{app,norm}}$  that are comparable among the radioligands. The obtained  $\text{MW}_{\text{app,norm}}$  between 1.9 kDa ( $^{177}\text{Lu}$ ]Lu-PSMA-I&T) and 39.9 kDa ( $^{177}\text{Lu}$ ]Lu-MC-1) covered a wide range indicating distinct HSA-binding strength among the analyzed compounds and, interestingly, significant differences were observed even among stereoisomers such as  $^{177}\text{Lu}$ ]Lu-rhPSMA-7.1 and  $^{177}\text{Lu}$ ]Lu-rhPSMA-7.2 (17.1 kDa and 21.7 kDa, respectively). Based on the sigmoidal correlation between molecular weight (MW) and glomerular sieving coefficients (GSC) of different human plasma proteins <sup>[327]</sup>,  $\text{GSC}_{\text{calc}}$  were calculated for the analyzed radioligands and ranged between 0.003 ( $^{177}\text{Lu}$ ]Lu-MC-1) and 0.992 ( $^{177}\text{Lu}$ ]Lu-PSMA-I&T). As the blood clearance kinetics of a renally excreted radioligand is mainly governed by the MW-dependent process of glomerular filtration,  $\text{MW}_{\text{app,norm}}$  and  $\text{GSC}_{\text{calc}}$  represent valuable preclinical parameters that might help to estimate the influence of a ligand’s HSA-binding on the blood clearance kinetics in patients. The radiohybrid ligand  $^{177}\text{Lu}$ ]Lu-rhPSMA-10.1 showed particularly interesting  $\text{MW}_{\text{app,norm}}$  of 17.2 kDa and  $\text{GSC}_{\text{calc}}$  of 0.644 which lies between the values obtained for  $^{177}\text{Lu}$ ]Lu-rhPSMA-7.3 ( $\text{MW}_{\text{app,norm}}$  = 20.7 kDa,  $\text{GSC}_{\text{calc}}$  = 0.408) and clinically established  $^{177}\text{Lu}$ ]Lu-PSMA-617 ( $\text{MW}_{\text{app,norm}}$  = 9.4 kDa,  $\text{GSC}_{\text{calc}}$  = 0.942).

In conclusion, AMSEC represents a unique methodology to possibly provide an estimation of the blood clearance kinetics of different radioligands already at the preclinical stage. If clinical data confirm this innovative approach, the novel parameters  $\text{MW}_{\text{app,norm}}$  and  $\text{GSC}_{\text{calc}}$  might help to identify optimized therapeutic lead compounds with suitable blood clearance kinetics in patients for clinical translation thus supporting the development of next-generation radioligands for RLT with improved therapeutic efficacy.

### **Author contribution**

The author of this thesis, Jan-Philip Kunert, was involved in the planning and conceptualization of this study and established all experimental procedures. He furthermore participated in the preparation of radioligands, acquired, analyzed and interpreted data, developed and executed the normalization procedure and wrote the original draft of the manuscript.

### 3.3. Synthesis and Preclinical Evaluation of Novel $^{99m}\text{Tc}$ -labeled PSMA Ligands for Radioguided Surgery of Prostate Cancer

Jan-Philip Kunert<sup>1</sup>, Max Müller<sup>1</sup>, Thomas Günther<sup>1</sup>, León Stopper<sup>1</sup>, Nicole Urtz-Urban<sup>1</sup>, Roswitha Beck<sup>1</sup> and Hans-Jürgen Wester<sup>1</sup>

<sup>1</sup> Chair of Pharmaceutical Radiochemistry, Department of Chemistry, Technical University of Munich (TUM), Walther-Meißner-Str 3, 85748 Garching, Germany.

*EJNMMI Research* **2023**, *13* (2), doi: 10.1186/s13550-022-00942-7.

Hyperlink: <https://ejnmmires.springeropen.com/articles/10.1186/s13550-022-00942-7>

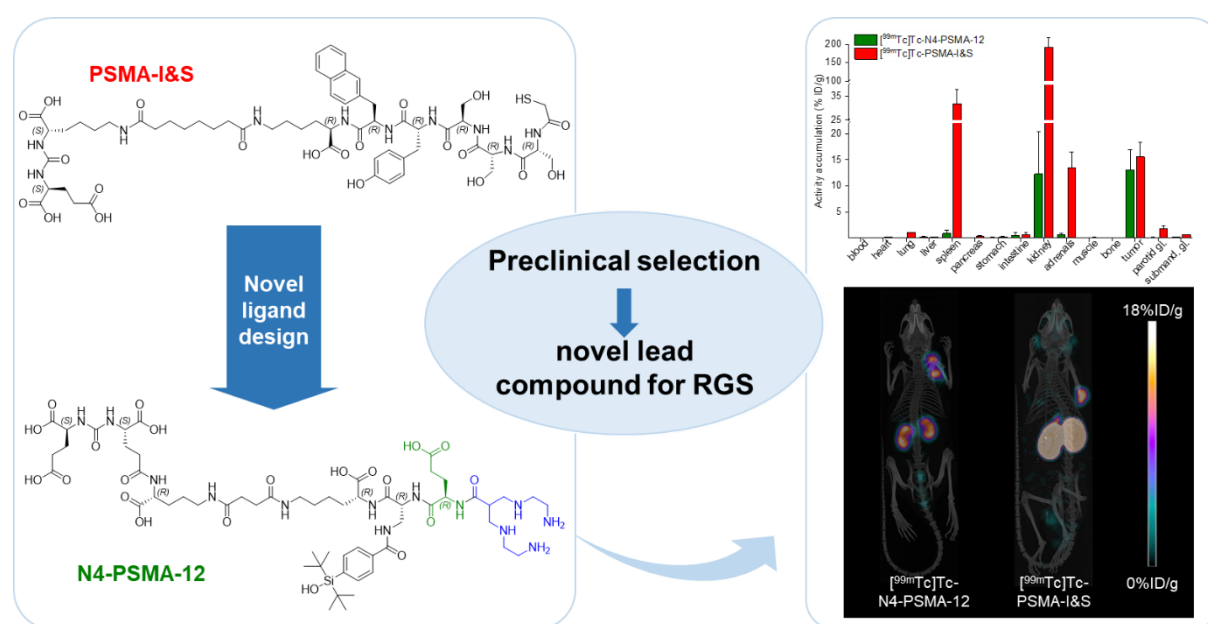


**Figure 16:** A series of novel  $^{99m}\text{Tc}$ -labeled PSMA ligands comprising a tetraamine (N4) chelator and a variable amino acid as pharmacokinetic modifier were evaluated in a preclinical selection process and compared to the reference compound [ $^{99m}\text{Tc}$ ]Tc-PSMA-I&S. The D-glutamate bearing derivative N4-PSMA-12 was identified as lead compound for application in RGS due to reduced lipophilicity and plasma protein binding *in vitro* and a favorable pharmacokinetic profile observed in biodistribution studies 6 h p.i., such as lower blood retention and superior tumor-to-background ratios as compared to other N4-PSMA ligands and PSMA-I&S.

With the introduction of  $^{99m}\text{Tc}$ -labeled PSMA-I&S RGS has become an accessible and attractive therapeutic intervention in primary or early recurrent PCa with regional pelvic lymph node metastases [259, 263]. Despite encouraging results in terms of metastases yield, biochemical response and suggested superiority over conventional lymph node dissection [259, 264-265], the incomplete resection especially of micrometastatic lesions remains a challenge and main reason for disease progression and metastatic spread. The unsatisfactory sensitivity for micrometastatic lesions can be attributed to a significant extent to insufficient tumor-to-background ratios when using [ $^{99m}\text{Tc}$ ]Tc-PSMA-I&S for radioguidance, a radioligand with rather slow whole-body clearance [263]. Therefore, the aim of this work

was to develop novel  $^{99m}\text{Tc}$ -labeled PSMA ligands for RGS with optimized pharmacokinetic properties to facilitate improved tumor-to-background ratios at the time of surgery.

Three novel  $^{99m}\text{Tc}$ -labeled PSMA ligands bearing a tetraamine (N4) chelator and a variable amino acid as pharmacokinetic modifier were synthesized and preclinically evaluated in comparison with the established tracer [ $^{99m}\text{Tc}$ ]Tc-PSMA-I&S. The novel compounds showed comparable affinity towards PSMA and generally reduced lipophilicity and plasma protein binding ( $-3.35$  to  $-2.78$  and  $55.1\%$  to  $88.5\%$ , respectively) as compared to [ $^{99m}\text{Tc}$ ]Tc-PSMA-I&S ( $-2.61$  and  $94.4\%$ , respectively). Thereby, the choice of the variable amino acid was found to modulate the extent of plasma protein binding and lipophilicity of the N4-PSMA radioligands. Biodistribution studies in LNCaP tumor-bearing xenografts at 6 h p.i. revealed markedly altered tissue distribution profiles for the novel compounds. Tumor uptake was comparable to [ $^{99m}\text{Tc}$ ]Tc-PSMA-I&S ( $P > 0.27$ ), however, significantly reduced retention in the kidneys and several other organs such as lungs, spleen, adrenals and parotid gland ( $P < 0.001$  each) was observed and resulted in largely increased tumor-to-background ratios. Especially [ $^{99m}\text{Tc}$ ]Tc-N4-PSMA-12 exhibited a superior pharmacokinetic profile with the lowest blood retention of all analyzed ligands ( $0.0200 \pm 0.0044$  %iD/g) and more than 15-fold reduced kidney uptake as well as superior tumor-to-background ratios in all analyzed organs as compared to [ $^{99m}\text{Tc}$ ]Tc-PSMA-I&S. Furthermore, a labeling procedure at patient scale was established for N4-PSMA-12 and reproducibly afforded the radioligand with excellent RCP of  $98.5 \pm 0.6\%$  at activities between 194 – 810 MBq ( $553 \pm 187$  MBq,  $n = 10$ ).

Its superior pharmacokinetic properties combined with the established labeling procedure suitable for routine clinical production render [ $^{99m}\text{Tc}$ ]Tc-N4-PSMA-12 a promising candidate for clinical investigations with the potential to tackle the limitations currently faced in RGS with [ $^{99m}\text{Tc}$ ]Tc-PSMA-I&S.

### **Author contribution**

The author of this thesis, Jan-Philip Kunert, planned the study, participated in the synthesis of evaluated compounds, carried out the majority of preclinical *in vitro* and *in vivo* experiments and was involved in the optimization of radiolabeling towards a clinically suitable procedure. Jan-Philip Kunert furthermore interpreted data, carried out statistical analysis and contributed significantly in the writing of the manuscript.

## 4. Conclusion and Outlook

The care of patients and potential cure of disease is oftentimes complex and, especially with oncologic diseases such as PCa, requires multidisciplinary efforts on various levels. Combination treatments, symbiosis of diagnostic and therapeutic interventions, aspects of clinical handling of side-effects and, with a wider perspective, even social and socioeconomic questions concerning accessibility and affordability of treatments need to be considered. Within that manifold challenge to improve the life of patients, the availability of ever-optimized drugs certainly is and will continue to be a fundamental cornerstone for improved patient care in the future. In the context of the management and treatment of PCa encouraging and highly impactful developments harnessing PSMA as molecular target for diagnostic and therapeutic interventions have rendered nuclear medicine a forerunner in modern precision oncology. The work presented in this thesis covers different aspects within the branch of radiopharmaceutical development towards therapeutic and theranostic applications in the management of PCa.

The evaluation of novel,  $^{177}\text{Lu}$ -labeled rhPSMA ligands for RLT presented in this work led to the identification of [ $^{177}\text{Lu}$ ]Lu-rhPSMA-10.1 as a highly attractive theranostic candidate for clinical translation. A first clinical phase I and II study to determine the radiation dosimetry, safety and efficacy of this novel radiopharmaceutical in mCRPC patients has already been initiated (NCT05413850), which represents a prime example for the constantly accelerating development of small-molecule radioligands for targeted RLT since the introduction of [ $^{177}\text{Lu}$ ]Lu-DOTATATE more than two decades ago [328]. Within the field of PCa, RLT is about to further increase its impact on patient management due to the recent regulatory approval of [ $^{177}\text{Lu}$ ]Lu-PSMA-617 [220]. Based on this milestone, the focus of PSMA-targeted RLT will likely shift from exclusive late-stage monotherapy applications towards earlier-line treatment, combination therapies and TAT [329-330]. However, due to intensified and potentially earlier application of PSMA-targeted RLT in the future, novel radioligands with improved therapeutic efficacy will be urgently needed to restrain radiotoxic side effects to a tolerable level while maximizing the dose delivered to cancerous lesions. If the therapeutic efficacy of novel tracers such as [ $^{177}\text{Lu}$ ]Lu-rhPSMA-10.1 should indeed prove superior compared to currently established radioligands, added benefits of improved pharmacokinetic properties on one hand and advantages of earlier-line or combination treatments on the other hand might be made available to PCa patients. Whether [ $^{177}\text{Lu}$ ]Lu-rhPSMA-10.1 indeed bears the expected potential needs to be evaluated by ongoing and future clinical studies. From a wider perspective, growing clinical experience with [ $^{177}\text{Lu}$ ]Lu-rhPSMA-10.1 might furthermore help to spread radiohybrid radiopharmaceuticals and their huge theranostic potential towards applications against other oncologic diseases beyond PCa.

The identification of novel radioligands with improved therapeutic efficacy for clinical translation requires preclinical methods that allow for an accurate estimation of a ligand's pharmacokinetic properties in humans. Therefore, the innovative methodology AMSEC was developed within the scope

of this thesis and the obtained preclinical parameters  $MW_{app,norm.}$  and  $GSC_{calc}$  might possibly help to draw conclusions on the blood clearance kinetics of therapeutic radioligands. While generated data show reasonable trends and impressive resolution, clinical data will be needed to verify and validate the hypothesized informative value of AMSEC experiments. It furthermore remains to be investigated whether precise estimations in terms of human blood clearance kinetics can indeed be derived from  $MW_{app,norm.}$  and  $GSC_{calc}$  or if these parameters are rather suited to relatively compare the blood clearance kinetics among structurally similar compounds. Furthermore, structural features were shown to influence non-specific interactions of evaluated radioligands with the SEC column matrix in AMSEC experiments. Therefore, future analysis of different classes of radioligands should be accompanied by thorough analysis of these ligand-specific interactions. If clinical data confirm the expected correlation between human blood clearance kinetics and the parameters  $MW_{app,norm.}$  and  $GSC_{calc}$ , AMSEC might serve as a valuable tool in the future development of therapeutic radioligands with optimized PK against various oncologic diseases. Additionally, AMSEC-guided pre-selection of radioligands for *in vivo* biodistribution studies could contribute to ameliorate animal welfare by reducing animal experiments in preclinical radioligand development.

Novel PSMA-targeted radioligands with optimized PK are also required in the context of RGS to improve the sensitivity for micrometastatic lesions. The novel  $^{99m}Tc$ -labeled PSMA-ligands developed in this thesis were preclinically compared to the routinely applied tracer  $[^{99m}Tc]Tc$ -PSMA-I&S and excellent targeting and physicochemical properties *in vitro* as well as markedly improved tumor-to-background ratios *in vivo* were achieved with  $[^{99m}Tc]Tc$ -N4-PSMA-12. Patient studies with this highly attractive candidate for clinical translation will be needed to ascertain whether the favorable preclinical pharmacokinetic characteristics will also result in improved sensitivity in RGS. As the approach of RGS is already established in many clinical centers, the introduction of an optimized ligand such as  $[^{99m}Tc]Tc$ -N4-PSMA-12 could exert an instant positive impact on PCa patient care building on its optimized pharmacokinetic properties and the infrastructure and workflows already established for the application of  $[^{99m}Tc]Tc$ -PSMA-I&S. Apart from RGS, the latter radioligand has also been successfully applied in diagnostic SPECT/CT-imaging of PCa patients<sup>[331]</sup>. Recent advancements in SPECT technology, such as solid-state detectors<sup>[332-333]</sup> and slant- or pinhole collimators<sup>[334-336]</sup>, allow for improved sensitivity and spatial resolution and strengthen the role of  $^{99m}Tc$ -labeled diagnostic tracers as valuable molecular imaging agents, especially where PET-imaging is not available<sup>[331]</sup>. Besides the application in RGS, the novel ligand  $[^{99m}Tc]Tc$ -N4-PSMA-12 might therefore also find application in diagnostic SPECT-imaging of PCa wherein the ease of tracer preparation with generator-based technetium-99m provides excellent availability not only in clinical but also in outpatient settings.

## 5. References

1. Sung, H.; Ferlay, J.; Siegel, R. L.; Laversanne, M.; Soerjomataram, I., et al., Global Cancer Statistics 2020: GLOBOCAN Estimates of Incidence and Mortality Worldwide for 36 Cancers in 185 Countries. *CA Cancer J Clin* **2021**, *71* (3), 209-249, 10.3322/caac.21660.
2. Ferlay, J.; Shin, H. R.; Bray, F.; Forman, D.; Mathers, C.; Parkin, D. M., Estimates of worldwide burden of cancer in 2008: GLOBOCAN 2008. *Int J Cancer* **2010**, *127* (12), 2893-2917, 10.1002/ijc.25516.
3. Ferlay, J.; Soerjomataram, I.; Dikshit, R.; Eser, S.; Mathers, C., et al., Cancer incidence and mortality worldwide: sources, methods and major patterns in GLOBOCAN 2012. *Int J Cancer* **2015**, *136* (5), E359-386, 10.1002/ijc.29210.
4. Bray, F.; Ferlay, J.; Soerjomataram, I.; Siegel, R. L.; Torre, L. A.; Jemal, A., Global cancer statistics 2018: GLOBOCAN estimates of incidence and mortality worldwide for 36 cancers in 185 countries. *CA Cancer J Clin* **2018**, *68* (6), 394-424, 10.3322/caac.21492.
5. Steinberg, G. D.; Carter, B. S.; Beaty, T. H.; Childs, B.; Walsh, P. C., Family history and the risk of prostate cancer. *Prostate* **1990**, *17* (4), 337-347, 10.1002/pros.2990170409.
6. Johns, L. E.; Houlston, R. S., A systematic review and meta-analysis of familial prostate cancer risk. *BJU Int* **2003**, *91* (9), 789-794, 10.1046/j.1464-410x.2003.04232.x.
7. Albright, F.; Stephenson, R. A.; Agarwal, N.; Teerlink, C. C.; Lowrance, W. T., et al., Prostate cancer risk prediction based on complete prostate cancer family history. *Prostate* **2015**, *75* (4), 390-398, 10.1002/pros.22925.
8. Gann, P. H.; Hennekens, C. H.; Ma, J.; Longcope, C.; Stampfer, M. J., Prospective study of sex hormone levels and risk of prostate cancer. *J Natl Cancer Inst* **1996**, *88* (16), 1118-1126, 10.1093/jnci/88.16.1118.
9. Ross, R. K.; Pike, M. C.; Coetzee, G. A.; Reichardt, J. K.; Yu, M. C., et al., Androgen metabolism and prostate cancer: establishing a model of genetic susceptibility. *Cancer Res* **1998**, *58* (20), 4497-4504.
10. Taplin, M. E.; Bubley, G. J.; Shuster, T. D.; Frantz, M. E.; Spooner, A. E., et al., Mutation of the androgen-receptor gene in metastatic androgen-independent prostate cancer. *N Engl J Med* **1995**, *332* (21), 1393-1398, 10.1056/NEJM199505253322101.
11. Robbins, C. M.; Hooker, S.; Kittles, R. A.; Carpten, J. D., EphB2 SNPs and sporadic prostate cancer risk in African American men. *PLoS One* **2011**, *6* (5), e19494, 10.1371/journal.pone.0019494.
12. Haiman, C. A.; Chen, G. K.; Blot, W. J.; Strom, S. S.; Berndt, S. I., et al., Characterizing genetic risk at known prostate cancer susceptibility loci in African Americans. *PLoS Genet* **2011**, *7* (5), e1001387, 10.1371/journal.pgen.1001387.
13. Jemal, A.; Center, M. M.; DeSantis, C.; Ward, E. M., Global patterns of cancer incidence and mortality rates and trends. *Cancer Epidemiol Biomarkers Prev* **2010**, *19* (8), 1893-1907, 10.1158/1055-9965.EPI-10-0437.
14. Prins, G. S.; Hu, W. Y.; Shi, G. B.; Hu, D. P.; Majumdar, S., et al., Bisphenol A promotes human prostate stem-progenitor cell self-renewal and increases in vivo carcinogenesis in human prostate epithelium. *Endocrinology* **2014**, *155* (3), 805-817, 10.1210/en.2013-1955.
15. Chamie, K.; DeVere White, R. W.; Lee, D.; Ok, J. H.; Ellison, L. M., Agent Orange exposure, Vietnam War veterans, and the risk of prostate cancer. *Cancer* **2008**, *113* (9), 2464-2470, 10.1002/cncr.23695.
16. Heshmat, M. Y.; Kaul, L.; Kovi, J.; Jackson, M. A.; Jackson, A. G., et al., Nutrition and prostate cancer: a case-control study. *Prostate* **1985**, *6* (1), 7-17, 10.1002/pros.2990060103.
17. Aronson, W. J.; Barnard, R. J.; Freedland, S. J.; Henning, S.; Elashoff, D., et al., Growth inhibitory effect of low fat diet on prostate cancer cells: results of a prospective, randomized dietary intervention trial in men with prostate cancer. *J Urol* **2010**, *183* (1), 345-350, 10.1016/j.juro.2009.08.104.
18. Laurent, V.; Guerard, A.; Mazerolles, C.; Le Gonidec, S.; Toulet, A., et al., Periprostatic adipocytes act as a driving force for prostate cancer progression in obesity. *Nat Commun* **2016**, *7*, 10230, 10.1038/ncomms10230.

19. Vidal, A. C.; Howard, L. E.; Moreira, D. M.; Castro-Santamaria, R.; Andriole, G. L., Jr.; Freedland, S. J., Obesity increases the risk for high-grade prostate cancer: results from the REDUCE study. *Cancer Epidemiol Biomarkers Prev* **2014**, *23* (12), 2936-2942, 10.1158/1055-9965.EPI-14-0795.
20. Moller, H.; Roswall, N.; Van Hemelrijck, M.; Larsen, S. B.; Cuzick, J., et al., Prostate cancer incidence, clinical stage and survival in relation to obesity: a prospective cohort study in Denmark. *Int J Cancer* **2015**, *136* (8), 1940-1947, 10.1002/ijc.29238.
21. Dennis, L. K.; Lynch, C. F.; Torner, J. C., Epidemiologic association between prostatitis and prostate cancer. *Urology* **2002**, *60* (1), 78-83, 10.1016/s0090-4295(02)01637-0.
22. De Marzo, A. M.; Platz, E. A.; Sutcliffe, S.; Xu, J.; Gronberg, H., et al., Inflammation in prostate carcinogenesis. *Nat Rev Cancer* **2007**, *7* (4), 256-269, 10.1038/nrc2090.
23. Jiang, J.; Li, J.; Yunxia, Z.; Zhu, H.; Liu, J.; Pumill, C., The role of prostatitis in prostate cancer: meta-analysis. *PLoS One* **2013**, *8* (12), e85179, 10.1371/journal.pone.0085179.
24. Rawla, P., Epidemiology of Prostate Cancer. *World J Oncol* **2019**, *10* (2), 63-89, 10.14740/wjon1191.
25. Bostwick, D. G.; Burke, H. B.; Djakiew, D.; Euling, S.; Ho, S. M., et al., Human prostate cancer risk factors. *Cancer* **2004**, *101* (10 Suppl), 2371-2490, 10.1002/cncr.20408.
26. Taitt, H. E., Global Trends and Prostate Cancer: A Review of Incidence, Detection, and Mortality as Influenced by Race, Ethnicity, and Geographic Location. *Am J Mens Health* **2018**, *12* (6), 1807-1823, 10.1177/1557988318798279.
27. Kaaks, R.; Stattin, P., Obesity, endogenous hormone metabolism, and prostate cancer risk: a conundrum of "highs" and "lows". *Cancer Prev Res (Phila)* **2010**, *3* (3), 259-262, 10.1158/1940-6207.CAPR-10-0014.
28. Mistry, K.; Cable, G., Meta-analysis of prostate-specific antigen and digital rectal examination as screening tests for prostate carcinoma. *J Am Board Fam Pract* **2003**, *16* (2), 95-101, 10.3122/jabfm.16.2.95.
29. Halpern, J. A.; Shoag, J. E.; Mittal, S.; Oromendia, C.; Ballman, K. V., et al., Prognostic Significance of Digital Rectal Examination and Prostate Specific Antigen in the Prostate, Lung, Colorectal and Ovarian (PLCO) Cancer Screening Arm. *J Urol* **2017**, *197* (2), 363-368, 10.1016/j.juro.2016.08.092.
30. Ahmed, H. U.; El-Shater Bosaily, A.; Brown, L. C.; Gabe, R.; Kaplan, R., et al., Diagnostic accuracy of multi-parametric MRI and TRUS biopsy in prostate cancer (PROMIS): a paired validating confirmatory study. *Lancet* **2017**, *389* (10071), 815-822, 10.1016/S0140-6736(16)32401-1.
31. Drost, F. H.; Osses, D. F.; Nieboer, D.; Steyerberg, E. W.; Bangma, C. H., et al., Prostate MRI, with or without MRI-targeted biopsy, and systematic biopsy for detecting prostate cancer. *Cochrane Database Syst Rev* **2019**, *4*, CD012663, 10.1002/14651858.CD012663.pub2.
32. Renfer, L. G.; Schow, D.; Thompson, I. M.; Optenberg, S., Is ultrasound guidance necessary for transrectal prostate biopsy? *J Urol* **1995**, *154* (4), 1390-1391, 10.1016/S0022-5347(01)66873-3.
33. Epstein, J. I.; Egevad, L.; Humphrey, P. A.; Montironi, R.; Members of the, I. I. i. D. U. P. G., Best practices recommendations in the application of immunohistochemistry in the prostate: report from the International Society of Urologic Pathology consensus conference. *Am J Surg Pathol* **2014**, *38* (8), e6-e19, 10.1097/PAS.0000000000000238.
34. Giberti, C.; Gallo, F.; Schenone, M.; Gastaldi, E.; Cortese, P., et al., Robotic prostatectomy versus brachytherapy for the treatment of low risk prostate cancer. *Can J Urol* **2017**, *24* (2), 8728-8733.
35. Galalae, R. M.; Martinez, A.; Mate, T.; Mitchell, C.; Edmundson, G., et al., Long-term outcome by risk factors using conformal high-dose-rate brachytherapy (HDR-BT) boost with or without neoadjuvant androgen suppression for localized prostate cancer. *Int J Radiat Oncol Biol Phys* **2004**, *58* (4), 1048-1055, 10.1016/j.ijrobp.2003.08.003.
36. Bill-Axelson, A.; Holmberg, L.; Ruutu, M.; Garmo, H.; Stark, J. R., et al., Radical prostatectomy versus watchful waiting in early prostate cancer. *N Engl J Med* **2011**, *364* (18), 1708-1717, 10.1056/NEJMoa1011967.
37. Swindle, P.; Eastham, J. A.; Otori, M.; Kattan, M. W.; Wheeler, T., et al., Do margins matter? The prognostic significance of positive surgical margins in radical prostatectomy specimens. *J Urol* **2005**, *174* (3), 903-907, 10.1097/01.ju.0000169475.00949.78.
38. Zietman, A. L.; DeSilvio, M. L.; Slater, J. D.; Rossi, C. J., Jr.; Miller, D. W., et al., Comparison of conventional-dose vs high-dose conformal radiation therapy in clinically localized adenocarcinoma

- of the prostate: a randomized controlled trial. *JAMA* **2005**, *294* (10), 1233-1239, 10.1001/jama.294.10.1233.
39. Beckendorf, V.; Guerif, S.; Le Prise, E.; Cosset, J. M.; Lefloch, O., et al., The GETUG 70 Gy vs. 80 Gy randomized trial for localized prostate cancer: feasibility and acute toxicity. *Int J Radiat Oncol Biol Phys* **2004**, *60* (4), 1056-1065, 10.1016/j.ijrobp.2004.05.033.
40. Kupelian, P. A.; Potters, L.; Khuntia, D.; Ciezki, J. P.; Reddy, C. A., et al., Radical prostatectomy, external beam radiotherapy <72 Gy, external beam radiotherapy > or =72 Gy, permanent seed implantation, or combined seeds/external beam radiotherapy for stage T1-T2 prostate cancer. *Int J Radiat Oncol Biol Phys* **2004**, *58* (1), 25-33, 10.1016/s0360-3016(03)00784-3.
41. King, C. R.; Collins, S.; Fuller, D.; Wang, P. C.; Kupelian, P., et al., Health-related quality of life after stereotactic body radiation therapy for localized prostate cancer: results from a multi-institutional consortium of prospective trials. *Int J Radiat Oncol Biol Phys* **2013**, *87* (5), 939-945, 10.1016/j.ijrobp.2013.08.019.
42. Chen, R. C.; Basak, R.; Meyer, A. M.; Kuo, T. M.; Carpenter, W. R., et al., Association Between Choice of Radical Prostatectomy, External Beam Radiotherapy, Brachytherapy, or Active Surveillance and Patient-Reported Quality of Life Among Men With Localized Prostate Cancer. *JAMA* **2017**, *317* (11), 1141-1150, 10.1001/jama.2017.1652.
43. Ip, S.; Dahabreh, I. J.; Chung, M.; Yu, W. W.; Balk, E. M., et al., An evidence review of active surveillance in men with localized prostate cancer. *Evid Rep Technol Assess (Full Rep)* **2011**, (204), 1-341.
44. Hamdy, F. C.; Donovan, J. L.; Lane, J. A.; Mason, M.; Metcalfe, C., et al., 10-Year Outcomes after Monitoring, Surgery, or Radiotherapy for Localized Prostate Cancer. *N Engl J Med* **2016**, *375* (15), 1415-1424, 10.1056/NEJMoa1606220.
45. Heidenreich, A.; Varga, Z.; Von Knobloch, R., Extended pelvic lymphadenectomy in patients undergoing radical prostatectomy: high incidence of lymph node metastasis. *J Urol* **2002**, *167* (4), 1681-1686, 10.1016/S0022-5347(05)65177-4.
46. Fossati, N.; Willemse, P. M.; Van den Broeck, T.; van den Bergh, R. C. N.; Yuan, C. Y., et al., The Benefits and Harms of Different Extents of Lymph Node Dissection During Radical Prostatectomy for Prostate Cancer: A Systematic Review. *Eur Urol* **2017**, *72* (1), 84-109, 10.1016/j.eururo.2016.12.003.
47. Briganti, A.; Chun, F. K.; Salonia, A.; Suardi, N.; Gallina, A., et al., Complications and other surgical outcomes associated with extended pelvic lymphadenectomy in men with localized prostate cancer. *Eur Urol* **2006**, *50* (5), 1006-1013, 10.1016/j.eururo.2006.08.015.
48. Pilepich, M. V.; Winter, K.; Lawton, C. A.; Krisch, R. E.; Wolkov, H. B., et al., Androgen suppression adjuvant to definitive radiotherapy in prostate carcinoma--long-term results of phase III RTOG 85-31. *Int J Radiat Oncol Biol Phys* **2005**, *61* (5), 1285-1290, 10.1016/j.ijrobp.2004.08.047.
49. Bolla, M.; Van Tienhoven, G.; Warde, P.; Dubois, J. B.; Mirimanoff, R.-O., et al., External irradiation with or without long-term androgen suppression for prostate cancer with high metastatic risk: 10-year results of an EORTC randomised study. *Lancet Oncol* **2010**, *11* (11), 1066-1073, 10.1016/S1470-2045(10)70223-0.
50. Tammela, T., Endocrine treatment of prostate cancer. *J Steroid Biochem Mol Biol* **2004**, *92* (4), 287-295, 10.1016/j.jsbmb.2004.10.005.
51. Gomella, L. G., Effective testosterone suppression for prostate cancer: is there a best castration therapy? *Rev Urol* **2009**, *11* (2), 52-60.
52. Fizazi, K.; Tran, N.; Fein, L.; Matsubara, N.; Rodriguez-Antolin, A., et al., Abiraterone acetate plus prednisone in patients with newly diagnosed high-risk metastatic castration-sensitive prostate cancer (LATITUDE): final overall survival analysis of a randomised, double-blind, phase 3 trial. *Lancet Oncol* **2019**, *20* (5), 686-700, 10.1016/S1470-2045(19)30082-8.
53. Armstrong, A. J.; Szmulewitz, R. Z.; Petrylak, D. P.; Holzbeierlein, J.; Villers, A., et al., ARCHES: A Randomized, Phase III Study of Androgen Deprivation Therapy With Enzalutamide or Placebo in Men With Metastatic Hormone-Sensitive Prostate Cancer. *J Clin Oncol* **2019**, *37* (32), 2974-2986, 10.1200/JCO.19.00799.
54. Ryan, C. J.; Smith, M. R.; de Bono, J. S.; Molina, A.; Logothetis, C. J., et al., Abiraterone in metastatic prostate cancer without previous chemotherapy. *N Engl J Med* **2013**, *368* (2), 138-148, 10.1056/NEJMoa1209096.

55. Beer, T. M.; Armstrong, A. J.; Rathkopf, D. E.; Loriot, Y.; Sternberg, C. N., et al., Enzalutamide in metastatic prostate cancer before chemotherapy. *N Engl J Med* **2014**, *371* (5), 424-433, 10.1056/NEJMoa1405095.
56. Berthold, D. R.; Pond, G. R.; Soban, F.; de Wit, R.; Eisenberger, M.; Tannock, I. F., Docetaxel plus prednisone or mitoxantrone plus prednisone for advanced prostate cancer: updated survival in the TAX 327 study. *J Clin Oncol* **2008**, *26* (2), 242-245, 10.1200/JCO.2007.12.4008.
57. de Wit, R.; de Bono, J.; Sternberg, C. N.; Fizazi, K.; Tombal, B., et al., Cabazitaxel versus Abiraterone or Enzalutamide in Metastatic Prostate Cancer. *N Engl J Med* **2019**, *381* (26), 2506-2518, 10.1056/NEJMoa1911206.
58. Parker, C.; Nilsson, S.; Heinrich, D.; Helle, S. I.; O'Sullivan, J. M., et al., Alpha emitter radium-223 and survival in metastatic prostate cancer. *N Engl J Med* **2013**, *369* (3), 213-223, 10.1056/NEJMoa1213755.
59. Smith, M.; Parker, C.; Saad, F.; Miller, K.; Tombal, B., et al., Addition of radium-223 to abiraterone acetate and prednisone or prednisolone in patients with castration-resistant prostate cancer and bone metastases (ERA 223): a randomised, double-blind, placebo-controlled, phase 3 trial. *Lancet Oncol* **2019**, *20* (3), 408-419, 10.1016/S1470-2045(18)30860-X.
60. Armstrong, C. M.; Gao, A. C., Drug resistance in castration resistant prostate cancer: resistance mechanisms and emerging treatment strategies. *Am J Clin Exp Urol* **2015**, *3* (2), 64-76.
61. de Bono, J. S.; Oudard, S.; Ozguroglu, M.; Hansen, S.; Machiels, J. P., et al., Prednisone plus cabazitaxel or mitoxantrone for metastatic castration-resistant prostate cancer progressing after docetaxel treatment: a randomised open-label trial. *Lancet* **2010**, *376* (9747), 1147-1154, 10.1016/S0140-6736(10)61389-X.
62. Antonarakis, E. S.; Lu, C.; Wang, H.; Luber, B.; Nakazawa, M., et al., AR-V7 and resistance to enzalutamide and abiraterone in prostate cancer. *N Engl J Med* **2014**, *371* (11), 1028-1038, 10.1056/NEJMoa1315815.
63. Dong, L.; Zieren, R. C.; Xue, W.; de Reijke, T. M.; Pienta, K. J., Metastatic prostate cancer remains incurable, why? *Asian J Urol* **2019**, *6* (1), 26-41, 10.1016/j.ajur.2018.11.005.
64. Kahn, D.; Williams, R. D.; Manyak, M. J.; Haseman, M. K.; Seldin, D. W., et al., <sup>111</sup>Indium-capromab pentetide in the evaluation of patients with residual or recurrent prostate cancer after radical prostatectomy. The ProstaScint Study Group. *J Urol* **1998**, *159* (6), 2041-2047, 10.1016/S0022-5347(01)63239-7.
65. Vallabhajosula, S.; Kuji, I.; Hamacher, K. A.; Konishi, S.; Kostakoglu, L., et al., Pharmacokinetics and biodistribution of <sup>111</sup>In- and <sup>177</sup>Lu-labeled J591 antibody specific for prostate-specific membrane antigen: prediction of <sup>90</sup>Y-J591 radiation dosimetry based on <sup>111</sup>In or <sup>177</sup>Lu? *J Nucl Med* **2005**, *46* (4), 634-641.
66. Vavere, A. L.; Kridel, S. J.; Wheeler, F. B.; Lewis, J. S., 1-<sup>11</sup>C-acetate as a PET radiopharmaceutical for imaging fatty acid synthase expression in prostate cancer. *J Nucl Med* **2008**, *49* (2), 327-334, 10.2967/jnumed.107.046672.
67. Kotzerke, J.; Volkmer, B. G.; Glatting, G.; van den Hoff, J.; Gschwend, J. E., et al., Intraindividual comparison of [<sup>11</sup>C]acetate and [<sup>11</sup>C]choline PET for detection of metastases of prostate cancer. *Nuklearmedizin* **2003**, *42* (1), 25-30, 10.1267/NUKL03010025.
68. Hara, T.; Kosaka, N.; Kishi, H., Development of <sup>18</sup>F-fluoroethylcholine for cancer imaging with PET: synthesis, biochemistry, and prostate cancer imaging. *J Nucl Med* **2002**, *43* (2), 187-199.
69. Israeli, R. S.; Powell, C. T.; Fair, W. R.; Heston, W. D., Molecular cloning of a complementary DNA encoding a prostate-specific membrane antigen. *Cancer Res* **1993**, *53* (2), 227-230.
70. Mesters, J. R.; Barinka, C.; Li, W.; Tsukamoto, T.; Majer, P., et al., Structure of glutamate carboxypeptidase II, a drug target in neuronal damage and prostate cancer. *EMBO J* **2006**, *25* (6), 1375-1384, 10.1038/sj.emboj.7600969.
71. Rajasekaran, A. K.; Anilkumar, G.; Christiansen, J. J., Is prostate-specific membrane antigen a multifunctional protein? *Am J Physiol Cell Physiol* **2005**, *288* (5), C975-981, 10.1152/ajpcell.00506.2004.
72. Davis, M. I.; Bennett, M. J.; Thomas, L. M.; Bjorkman, P. J., Crystal structure of prostate-specific membrane antigen, a tumor marker and peptidase. *Proc Natl Acad Sci U S A* **2005**, *102* (17), 5981-5986, 10.1073/pnas.0502101102.

73. Heston, W. D., Characterization and glutamyl preferring carboxypeptidase function of prostate specific membrane antigen: a novel folate hydrolase. *Urology* **1997**, *49* (3A Suppl), 104-112, 10.1016/s0090-4295(97)00177-5.
74. Barinka, C.; Starkova, J.; Konvalinka, J.; Lubkowski, J., A high-resolution structure of ligand-free human glutamate carboxypeptidase II. *Acta Crystallogr Sect F Struct Biol Cryst Commun* **2007**, *63* (Pt 3), 150-153, 10.1107/S174430910700379X.
75. Schulke, N.; Varlamova, O. A.; Donovan, G. P.; Ma, D.; Gardner, J. P., et al., The homodimer of prostate-specific membrane antigen is a functional target for cancer therapy. *Proc Natl Acad Sci U S A* **2003**, *100* (22), 12590-12595, 10.1073/pnas.1735443100.
76. Barinka, C.; Sacha, P.; Sklenar, J.; Man, P.; Bezouska, K., et al., Identification of the N-glycosylation sites on glutamate carboxypeptidase II necessary for proteolytic activity. *Protein Sci* **2004**, *13* (6), 1627-1635, 10.1110/ps.04622104.
77. Ghosh, A.; Heston, W. D., Effect of carbohydrate moieties on the folate hydrolysis activity of the prostate specific membrane antigen. *Prostate* **2003**, *57* (2), 140-151, 10.1002/pros.10289.
78. Robinson, M. B.; Blakely, R. D.; Couto, R.; Coyle, J. T., Hydrolysis of the brain dipeptide N-acetyl-L-aspartyl-L-glutamate. Identification and characterization of a novel N-acetylated alpha-linked acidic dipeptidase activity from rat brain. *J Biol Chem* **1987**, *262* (30), 14498-14506, 10.1016/S0021-9258(18)47823-4.
79. Neale, J. H.; Bzdega, T.; Wroblewska, B., N-Acetylaspartylglutamate: the most abundant peptide neurotransmitter in the mammalian central nervous system. *J Neurochem* **2000**, *75* (2), 443-452, 10.1046/j.1471-4159.2000.0750443.x.
80. Niswender, C. M.; Conn, P. J., Metabotropic glutamate receptors: physiology, pharmacology, and disease. *Annu Rev Pharmacol Toxicol* **2010**, *50*, 295-322, 10.1146/annurev.pharmtox.011008.145533.
81. Barinka, C.; Rojas, C.; Slusher, B.; Pomper, M., Glutamate carboxypeptidase II in diagnosis and treatment of neurologic disorders and prostate cancer. *Curr Med Chem* **2012**, *19* (6), 856-870, 10.2174/092986712799034888.
82. Thomas, A. G.; Corse, A. M.; Coccia, C. F.; Bilak, M. M.; Rothstein, J. D.; Slusher, B. S., NAALADase inhibition protects motor neurons against chronic glutamate toxicity. *Eur J Pharmacol* **2003**, *471* (3), 177-184, 10.1016/s0014-2999(03)01832-6.
83. Witkin, J. M.; Gasior, M.; Schad, C.; Zapata, A.; Shippenberg, T., et al., NAALADase (GCP II) inhibition prevents cocaine-kindled seizures. *Neuropharmacology* **2002**, *43* (3), 348-356, 10.1016/s0028-3908(02)00124-7.
84. Profaci, C. P.; Krolkowski, K. A.; Olszewski, R. T.; Neale, J. H., Group II mGluR agonist LY354740 and NAAG peptidase inhibitor effects on prepulse inhibition in PCP and D-amphetamine models of schizophrenia. *Psychopharmacology (Berl)* **2011**, *216* (2), 235-243, 10.1007/s00213-011-2200-0.
85. Zhao, R.; Matherly, L. H.; Goldman, I. D., Membrane transporters and folate homeostasis: intestinal absorption and transport into systemic compartments and tissues. *Expert Rev Mol Med* **2009**, *11*, e4, 10.1017/S1462399409000969.
86. Qiu, A.; Jansen, M.; Sakaris, A.; Min, S. H.; Chattopadhyay, S., et al., Identification of an intestinal folate transporter and the molecular basis for hereditary folate malabsorption. *Cell* **2006**, *127* (5), 917-928, 10.1016/j.cell.2006.09.041.
87. Pinto, J. T.; Suffoletto, B. P.; Berzin, T. M.; Qiao, C. H.; Lin, S., et al., Prostate-specific membrane antigen: a novel folate hydrolase in human prostatic carcinoma cells. *Clin Cancer Res* **1996**, *2* (9), 1445-1451.
88. Silver, D. A.; Pellicer, I.; Fair, W. R.; Heston, W. D.; Cordon-Cardo, C., Prostate-specific membrane antigen expression in normal and malignant human tissues. *Clin Cancer Res* **1997**, *3* (1), 81-85.
89. Wright, G. L., Jr.; Haley, C.; Beckett, M. L.; Schellhammer, P. F., Expression of prostate-specific membrane antigen in normal, benign, and malignant prostate tissues. *Urol Oncol* **1995**, *1* (1), 18-28, 10.1016/1078-1439(95)00002-y.
90. Kinoshita, Y.; Kuratsukuri, K.; Landas, S.; Imaida, K.; Rovito, P. M., Jr., et al., Expression of prostate-specific membrane antigen in normal and malignant human tissues. *World J Surg* **2006**, *30* (4), 628-636, 10.1007/s00268-005-0544-5.

91. Mhaweche-Fauceglia, P.; Zhang, S.; Terracciano, L.; Sauter, G.; Chadhuri, A., et al., Prostate-specific membrane antigen (PSMA) protein expression in normal and neoplastic tissues and its sensitivity and specificity in prostate adenocarcinoma: an immunohistochemical study using multiple tumour tissue microarray technique. *Histopathology* **2007**, *50* (4), 472-483, 10.1111/j.1365-2559.2007.02635.x.
92. Bostwick, D. G.; Pacelli, A.; Blute, M.; Roche, P.; Murphy, G. P., Prostate specific membrane antigen expression in prostatic intraepithelial neoplasia and adenocarcinoma: a study of 184 cases. *Cancer* **1998**, *82* (11), 2256-2261, 10.1002/(sici)1097-0142(19980601)82:11<2256::aid-cncr22>3.0.co;2-s.
93. Sweat, S. D.; Pacelli, A.; Murphy, G. P.; Bostwick, D. G., Prostate-specific membrane antigen expression is greatest in prostate adenocarcinoma and lymph node metastases. *Urology* **1998**, *52* (4), 637-640, 10.1016/s0090-4295(98)00278-7.
94. Perner, S.; Hofer, M. D.; Kim, R.; Shah, R. B.; Li, H., et al., Prostate-specific membrane antigen expression as a predictor of prostate cancer progression. *Hum Pathol* **2007**, *38* (5), 696-701, 10.1016/j.humpath.2006.11.012.
95. Su, S. L.; Huang, I. P.; Fair, W. R.; Powell, C. T.; Heston, W. D., Alternatively spliced variants of prostate-specific membrane antigen RNA: ratio of expression as a potential measurement of progression. *Cancer Res* **1995**, *55* (7), 1441-1443.
96. Schmittgen, T. D.; Teske, S.; Vessella, R. L.; True, L. D.; Zakrajsek, B. A., Expression of prostate specific membrane antigen and three alternatively spliced variants of PSMA in prostate cancer patients. *Int J Cancer* **2003**, *107* (2), 323-329, 10.1002/ijc.11402.
97. Minner, S.; Wittmer, C.; Graefen, M.; Salomon, G.; Steuber, T., et al., High level PSMA expression is associated with early PSA recurrence in surgically treated prostate cancer. *Prostate* **2011**, *71* (3), 281-288, 10.1002/pros.21241.
98. Hupe, M. C.; Philippi, C.; Roth, D.; Kumpers, C.; Ribbat-Idel, J., et al., Expression of Prostate-Specific Membrane Antigen (PSMA) on Biopsies Is an Independent Risk Stratifier of Prostate Cancer Patients at Time of Initial Diagnosis. *Front Oncol* **2018**, *8*, 623, 10.3389/fonc.2018.00623.
99. Ghosh, A.; Wang, X.; Klein, E.; Heston, W. D., Novel role of prostate-specific membrane antigen in suppressing prostate cancer invasiveness. *Cancer Res* **2005**, *65* (3), 727-731, 10.1158/0008-5472.727.65.3.
100. Yao, V.; Bacich, D. J., Prostate specific membrane antigen (PSMA) expression gives prostate cancer cells a growth advantage in a physiologically relevant folate environment in vitro. *Prostate* **2006**, *66* (8), 867-875, 10.1002/pros.20361.
101. Yao, V.; Berkman, C. E.; Choi, J. K.; O'Keefe, D. S.; Bacich, D. J., Expression of prostate-specific membrane antigen (PSMA), increases cell folate uptake and proliferation and suggests a novel role for PSMA in the uptake of the non-polyglutamated folate, folic acid. *Prostate* **2010**, *70* (3), 305-316, 10.1002/pros.21065.
102. Spatz, S.; Tolkach, Y.; Jung, K.; Stephan, C.; Busch, J., et al., Comprehensive Evaluation of Prostate Specific Membrane Antigen Expression in the Vasculature of Renal Tumors: Implications for Imaging Studies and Prognostic Role. *J Urol* **2018**, *199* (2), 370-377, 10.1016/j.juro.2017.08.079.
103. Haffner, M. C.; Kronberger, I. E.; Ross, J. S.; Sheehan, C. E.; Zitt, M., et al., Prostate-specific membrane antigen expression in the neovasculature of gastric and colorectal cancers. *Hum Pathol* **2009**, *40* (12), 1754-1761, 10.1016/j.humpath.2009.06.003.
104. Kasoha, M.; Unger, C.; Solomayer, E. F.; Bohle, R. M.; Zaharia, C., et al., Prostate-specific membrane antigen (PSMA) expression in breast cancer and its metastases. *Clin Exp Metastasis* **2017**, *34* (8), 479-490, 10.1007/s10585-018-9878-x.
105. Bychkov, A.; Vutrapongwatana, U.; Tepmongkol, S.; Keelawat, S., PSMA expression by microvasculature of thyroid tumors - Potential implications for PSMA theranostics. *Sci Rep* **2017**, *7* (1), 5202, 10.1038/s41598-017-05481-z.
106. Van de Wiele, C.; Sathekege, M.; de Spiegeleer, B.; de Jonghe, P. J.; Beels, L.; Maes, A., PSMA-Targeting Positron Emission Agents for Imaging Solid Tumors Other Than Non-Prostate Carcinoma: A Systematic Review. *Int J Mol Sci* **2019**, *20* (19), 4886, 10.3390/ijms20194886.
107. Uijen, M. J. M.; Derks, Y. H. W.; Merks, R. I. J.; Schilham, M. G. M.; Roosen, J., et al., PSMA radioligand therapy for solid tumors other than prostate cancer: background, opportunities, challenges, and first clinical reports. *Eur J Nucl Med Mol Imaging* **2021**, *48* (13), 4350-4368, 10.1007/s00259-021-05433-w.

108. Backhaus, P.; Noto, B.; Avramovic, N.; Grubert, L. S.; Huss, S., et al., Targeting PSMA by radioligands in non-prostate disease-current status and future perspectives. *Eur J Nucl Med Mol Imaging* **2018**, *45* (5), 860-877, 10.1007/s00259-017-3922-y.
109. Horoszewicz, J. S.; Kawinski, E.; Murphy, G. P., Monoclonal antibodies to a new antigenic marker in epithelial prostatic cells and serum of prostatic cancer patients. *Anticancer Res* **1987**, *7* (5B), 927-935.
110. Elgamal, A. A.; Troychak, M. J.; Murphy, G. P., ProstaScint scan may enhance identification of prostate cancer recurrences after prostatectomy, radiation, or hormone therapy: analysis of 136 scans of 100 patients. *Prostate* **1998**, *37* (4), 261-269, 10.1002/(sici)1097-0045(19981201)37:4<261::aid-pros8>3.0.co;2-#.
111. Liu, H.; Moy, P.; Kim, S.; Xia, Y.; Rajasekaran, A., et al., Monoclonal antibodies to the extracellular domain of prostate-specific membrane antigen also react with tumor vascular endothelium. *Cancer Res* **1997**, *57* (17), 3629-3634.
112. Henry, M. D.; Wen, S.; Silva, M. D.; Chandra, S.; Milton, M.; Worland, P. J., A prostate-specific membrane antigen-targeted monoclonal antibody-chemotherapeutic conjugate designed for the treatment of prostate cancer. *Cancer Res* **2004**, *64* (21), 7995-8001, 10.1158/0008-5472.CAN-04-1722.
113. Tagawa, S. T.; Osborne, J.; Dallos, M.; Nauseef, J.; Sternberg, C. N., et al., Phase I/II trial of pembrolizumab and AR signaling inhibitor+/-<sup>225</sup>Ac-J591 for chemo-naive metastatic castration-resistant prostate cancer (mCRPC). *Clin Oncol* **2022**, *40* (6\_suppl), 10.1200/JCO.2022.40.6\_suppl.TPS216.
114. Subasinghe, N.; Schulte, M.; Chan, M. Y.; Roon, R. J.; Koerner, J. F.; Johnson, R. L., Synthesis of acyclic and dehydroaspartic acid analogues of Ac-Asp-Glu-OH and their inhibition of rat brain N-acetylated alpha-linked acidic dipeptidase (NAALA dipeptidase). *J Med Chem* **1990**, *33* (10), 2734-2744, 10.1021/jm00172a009.
115. Serval, V.; Galli, T.; Cheramy, A.; Glowinski, J.; Lavielle, S., In vitro and in vivo inhibition of N-acetyl-L-aspartyl-L-glutamate catabolism by N-acylated L-glutamate analogs. *J Pharmacol Exp Ther* **1992**, *260* (3), 1093-1100.
116. Jackson, P. F.; Cole, D. C.; Slusher, B. S.; Stetz, S. L.; Ross, L. E., et al., Design, synthesis, and biological activity of a potent inhibitor of the neuropeptidase N-acetylated alpha-linked acidic dipeptidase. *J Med Chem* **1996**, *39* (2), 619-622, 10.1021/jm950801q.
117. Klusak, V.; Barinka, C.; Plechanovova, A.; Mlcochova, P.; Konvalinka, J., et al., Reaction mechanism of glutamate carboxypeptidase II revealed by mutagenesis, X-ray crystallography, and computational methods. *Biochemistry* **2009**, *48* (19), 4126-4138, 10.1021/bi900220s.
118. Barinka, C.; Byun, Y.; Dusich, C. L.; Banerjee, S. R.; Chen, Y., et al., Interactions between human glutamate carboxypeptidase II and urea-based inhibitors: structural characterization. *J Med Chem* **2008**, *51* (24), 7737-7743, 10.1021/jm800765e.
119. Novakova, Z.; Cerny, J.; Choy, C. J.; Nedrow, J. R.; Choi, J. K., et al., Design of composite inhibitors targeting glutamate carboxypeptidase II: the importance of effector functionalities. *FEBS J* **2016**, *283* (1), 130-143, 10.1111/febs.13557.
120. Jackson, P. F.; Tays, K. L.; Maclin, K. M.; Ko, Y. S.; Li, W., et al., Design and pharmacological activity of phosphinic acid based NAALADase inhibitors. *J Med Chem* **2001**, *44* (24), 4170-4175, 10.1021/jm0001774.
121. Kozikowski, A. P.; Nan, F.; Conti, P.; Zhang, J.; Ramadan, E., et al., Design of remarkably simple, yet potent urea-based inhibitors of glutamate carboxypeptidase II (NAALADase). *J Med Chem* **2001**, *44* (3), 298-301, 10.1021/jm000406m.
122. Barinka, C.; Rovenska, M.; Mlcochova, P.; Hlouchova, K.; Plechanovova, A., et al., Structural insight into the pharmacophore pocket of human glutamate carboxypeptidase II. *J Med Chem* **2007**, *50* (14), 3267-3273, 10.1021/jm070133w.
123. Kopka, K.; Benesova, M.; Barinka, C.; Haberkorn, U.; Babich, J., Glu-Ureido-Based Inhibitors of Prostate-Specific Membrane Antigen: Lessons Learned During the Development of a Novel Class of Low-Molecular-Weight Theranostic Radiotracers. *J Nucl Med* **2017**, *58* (Suppl 2), 17S-26S, 10.2967/jnumed.116.186775.
124. Chen, Y.; Foss, C. A.; Byun, Y.; Nimmagadda, S.; Pullambhatla, M., et al., Radiohalogenated prostate-specific membrane antigen (PSMA)-based ureas as imaging agents for prostate cancer. *J Med Chem* **2008**, *51* (24), 7933-7943, 10.1021/jm801055h.

125. Mease, R. C.; Dusich, C. L.; Foss, C. A.; Ravert, H. T.; Dannals, R. F., et al., N-[N-[(S)-1,3-Dicarboxypropyl]carbamoyl]-4-[<sup>18</sup>F]fluorobenzyl-L-cysteine, [<sup>18</sup>F]DCFBC: a new imaging probe for prostate cancer. *Clin Cancer Res* **2008**, *14* (10), 3036-3043, 10.1158/1078-0432.CCR-07-1517.
126. Zhang, A. X.; Murelli, R. P.; Barinka, C.; Michel, J.; Cocleaza, A., et al., A remote arene-binding site on prostate specific membrane antigen revealed by antibody-recruiting small molecules. *J Am Chem Soc* **2010**, *132* (36), 12711-12716, 10.1021/ja104591m.
127. Maresca, K. P.; Hillier, S. M.; Femia, F. J.; Keith, D.; Barone, C., et al., A series of halogenated heterodimeric inhibitors of prostate specific membrane antigen (PSMA) as radiolabeled probes for targeting prostate cancer. *J Med Chem* **2009**, *52* (2), 347-357, 10.1021/jm800994j.
128. Lesche, R.; Kettschau, G.; Gromov, A. V.; Bohnke, N.; Borkowski, S., et al., Preclinical evaluation of BAY 1075553, a novel <sup>18</sup>F-labelled inhibitor of prostate-specific membrane antigen for PET imaging of prostate cancer. *Eur J Nucl Med Mol Imaging* **2014**, *41* (1), 89-101, 10.1007/s00259-013-2527-3.
129. Chen, Y.; Pullambhatla, M.; Foss, C. A.; Byun, Y.; Nimmagadda, S., et al., 2-(3-{1-Carboxy-5-[(6-[<sup>18</sup>F]fluoro-pyridine-3-carbonyl)-amino]-pentyl}-ureido)-pentanedioic acid, [<sup>18</sup>F]DCFPyL, a PSMA-based PET imaging agent for prostate cancer. *Clin Cancer Res* **2011**, *17* (24), 7645-7653, 10.1158/1078-0432.CCR-11-1357.
130. Baranski, A. C.; Schafer, M.; Bauder-Wust, U.; Roscher, M.; Schmidt, J., et al., PSMA-11-Derived Dual-Labeled PSMA Inhibitors for Preoperative PET Imaging and Precise Fluorescence-Guided Surgery of Prostate Cancer. *J Nucl Med* **2018**, *59* (4), 639-645, 10.2967/jnumed.117.201293.
131. Boinapally, S.; Ahn, H. H.; Cheng, B.; Brummet, M.; Nam, H., et al., A prostate-specific membrane antigen (PSMA)-targeted prodrug with a favorable in vivo toxicity profile. *Sci Rep* **2021**, *11* (1), 7114, 10.1038/s41598-021-86551-1.
132. Wang, X.; Tsui, B.; Ramamurthy, G.; Zhang, P.; Meyers, J., et al., Theranostic Agents for Photodynamic Therapy of Prostate Cancer by Targeting Prostate-Specific Membrane Antigen. *Mol Cancer Ther* **2016**, *15* (8), 1834-1844, 10.1158/1535-7163.MCT-15-0722.
133. Kirby, M.; Hirst, C.; Crawford, E. D., Characterising the castration-resistant prostate cancer population: a systematic review. *Int J Clin Pract* **2011**, *65* (11), 1180-1192, 10.1111/j.1742-1241.2011.02799.x.
134. Berruti, A.; Tucci, M.; Mosca, A.; Tarabuzzi, R.; Gorzegno, G., et al., Predictive factors for skeletal complications in hormone-refractory prostate cancer patients with metastatic bone disease. *Br J Cancer* **2005**, *93* (6), 633-638, 10.1038/sj.bjc.6602767.
135. Inoue, T.; Segawa, T.; Kamba, T.; Yoshimura, K.; Nakamura, E., et al., Prevalence of skeletal complications and their impact on survival of hormone refractory prostate cancer patients in Japan. *Urology* **2009**, *73* (5), 1104-1109, 10.1016/j.urology.2008.07.062.
136. Smith, M. R.; Kabbavar, F.; Saad, F.; Hussain, A.; Gittelman, M. C., et al., Natural history of rising serum prostate-specific antigen in men with castrate nonmetastatic prostate cancer. *J Clin Oncol* **2005**, *23* (13), 2918-2925, 10.1200/JCO.2005.01.529.
137. Milowsky, M. I.; Nanus, D. M.; Kostakoglu, L.; Vallabhajosula, S.; Goldsmith, S. J.; Bander, N. H., Phase I trial of yttrium-90-labeled anti-prostate-specific membrane antigen monoclonal antibody J591 for androgen-independent prostate cancer. *J Clin Oncol* **2004**, *22* (13), 2522-2531, 10.1200/JCO.2004.09.154.
138. Bander, N. H.; Milowsky, M. I.; Nanus, D. M.; Kostakoglu, L.; Vallabhajosula, S.; Goldsmith, S. J., Phase I trial of <sup>177</sup>lutetium-labeled J591, a monoclonal antibody to prostate-specific membrane antigen, in patients with androgen-independent prostate cancer. *J Clin Oncol* **2005**, *23* (21), 4591-4601, 10.1200/JCO.2005.05.160.
139. Foss, C. A.; Mease, R. C.; Fan, H.; Wang, Y.; Ravert, H. T., et al., Radiolabeled small-molecule ligands for prostate-specific membrane antigen: in vivo imaging in experimental models of prostate cancer. *Clin Cancer Res* **2005**, *11* (11), 4022-4028, 10.1158/1078-0432.CCR-04-2690.
140. Barrett, J. A.; Coleman, R. E.; Goldsmith, S. J.; Vallabhajosula, S.; Petry, N. A., et al., First-in-man evaluation of 2 high-affinity PSMA-avid small molecules for imaging prostate cancer. *J Nucl Med* **2013**, *54* (3), 380-387, 10.2967/jnumed.112.111203.
141. Baum, R. P.; Kulkarni, H. R., THERANOSTICS: From Molecular Imaging Using Ga-68 Labeled Tracers and PET/CT to Personalized Radionuclide Therapy - The Bad Berka Experience. *Theranostics* **2012**, *2* (5), 437-447, 10.7150/thno.3645.

142. Turner, J. H., Recent advances in theranostics and challenges for the future. *Br J Radiol* **2018**, *91* (1091), 20170893, 10.1259/bjr.20170893.
143. Yordanova, A.; Eppard, E.; Kurpig, S.; Bundschuh, R. A.; Schonberger, S., et al., Theranostics in nuclear medicine practice. *Onco Targets Ther* **2017**, *10*, 4821-4828, 10.2147/OTT.S140671.
144. Langbein, T.; Weber, W. A.; Eiber, M., Future of Theranostics: An Outlook on Precision Oncology in Nuclear Medicine. *J Nucl Med* **2019**, *60* (Suppl 2), 13S-19S, 10.2967/jnumed.118.220566.
145. Barwick, T.; Murray, I.; Megadmi, H.; Drake, W. M.; Plowman, P. N., et al., Single photon emission computed tomography (SPECT)/computed tomography using Iodine-123 in patients with differentiated thyroid cancer: additional value over whole body planar imaging and SPECT. *Eur J Endocrinol* **2010**, *162* (6), 1131-1139, 10.1530/EJE-09-1023.
146. Wong, K. K.; Zarzhevsky, N.; Cahill, J. M.; Frey, K. A.; Avram, A. M., Incremental value of diagnostic <sup>131</sup>I SPECT/CT fusion imaging in the evaluation of differentiated thyroid carcinoma. *AJR Am J Roentgenol* **2008**, *191* (6), 1785-1794, 10.2214/AJR.08.1218.
147. Van Nostrand, D.; Aiken, M.; Atkins, F.; Moreau, S.; Garcia, C., et al., The utility of radioiodine scans prior to iodine 131 ablation in patients with well-differentiated thyroid cancer. *Thyroid* **2009**, *19* (8), 849-855, 10.1089/thy.2008.0419.
148. Sweeney, D. C.; Johnston, G. S., Radioiodine therapy for thyroid cancer. *Endocrinol Metab Clin North Am* **1995**, *24* (4), 803-839, 10.1016/S0889-8529(18)30022-7.
149. Tuttle, R. M.; Ahuja, S.; Avram, A. M.; Bernet, V. J.; Bourguet, P., et al., Controversies, Consensus, and Collaboration in the Use of <sup>131</sup>I Therapy in Differentiated Thyroid Cancer: A Joint Statement from the American Thyroid Association, the European Association of Nuclear Medicine, the Society of Nuclear Medicine and Molecular Imaging, and the European Thyroid Association. *Thyroid* **2019**, *29* (4), 461-470, 10.1089/thy.2018.0597.
150. Seidlin, S. M.; Marinelli, L. D.; Oshry, E., Radioactive iodine therapy; effect on functioning metastases of adenocarcinoma of the thyroid. *J Am Med Assoc* **1946**, *132* (14), 838-847, 10.1001/jama.1946.02870490016004.
151. Seidlin, S. M.; Rossman, I.; et al., Radioiodine therapy of metastases from carcinoma of the thyroid; a 6-year progress report. *J Clin Endocrinol Metab* **1949**, *9* (11), 1122-1137, 10.1210/jcem-9-11-1122.
152. Zechmann, C. M.; Afshar-Oromieh, A.; Armor, T.; Stubbs, J. B.; Mier, W., et al., Radiation dosimetry and first therapy results with a <sup>124</sup>I/<sup>131</sup>I-labeled small molecule (MIP-1095) targeting PSMA for prostate cancer therapy. *Eur J Nucl Med Mol Imaging* **2014**, *41* (7), 1280-1292, 10.1007/s00259-014-2713-y.
153. Banerjee, S. R.; Pullambhatla, M.; Foss, C. A.; Nimmagadda, S.; Ferdani, R., et al., <sup>64</sup>Cu-labeled inhibitors of prostate-specific membrane antigen for PET imaging of prostate cancer. *J Med Chem* **2014**, *57* (6), 2657-2669, 10.1021/jm401921j.
154. Xie, F.; Wei, W., [<sup>64</sup>Cu]Cu-ATSM: an emerging theranostic agent for cancer and neuroinflammation. *Eur J Nucl Med Mol Imaging* **2022**, *49*, 3964-3972, 10.1007/s00259-022-05887-6.
155. Qin, C.; Liu, H.; Chen, K.; Hu, X.; Ma, X., et al., Theranostics of malignant melanoma with <sup>64</sup>CuCl<sub>2</sub>. *J Nucl Med* **2014**, *55* (5), 812-817, 10.2967/jnumed.113.133850.
156. Anderson, C. J.; Ferdani, R., Copper-64 radiopharmaceuticals for PET imaging of cancer: advances in preclinical and clinical research. *Cancer Biother Radiopharm* **2009**, *24* (4), 379-393, 10.1089/cbr.2009.0674.
157. Medvedev, D. G.; Mausner, L. F.; Meinken, G. E.; Kurczak, S. O.; Schnakenberg, H., et al., Development of a large scale production of <sup>67</sup>Cu from <sup>68</sup>Zn at the high energy proton accelerator: closing the <sup>68</sup>Zn cycle. *Appl Radiat Isot* **2012**, *70* (3), 423-429, 10.1016/j.apradiso.2011.10.007.
158. Hicks, R. J.; Jackson, P.; Kong, G.; Ware, R. E.; Hofman, M. S., et al., <sup>64</sup>Cu-SARTATE PET Imaging of Patients with Neuroendocrine Tumors Demonstrates High Tumor Uptake and Retention, Potentially Allowing Prospective Dosimetry for Peptide Receptor Radionuclide Therapy. *J Nucl Med* **2019**, *60* (6), 777-785, 10.2967/jnumed.118.217745.
159. Kelly, J. M.; Ponnala, S.; Amor-Coarasa, A.; Zia, N. A.; Nikolopoulou, A., et al., Preclinical Evaluation of a High-Affinity Sarcophagine-Containing PSMA Ligand for <sup>64</sup>Cu/<sup>67</sup>Cu-Based Theranostics in Prostate Cancer. *Mol Pharm* **2020**, *17* (6), 1954-1962, 10.1021/acs.molpharmaceut.0c00060.

160. Keinanen, O.; Fung, K.; Brennan, J. M.; Zia, N.; Harris, M., et al., Harnessing  $^{64}\text{Cu}/^{67}\text{Cu}$  for a theranostic approach to pretargeted radioimmunotherapy. *Proc Natl Acad Sci U S A* **2020**, *117* (45), 28316-28327, 10.1073/pnas.2009960117.
161. Müller, C.; Zhernosekov, K.; Koster, U.; Johnston, K.; Dorrer, H., et al., A unique matched quadruplet of terbium radioisotopes for PET and SPECT and for alpha- and beta- radionuclide therapy: an in vivo proof-of-concept study with a new receptor-targeted folate derivative. *J Nucl Med* **2012**, *53* (12), 1951-1959, 10.2967/jnumed.112.107540.
162. Naskar, N.; Lahiri, S., Theranostic Terbium Radioisotopes: Challenges in Production for Clinical Application. *Front Med (Lausanne)* **2021**, *8*, 675014, 10.3389/fmed.2021.675014.
163. Cavaier, R. F.; Haddad, F.; Sounalet, T.; Stora, T.; Zahi, I., Terbium radionuclides for theranostics applications: a focus on MEDICIS-PROMED. *Physics Procedia* **2017**, *90*, 157-163, 10.1016/j.phpro.2017.09.053.
164. de Jong, M.; Breeman, W. A.; Bernard, B. F.; Rolleman, E. J.; Hofland, L. J., et al., Evaluation in vitro and in rats of  $^{161}\text{Tb}$ -DTPA-octreotide, a somatostatin analogue with potential for intraoperative scanning and radiotherapy. *Eur J Nucl Med* **1995**, *22* (7), 608-616, 10.1007/BF01254561.
165. Beyer, G. J.; Miederer, M.; Vranjes-Duric, S.; Comor, J. J.; Kunzi, G., et al., Targeted alpha therapy in vivo: direct evidence for single cancer cell kill using  $^{149}\text{Tb}$ -rituximab. *Eur J Nucl Med Mol Imaging* **2004**, *31* (4), 547-554, 10.1007/s00259-003-1413-9.
166. Baum, R. P.; Singh, A.; Benesova, M.; Vermeulen, C.; Gnesin, S., et al., Clinical evaluation of the radiolanthanide terbium-152: first-in-human PET/CT with  $^{152}\text{Tb}$ -DOTATOC. *Dalton Trans* **2017**, *46* (42), 14638-14646, 10.1039/c7dt01936j.
167. Müller, C.; Singh, A.; Umbricht, C. A.; Kulkarni, H. R.; Johnston, K., et al., Preclinical investigations and first-in-human application of  $^{152}\text{Tb}$ -PSMA-617 for PET/CT imaging of prostate cancer. *EJNMMI Res* **2019**, *9* (1), 68, 10.1186/s13550-019-0538-1.
168. Baum, R. P.; Singh, A.; Kulkarni, H. R.; Bernhardt, P.; Ryden, T., et al., First-in-Humans Application of  $^{161}\text{Tb}$ : A Feasibility Study Using  $^{161}\text{Tb}$ -DOTATOC. *J Nucl Med* **2021**, *62* (10), 1391-1397, 10.2967/jnumed.120.258376.
169. Banerjee, S.; Pillai, M. R.; Knapp, F. F., Lutetium-177 therapeutic radiopharmaceuticals: linking chemistry, radiochemistry, and practical applications. *Chem Rev* **2015**, *115* (8), 2934-2974, 10.1021/cr500171e.
170. Parus, J. L.; Pawlak, D.; Mikolajczak, R.; Duatti, A., Chemistry and bifunctional chelating agents for binding  $^{177}\text{Lu}$ . *Curr Radiopharm* **2015**, *8* (2), 86-94, 10.2174/1874471008666150312160440.
171. Lassmann, M.; Eberlein, U., Radiation Dosimetry Aspects of  $^{177}\text{Lu}$ . *Curr Radiopharm* **2015**, *8* (2), 139-144, 10.2174/1874471008666150313104212.
172. Kratochwil, C.; Bruchertseifer, F.; Giesel, F. L.; Weis, M.; Verburg, F. A., et al.,  $^{225}\text{Ac}$ -PSMA-617 for PSMA-Targeted alpha-Radiation Therapy of Metastatic Castration-Resistant Prostate Cancer. *J Nucl Med* **2016**, *57* (12), 1941-1944, 10.2967/jnumed.116.178673.
173. Ballal, S.; Yadav, M. P.; Bal, C.; Sahoo, R. K.; Tripathi, M., Broadening horizons with  $^{225}\text{Ac}$ -DOTATATE targeted alpha therapy for gastroenteropancreatic neuroendocrine tumour patients stable or refractory to  $^{177}\text{Lu}$ -DOTATATE PRRT: first clinical experience on the efficacy and safety. *Eur J Nucl Med Mol Imaging* **2020**, *47* (4), 934-946, 10.1007/s00259-019-04567-2.
174. Zacherl, M. J.; Gildehaus, F. J.; Mittlmeier, L.; Boning, G.; Gosewisch, A., et al., First Clinical Results for PSMA-Targeted alpha-Therapy Using  $^{225}\text{Ac}$ -PSMA-I&T in Advanced-mCRPC Patients. *J Nucl Med* **2021**, *62* (5), 669-674, 10.2967/jnumed.120.251017.
175. Poeppel, T. D.; Binse, I.; Petersenn, S.; Lahner, H.; Schott, M., et al.,  $^{68}\text{Ga}$ -DOTATOC versus  $^{68}\text{Ga}$ -DOTATATE PET/CT in functional imaging of neuroendocrine tumors. *J Nucl Med* **2011**, *52* (12), 1864-1870, 10.2967/jnumed.111.091165.
176. Bodei, L.; Cremonesi, M.; Grana, C. M.; Fazio, N.; Iodice, S., et al., Peptide receptor radionuclide therapy with  $^{177}\text{Lu}$ -DOTATATE: the IEO phase I-II study. *Eur J Nucl Med Mol Imaging* **2011**, *38* (12), 2125-2135, 10.1007/s00259-011-1902-1.
177. Heinzl, A.; Boghos, D.; Mottaghy, F. M.; Gaertner, F.; Essler, M., et al.,  $^{68}\text{Ga}$ -PSMA PET/CT for monitoring response to  $^{177}\text{Lu}$ -PSMA-617 radioligand therapy in patients with metastatic castration-resistant prostate cancer. *Eur J Nucl Med Mol Imaging* **2019**, *46* (5), 1054-1062, 10.1007/s00259-019-4258-6.
178. Heppeler, A.; Froidevaux, S.; Mäcke, H. R.; Jermann, E.; Béhé, M., et al., Radiometal-labelled macrocyclic chelator-derivatised somatostatin analogue with superb tumour-targeting properties and

- potential for receptor-mediated internal radiotherapy. *Chem Eur J* **1999**, *5* (7), 1974-1981, 10.1002/(SICI)1521-3765(19990702)5:7<1974::AID-CHEM1974>3.0.CO;2-X.
179. Umbricht, C. A.; Benesova, M.; Schmid, R. M.; Turler, A.; Schibli, R., et al., <sup>44</sup>Sc-PSMA-617 for radiotheragnostics in tandem with <sup>177</sup>Lu-PSMA-617-preclinical investigations in comparison with <sup>68</sup>Ga-PSMA-11 and <sup>68</sup>Ga-PSMA-617. *EJNMMI Res* **2017**, *7* (1), 9, 10.1186/s13550-017-0257-4.
180. Iovkova, L.; Wangler, B.; Schirmmayer, E.; Schirmmayer, R.; Quandt, G., et al., para-Functionalized aryl-di-tert-butylfluorosilanes as potential labeling synthons for <sup>18</sup>F radiopharmaceuticals. *Chemistry* **2009**, *15* (9), 2140-2147, 10.1002/chem.200802266.
181. Bernard-Gauthier, V.; Wangler, C.; Schirmmayer, E.; Kostikov, A.; Jurkschat, K., et al., <sup>18</sup>F-labeled silicon-based fluoride acceptors: potential opportunities for novel positron emitting radiopharmaceuticals. *Biomed Res Int* **2014**, *2014*, 454503, 10.1155/2014/454503.
182. Wurzer, A.; Di Carlo, D.; Schmidt, A.; Beck, R.; Eiber, M., et al., Radiohybrid Ligands: A Novel Tracer Concept Exemplified by <sup>18</sup>F- or <sup>68</sup>Ga-Labeled rhPSMA Inhibitors. *J Nucl Med* **2020**, *61* (5), 735-742, 10.2967/jnumed.119.234922.
183. Wurzer, A.; Parzinger, M.; Konrad, M.; Beck, R.; Gunther, T., et al., Preclinical comparison of four [<sup>18</sup>F, <sup>nat</sup>Ga]rhPSMA-7 isomers: influence of the stereoconfiguration on pharmacokinetics. *EJNMMI Res* **2020**, *10* (1), 149, 10.1186/s13550-020-00740-z.
184. Eiber, M.; Kroenke, M.; Wurzer, A.; Ulbrich, L.; Jooss, L., et al., <sup>18</sup>F-rhPSMA-7 PET for the Detection of Biochemical Recurrence of Prostate Cancer After Radical Prostatectomy. *J Nucl Med* **2020**, *61* (5), 696-701, 10.2967/jnumed.119.234914.
185. Kroenke, M.; Mirzoyan, L.; Horn, T.; Peecken, J. C.; Wurzer, A., et al., Matched-Pair Comparison of <sup>68</sup>Ga-PSMA-11 and <sup>18</sup>F-rhPSMA-7 PET/CT in Patients with Primary and Biochemical Recurrence of Prostate Cancer: Frequency of Non-Tumor-Related Uptake and Tumor Positivity. *J Nucl Med* **2021**, *62* (8), 1082-1088, 10.2967/jnumed.120.251447.
186. Kroenke, M.; Wurzer, A.; Schwamborn, K.; Ulbrich, L.; Jooss, L., et al., Histologically Confirmed Diagnostic Efficacy of <sup>18</sup>F-rhPSMA-7 PET for N-Staging of Patients with Primary High-Risk Prostate Cancer. *J Nucl Med* **2020**, *61* (5), 710-715, 10.2967/jnumed.119.234906.
187. Langbein, T.; Wang, H.; Rauscher, I.; Kronke, M.; Knorr, K., et al., Utility of <sup>18</sup>F-rhPSMA-7.3 positron emission tomography for imaging of primary prostate cancer and pre-operative efficacy in N-staging of unfavorable intermediate to very high-risk patients validated by histopathology. *J Nucl Med* **2022**, 10.2967/jnumed.121.263440.
188. Kesch, C.; Kratochwil, C.; Mier, W.; Kopka, K.; Giesel, F. L., <sup>68</sup>Ga or <sup>18</sup>F for Prostate Cancer Imaging? *J Nucl Med* **2017**, *58* (5), 687-688, 10.2967/jnumed.117.190157.
189. Sanchez-Crespo, A., Comparison of Gallium-68 and Fluorine-18 imaging characteristics in positron emission tomography. *Appl Radiat Isot* **2013**, *76*, 55-62, 10.1016/j.apradiso.2012.06.034.
190. Benesova, M.; Schafer, M.; Bauder-Wust, U.; Afshar-Oromieh, A.; Kratochwil, C., et al., Preclinical Evaluation of a Tailor-Made DOTA-Conjugated PSMA Inhibitor with Optimized Linker Moiety for Imaging and Endoradiotherapy of Prostate Cancer. *J Nucl Med* **2015**, *56* (6), 914-920, 10.2967/jnumed.114.147413.
191. Weineisen, M.; Schottelius, M.; Simecek, J.; Baum, R. P.; Yildiz, A., et al., <sup>68</sup>Ga- and <sup>177</sup>Lu-Labeled PSMA I&T: Optimization of a PSMA-Targeted Theranostic Concept and First Proof-of-Concept Human Studies. *J Nucl Med* **2015**, *56* (8), 1169-1176, 10.2967/jnumed.115.158550.
192. Eder, M.; Schafer, M.; Bauder-Wust, U.; Hull, W. E.; Wangler, C., et al., <sup>68</sup>Ga-complex lipophilicity and the targeting property of a urea-based PSMA inhibitor for PET imaging. *Bioconjug Chem* **2012**, *23* (4), 688-697, 10.1021/bc200279b.
193. Afshar-Oromieh, A.; Zechmann, C. M.; Malcher, A.; Eder, M.; Eisenhut, M., et al., Comparison of PET imaging with a <sup>68</sup>Ga-labelled PSMA ligand and <sup>18</sup>F-choline-based PET/CT for the diagnosis of recurrent prostate cancer. *Eur J Nucl Med Mol Imaging* **2014**, *41* (1), 11-20, 10.1007/s00259-013-2525-5.
194. Eder, M.; Kopka, K.; Schäfer, M.; Bauder-Wüst, U.; Haberkorn, U. LABELED INHIBITORS OF PROSTATE SPECIFIC MEMBRANE ANTIGEN (PSMA), THEIR USE AS IMAGING AGENTS AND PHARMACEUTICAL AGENTS FOR THE TREATMENT OF PROSTATE CANCER. *WO2015055318A1*, **2015**.
195. Banerjee, S. R.; Pullambhatla, M.; Byun, Y.; Nimmagadda, S.; Green, G., et al., <sup>68</sup>Ga-labeled inhibitors of prostate-specific membrane antigen (PSMA) for imaging prostate cancer. *J Med Chem* **2010**, *53* (14), 5333-5341, 10.1021/jm100623e.

196. Weineisen, M.; Simecek, J.; Schottelius, M.; Schwaiger, M.; Wester, H. J., Synthesis and preclinical evaluation of DOTAGA-conjugated PSMA ligands for functional imaging and endoradiotherapy of prostate cancer. *EJNMMI Res* **2014**, *4* (1), 63, 10.1186/s13550-014-0063-1.
197. Kulkarni, H. R.; Singh, A.; Schuchardt, C.; Niepsch, K.; Sayeg, M., et al., PSMA-Based Radioligand Therapy for Metastatic Castration-Resistant Prostate Cancer: The Bad Berka Experience Since 2013. *J Nucl Med* **2016**, *57* (Suppl 3), 97S-104S, 10.2967/jnumed.115.170167.
198. Müller, C.; Umbricht, C. A.; Gracheva, N.; Tschan, V. J.; Pellegrini, G., et al., Terbium-161 for PSMA-targeted radionuclide therapy of prostate cancer. *Eur J Nucl Med Mol Imaging* **2019**, *46* (9), 1919-1930, 10.1007/s00259-019-04345-0.
199. Meier, J.; Bhuiyan, M.; Zhang, H.; Tsai, H.-M.; Berens, L., et al., Development of  $^{43}\text{Sc}/^{47}\text{Sc}$ -PSMA-617 as Theranostics for Prostate Cancer: Preliminary Cellular and Animal Studies. *J Nucl Med* **2022**, *63* (Suppl 2), 2895.
200. Nambisan, A.; Khan, M.; Babeker, H.; Ketchemen, J. P.; Tikum, A., et al., Preclinical evaluation of  $^{67}\text{Cu}$ -PSMA-617 theranostic as an alternative to  $^{177}\text{Lu}$ -PSMA-617 for prostate cancer. *J Nucl Med* **2022**, *63* (Suppl 2), 4024.
201. Grubmüller, B.; Baum, R. P.; Capasso, E.; Singh, A.; Ahmadi, Y., et al.,  $^{64}\text{Cu}$ -PSMA-617 PET/CT Imaging of Prostate Adenocarcinoma: First In-Human Studies. *Cancer Biother Radiopharm* **2016**, *31* (8), 277-286, 10.1089/cbr.2015.1964.
202. Rathke, H.; Flechsig, P.; Mier, W.; Bronzel, M.; Mavriopoulou, E., et al., Dosimetry Estimate and Initial Clinical Experience with  $^{90}\text{Y}$ -PSMA-617. *J Nucl Med* **2019**, *60* (6), 806-811, 10.2967/jnumed.118.218917.
203. O'Donoghue, J. A.; Bardies, M.; Wheldon, T. E., Relationships between tumor size and curability for uniformly targeted therapy with beta-emitting radionuclides. *J Nucl Med* **1995**, *36* (10), 1902-1909.
204. Enger, S. A.; Hartman, T.; Carlsson, J.; Lundqvist, H., Cross-fire doses from beta-emitting radionuclides in targeted radiotherapy. A theoretical study based on experimentally measured tumor characteristics. *Phys Med Biol* **2008**, *53* (7), 1909-1920, 10.1088/0031-9155/53/7/007.
205. Rahbar, K.; Ahmadzadehfar, H.; Kratochwil, C.; Haberkorn, U.; Schafers, M., et al., German Multicenter Study Investigating  $^{177}\text{Lu}$ -PSMA-617 Radioligand Therapy in Advanced Prostate Cancer Patients. *J Nucl Med* **2017**, *58* (1), 85-90, 10.2967/jnumed.116.183194.
206. Hofman, M. S.; Violet, J.; Hicks, R. J.; Ferdinandus, J.; Thang, S. P., et al., [ $^{177}\text{Lu}$ ]-PSMA-617 radionuclide treatment in patients with metastatic castration-resistant prostate cancer (LuPSMA trial): a single-centre, single-arm, phase 2 study. *Lancet Oncol* **2018**, *19* (6), 825-833, 10.1016/S1470-2045(18)30198-0.
207. Fendler, W. P.; Reinhardt, S.; Ilhan, H.; Delker, A.; Boning, G., et al., Preliminary experience with dosimetry, response and patient reported outcome after  $^{177}\text{Lu}$ -PSMA-617 therapy for metastatic castration-resistant prostate cancer. *Oncotarget* **2017**, *8* (2), 3581-3590, 10.18632/oncotarget.12240.
208. Kratochwil, C.; Giesel, F. L.; Stefanova, M.; Benesova, M.; Bronzel, M., et al., PSMA-Targeted Radionuclide Therapy of Metastatic Castration-Resistant Prostate Cancer with  $^{177}\text{Lu}$ -Labeled PSMA-617. *J Nucl Med* **2016**, *57* (8), 1170-1176, 10.2967/jnumed.115.171397.
209. Violet, J.; Jackson, P.; Ferdinandus, J.; Sandhu, S.; Akhurst, T., et al., Dosimetry of  $^{177}\text{Lu}$ -PSMA-617 in Metastatic Castration-Resistant Prostate Cancer: Correlations Between Pretherapeutic Imaging and Whole-Body Tumor Dosimetry with Treatment Outcomes. *J Nucl Med* **2019**, *60* (4), 517-523, 10.2967/jnumed.118.219352.
210. Delker, A.; Fendler, W. P.; Kratochwil, C.; Brungraf, A.; Gosewisch, A., et al., Dosimetry for  $^{177}\text{Lu}$ -DKFZ-PSMA-617: a new radiopharmaceutical for the treatment of metastatic prostate cancer. *Eur J Nucl Med Mol Imaging* **2016**, *43* (1), 42-51, 10.1007/s00259-015-3174-7.
211. Kramer, V.; Fernandez, R.; Lehnert, W.; Jimenez-Franco, L. D.; Soza-Ried, C., et al., Biodistribution and dosimetry of a single dose of albumin-binding ligand [ $^{177}\text{Lu}$ ]Lu-PSMA-ALB-56 in patients with mCRPC. *Eur J Nucl Med Mol Imaging* **2021**, *48*, 893-903, 10.1007/s00259-020-05022-3.
212. Rahbar, K.; Bode, A.; Weckesser, M.; Avramovic, N.; Claesener, M., et al., Radioligand Therapy With  $^{177}\text{Lu}$ -PSMA-617 as A Novel Therapeutic Option in Patients With Metastatic Castration Resistant Prostate Cancer. *Clin Nucl Med* **2016**, *41* (7), 522-528, 10.1097/RLU.0000000000001240.
213. Scarpa, L.; Buxbaum, S.; Kendler, D.; Fink, K.; Bektic, J., et al., The  $^{68}\text{Ga}/^{177}\text{Lu}$  theragnostic concept in PSMA targeting of castration-resistant prostate cancer: correlation of SUVmax values and

- absorbed dose estimates. *Eur J Nucl Med Mol Imaging* **2017**, *44* (5), 788-800, 10.1007/s00259-016-3609-9.
214. Emami, B.; Lyman, J.; Brown, A.; Coia, L.; Goitein, M., et al., Tolerance of normal tissue to therapeutic irradiation. *Int J Radiat Oncol Biol Phys* **1991**, *21* (1), 109-122, 10.1016/0360-3016(91)90171-y.
215. Ahmadzadehfar, H.; Eppard, E.; Kurpig, S.; Fimmers, R.; Yordanova, A., et al., Therapeutic response and side effects of repeated radioligand therapy with <sup>177</sup>Lu-PSMA-DKFZ-617 of castrate-resistant metastatic prostate cancer. *Oncotarget* **2016**, *7* (11), 12477-12488, 10.18632/oncotarget.7245.
216. Okamoto, S.; Thieme, A.; Allmann, J.; D'Alessandria, C.; Maurer, T., et al., Radiation Dosimetry for <sup>177</sup>Lu-PSMA I&T in Metastatic Castration-Resistant Prostate Cancer: Absorbed Dose in Normal Organs and Tumor Lesions. *J Nucl Med* **2017**, *58* (3), 445-450, 10.2967/jnumed.116.178483.
217. Baum, R. P.; Kulkarni, H. R.; Schuchardt, C.; Singh, A.; Wirtz, M., et al., <sup>177</sup>Lu-Labeled Prostate-Specific Membrane Antigen Radioligand Therapy of Metastatic Castration-Resistant Prostate Cancer: Safety and Efficacy. *J Nucl Med* **2016**, *57* (7), 1006-1013, 10.2967/jnumed.115.168443.
218. Karimzadeh, A.; Heck, M.; Tauber, R.; Knorr, K.; Haller, B., et al., <sup>177</sup>Lu-PSMA-I&T for treatment of metastatic castration resistant prostate cancer: prognostic value of scintigraphic and clinical biomarkers. *J Nucl Med* **2023**, *64* (3), 402-409, 10.2967/jnumed.122.264402.
219. Rahbar, K.; Boegemann, M.; Yordanova, A.; Eveslage, M.; Schafers, M., et al., PSMA targeted radioligandtherapy in metastatic castration resistant prostate cancer after chemotherapy, abiraterone and/or enzalutamide. A retrospective analysis of overall survival. *Eur J Nucl Med Mol Imaging* **2018**, *45* (1), 12-19, 10.1007/s00259-017-3848-4.
220. FDA approves Pluvicto for metastatic castration-resistant prostate cancer. <https://www.fda.gov/drugs/resources-information-approved-drugs/fda-approves-pluvicto-metastatic-castration-resistant-prostate-cancer> (accessed 8 March 2023).
221. Sartor, O.; de Bono, J.; Chi, K. N.; Fizazi, K.; Herrmann, K., et al., Lutetium-177-PSMA-617 for Metastatic Castration-Resistant Prostate Cancer. *N Engl J Med* **2021**, *385* (12), 1091-1103, 10.1056/NEJMoa2107322.
222. Rahbar, K.; Bodei, L.; Morris, M. J., Is the Vision of Radioligand Therapy for Prostate Cancer Becoming a Reality? An Overview of the Phase III VISION Trial and Its Importance for the Future of Theranostics. *J Nucl Med* **2019**, *60* (11), 1504-1506, 10.2967/jnumed.119.234054.
223. Kassis, A. I., Therapeutic radionuclides: biophysical and radiobiologic principles. *Semin Nucl Med* **2008**, *38* (5), 358-366, 10.1053/j.semnuclmed.2008.05.002.
224. Navalkisoor, S.; Grossman, A., Targeted Alpha Particle Therapy for Neuroendocrine Tumours: The Next Generation of Peptide Receptor Radionuclide Therapy. *Neuroendocrinology* **2019**, *108* (3), 256-264, 10.1159/000494760.
225. Dodson, H.; Wheatley, S. P.; Morrison, C. G., Involvement of centrosome amplification in radiation-induced mitotic catastrophe. *Cell Cycle* **2007**, *6* (3), 364-370, 10.4161/cc.6.3.3834.
226. Sgouros, G.; Roeske, J. C.; McDevitt, M. R.; Palm, S.; Allen, B. J., et al., MIRD Pamphlet No. 22 (abridged): radiobiology and dosimetry of alpha-particle emitters for targeted radionuclide therapy. *J Nucl Med* **2010**, *51* (2), 311-328, 10.2967/jnumed.108.058651.
227. Kratochwil, C.; Bruchertseifer, F.; Rathke, H.; Hohenfellner, M.; Giesel, F. L., et al., Targeted alpha-Therapy of Metastatic Castration-Resistant Prostate Cancer with <sup>225</sup>Ac-PSMA-617: Swimmer-Plot Analysis Suggests Efficacy Regarding Duration of Tumor Control. *J Nucl Med* **2018**, *59* (5), 795-802, 10.2967/jnumed.117.203539.
228. Sathekge, M.; Bruchertseifer, F.; Knoesen, O.; Reyneke, F.; Lawal, I., et al., <sup>225</sup>Ac-PSMA-617 in chemotherapy-naïve patients with advanced prostate cancer: a pilot study. *Eur J Nucl Med Mol Imaging* **2019**, *46* (1), 129-138, 10.1007/s00259-018-4167-0.
229. Gosewisch, A.; Schleske, M.; Gildehaus, F. J.; Berg, I.; Kaiser, L., et al., Image-based dosimetry for <sup>225</sup>Ac-PSMA-I&T therapy using quantitative SPECT. *Eur J Nucl Med Mol Imaging* **2021**, *48* (4), 1260-1261, 10.1007/s00259-020-05024-1.
230. Rathke, H.; Bruchertseifer, F.; Kratochwil, C.; Keller, H.; Giesel, F. L., et al., First patient exceeding 5-year complete remission after <sup>225</sup>Ac-PSMA-TAT. *Eur J Nucl Med Mol Imaging* **2021**, *48* (1), 311-312, 10.1007/s00259-020-04875-y.
231. Feuerecker, B.; Tauber, R.; Knorr, K.; Heck, M.; Beheshti, A., et al., Activity and Adverse Events of Actinium-225-PSMA-617 in Advanced Metastatic Castration-resistant Prostate Cancer After Failure of Lutetium-177-PSMA. *Eur Urol* **2021**, *79* (3), 343-350, 10.1016/j.eururo.2020.11.013.

232. Heynickx, N.; Herrmann, K.; Vermeulen, K.; Baatout, S.; Aerts, A., The salivary glands as a dose limiting organ of PSMA- targeted radionuclide therapy: A review of the lessons learnt so far. *Nucl Med Biol* **2021**, 98-99, 30-39, 10.1016/j.nucmedbio.2021.04.003.
233. Felber, V. B.; Valentin, M. A.; Wester, H. J., Design of PSMA ligands with modifications at the inhibitor part: an approach to reduce the salivary gland uptake of radiolabeled PSMA inhibitors? *EJNMMI Radiopharm Chem* **2021**, 6 (1), 10, 10.1186/s41181-021-00124-1.
234. Duan, X.; Liu, F.; Kwon, H.; Byun, Y.; Minn, I., et al., (S)-3-(Carboxyformamido)-2-(3-(carboxymethyl)ureido)propanoic Acid as a Novel PSMA Targeting Scaffold for Prostate Cancer Imaging. *J Med Chem* **2020**, 63 (7), 3563-3576, 10.1021/acs.jmedchem.9b02031.
235. Duan, X.; Cao, Z.; Zhu, H.; Liu, C.; Zhang, X., et al., <sup>68</sup>Ga-labeled ODAP-Urea-based PSMA agents in prostate cancer: first-in-human imaging of an optimized agent. *Eur J Nucl Med Mol Imaging* **2022**, 49 (3), 1030-1040, 10.1007/s00259-021-05486-x.
236. Kuo, H. T.; Lin, K. S.; Zhang, Z.; Zhang, C.; Merckens, H., et al., What a difference a methylene makes: replacing Glu with Asp or Aad in the Lys-urea-Glu pharmacophore of PSMA-targeting radioligands to reduce kidney and salivary gland uptake. *Theranostics* **2022**, 12 (14), 6179-6188, 10.7150/thno.76571.
237. Carlos Dos Santos, J.; Beijer, B.; Bauder-Wust, U.; Schafer, M.; Leotta, K., et al., Development of Novel PSMA Ligands for Imaging and Therapy with Copper Isotopes. *J Nucl Med* **2020**, 61 (1), 70-79, 10.2967/jnumed.119.229054.
238. Kelly, J. M.; Amor-Coarasa, A.; Ponnala, S.; Nikolopoulou, A.; Williams, C., Jr., et al., A Single Dose of <sup>225</sup>Ac-RPS-074 Induces a Complete Tumor Response in an LNCaP Xenograft Model. *J Nucl Med* **2019**, 60 (5), 649-655, 10.2967/jnumed.118.219592.
239. Li, L.; Jaraquemada-Pelaez, M. G.; Kuo, H. T.; Merckens, H.; Choudhary, N., et al., Functionally Versatile and Highly Stable Chelator for <sup>111</sup>In and <sup>177</sup>Lu: Proof-of-Principle Prostate-Specific Membrane Antigen Targeting. *Bioconjug Chem* **2019**, 30 (5), 1539-1553, 10.1021/acs.bioconjchem.9b00225.
240. Abou, D. S.; Thiele, N. A.; Gutsche, N. T.; Villmer, A.; Zhang, H., et al., Towards the stable chelation of radium for biomedical applications with an 18-membered macrocyclic ligand. *Chem Sci* **2021**, 12 (10), 3733-3742, 10.1039/d0sc06867e.
241. Eppard, E.; de la Fuente, A.; Benesova, M.; Khawar, A.; Bundschuh, R. A., et al., Clinical Translation and First In-Human Use of [<sup>44</sup>Sc]Sc-PSMA-617 for PET Imaging of Metastasized Castrate-Resistant Prostate Cancer. *Theranostics* **2017**, 7 (18), 4359-4369, 10.7150/thno.20586.
242. Plechanovova, A.; Byun, Y.; Alquicer, G.; Skultetyova, L.; Mlcochova, P., et al., Novel substrate-based inhibitors of human glutamate carboxypeptidase II with enhanced lipophilicity. *J Med Chem* **2011**, 54 (21), 7535-7546, 10.1021/jm200807m.
243. Wang, H.; Byun, Y.; Barinka, C.; Pullambhatla, M.; Bhang, H. E., et al., Bioisosterism of urea-based GCPII inhibitors: Synthesis and structure-activity relationship studies. *Bioorg Med Chem Lett* **2010**, 20 (1), 392-397, 10.1016/j.bmcl.2009.10.061.
244. Banerjee, S. R.; Kumar, V.; Lisok, A.; Chen, J.; Minn, I., et al., <sup>177</sup>Lu-labeled low-molecular-weight agents for PSMA-targeted radiopharmaceutical therapy. *Eur J Nucl Med Mol Imaging* **2019**, 46 (12), 2545-2557, 10.1007/s00259-019-04434-0.
245. Dos Santos, J. C.; Schafer, M.; Bauder-Wust, U.; Beijer, B.; Eder, M., et al., Refined Chelator Spacer Moieties Ameliorate the Pharmacokinetics of PSMA-617. *Front Chem* **2022**, 10, 898692, 10.3389/fchem.2022.898692.
246. Wang, Z.; Tian, R.; Niu, G.; Ma, Y.; Lang, L., et al., Single Low-Dose Injection of Evans Blue Modified PSMA-617 Radioligand Therapy Eliminates Prostate-Specific Membrane Antigen Positive Tumors. *Bioconjug Chem* **2018**, 29 (9), 3213-3221, 10.1021/acs.bioconjchem.8b00556.
247. Umbricht, C. A.; Benesova, M.; Schibli, R.; Muller, C., Preclinical Development of Novel PSMA-Targeting Radioligands: Modulation of Albumin-Binding Properties To Improve Prostate Cancer Therapy. *Mol Pharm* **2018**, 15 (6), 2297-2306, 10.1021/acs.molpharmaceut.8b00152.
248. Zang, J.; Fan, X.; Wang, H.; Liu, Q.; Wang, J., et al., First-in-human study of <sup>177</sup>Lu-EB-PSMA-617 in patients with metastatic castration-resistant prostate cancer. *Eur J Nucl Med Mol Imaging* **2019**, 46 (1), 148-158, 10.1007/s00259-018-4096-y.
249. Mariani, M. F.; Fugazza, L.; Chicco, D.; Pomper, M. G.; Ray, S. PROSTATE SPECIFIC MEMBRANE ANTIGEN (PSMA) LIGANDS AND USES THEREOF. *WO2021001360A1*, **2021**.

250. Feuerecker, B.; Chantadisai, M.; Allmann, A.; Tauber, R.; Allmann, J., et al., Pretherapeutic Comparative Dosimetry of  $^{177}\text{Lu}$ -rhPSMA-7.3 and  $^{177}\text{Lu}$ -PSMA I&T in Patients with Metastatic Castration-Resistant Prostate Cancer. *J Nucl Med* **2022**, *63* (6), 833-839, 10.2967/jnumed.121.262671.
251. Selverstone, B.; Sweet, W. H.; Robinson, C. V., The clinical use of radioactive phosphorus in the surgery of brain tumors. *Ann Surg* **1949**, *130* (4), 643-651.
252. Aitken, D. R.; Hinkle, G. H.; Thurston, M. O.; Tuttle, S. E.; Martin, D. T., et al., A gamma-detecting probe for radioimmune detection of CEA-producing tumors. Successful experimental use and clinical case report. *Dis Colon Rectum* **1984**, *27* (5), 279-282, 10.1007/BF02555625.
253. Pijpers, R.; Collet, G. J.; Meijer, S.; Hoekstra, O. S., The impact of dynamic lymphoscintigraphy and gamma probe guidance on sentinel node biopsy in melanoma. *Eur J Nucl Med* **1995**, *22* (11), 1238-1241, 10.1007/BF00801606.
254. Kapteijn, B. A.; Nieweg, O. E.; Muller, S. H.; Liem, I. H.; Hoefnagel, C. A., et al., Validation of gamma probe detection of the sentinel node in melanoma. *J Nucl Med* **1997**, *38* (3), 362-366.
255. Casara, D.; Rubello, D.; Piotta, A.; Pelizzo, M. R.,  $^{99\text{m}}\text{Tc}$ -MIBI radio-guided minimally invasive parathyroid surgery planned on the basis of a preoperative combined  $^{99\text{m}}\text{Tc}$ -pertechnetate/ $^{99\text{m}}\text{Tc}$ -MIBI and ultrasound imaging protocol. *Eur J Nucl Med* **2000**, *27* (9), 1300-1304, 10.1007/s002590000297.
256. Gulec, S. A.; Baum, R., Radio-guided surgery in neuroendocrine tumors. *J Surg Oncol* **2007**, *96* (4), 309-315, 10.1002/jso.20868.
257. Povoski, S. P.; Neff, R. L.; Mojzisek, C. M.; O'Malley, D. M.; Hinkle, G. H., et al., A comprehensive overview of radioguided surgery using gamma detection probe technology. *World J Surg Oncol* **2009**, *7*, 11, 10.1186/1477-7819-7-11.
258. Maurer, T.; Weirich, G.; Schottelius, M.; Weineisen, M.; Frisch, B., et al., Prostate-specific membrane antigen-radioguided surgery for metastatic lymph nodes in prostate cancer. *Eur Urol* **2015**, *68* (3), 530-534, 10.1016/j.eururo.2015.04.034.
259. Maurer, T.; Robu, S.; Schottelius, M.; Schwamborn, K.; Rauscher, I., et al.,  $^{99\text{m}}\text{Tc}$ -Technetium-based Prostate-specific Membrane Antigen-radioguided Surgery in Recurrent Prostate Cancer. *Eur Urol* **2019**, *75* (4), 659-666, 10.1016/j.eururo.2018.03.013.
260. Schottelius, M.; Wirtz, M.; Eiber, M.; Maurer, T.; Wester, H. J., [ $^{111}\text{In}$ ]PSMA-I&T: expanding the spectrum of PSMA-I&T applications towards SPECT and radioguided surgery. *EJNMMI Res* **2015**, *5* (1), 68, 10.1186/s13550-015-0147-6.
261. Papagiannopoulou, D., Technetium-99m radiochemistry for pharmaceutical applications. *J Labelled Comp Radiopharm* **2017**, *60* (11), 502-520, 10.1002/jlcr.3531.
262. Eckelman, W. C., Unparalleled contribution of technetium-99m to medicine over 5 decades. *JACC Cardiovasc Imaging* **2009**, *2* (3), 364-368, 10.1016/j.jcmg.2008.12.013.
263. Robu, S.; Schottelius, M.; Eiber, M.; Maurer, T.; Gschwend, J., et al., Preclinical Evaluation and First Patient Application of  $^{99\text{m}}\text{Tc}$ -PSMA-I&S for SPECT Imaging and Radioguided Surgery in Prostate Cancer. *J Nucl Med* **2017**, *58* (2), 235-242, 10.2967/jnumed.116.178939.
264. Horn, T.; Kronke, M.; Rauscher, I.; Haller, B.; Robu, S., et al., Single Lesion on Prostate-specific Membrane Antigen-ligand Positron Emission Tomography and Low Prostate-specific Antigen Are Prognostic Factors for a Favorable Biochemical Response to Prostate-specific Membrane Antigen-targeted Radioguided Surgery in Recurrent Prostate Cancer. *Eur Urol* **2019**, *76* (4), 517-523, 10.1016/j.eururo.2019.03.045.
265. Knipper, S.; Tilki, D.; Mansholt, J.; Berliner, C.; Bernreuther, C., et al., Metastases-yield and Prostate-specific Antigen Kinetics Following Salvage Lymph Node Dissection for Prostate Cancer: A Comparison Between Conventional Surgical Approach and Prostate-specific Membrane Antigen-radioguided Surgery. *Eur Urol Focus* **2019**, *5* (1), 50-53, 10.1016/j.euf.2018.09.014.
266. Jeschke, S.; Beri, A.; Grull, M.; Ziegerhofer, J.; Prammer, P., et al., Laparoscopic radioisotope-guided sentinel lymph node dissection in staging of prostate cancer. *Eur Urol* **2008**, *53* (1), 126-132, 10.1016/j.eururo.2007.03.064.
267. de Barros, H. A.; van Oosterom, M. N.; Donswijk, M. L.; Hendriks, J.; Vis, A. N., et al., Robot-assisted Prostate-specific Membrane Antigen-radioguided Salvage Surgery in Recurrent Prostate Cancer Using a DROP-IN Gamma Probe: The First Prospective Feasibility Study. *Eur Urol* **2022**, *82* (1), 97-105, 10.1016/j.eururo.2022.03.002.
268. van Oosterom, M. N.; Simon, H.; Mengus, L.; Welling, M. M.; van der Poel, H. G., et al., Revolutionizing (robot-assisted) laparoscopic gamma tracing using a drop-in gamma probe technology. *Am J Nucl Med Mol Imaging* **2016**, *6* (1), 1-17.

269. Meershoek, P.; van Oosterom, M. N.; Simon, H.; Mengus, L.; Maurer, T., et al., Robot-assisted laparoscopic surgery using DROP-IN radioguidance: first-in-human translation. *Eur J Nucl Med Mol Imaging* **2019**, *46* (1), 49-53, 10.1007/s00259-018-4095-z.
270. Azargoshasb, S.; van Alphen, S.; Slof, L. J.; Rosiello, G.; Puliatti, S., et al., The Click-On gamma probe, a second-generation tethered robotic gamma probe that improves dexterity and surgical decision-making. *Eur J Nucl Med Mol Imaging* **2021**, *48* (13), 4142-4151, 10.1007/s00259-021-05387-z.
271. Koehler, D.; Sauer, M.; Klutmann, S.; Apostolova, I.; Lehnert, W., et al., Feasibility of <sup>99m</sup>Tc-MIP-1404 for SPECT/CT imaging and subsequent PSMA-radioguided surgery in early biochemical recurrent prostate cancer: a case series of 9 patients. *J Nucl Med* **2022**, 10.2967/jnumed.122.263892.
272. Vallabhajosula, S.; Nikolopoulou, A.; Babich, J. W.; Osborne, J. R.; Tagawa, S. T., et al., <sup>99m</sup>Tc-labeled small-molecule inhibitors of prostate-specific membrane antigen: pharmacokinetics and biodistribution studies in healthy subjects and patients with metastatic prostate cancer. *J Nucl Med* **2014**, *55* (11), 1791-1798, 10.2967/jnumed.114.140426.
273. Urban, S.; Meyer, C.; Dahlbom, M.; Farkas, I.; Sipka, G., et al., Radiation Dosimetry of <sup>99m</sup>Tc-PSMA I&S: A Single-Center Prospective Study. *J Nucl Med* **2021**, *62* (8), 1075-1081, 10.2967/jnumed.120.253476.
274. Buckle, T.; van Willigen, D. M.; Spa, S. J.; Hensbergen, A. W.; van der Wal, S., et al., Tracers for Fluorescence-Guided Surgery: How Elongation of the Polymethine Chain in Cyanine Dyes Alters the Pharmacokinetics of a Dual-Modality c[RGDyK] Tracer. *J Nucl Med* **2018**, *59* (6), 986-992, 10.2967/jnumed.117.205575.
275. Derks, Y. H. W.; Lowik, D.; Sedelaar, J. P. M.; Gotthardt, M.; Boerman, O. C., et al., PSMA-targeting agents for radio- and fluorescence-guided prostate cancer surgery. *Theranostics* **2019**, *9* (23), 6824-6839, 10.7150/thno.36739.
276. van Leeuwen, F. W. B.; Schottelius, M.; Brouwer, O. R.; Vidal-Sicart, S.; Achilefu, S., et al., Trending: Radioactive and Fluorescent Bimodal/Hybrid Tracers as Multiplexing Solutions for Surgical Guidance. *J Nucl Med* **2020**, *61* (1), 13-19, 10.2967/jnumed.119.228684.
277. Schottelius, M.; Wurzer, A.; Wissmiller, K.; Beck, R.; Koch, M., et al., Synthesis and Preclinical Characterization of the PSMA-Targeted Hybrid Tracer PSMA-I&F for Nuclear and Fluorescence Imaging of Prostate Cancer. *J Nucl Med* **2019**, *60* (1), 71-78, 10.2967/jnumed.118.212720.
278. Hensbergen, A. W.; Buckle, T.; van Willigen, D. M.; Schottelius, M.; Welling, M. M., et al., Hybrid Tracers Based on Cyanine Backbones Targeting Prostate-Specific Membrane Antigen: Tuning Pharmacokinetic Properties and Exploring Dye-Protein Interaction. *J Nucl Med* **2020**, *61* (2), 234-241, 10.2967/jnumed.119.233064.
279. Aras, O.; Demirdag, C.; Kommidi, H.; Guo, H.; Pavlova, I., et al., Small Molecule, Multimodal, [<sup>18</sup>F]-PET and Fluorescence Imaging Agent Targeting Prostate-Specific Membrane Antigen: First-in-Human Study. *Clin Genitourin Cancer* **2021**, *19* (5), 405-416, 10.1016/j.clgc.2021.03.011.
280. Eder, A. C.; Schafer, M.; Schmidt, J.; Bauder-Wust, U.; Roscher, M., et al., Rational Linker Design to Accelerate Excretion and Reduce Background Uptake of Peptidomimetic PSMA-Targeting Hybrid Molecules. *J Nucl Med* **2021**, *62* (10), 1461-1467, 10.2967/jnumed.120.248443.
281. Eder, A. C.; Omrane, M. A.; Stadlbauer, S.; Roscher, M.; Khoder, W. Y., et al., The PSMA-11-derived hybrid molecule PSMA-914 specifically identifies prostate cancer by preoperative PET/CT and intraoperative fluorescence imaging. *Eur J Nucl Med Mol Imaging* **2021**, *48* (6), 2057-2058, 10.1007/s00259-020-05184-0.
282. Dell'Oglio, P.; van Willigen, D. M.; van Oosterom, M. N.; Bauwens, K.; Hensbergen, F., et al., Feasibility of fluorescence imaging at microdosing using a hybrid PSMA tracer during robot-assisted radical prostatectomy in a large animal model. *EJNMMI Res* **2022**, *12* (1), 14, 10.1186/s13550-022-00886-y.
283. Eddershaw, P. J.; Beresford, A. P.; Bayliss, M. K., ADME/PK as part of a rational approach to drug discovery. *Drug Discov Today* **2000**, *5* (9), 409-414, 10.1016/s1359-6446(00)01540-3.
284. Lucas, A. J.; Sproston, J. L.; Barton, P.; Riley, R. J., Estimating human ADME properties, pharmacokinetic parameters and likely clinical dose in drug discovery. *Expert Opin Drug Discov* **2019**, *14* (12), 1313-1327, 10.1080/17460441.2019.1660642.
285. Evans, B. J.; King, A. T.; Katsifis, A.; Matesic, L.; Jamie, J. F., Methods to Enhance the Metabolic Stability of Peptide-Based PET Radiopharmaceuticals. *Molecules* **2020**, *25* (10), 2314, 10.3390/molecules25102314.

286. Akizawa, H.; Uehara, T.; Arano, Y., Renal uptake and metabolism of radiopharmaceuticals derived from peptides and proteins. *Adv Drug Deliv Rev* **2008**, *60* (12), 1319-1328, 10.1016/j.addr.2008.04.005.
287. Shipp, M. A.; Tarr, G. E.; Chen, C. Y.; Switzer, S. N.; Hersh, L. B., et al., CD10/neutral endopeptidase 24.11 hydrolyzes bombesin-like peptides and regulates the growth of small cell carcinomas of the lung. *Proc Natl Acad Sci U S A* **1991**, *88* (23), 10662-10666, 10.1073/pnas.88.23.10662.
288. Pauwels, S.; Najdovski, T.; Dimaline, R.; Lee, C. M.; Deschodt-Lanckman, M., Degradation of human gastrin and CCK by endopeptidase 24.11: differential behaviour of the sulphated and unsulphated peptides. *Biochim Biophys Acta* **1989**, *996* (1-2), 82-88, 10.1016/0167-4838(89)90098-8.
289. Dubreuil, P.; Fulcrand, P.; Rodriguez, M.; Fulcrand, H.; Laur, J.; Martinez, J., Novel activity of angiotensin-converting enzyme. Hydrolysis of cholecystokinin and gastrin analogues with release of the amidated C-terminal dipeptide. *Biochem J* **1989**, *262* (1), 125-130, 10.1042/bj2620125.
290. Kratochwil, C.; Giesel, F. L.; Leotta, K.; Eder, M.; Hoppe-Tich, T., et al., PMPA for nephroprotection in PSMA-targeted radionuclide therapy of prostate cancer. *J Nucl Med* **2015**, *56* (2), 293-298, 10.2967/jnumed.114.147181.
291. Wirtz, M. Development of biomarkers for molecular imaging and endoradiotherapy of prostate cancer. PhD thesis, *Technical University Munich*, Munich, **2015**.
292. Vaidyanathan, G.; Kang, C. M.; McDougald, D.; Minn, I.; Brummet, M., et al., Brush border enzyme-cleavable linkers: Evaluation for reducing renal uptake of radiolabeled prostate-specific membrane antigen inhibitors. *Nucl Med Biol* **2018**, *62-63*, 18-30, 10.1016/j.nucmedbio.2018.05.002.
293. Bendre, S.; Zhang, Z.; Kuo, H. T.; Rousseau, J.; Zhang, C., et al., Evaluation of Met-Val-Lys as a Renal Brush Border Enzyme-Cleavable Linker to Reduce Kidney Uptake of <sup>68</sup>Ga-Labeled DOTA-Conjugated Peptides and Peptidomimetics. *Molecules* **2020**, *25* (17), 3854, 10.3390/molecules25173854.
294. Arano, Y., Renal brush border strategy: A developing procedure to reduce renal radioactivity levels of radiolabeled polypeptides. *Nucl Med Biol* **2021**, *92*, 149-155, 10.1016/j.nucmedbio.2020.03.001.
295. Lau, J.; Lee, H.; Rousseau, J.; Benard, F.; Lin, K. S., Application of Cleavable Linkers to Improve Therapeutic Index of Radioligand Therapies. *Molecules* **2022**, *27* (15), 4959, 10.3390/molecules27154959.
296. Kuo, H. T.; Pan, J.; Zhang, Z.; Lau, J.; Merkens, H., et al., Effects of Linker Modification on Tumor-to-Kidney Contrast of <sup>68</sup>Ga-Labeled PSMA-Targeted Imaging Probes. *Mol Pharm* **2018**, *15* (8), 3502-3511, 10.1021/acs.molpharmaceut.8b00499.
297. Eder, M.; Lohr, T.; Bauder-Wust, U.; Reber, M.; Mier, W., et al., Pharmacokinetic properties of peptidic radiopharmaceuticals: reduced uptake of (EH)<sub>3</sub>-conjugates in important organs. *J Nucl Med* **2013**, *54* (8), 1327-1330, 10.2967/jnumed.112.114512.
298. Baranski, A. C.; Schafer, M.; Bauder-Wust, U.; Wacker, A.; Schmidt, J., et al., Improving the Imaging Contrast of <sup>68</sup>Ga-PSMA-11 by Targeted Linker Design: Charged Spacer Moieties Enhance the Pharmacokinetic Properties. *Bioconjug Chem* **2017**, *28* (9), 2485-2492, 10.1021/acs.bioconjchem.7b00458.
299. Wurzer, A.; Wester, H. J.; Fischer, S.; Kunert, J. P. SILICON-CONTAINING LIGAND COMPOUNDS. *WO2022018264A1*, **2022**.
300. Fasano, M.; Curry, S.; Terreno, E.; Galliano, M.; Fanali, G., et al., The extraordinary ligand binding properties of human serum albumin. *IUBMB Life* **2005**, *57* (12), 787-796, 10.1080/15216540500404093.
301. Bteich, M., An overview of albumin and alpha-1-acid glycoprotein main characteristics: highlighting the roles of amino acids in binding kinetics and molecular interactions. *Heliyon* **2019**, *5* (11), e02879, 10.1016/j.heliyon.2019.e02879.
302. Fanali, G.; di Masi, A.; Trezza, V.; Marino, M.; Fasano, M.; Ascenzi, P., Human serum albumin: from bench to bedside. *Mol Aspects Med* **2012**, *33* (3), 209-290, 10.1016/j.mam.2011.12.002.
303. Ghuman, J.; Zunszain, P. A.; Petitpas, I.; Bhattacharya, A. A.; Otagiri, M.; Curry, S., Structural basis of the drug-binding specificity of human serum albumin. *J Mol Biol* **2005**, *353* (1), 38-52, 10.1016/j.jmb.2005.07.075.
304. Sudlow, G.; Birkett, D. J.; Wade, D. N., The characterization of two specific drug binding sites on human serum albumin. *Mol Pharmacol* **1975**, *11* (6), 824-832.

305. Sudlow, G.; Birkett, D. J.; Wade, D. N., Further characterization of specific drug binding sites on human serum albumin. *Mol Pharmacol* **1976**, *12* (6), 1052-1061.
306. Birkett, D. J.; Myers, S. P.; Sudlow, G., Effects of fatty acids on two specific drug binding sites on human serum albumin. *Mol Pharmacol* **1977**, *13* (6), 987-992.
307. Zsila, F., Subdomain IB is the third major drug binding region of human serum albumin: toward the three-sites model. *Mol Pharm* **2013**, *10* (5), 1668-1682, 10.1021/mp400027q.
308. Dumelin, C. E.; Trussel, S.; Buller, F.; Trachsel, E.; Bootz, F., et al., A portable albumin binder from a DNA-encoded chemical library. *Angew Chem Int Ed Engl* **2008**, *47* (17), 3196-3201, 10.1002/anie.200704936.
309. Trussel, S.; Dumelin, C.; Frey, K.; Villa, A.; Buller, F.; Neri, D., New strategy for the extension of the serum half-life of antibody fragments. *Bioconjug Chem* **2009**, *20* (12), 2286-2292, 10.1021/bc9002772.
310. Müller, C.; Struthers, H.; Winiger, C.; Zhernosekov, K.; Schibli, R., DOTA conjugate with an albumin-binding entity enables the first folic acid-targeted <sup>177</sup>Lu-radionuclide tumor therapy in mice. *J Nucl Med* **2013**, *54* (1), 124-131, 10.2967/jnumed.112.107235.
311. Kaeppli, S. A. M.; Jodal, A.; Gotthardt, M.; Schibli, R.; Behe, M., Exendin-4 Derivatives with an Albumin-Binding Moiety Show Decreased Renal Retention and Improved GLP-1 Receptor Targeting. *Mol Pharm* **2019**, *16* (9), 3760-3769, 10.1021/acs.molpharmaceut.9b00271.
312. Koustoulidou, S.; Handula, M.; de Ridder, C.; Stuurman, D.; Beekman, S., et al., Synthesis and Evaluation of Two Long-Acting SSTR2 Antagonists for Radionuclide Therapy of Neuroendocrine Tumors. *Pharmaceuticals (Basel)* **2022**, *15* (9), 1155, 10.3390/ph15091155.
313. Kelly, J. M.; Jeitner, T. M.; Ponnala, S.; Williams, C., Jr.; Nikolopoulou, A., et al., A Trifunctional Theranostic Ligand Targeting Fibroblast Activation Protein- $\alpha$  (FAP $\alpha$ ). *Mol Imaging Biol* **2021**, *23* (5), 686-696, 10.1007/s11307-021-01593-1.
314. Benesova, M.; Umbricht, C. A.; Schibli, R.; Muller, C., Albumin-Binding PSMA Ligands: Optimization of the Tissue Distribution Profile. *Mol Pharm* **2018**, *15* (3), 934-946, 10.1021/acs.molpharmaceut.7b00877.
315. Robu, S.; Schmidt, A.; Eiber, M.; Schottelius, M.; Gunther, T., et al., Synthesis and preclinical evaluation of novel <sup>18</sup>F-labeled Glu-urea-Glu-based PSMA inhibitors for prostate cancer imaging: a comparison with <sup>18</sup>F-DCFPyl and <sup>18</sup>F-PSMA-1007. *EJNMMI Res* **2018**, *8* (1), 30, 10.1186/s13550-018-0382-8.
316. Schmidt, A.; Wirtz, M.; Farber, S. F.; Osl, T.; Beck, R., et al., Effect of Carbohydratation on the Theranostic Tracer PSMA I&T. *ACS Omega* **2018**, *3* (7), 8278-8287, 10.1021/acsomega.8b00790.
317. Deberle, L. M.; Benesova, M.; Umbricht, C. A.; Borgna, F.; Buchler, M., et al., Development of a new class of PSMA radioligands comprising ibuprofen as an albumin-binding entity. *Theranostics* **2020**, *10* (4), 1678-1693, 10.7150/thno.40482.
318. Deberle, L. M.; Tschan, V. J.; Borgna, F.; Sozzi-Guo, F.; Bernhardt, P., et al., Albumin-Binding PSMA Radioligands: Impact of Minimal Structural Changes on the Tissue Distribution Profile. *Molecules* **2020**, *25* (11), 2542, 10.3390/molecules25112542.
319. Kelly, J. M.; Amor-Coarasa, A.; Nikolopoulou, A.; Wustemann, T.; Barelli, P., et al., Dual-Target Binding Ligands with Modulated Pharmacokinetics for Endoradiotherapy of Prostate Cancer. *J Nucl Med* **2017**, *58* (9), 1442-1449, 10.2967/jnumed.116.188722.
320. Kelly, J. M.; Amor-Coarasa, A.; Ponnala, S.; Nikolopoulou, A.; Williams, C., Jr., et al., Albumin-Binding PSMA Ligands: Implications for Expanding the Therapeutic Window. *J Nucl Med* **2019**, *60* (5), 656-663, 10.2967/jnumed.118.221150.
321. Kuo, H. T.; Lin, K. S.; Zhang, Z.; Uribe, C. F.; Merckens, H., et al., <sup>177</sup>Lu-Labeled Albumin-Binder-Conjugated PSMA-Targeting Agents with Extremely High Tumor Uptake and Enhanced Tumor-to-Kidney Absorbed Dose Ratio. *J Nucl Med* **2021**, *62* (4), 521-527, 10.2967/jnumed.120.250738.
322. Fendler, W. P.; Rahbar, K.; Herrmann, K.; Kratochwil, C.; Eiber, M., <sup>177</sup>Lu-PSMA Radioligand Therapy for Prostate Cancer. *J Nucl Med* **2017**, *58* (8), 1196-1200, 10.2967/jnumed.117.191023.
323. Toma, C.-M.; Imre, S.; Vari, C.-E.; Muntean, D.-L.; Tero-Vescan, A., Ultrafiltration Method for Plasma Protein Binding Studies and Its Limitations. *Processes* **2021**, *9* (2), 382-388, 10.3390/pr9020382.

324. Hage, D. S., High-performance affinity chromatography: a powerful tool for studying serum protein binding. *J Chromatogr B Analyt Technol Biomed Life Sci* **2002**, 768 (1), 3-30, 10.1016/s0378-4347(01)00482-0.
325. Shibukawa, A.; Kuroda, Y.; Nakagawa, T., High-performance frontal analysis for drug-protein binding study. *J Pharm Biomed Anal* **1999**, 18 (6), 1047-1055, 10.1016/s0731-7085(98)00201-5.
326. Knorr, K.; Oh, S. W.; Kronke, M.; Wurzer, A.; D'Alessandria, C., et al., Preclinical biodistribution and dosimetry and human biodistribution comparing  $^{18}\text{F}$ -rhPSMA-7 and single isomer  $^{18}\text{F}$ -rhPSMA-7.3. *EJNMMI Res* **2022**, 12 (1), 8, 10.1186/s13550-021-00872-w.
327. Norden, A. G.; Lapsley, M.; Lee, P. J.; Pusey, C. D.; Scheinman, S. J., et al., Glomerular protein sieving and implications for renal failure in Fanconi syndrome. *Kidney Int* **2001**, 60 (5), 1885-1892, 10.1046/j.1523-1755.2001.00016.x.
328. Kwekkeboom, D. J.; Bakker, W. H.; Kooij, P. P.; Konijnenberg, M. W.; Srinivasan, A., et al., [ $^{177}\text{Lu}$ -DOTAOTyr3]octreotate: comparison with [ $^{111}\text{In}$ -DTPAo]octreotide in patients. *Eur J Nucl Med* **2001**, 28 (9), 1319-1325, 10.1007/s002590100574.
329. Jang, A.; Kendi, A. T.; Sartor, O., Status of PSMA-targeted radioligand therapy in prostate cancer: current data and future trials. *Ther Adv Med Oncol* **2023**, 15, 10.1177/17588359231157632.
330. Ramnarain, B.; Sartor, O., PSMA-Targeted Radiopharmaceuticals in Prostate Cancer: Current Data and New Trials. *The Oncologist* **2023**, 10.1093/oncolo/oyac279.
331. Werner, P.; Neumann, C.; Eiber, M.; Wester, H. J.; Schottelius, M., [ $^{99\text{m}}\text{Tc}$ ]Tc-PSMA-I&S-SPECT/CT: experience in prostate cancer imaging in an outpatient center. *EJNMMI Res* **2020**, 10 (1), 45, 10.1186/s13550-020-00635-z.
332. Sharir, T.; Slomka, P. J.; Berman, D. S., Solid-state SPECT technology: fast and furious. *J Nucl Cardiol* **2010**, 17 (5), 890-896, 10.1007/s12350-010-9284-5.
333. Song, H.; Ferri, V.; Duan, H.; Aparici, C. M.; Davidzon, G., et al., SPECT at the speed of PET: a feasibility study of CZT-based whole-body SPECT/CT in the post  $^{177}\text{Lu}$ -DOTATATE and  $^{177}\text{Lu}$ -PSMA617 setting. *Eur J Nucl Med Mol Imaging* **2023**, 10.1007/s00259-023-06176-6.
334. Rahmim, A.; Zaidi, H., PET versus SPECT: strengths, limitations and challenges. *Nucl Med Commun* **2008**, 29 (3), 193-207, 10.1097/MNM.0b013e3282f3a515.
335. Clack, R.; Christian, P. E.; Defrise, M.; Welch, A. E., Image reconstruction for a novel SPECT system with rotating slant-hole collimators. *Proceedings of 1994 IEEE Nuclear Science Symposium - NSS'94* **1994**, 4, 1948-1952, 10.1109/NSSMIC.1994.474685.
336. Beekman, F.; van der Have, F., The pinhole: gateway to ultra-high-resolution three-dimensional radionuclide imaging. *Eur J Nucl Med Mol Imaging* **2007**, 34 (2), 151-161, 10.1007/s00259-006-0248-6.

## 6. Appendix

### 6.1. List of Figures

**Figure 1:** Crystal structure of the membrane-bound homo-dimer of prostate-specific membrane antigen (PSMA, left monomer depicted in grey, right monomer depicted in color). The extracellular domain consists of three subdomains: helical domain (yellow), apical domain (blue) and protease domain (green). The binuclear active site of PSMA is located at the interface of the three subdomains and bears two zinc ions (red spheres). N-glycosylations are depicted in cyan. Left side: in the nervous system PSMA catabolizes the neurotransmitter N-acetyl-aspartyl-glutamate (NAAG) and the hydrolysis products N-acetyl-aspartate (NAA) and glutamate (Glu) are transported into neuronal glial cells. Right side: in the membrane brush border of the small intestine mono-glutamylated folate (folic acid) is provided via iterative cleavage of C-terminal glutamates from foylyl-poly- $\gamma$ -glutamate (FPG<sub>n</sub>) by PSMA. Folic acid can subsequently be selectively transported into the enterocytes (figure adapted from *Barinka et al. Glutamate Carboxypeptidase II in Diagnosis and Treatment of Neurologic Disorders and Prostate Cancer. Curr Med Chem. 2012;19(6):856-870. Copyright © 2012 Bentham Science Publishers*). ..... **4**

**Figure 2:** Schematic representation of the natural substrate NAAG and urea-based inhibitors within the active site of PSMA. The S1' pharmacophore pocket and S1 pocket are indicated in pale blue and pale orange, respectively. Zinc ions are depicted as red spheres, the P1' side and P1 side of substrate and inhibitors are colored green and blue, respectively. A) Orientation of NAAG within the active site of PSMA. Glutamate is coordinated by the glutarate sensor, the amide bond oxygen coordinates to zinc-ion A and a water molecule (polarized by Zn-ions A and B and the catalytic base E424) acts as hydrolytic nucleophile (mechanism indicated by grey arrows). The aspartyl carboxylate is coordinated by guanidinium groups of the arginine patch (interactions between substrate and binding pocket according to crystal structures reported by *Klusak et al. Reaction mechanism of glutamate carboxypeptidase II revealed by mutagenesis, X-ray crystallography, and computational methods. Biochemistry 2009;48(19):4126–38*). B) Orientation of a urea-based PSMA-inhibitors within the active site of PSMA. Glutamate recognition resembles NAAG, the hydrolysis-resistant urea group coordinates to zinc-ion A and H553, and the P1 carboxylate interacts with guanidinium groups of the arginine patch (interactions between substrate and binding pocket according to *Barinka et al. Interactions between Human Glutamate Carboxypeptidase II and Urea-Based Inhibitors: Structural Characterization. J Med Chem. 2008;51(24):7737–7743*). ..... **6**

**Figure 3:** A) PSMA binding pocket with superimposed structures of different PSMA-inhibitors. Active site and secondary binding sites are indicated with arrows. B) Arginine patch in uncomplexed PSMA. Residue R536 is flexible and adopts either 'stacking' (R536s) or 'binding' (R536b) position. Residue R463 adopts 'up' (R463u) position. The S1 accessory pocket is not accessible. C) In NAAG-complexed PSMA the conformation R536b and R463d ('down' position) occlude the S1 accessory pocket. D) Upon complexation with IBA-KuE, R536b and R463u conformation of the arginine patch opens the S1 accessory pocket for interaction with the 4-iodobenzyl moiety of the inhibitor. E) Complexation of PSMA with inhibitor ARM-P4 promotes an open conformation of the entrance lid (blue) and residues forming the arene binding site (red) can interact with the dinitroarene in ARM-P4. F) When complexed with IBA-KuE the entrance lid of PSMA (blue) remains in a closed conformation and residues forming the arene binding site are relatively dislocated. Ligand structures of ARM-P4 and IBA-KuE are superimposed in panels E and F (figure A modified from *Kopka et al. Glu-Ureido-Based Inhibitors of Prostate-Specific Membrane Antigen: Lessons Learned During the Development of a Novel Class of Low-Molecular-Weight Theranostic Radiotracers. J Nucl Med. 2017;58(S2):17S-26S. Copyright © 2017 SNMMI*; figures B-D reproduced from *Barinka et al. Interactions between Human Glutamate Carboxypeptidase II and Urea-Based Inhibitors: Structural Characterization. J Med Chem. 2008;51(24):7737–7743. Copyright © 2008 American Chemical Society*; figures E and F reproduced from *Zhang et al. A Remote Arene-Binding Site on Prostate Specific Membrane Antigen Revealed by Antibody-Recruiting Small Molecules. J Am Chem Soc. 2010;132(36):12711–12716. Copyright © 2010 American Chemical Society*). ..... **8**

**Figure 4:** Structures of some important small-molecule, urea-based PSMA-inhibitors. A) Schematic structure of PSMA-targeted ligands consisting of a urea-based targeting vector (A, blue), an optional linker moiety (B, green) and a site for either covalent radiolabeling or radiometal complexation (C, yellow). In panels B-F, urea binding motives are indicated with blue dotted squares, linker regions displayed by green dotted ellipsoids and sites of radiolabeling are highlighted by yellow dotted edging. B) MIP-1095 comprises the common KuE binding motive, a 4-iodo-phenyl group enhances affinity via interaction with the S1 accessory pocket and furthermore serves for radiolabeling with isotopes of iodine. C) PSMA-11 comprises a HBED-CC chelator for labeling with gallium-68. A linear linker provides optimal distance between the KuE binding motive and the chelator. D) PSMA-I&T comprises a DOTAGA chelator for labeling with diagnostic and therapeutic radionuclides. The linker region is composed of D-amino acids for enhanced metabolic stability and lipophilic interactions with the arene binding site in PSMA. E) The linker region in PSMA-617 was specifically optimized for enhanced internalization. A DOTA chelator allows for use in theranostic applications. F) PSMA-1007 was developed for  $^{18}\text{F}$ -based PET-imaging. The linker moiety is derived from PSMA-617 and comprises two glutamates to counteract the compound's high lipophilicity. Labeling with fluorine-18 is facilitated by a nicotinic acid prosthetic group. .... 9

**Figure 5:** Schematic overview of clinical patient management using theranostic radioligands. The diagnostic companion of the theranostic pair (related procedures are indicated in blue) is used for initial diagnosis via molecular imaging. Dosage of subsequent radioligand therapy (RLT) with the therapeutic companion (indicated in red) is based on dosimetry calculations derived from quantitative imaging with the diagnostic companion. Response to RLT can be controlled via post-therapeutic imaging which contributes to subsequent decision-making towards further RLT cycles or alternative treatment options. .... 12

**Figure 6:** Radiohybrid theranostic ligands contain a chelating unit (square in schematic depiction, red in chemical structure) for the complexation of either the natural isotope ( $^{\text{nat}}\text{M}$ ) or the therapeutic radionuclide ( $^*\text{M}$ ) of a metal such as lutetium and a silicon-fluoride acceptor (SiFA) moiety (small circle in schematic depiction, blue in chemical structure) that can be labeled with fluorine-18 for PET-imaging. The diagnostic twin is labeled with fluorine-18 (blue) and complexed with a non-radioactive metal ion (e.g.  $^{\text{nat}}\text{Lu}^{3+}$ ), while the therapeutic twin contains non-radioactive fluorine-19 and a therapeutic radiometal (red, e.g.  $^{177}\text{Lu}^{3+}$ ) complexed to the chelating unit. Examples for diagnostic and therapeutic twins are  $^{18}\text{F}$ [ $^{\text{nat}}\text{Lu}$ ]Lu-rhPSMA-7 and  $^{19}\text{F}$ [ $^{177}\text{Lu}$ ]Lu-rhPSMA-7, respectively. .... 14

**Figure 7:** The molecular structure of PSMA-617 (upper row) was developed by introduction of a DOTA chelator into a PSMA-11-derived compound (DOTA-Ahx-KuE) and subsequent optimization of the linker unit focusing on lipophilic interaction with the PSMA binding pocket. The structure of DOTA-FFK-Sub-KuE (bottom row) was in a first step optimized by replacement of DOTA by DOTAGA. Subsequent introduction of D-configured amino acids in the linker for enhanced metabolic stability and substitution of N-terminal phenylalanine by 3-iodo-tyrosine for ameliorated interaction with the arene binding site led to the development of PSMA-I&T. Iterative chemical modifications are indicated in red. .... 16

**Figure 8:** Pre-, intra- and post-therapeutic  $^{68}\text{Ga}$ ]Ga-PSMA-11 PET scans of a mCRPC patient presenting with peritoneal carcinomatosis and liver metastases (A). After disease progression under RLT with  $^{177}\text{Lu}$ ]Lu-PSMA-617 (B), complete biochemical and radiographic response to targeted  $\alpha$ -therapy was achieved using  $^{225}\text{Ac}$ ]Ac-PSMA-617 (C, D). Severe radiotoxicity to the salivary glands was reported and is reflected by reduced uptake of the diagnostic tracer in the respective organs observed in scans C and D (figure adapted from *Kratochwil et al.*  $^{225}\text{Ac}$ -PSMA-617 for PSMA-Targeted  $\alpha$ -Radiation Therapy of Metastatic Castration-Resistant Prostate Cancer. *J Nucl Med.* 2016;57(12):1941-44. Copyright © 2016 SNMMI). .... 19

**Figure 9:** Principle of radioguided surgery (RGS). A) Patients are initially stratified by PET/CT-imaging using  $^{68}\text{Ga}$ ]Ga-PSMA-11. Patients eligible for RGS receive an injection of  $^{99\text{m}}\text{Tc}$ ]Tc-PSMA-I&S approximately 20-24h prior to RGS and uptake in metastatic lesions is verified using SPECT/CT-imaging. B) A handheld  $\gamma$ -probe is applied to localize metastatic lesions

intraoperatively. C) Outside the surgical field, PSMA-positivity in resected tissue samples can instantly be verified by *ex vivo* activity measurements. D) Histopathology of resected tissue specimens is used for final identification of metastatic lesions (figure A adapted from Maurer *et al.* <sup>99m</sup>Tc-based Prostate-specific Membrane Antigen–radioguided Surgery in Recurrent Prostate Cancer. *Eur Urol.* 2019;75(4):659-666. Copyright © 2018 European Association of Urology. Figures B and C reproduced from Eiber *et al.* Prostate-Specific Membrane Antigen Ligands for Imaging and Therapy. *J Nucl Med.* 2017;58(S2):67S-76S. Copyright © 2017 SNMMI. Figure D reproduced from Maurer *et al.* Prostate-specific Membrane Antigen–radioguided Surgery for Metastatic Lymph Nodes in Prostate Cancer. *Eur Urol.* 2015;68(3):530-534. Copyright © 2015 European Association of Urology)..... **22**

**Figure 10:** Structure of [<sup>99m</sup>Tc]Tc-PSMA-I&S (upper row) for RGS and hybrid tracer [<sup>99m</sup>Tc]Tc-EuK-(SO<sub>3</sub>)Cy5-mas<sub>3</sub> (bottom row) for radio- and fluorescence-guidance. Both tracers share the common glutamate-urea-based PSMA binding motive (blue) and a mas<sub>3</sub>-chelator (red). The linker of PSMA-I&S contains lipophilic amino acids (green) for optimal target interaction while a SO<sub>3</sub>-substituted Cy5 fluorescent dye (purple) is incorporated in EuK-(SO<sub>3</sub>)Cy5-mas<sub>3</sub> to facilitate fluorescence-guidance. .... **23**

**Figure 11:** Examples of PSMA ligands incorporating distinct structural modifications to alter their pharmacokinetic profile. A repeat of glutamyl-histidine (blue) in EuK-Ahx-HBED-CC-(EH)<sub>3</sub> leads to reduced renal and hepatic uptake of the <sup>68</sup>Ga-labeled radioligand in mice. An enzyme-cleavable glycyl-tyrosine sequence (green) in IBA-G-Y-KuE aims for reduced kidney uptake by metabolic cleavage in the proximal tubule. The hydroxyl functionality (red) in SiOH-PSMA-7.3 replacing the corresponding fluoride in the analog radiohybrid compound leads to accelerated clearance and an increased tumor-to-kidney ratio of the <sup>177</sup>Lu-labeled radioligand in mice. .... **26**

**Figure 12:** A) Crystal structure of human serum albumin (HSA) complexed with myristic acid and R-(+)-warfarin (Protein Data Base (PDB) ID: 1H9Z; doi: 10.2210/pdb1H9Z/pdb). Subdomains are indicated by color code: subdomain IA: dark blue; subdomain IB: pale blue; subdomain IIA: yellow; subdomain IIB: orange; subdomain IIIA: rose; subdomain IIIB: red. Green stars indicate the location of six myristic acid molecules in fatty acid binding sites (FA) 1-6 of HSA. The pink star indicates Sudlow's site I occupied by R-(+)-warfarin (pink stick representation) with the latter impeding the binding of another myristic acid molecule to FA7. Sudlow's site II is indicated with an arrow and overlaps with FA3 and FA4. B) Chemical structures of some HSA-binding compounds. Their site of binding is represented in panels A and C-E. C) Orientation of R-(+)-warfarin (pink stick representation) in Sudlow's site I (PDB ID: 1H9Z). Major interactions are H-bonds (blue dotted lines) of oxo-groups with arginine (R222) and histidine (H242) residues and a water molecule as well as  $\pi$ -interactions (green dotted lines) with a tryptophan (W214) residue. D) Orientation of S-(+)-ibuprofen (pink stick representation) in Sudlow's site II (PDB ID: 2BXG; doi: 10.2210/pdb2BXG/pdb). The aromatic portion is located in an apolar pocket and the carboxylate is oriented towards a polar patch formed by residues of arginine (R410), tyrosine (Y411) and lysine (K414). E) Orientation of 4-phenylbutanoic acid (pink stick representation) in Sudlow's site II (PDB ID: 5YOQ; doi: 10.2210/pdb5YOQ/pdb). In analogy to ibuprofen the molecule's aromatic portion covers a hydrophobic pocket while amino acid residues of the polar patch (predominantly Y411 and K414) coordinate the carboxylate..... **28**

**Figure 13:** Chemical structures of selected HSA-binding PSMA-ligands with moieties conferring plasma protein binding properties highlighted in blue. Multiple compounds were derived from PSMA-617 by insertion of an albumin-binding motive between EuK-2-Nal-Thx (abbreviated as R) and the chelating moiety. EB-PSMA-617 and PSMA-ALB-56 contain the strong albumin-binding motives Evans Blue and 4-(*p*-tolyl)butanoic acid, respectively. Ibu-DAB-PSMA contains an altered linker structure (depicted in green) to modulate the effective albumin binding capacity of ibuprofen. The SiFA-group in rhPSMA-7.3 serves labeling with fluorine-18 and enhances PSMA affinity. Its lipophilic character, however, also endows significant plasma protein binding to the entire ligand. In a similar fashion, the naphthyl-group in PSMA-617 primarily serves enhanced target interactions but also confers moderate plasma protein binding to this rather fast clearing compound..... **30**

- Figure 14:** In a comparative preclinical selection process including thorough *in vitro* evaluation and *in vivo* biodistribution studies at 24 h p.i. among a group of six theranostic  $^{177}\text{Lu}$ -labeled rhPSMA ligands, [ $^{177}\text{Lu}$ ]Lu-rhPSMA-10.1 was identified as therapeutic lead compound. [ $^{177}\text{Lu}$ ]Lu-rhPSMA-10.1 exhibits an improved pharmacokinetic profile compared to [ $^{177}\text{Lu}$ ]Lu-rhPSMA-7.3, e.g. low blood retention and increased tumor-to-kidney ratio. Figure reproduced with the permission of the publisher. © 2022 by the Society of Nuclear Medicine and Molecular Imaging, Inc. .... 33
- Figure 15:** Conceptual design of ‘albumin-mediated size exclusion chromatography’ (AMSEC). A size exclusion column is equilibrated with 700  $\mu\text{M}$  HSA in phosphate buffered saline (PBS) and radioligands with a molecular mass below the column fractionation range are injected. A ligand-specific, HSA-mediated retention time is observed according to the strength of interaction between radioligand and HSA during the chromatographic run. Based on the acquired retention time an apparent molecular weight  $\text{MW}_{\text{app}}$  can be determined which can be used to calculate glomerular sieving coefficients of the radioligands. Figure reproduced with the permission of the publisher. © 2022 by the authors..... 35
- Figure 16:** A series of novel  $^{99\text{m}}\text{Tc}$ -labeled PSMA ligands comprising a tetraamine (N4) chelator and a variable amino acid as pharmacokinetic modifier were evaluated in a preclinical selection process and compared to the reference compound [ $^{99\text{m}}\text{Tc}$ ]Tc-PSMA-I&S. The D-glutamate bearing derivative N4-PSMA-12 was identified as lead compound for application in RGS due to reduced lipophilicity and plasma protein binding *in vitro* and a favorable pharmacokinetic profile observed in biodistribution studies 6 h p.i., such as lower blood retention and superior tumor-to-background ratios as compared to other N4-PSMA ligands and PSMA-I&S. .... 37

## 6.2. Reprint Permissions and Reprints of Original Publications

In the following section reprint permissions and original articles are given for the three publications incorporated in this thesis.

### 6.2.1. *The Journal of Nuclear Medicine – Synthesis and Preclinical Evaluation of <sup>177</sup>Lu-labeled Radiohybrid PSMA Ligands for Endoradiotherapy of Prostate Cancer*

Reprint permission for the peer-reviewed article “*Synthesis and Preclinical Evaluation of <sup>177</sup>Lu-labeled Radiohybrid PSMA Ligands for Endoradiotherapy of Prostate Cancer*” has been granted upon request under reference to the JNM Author’s Permission to Reprint policy (online available under <https://jnm.snmjournals.org/page/permissions>). A screenshot of the communication with the editorial office of the journal is provided below.

Dear Jan-Philip Kunert,

As you are an author on the original paper, permission for your request is granted per JNM Author’s Permission to Reprint policy (<https://jnm.snmjournals.org/page/permissions>). This policy allows authors to republish their original articles as part of academic theses or dissertations with proper citation. This policy is part of and enforced by your Assignment of Copyright form. No additional formal permission is required. This applies to original materials only and does not include materials reprinted from prior sources.

**Mark Sumimoto**



*Editorial Project Manager*

SNMMI | The Society of Nuclear Medicine and Molecular Imaging

phone: 703.652.6777 | fax: 703.708.9018

email: [msumimoto@snmmi.org](mailto:msumimoto@snmmi.org)

[www.snmmi.org](http://www.snmmi.org)

Please turn to the next page for the reprint of the original publication and the supplementary material.

# Synthesis and Preclinical Evaluation of $^{177}\text{Lu}$ -Labeled Radiohybrid PSMA Ligands for Endoradiotherapy of Prostate Cancer

Alexander Wurzer\*<sup>1</sup>, Jan-Philip Kunert\*<sup>1</sup>, Sebastian Fischer<sup>1</sup>, Veronika Felber<sup>1</sup>, Roswitha Beck<sup>1</sup>, Francesco de Rose<sup>2</sup>, Calogero D'Alessandria<sup>2</sup>, Wolfgang Weber<sup>2</sup>, and Hans-Jürgen Wester<sup>1</sup>

<sup>1</sup>Chair of Pharmaceutical Radiochemistry, Technical University of Munich, Garching, Germany; and <sup>2</sup>Department of Nuclear Medicine, Klinikum Rechts der Isar, Technical University of Munich, Munich, Germany

The prostate-specific membrane antigen (PSMA)-targeted radiohybrid (rh) ligand [ $^{177}\text{Lu}$ ]Lu-rhPSMA-7.3 has recently been assessed in a pretherapeutic dosimetry study on prostate cancer patients. In comparison to [ $^{177}\text{Lu}$ ]Lu-PSMA I&T, application of [ $^{177}\text{Lu}$ ]Lu-rhPSMA-7.3 resulted in a significantly improved tumor dose but also higher kidney accumulation. Although rhPSMA-7.3 has been initially selected as the lead compound for diagnostic application based on the characterization of its gallium complex, a systematic comparison of the most promising  $^{177}\text{Lu}$ -labeled rhPSMA ligands is still missing. Thus, this study aimed to identify the rhPSMA ligand with the most favorable pharmacokinetics for  $^{177}\text{Lu}$ -radioligand therapy. **Methods:** The 4 isomers of [ $^{177}\text{Lu}$ ]Lu-rhPSMA-7 (namely [ $^{177}\text{Lu}$ ]Lu-rhPSMA-7.1, -7.2, -7.3, and -7.4), along with the novel radiohybrid ligands [ $^{177}\text{Lu}$ ]Lu-rhPSMA-10.1 and -10.2, were compared with the state-of-the-art compounds [ $^{177}\text{Lu}$ ]Lu-PSMA I&T and [ $^{177}\text{Lu}$ ]Lu-PSMA-617. The comparative evaluation comprised affinity studies (half-maximal inhibitory concentration) and internalization experiments on LNCaP cells, as well as lipophilicity measurements. In addition, we determined the apparent molecular weight (AMW) of each tracer as a parameter for human serum albumin (HSA) binding. Biodistribution studies and small-animal SPECT imaging were performed on LNCaP-tumor bearing mice at 24 h after injection. **Results:**  $^{177}\text{Lu}$  labeling of the radiohybrids was performed according to the established procedures for the currently established PSMA-targeted ligands. All ligands showed potent binding to PSMA-expressing LNCaP cells, with affinities in the low nanomolar range and high internalization rates. Surprisingly, the most pronounced differences regarded the HSA-related AMW. Although [ $^{177}\text{Lu}$ ]Lu-rhPSMA-7 isomers demonstrated the highest AMW and thus strongest HSA interactions, [ $^{177}\text{Lu}$ ]Lu-rhPSMA-10.1 showed an AMW lower than for [ $^{177}\text{Lu}$ ]Lu-rhPSMA-7.3 but higher than for the  $^{177}\text{Lu}$ -labeled references PSMA I&T and PSMA-617. In biodistribution studies, [ $^{177}\text{Lu}$ ]Lu-rhPSMA-10.1 exhibited the lowest kidney uptake and fastest excretion from the blood pool of all rhPSMA ligands while preserving a high tumor accumulation. **Conclusion:** Clinical investigation of [ $^{177}\text{Lu}$ ]Lu-rhPSMA-10.1 is highly warranted to determine whether the favorable pharmacokinetics observed in mice will also result in high tumor uptake and decreased absorbed dose to kidneys and other non-target tissues in patients.

**Key Words:** radiohybrid; rhPSMA; PSMA; radioligand therapy; prostate cancer

**J Nucl Med 2022; 63:1489–1495**

DOI: 10.2967/jnumed.121.263371

**R**adioligand therapy (RLT) of metastatic castration-resistant prostate cancer with ligands targeting prostate-specific membrane antigen (PSMA) holds great promise for patients who have exhausted conventional treatment regimens. Currently,  $^{177}\text{Lu}$ -labeled PSMA-617 (1) and PSMA I&T (2) are the most extensively evaluated agents in this class and have demonstrated favorable safety and good treatment response rates (3,4). Although regulatory approval is still awaited for both agents, their application in compassionate-use programs has recently been reaffirmed by the European Association of Nuclear Medicine procedure guidelines for  $^{177}\text{Lu}$ -PSMA therapy (5). [ $^{177}\text{Lu}$ ]Lu-PSMA-617 has been evaluated by Novartis in a phase 3 clinical trial (NCT 03511664) on patients with metastatic castration-resistant prostate cancer. In that trial, [ $^{177}\text{Lu}$ ]Lu-PSMA-617 was compared with the best standard of care. The investigators recently announced that both primary endpoints—overall and radiographic progression-free survival—were met (6). In addition, an ongoing phase 3 trial investigating [ $^{177}\text{Lu}$ ]Lu-PSMA I&T (NCT 04647526) is evaluating its efficacy versus abiraterone or enzalutamide in delaying radiographic progression in patients with metastatic castration-resistant prostate cancer after second-line hormonal treatment. Retrospective clinical comparison of  $^{177}\text{Lu}$ -labeled PSMA-617 and PSMA I&T point toward nearly identical pharmacokinetics for both tracers, and clinical efficacy is assumed to be similar, with no clear advantage to either compound (7).

Recently, the novel class of radiohybrid (rh) PSMA-targeted ligands was introduced by our group (8). These compounds combine a silicon-fluoride acceptor for  $^{19}\text{F}/^{18}\text{F}$ -isotopic exchange radiolabeling and a chelator for complexation of a metal or radiometal (e.g.,  $^{177}\text{Lu}$ ,  $^{68}\text{Ga}$ , or  $^{225}\text{Ac}$ ). Respective ligand pairs of  $^{18}\text{F}$ /nonradioactive metal and  $^{19}\text{F}$ /radiometal, such as [ $^{18}\text{F}$ ]Lu-rhPSMA and [ $^{177}\text{Lu}$ ]Lu-rhPSMA, are chemically identical and thus display identical pharmacokinetics, offering unique possibilities for theranostic applications (Fig. 1).

For prostate cancer diagnosis, the first clinical evaluations were conducted with the  $^{18}\text{F}$ -labeled  $^{nat}\text{Ga}$  chelate of rhPSMA-7, which demonstrated a favorable biodistribution and indicated a high diagnostic performance for N-staging and localization of biochemical recurrence in patients with prostate cancer (9–11). Since rhPSMA-7

Received Oct. 12, 2021; revision accepted Jan. 18, 2022.

For correspondence or reprints, contact Alexander Wurzer (alexander.wurzer@tum.de).

\*Contributed equally to this work.

Published online Jan. 27, 2022.

Immediate Open Access: Creative Commons Attribution 4.0 International License (CC BY) allows users to share and adapt with attribution, excluding materials credited to previous publications. License: <https://creativecommons.org/licenses/by/4.0/>. Details: <http://jnm.snmjournals.org/site/misc/permission.xhtml>.

COPYRIGHT © 2022 by the Society of Nuclear Medicine and Molecular Imaging.

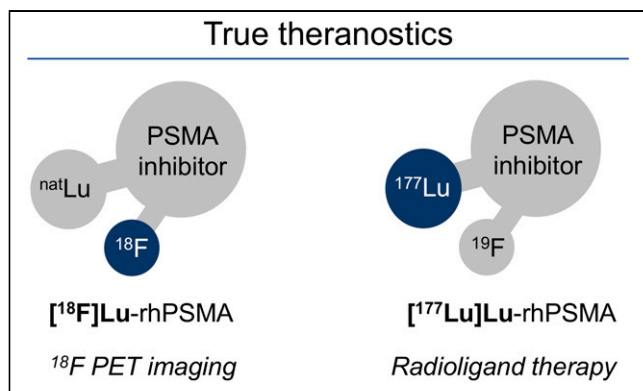


**FIGURE 1.** Theranostic radiohybrid concept applied to PSMA-targeted ligands. Molecules offer 2 labeling sites for radionuclides, silicon-fluorine acceptor site for  $^{18}\text{F}$  labeling via isotopic exchange and chelator for radiometallation.  $^{18}\text{F}$ -labeled cold lutetium-complexed ligand ( $^{18}\text{F}$ Lu-rhPSMA) is chemically identical to  $^{177}\text{Lu}$ -labeled cold fluorine compound ( $^{177}\text{Lu}$ Lu-rhPSMA), therefore representing true theranostic agents for PET imaging and RLT.

was found to comprise 4 diastereoisomers (rhPSMA-7.1, -7.2, -7.3, and -7.4), a preclinical selection process was initiated that identified  $^{18}\text{F}$ Ga-rhPSMA-7.3 (often abbreviated as  $^{18}\text{F}$ -rhPSMA-7.3) as the novel diagnostic lead compound (12) for current phase 3 clinical trials (NCT04186819 and NCT04186845).

For initial evaluation of the radiohybrid technology for therapeutic applications, rhPSMA-7.3 was labeled with  $^{177}\text{Lu}$  and compared with  $^{177}\text{Lu}$ Lu-PSMA I&T in biodistribution and dosimetry studies on mice. Both ligands showed similar uptake in healthy organs, resulting in a similar dose to all major organs, including bone marrow and kidney (13). Compared with  $^{177}\text{Lu}$ Lu-PSMA I&T,  $^{177}\text{Lu}$ Lu-rhPSMA-7.3 exhibited a 2.8- and 4.7-fold higher tumor uptake at 1 and 168 h after injection, respectively, resulting in a significantly higher dose at the tumor and a superior treatment response (13).

In a pretherapeutic comparative dosimetry study of  $^{177}\text{Lu}$ -labeled rhPSMA-7.3 and PSMA I&T on a small patient cohort ( $n = 6$ , intra-individual comparison), an approximately 2.4-fold higher mean absorbed dose for tumor lesions of the radiohybrid ligand was found, consistent with the preclinical observations (14). However, contradictory to animal studies, the mean absorbed dose to different healthy organs was also higher—for example, 2.3-fold higher doses to kidneys and 2.2-fold higher doses to bone marrow for  $^{177}\text{Lu}$ Lu-rhPSMA-7.3 versus  $^{177}\text{Lu}$ Lu-PSMA I&T. The authors concluded that the radiohybrid tracer holds promise for therapeutic effects similar to those obtained with  $^{177}\text{Lu}$ Lu-PSMA I&T while offering potential economic advantages by an approximately 2-fold reduction in the injected radioactive doses (14).

The selection of rhPSMA-7.3 as lead compound for diagnostic application was based on the evaluation of gallium chelates  $^{18}\text{F}$ Ga-rhPSMA-7.1, -7.2, -7.3, and -7.4 (12). Since it is known from the literature that the complex structure of the metal chelate (e.g., [Ga]DOTAGA and [Lu]DOTAGA) within a radioligand can influence its pharmacokinetic properties (15,16), all  $^{177}\text{Lu}$ -labeled isomers of rhPSMA-7 have been included in this comparison. The isomers differ in the stereoconfiguration of the diamino propionic acid branching unit (D-Dap or L-Dap) and the glutamic acid arm at the DOTAGA chelator (R- or S-DOTAGA: rhPSMA-7.1 [D-Dap-R-DOTAGA], rhPSMA-7.2 [L-Dap-R-DOTAGA], rhPSMA-7.3 [D-Dap-S-DOTAGA], rhPSMA-7.4 [L-Dap-S-DOTAGA]).

Given the promising initial data from  $^{177}\text{Lu}$ -labeled rhPSMA-7.3, the aim of the present study was to evaluate whether other isomers of  $^{177}\text{Lu}$ -labeled rhPSMA-7 or the closely related compounds [ $^{177}\text{Lu}$ ]Lu-rhPSMA-10.1 (D-Dap) and -10.2 (L-Dap) (where DOTAGA replaces the DOTAGA chelator) might have further improved biodistribution kinetics in normal organs while maintaining the high tumor uptake found with [ $^{177}\text{Lu}$ ]Lu-rhPSMA-7.3. We evaluated the ligands in comparison with reference ligands [ $^{177}\text{Lu}$ ]Lu-PSMA-617 and [ $^{177}\text{Lu}$ ]Lu-PSMA I&T (Fig. 2) in vitro (lipophilicity, half-maximal inhibitory concentration, internalization into LNCaP cells, binding to human serum albumin [HSA]) and in biodistribution studies on LNCaP tumor-bearing mice.

## MATERIALS AND METHODS

A detailed description of the chemical synthesis of rhPSMA and the analytic instruments is provided in the supplemental materials (available at <http://jnm.snmjournals.org>).

### Radiolabeling

Radiolabeling with no-carrier-added  $^{177}\text{Lu}$  was performed according to the established procedures for PSMA-targeted ligands (1,2). Briefly, the precursor (1.0 nmol, 10  $\mu\text{L}$ , 0.1 mM in dimethylsulfoxide) was added to 10  $\mu\text{L}$  of 1.0 M aqueous NaOAc buffer (pH 5.5). Subsequently, 20–50 MBq of [ $^{177}\text{Lu}$ ]LuCl<sub>3</sub> (specific activity > 3,000 GBq/mg at the time of radiolabeling, 740 MBq/mL, 0.04 M HCl; ITM) was added, and the mixture was filled up to 100  $\mu\text{L}$  with 0.04 M HCl. The reaction mixture was heated for 20–30 min at 90°C, and the radiochemical purity was determined using radio-high-performance liquid chromatography and radio-thin-layer chromatography with 0.1 M sodium citrate buffer on instant thin-layer chromatography–silica gel chromatography paper (Agilent) and 1.0 M NH<sub>4</sub>OAc/dimethylformamide buffer (1/1; v/v) on thin-layer chromatography silica gel 60 F<sub>254</sub> plates (Merck Millipore).

### Lipophilicity

Approximately 1 MBq of the  $^{177}\text{Lu}$ -labeled PSMA ligand was dissolved in 1 mL of a 1:1 mixture (v/v) of phosphate-buffered saline (pH 7.4) and *n*-octanol ( $n = 6$ ). After vigorous mixing of the suspension for 3 min, the vial was centrifuged at 15,000g for 3 min, and 100- $\mu\text{L}$  aliquots of both layers were measured in a  $\gamma$ -counter. Finally, the ratio of the radioactivity detected in the *n*-octanol sample and the phosphate-buffered saline buffer was calculated and expressed as distribution ratio  $\log D_{7.4}$ .

### Binding to HSA

Binding of  $^{177}\text{Lu}$ -labeled ligands to HSA was assessed by albumin-mediated size-exclusion chromatography (AMSEC), a novel method that has recently been developed by our group to determine the apparent molecular weight (AMW) of a compound in the presence of HSA. A dedicated and detailed description of the AMSEC method will be published elsewhere to cover the context and the development process of this method in its entirety. Briefly, a gel filtration size-exclusion column (Superdex 75 Increase 10/300 GL; fractionation range, 70–3 kDa; GE Healthcare) was calibrated as recommended by the manufacturer using a commercially available set of proteins (Gel Filtration LMW Calibration Kit; GE Healthcare). AMSEC experiments were performed by injection of the various radioligands using an HSA buffer at physiologic concentration (Biowest) as the mobile phase at room temperature. Depending on the strength of the HSA/ligand interaction during the chromatographic procedure, an injected radioligand (1.0 MBq, 10–20 GBq/ $\mu\text{mol}$ ) can show a reduced retention time that correlates to AMWs higher than the actual, physical, molecular weight (the latter being for all investigated ligands < 2 kDa, and thus below the column fractionation range). The stronger this interaction, the longer the mean time the ligand is bound to HSA during the chromatographic process and the faster the ligand is

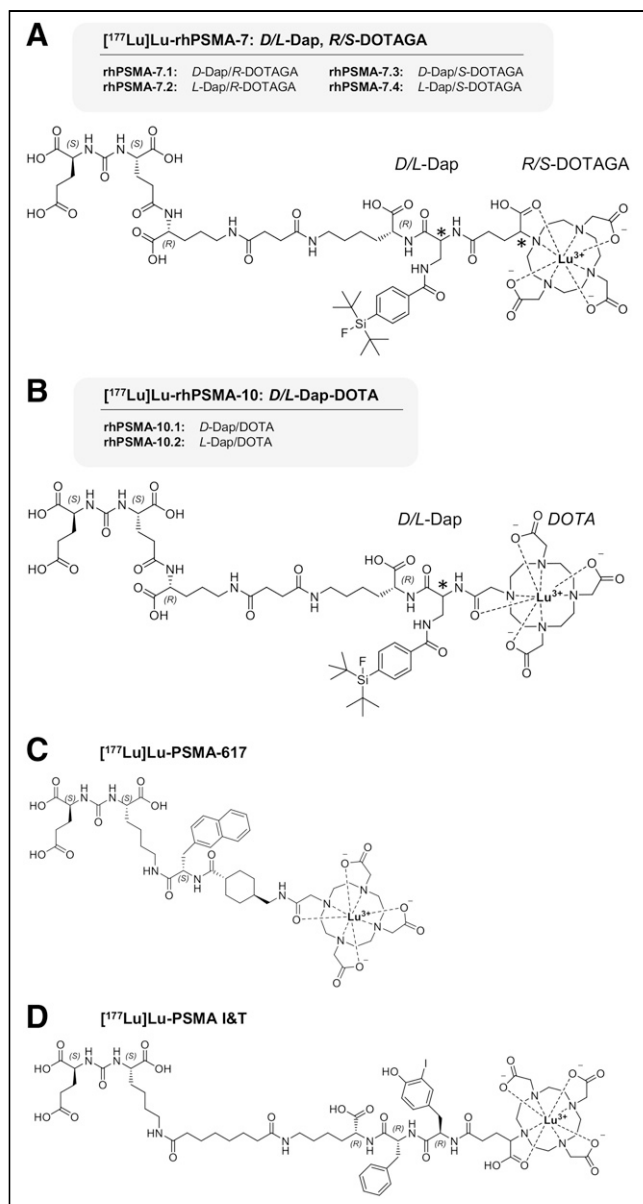


**FIGURE 2.** (A) rhPSMA-7 isomers differ in stereoconfiguration of diaminopropionic acid branching unit (*D*- or *L*-Dap) and glutamic acid arm at DOTAGA chelator (*R*- or *S*-DOTAGA). (B) rhPSMA-10.1 (*D*-Dap) and rhPSMA-10.2 (*L*-Dap), both equipped with DOTA chelator, also differ in stereoconfiguration of branching unit (*D*- or *L*-Dap). Well-established PSMA-addressing ligands PSMA-617 (C) and PSMA I&T (D) served as reference compounds (1,2).

eluted from the column. By means of calibration, the retention time can be translated into a ligand-specific AMW (expressed in kDa) as a parameter allowing quantification of the extent of HSA binding. The detection window ranges between 2.1 kDa (cutoff value, determined by [<sup>18F</sup>]fluoride; no HSA interaction) and 70.2 kDa (experimental molecular weight of HSA; maximum HSA interaction). [<sup>177Lu</sup>]Lu-rhPSMA-7.3 served as an internal standard during AMSEC studies (30.4 ± 0.5 kDa; *n* = 10).

#### Affinity Determinations (Half-Maximal Inhibitory Concentration) and Internalization Studies

Competitive binding studies were determined on LNCaP cells (1.5 × 10<sup>5</sup> cells in 0.25 mL/well) after incubation at 4°C for 1 h, using

(*(S)*-1-carboxy-5-(4-([<sup>125</sup>I]iodo)benzamido)pentyl)carbamoyl-L-glutamic acid ([<sup>125</sup>I]IBA)KuE; 0.2 nM/well) as the reference radioligand (*n* = 3). Internalization studies of the radiolabeled ligands (1.0 nM/well) were performed on LNCaP cells (1.25 × 10<sup>5</sup> cells in 0.25 mL/well) at 37°C for 1 h and accompanied by ([<sup>125</sup>I]IBA)KuE (0.2 nM/well) as a reference. Data were corrected for nonspecific binding and normalized to the specific internalization observed for the reference (*n* = 3), as previously published (8).

#### In Vivo Experiments

All animal experiments were conducted in accordance with general animal welfare regulations in Germany (German animal protection act, as amended on May 18, 2018, article 141 G, version March 29, 2017, I 626, approval 55.2-1-54-2532-71-13) and the institutional guidelines for the care and use of animals. LNCaP tumor xenografts were established in 6- to 8-wk-old male CB-17 SCID mice as described previously (8).

**Biodistribution Studies.** The <sup>177</sup>Lu-labeled PSMA ligands (2–5 MBq; 0.1 nmol) were injected under isoflurane anesthesia into the tail vein of mice, which were euthanized 24 h after injection (*n* = 4–5). Selected organs were removed, weighed, and measured in a  $\gamma$ -counter. All rhPSMA ligands were evaluated during the same period (first quarter of 2020), whereas <sup>177</sup>Lu-labeled PSMA-617 and PSMA I&T (17) were assessed in 2016, using the identical cell line, mouse model, and experimental procedure.

**Small-Animal SPECT/CT Imaging.** Static images of <sup>177</sup>Lu-labeled ligands in euthanized mice were recorded 24 h after injection directly after blood collection, with an acquisition time of 45 min using a high-energy, general-purpose rat-and-mouse collimator and a stepwise multiplanar bed movement. For imaging studies, a VECTOR4 small-animal SPECT/PET/optical imaging/CT device from MILabs was applied. Data were reconstructed using MILabs.Rec software (version 10.02) and PMOD software (version 4.0; PMOD Technologies LLC). After imaging, the mice underwent biodistribution studies.

## RESULTS

### Synthesis and Radiolabeling

Uncomplexed PSMA ligands were obtained via a solid-phase/solution-phase synthetic strategy with chemical purities of more than 97% as determined by high-performance liquid chromatography (absorbance at 220 nm). Identity was confirmed by mass spectrometry. Complexation with a 2.5-fold molar excess of LuCl<sub>3</sub> led to quantitative formation of the respective lutetium-PSMA ligands, which were used for in vitro studies. <sup>177</sup>Lu labeling of PSMA ligands according to standard manual procedures resulted in a radiochemical purity of more than 95%, determined by radio-high-performance liquid chromatography and radio-thin-layer chromatography (Supplemental Table 1).

### In Vitro Characterization

Results of the in vitro evaluation of all rhPSMAs and the reference ligands PSMA-617 (1) and PSMA I&T (2) are summarized in Figure 3 and Supplemental Table 2. PSMA binding affinity (half-maximal inhibitory concentration; Fig. 3A) was high and in the low nanomolar range for all lutetium-rhPSMA ligands (range, 2.8 ± 0.5 to 3.6 ± 0.6 nM) and the 2 reference ligands ([<sup>177</sup>Lu]Lu-PSMA I&T, 4.2 ± 0.8 nM; [<sup>177</sup>Lu]Lu-PSMA-617, 3.3 ± 0.2 nM).

Slight differences between the ligands were found for the PSMA-mediated internalization into LNCaP cells (1 h, 37°C), which is expressed as a percentage of the specific internalization of the reference ligand ([<sup>125</sup>I]IBA)KuE (Fig. 3B). Although [<sup>177</sup>Lu]Lu-rhPSMA-7.1 and [<sup>177</sup>Lu]Lu-PSMA I&T showed the lowest internalization rates, with values of 137% ± 6% and 145% ± 14%, respectively, the other rhPSMA compounds showed an approximately 1.4-fold higher

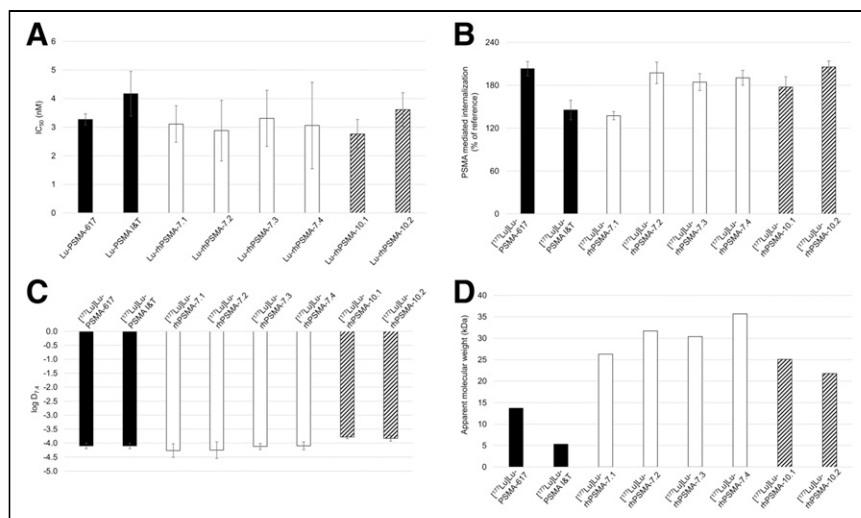


**FIGURE 3.** (A) Binding affinities (half-maximal inhibitory concentration [IC<sub>50</sub>; nM], 1 h, 4°C) of [<sup>177</sup>Lu]Lu-rhPSMA-7.1 to -7.4 (white; n = 3), [<sup>177</sup>Lu]Lu-rhPSMA-10.1 and -10.2 (black/white stripes; n = 3), and references [<sup>177</sup>Lu]Lu-PSMA-617 and [<sup>177</sup>Lu]Lu-PSMA I&T (black; n = 3). (B) PSMA-mediated internalization of [<sup>177</sup>Lu]Lu-rhPSMA-7.1 to -7.4 (white; n = 3), [<sup>177</sup>Lu]Lu-rhPSMA-10.1 and -10.2 (black/white stripes; n = 3), and references [<sup>177</sup>Lu]Lu-PSMA-617 and [<sup>177</sup>Lu]Lu-PSMA I&T (black; n = 3) by LNCaP cells (1 h, 37°C) as percentage of reference ligand ([<sup>125</sup>I]HBA)KuE). (C) Lipophilicity of [<sup>177</sup>Lu]Lu-rhPSMA-7.1 to -7.4 (white; n = 6), [<sup>177</sup>Lu]Lu-rhPSMA-10.1 and -10.2 (black/white stripes; n = 6), and references [<sup>177</sup>Lu]Lu-PSMA-617 and [<sup>177</sup>Lu]Lu-PSMA I&T (black; n = 6), expressed as partition coefficient (log D<sub>7.4</sub> in n-octanol/phosphate-buffered saline, pH 7.4). (D) AMW of [<sup>177</sup>Lu]Lu-rhPSMA-7.1 to -7.4 (white), [<sup>177</sup>Lu]Lu-rhPSMA-10.1 and -10.2 (black/white stripes), and references [<sup>177</sup>Lu]Lu-PSMA-617 and [<sup>177</sup>Lu]Lu-PSMA I&T (black), as determined by HSA-mediated size-exclusion chromatography.

internalization (range, 177% ± 15% to 206% ± 8%), similar to that of [<sup>177</sup>Lu]Lu-PSMA-617 (203% ± 10%).

The <sup>177</sup>Lu-labeled rhPSMA-7 isomers, as well as the references ([<sup>177</sup>Lu]Lu-PSMA I&T and [<sup>177</sup>Lu]Lu-PSMA-617), demonstrated a high and similar hydrophilicity, expressed as a partition coefficient (log D<sub>7.4</sub>; n-octanol and phosphate-buffered saline, pH 7.4) with values between -4.1 ± 0.1 and -4.3 ± 0.3. The DOTA conjugates [<sup>177</sup>Lu]Lu-rhPSMA-10.1 and -10.2 showed a slightly lower hydrophilicity, with a log D<sub>7.4</sub> of -3.8 (Fig. 3C).

The AMW of the tracers was determined to compare the relative HSA-binding strength of the ligands. Exemplary chromatograms of AMSEC experiments showing ligand-specific retention times are provided in Supplemental Figures 1–3. Interestingly, remarkable differences were found for the AMWs of the state-of-the-art references and even among the single isomers of <sup>177</sup>Lu-labeled rhPSMA-7 and rhPSMA-10 (Fig. 3D). Although [<sup>177</sup>Lu]Lu-PSMA I&T showed the lowest HSA interaction (AMW, 5.3 kDa), followed by [<sup>177</sup>Lu]Lu-PSMA-617 (AMW, 13.7 kDa), all radiohybrid ligands demonstrated an at least 1.5-fold higher AMW, with values between 21.8 and 35.7 kDa. Among the radiohybrids, the 2 DOTA conjugates, [<sup>177</sup>Lu]Lu-rhPSMA-10.1 and -10.2, showed the lowest AMWs (25.1 and 21.8 kDa, respectively), whereas D-Dap-configured [<sup>177</sup>Lu]Lu-rhPSMA-7.1 (molecular weight, 26.3 kDa) and [<sup>177</sup>Lu]Lu-rhPSMA-7.3 (molecular weight, 30.4 kDa) showed the lowest AMWs within the rhPSMA-7 series (AMWs of L-Dap-comprising isomers: [<sup>177</sup>Lu]Lu-rhPSMA-7.2, 31.7 kDa; [<sup>177</sup>Lu]Lu-rhPSMA-7.4, 35.7 kDa).

### In Vivo Characterization

**Biodistribution Studies.** Overall, the comparative biodistribution study of the <sup>177</sup>Lu-labeled PSMA ligands in LNCaP tumor-bearing

mice at 24 h after injection revealed a quite similar distribution pattern with high tumor uptake, fast excretion from background organs, but a varying degree of activity retention in the kidneys (Fig. 4; Supplemental Tables 3 and 4).

At 24 h after injection, the highest activity retention in the kidneys was found for [<sup>177</sup>Lu]Lu-PSMA I&T (34.7 ± 17.2 percentage injected dose [%ID]/g), whereas [<sup>177</sup>Lu]Lu-PSMA-617 (1.4 ± 0.4 %ID/g) and [<sup>177</sup>Lu]Lu-rhPSMA-10.1 (2.0 ± 0.8 %ID/g) demonstrated the fastest renal clearance. Kidney uptake of the former lead compound, [<sup>177</sup>Lu]Lu-rhPSMA-7.3, was found to be 9.8 ± 2.7 %ID/g, thus showing slower renal clearance than [<sup>177</sup>Lu]Lu-rhPSMA-7.1 (4.1 ± 0.8 %ID/g), [<sup>177</sup>Lu]Lu-rhPSMA-10.1 (2.0 ± 0.8 %ID/g), and [<sup>177</sup>Lu]Lu-rhPSMA-10.2 (8.1 ± 1.7 %ID/g). These differences are also well illustrated in the small-animal SPECT/CT images (Fig. 5). Tumor uptake was highest for all [<sup>177</sup>Lu]Lu-rhPSMA-7 isomers and in the range of 11.6–12.7 %ID/g, followed by [<sup>177</sup>Lu]Lu-rhPSMA-10.2 (10.5 ± 3.3 %ID/g) and -10.1 (9.8 ± 0.3 %ID/g), whereas the references, <sup>177</sup>Lu-labeled PSMA-617 (7.5 ± 0.9 %ID/g) and PSMA I&T (4.1 ± 1.1 %ID/g), exhibited a lower tumor uptake.

**Tumor-to-Organ Ratios.** Interestingly, all

radiohybrid ligands are cleared from the blood pool and background tissues with a kinetic profile that resembles that of small molecules more than that of larger proteins, despite their extensive binding to HSA. Among all radiohybrids, the highest tumor-to-blood and tumor-to-kidney ratios were found for [<sup>177</sup>Lu]Lu-rhPSMA-10.1 (tumor-to-blood, 11,498; tumor-to-kidney, 5.7), followed by [<sup>177</sup>Lu]Lu-rhPSMA-7.1 (tumor-to-blood, 5,971; tumor-to-kidney, 3.2), whereas [<sup>177</sup>Lu]Lu-rhPSMA-7.3 showed inferior values (tumor-to-blood, 3,843; tumor-to-kidney, 1.2). Although [<sup>177</sup>Lu]Lu-PSMA I&T (tumor-to-blood, 408; tumor-to-kidney, 0.2) exhibited rather slow excretion in mice, [<sup>177</sup>Lu]Lu-PSMA-617 showed the highest tumor-to-kidney ratio (tumor-to-blood, 1,424; tumor-to-kidney, 5.9), whereas its tumor-to-blood ratio was lower than all radiohybrid ligands (Supplemental Tables 5 and 6).

### DISCUSSION

Although it has recently been demonstrated in patients that the uptake of [<sup>177</sup>Lu]Lu-rhPSMA-7.3 in tumor lesions was on average 2- to 3-fold higher than that of [<sup>177</sup>Lu]Lu-PSMA I&T, the slower clearance resulted in a comparatively higher dose to the kidney as the organ at risk (14). In retrospect, this result is hardly surprising, since the selection process of the best diagnostic rhPSMA-7 isomer was based on criteria that are considered suboptimal for therapy: fast blood clearance to reach high tumor-to-background ratios at early time points, predominantly renal clearance, and high kidney retention to ensure low activity in the bladder at early time points. In contrast, the selection criteria for the best therapeutic isomer are different. Compared with today's therapeutic ligands, a slightly delayed blood clearance is preferred. The ligand should be excreted renally while showing almost no retention in the kidneys.

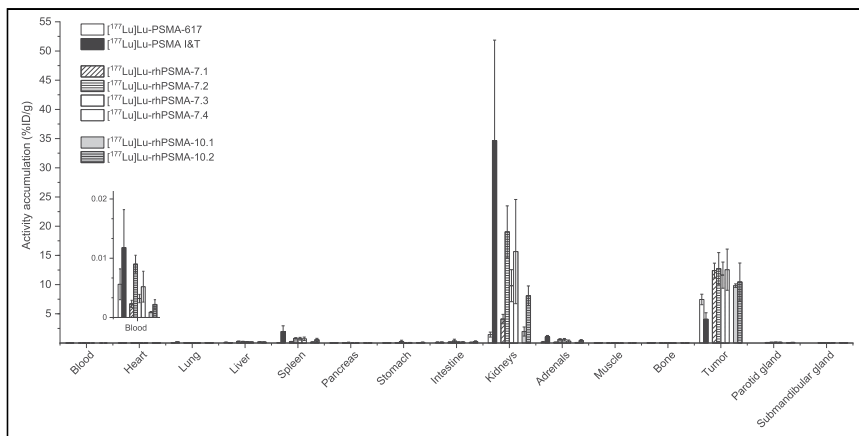


**FIGURE 4.** Biodistribution of [ $^{177}\text{Lu}$ ]Lu-rhPSMA-7.1 to -7.4, [ $^{177}\text{Lu}$ ]Lu-rhPSMA-10.1 and -10.2, and references [ $^{177}\text{Lu}$ ]Lu-PSMA-617 and [ $^{177}\text{Lu}$ ]Lu-PSMA I&T at 24 h after injection in male LNCaP tumor-bearing SCID mice. Data are expressed as %ID/g, mean  $\pm$  SD ( $n = 4 - 5$ ). Values of [ $^{177}\text{Lu}$ ]Lu-PSMA I&T were taken from previously published study by our group (17) that was performed under identical conditions.

It must also be considered that the change in the isotope (lutetium for RLT instead of gallium for the diagnostic compound) results in a different structure and charge at the chelate-metal complex (gallium-DOTA: hexadentate, zwitterionic; lutetium-DOTA: octadentate, uncharged) (15). This matter obviously influences the pharmacokinetic properties of the entire ligand, as demonstrated by the prolonged clearance kinetics of the  $^{177}\text{Lu}$ -labeled “best diagnostic isomer” rhPSMA-7.3 in patients (14).

With the aim of addressing these therapeutic criteria and of identifying a  $^{177}\text{Lu}$ -labeled rhPSMA tracer with more favorable characteristics for RLT, we performed a coevaluation of 6 different rhPSMA ligands (4 rhPSMA-7 isomers and 2 rhPSMA-10 isomers) and compared the results with preclinical data on the 2 reference compounds, PSMA-617 and PSMA I&T.

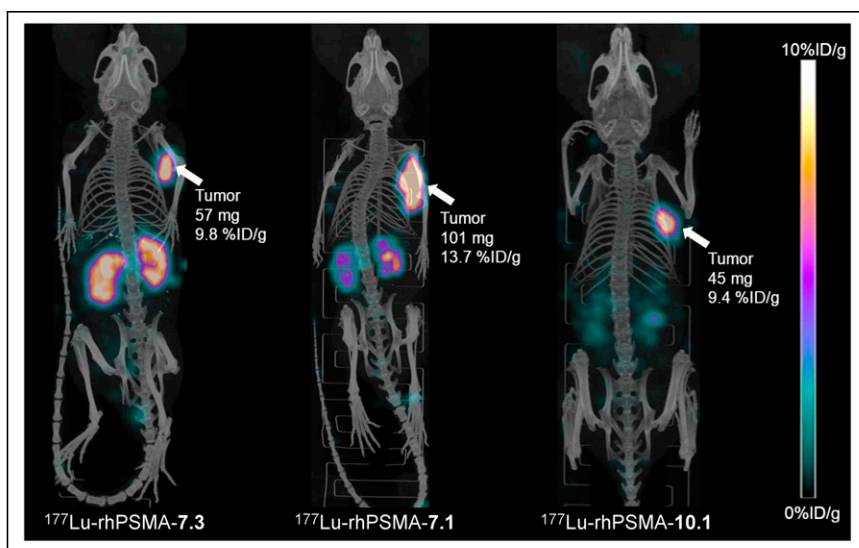


**FIGURE 5.** Static small-animal SPECT/CT images (maximum-intensity projections) of  $^{177}\text{Lu}$ -labeled rhPSMA-7.3, -7.1, and -10.1 in LNCaP tumor-bearing mice, euthanized 24 h after injection and imaged directly after blood collection, with acquisition time of 45 min on VECTor4 small-animal SPECT/PET/optimal imaging/CT device. Tumor weight and tracer uptake in tumor (%ID/g) were determined from subsequent biodistribution studies.

All lutetium-complexed radiohybrid tracers and the external references, PSMA I&T and PSMA-617, demonstrated potent binding to LNCaP cells with an excellent affinity in the low-nanomolar range and high internalization rates, which did not allow prioritization of certain candidates for further evaluation.

In the context of PSMA-targeted RLT, the kidney and then the bone marrow are still considered the main organs at risk, and uptake in these should be carefully considered (18).

In our comparative biodistribution studies, pronounced differences in kidney uptake values were observed. Whereas our internal reference, D-Dap-S-DOTAGA-configured [ $^{177}\text{Lu}$ ]Lu-rhPSMA-7.3, showed a kidney uptake of  $9.8 \pm 2.7$  %ID/g at 24 h after injection, the uptake of the D-Dap-DOTA derivative, [ $^{177}\text{Lu}$ ]Lu-rhPSMA-10.1, reached only 20% of that value ( $2.0 \pm 0.8$  %ID/g). Moreover, the stereoconfiguration of the Dap-

branching unit (D-Dap or L-Dap) also resulted in a pronounced different kidney uptake, as shown for [ $^{177}\text{Lu}$ ]Lu-rhPSMA-7.1 (D-Dap,  $4.1 \pm 0.8$  %ID/g) and the 5-fold higher value of the corresponding L-Dap version, [ $^{177}\text{Lu}$ ]Lu-rhPSMA-7.2 ( $19.0 \pm 4.5$  %ID/g). As already demonstrated in a previous study of [ $^{18}\text{F}$ ]Ga-rhPSMA ligands (12), these results impressively demonstrate once more that even small modifications in the arene binding region of PSMA-targeted ligands can have a remarkable influence on the biodistribution. In this former study, the modification of the stereoconfiguration of the Dap branching unit and the DOTAGA chelator resulted in superior pharmacokinetics of [ $^{18}\text{F}$ ]Ga-rhPSMA-7.3 in mice compared with the diastereomeric mixture [ $^{18}\text{F}$ ]Ga-rhPSMA-7. This result was confirmed in patient studies, revealing a 5-fold lower excretion of [ $^{18}\text{F}$ ]Ga-rhPSMA-7.3 into the bladder, a 1.6-fold lower kidney uptake, and a 1.6-fold higher tumor uptake than for the diastereomeric mixture [ $^{18}\text{F}$ ]Ga-rhPSMA-7 (19).

Even though the results of our preclinical comparison are highly promising, there are many examples in the literature that question the direct transferability of the preclinical results to clinical studies, particularly with regard to kidney clearance and kidney retention. The low kidney uptake of [ $^{177}\text{Lu}$ ]Lu-PSMA-617 ( $1.4 \pm 0.4$  %ID/g at 24 h after injection) in mice has often been highlighted as a major selection criterion that promoted its rapid clinical development and thus was considered a major advantage compared with [ $^{177}\text{Lu}$ ]Lu-PSMA I&T (kidney uptake,  $34.7 \pm 17.2$  %ID/g at 24 h after injection) (20). However, in contrast to preclinical results, head-to-head comparison of both ligands in patients has impressively demonstrated a nearly identical kidney uptake and clearance kinetic of both tracers (7). Moreover, a similar absorbed dose to the kidney was found in dosimetry studies:  $0.4 \pm 0.2$  to  $0.8 \pm 0.3$  Gy/GBq for [ $^{177}\text{Lu}$ ]Lu-PSMA-617 (21–23) and

0.7 ± 0.2 Gy/GBq for [<sup>177</sup>Lu]Lu-PSMA I&T (24). Until further investigations improve our understanding of species-dependent renal handling of PSMA tracers, and in the absence of alternative and more valid selection criteria, the evaluation of the biodistribution in mice, including the assessment of the different excretion behavior, will remain our only viable option—although we should treat such data with appropriate caution.

Regarding important nontarget organs such as liver, muscle, and heart, all ligands demonstrated almost identical and complete clearance 24 h after injection. Even though only low activity levels were found in the blood pool for all ligands, [<sup>177</sup>Lu]Lu-rhPSMA-10.1 showed the best clearance of all investigated PSMA ligands, and this superior clearance is also expressed by the highest tumor-to-blood ratio (11,498): 3 times higher than for [<sup>177</sup>Lu]Lu-rhPSMA-7.3 and 8 times higher than for [<sup>177</sup>Lu]Lu-PSMA-617.

The tendency of both DOTA-conjugated [<sup>177</sup>Lu]Lu-rhPSMA-10 isomers to clear more quickly can at least in part be explained by the HSA-binding experiments and our newly introduced in vitro parameter, AMW. The molecular weight of a molecule is known to have a direct implication in the glomerular sieving coefficient (GSC) (as a rule of thumb, the lower the molecular weight, the higher the GSC and the faster the excretion kinetics) (25). Thus, the stronger the interaction of a molecule with HSA or the higher the ratio of HSA-bound ligand to free ligand, the less ligand is subjected to glomerular filtration and thus the less ligand is excreted. In our assay, this ratio is indirectly determined by calculating the AMW of each compound (details on these methods will be described elsewhere).

Looking at the AMW of <sup>177</sup>Lu-labeled PSMA-617 (13.7 kDa) and PSMA-I&T (5.3 kDa) as key reference points, the 2.3-fold lower AMW of PSMA I&T appears *prima facie* unproportional: Kulkarni et al. could demonstrate that [<sup>177</sup>Lu]Lu-PSMA-617 exhibits only a marginally slower clearance in patients than does [<sup>177</sup>Lu]Lu-PSMA I&T (7). However, taking into account the non-linear correlation of the molecular weight and GSC and the tiny changes in the GSC at low molecular weights, the differences in the AMW of PSMA I&T and PSMA-617 result in only slightly different GSCs, which explains the similar kidney excretion kinetics of these 2 ligands in patients (25). In contrast, the higher AMW of [<sup>177</sup>Lu]Lu-rhPSMA-7.3 (molecular weight, 30.4) would translate into a markedly lower GSC and thus a delayed clearance, which has been confirmed by clinical results from Feurecker et al. (14). On the basis of these results, we expect that the blood clearance kinetics of [<sup>177</sup>Lu]Lu-rhPSMA-10.1 and -10.2 in humans will be somewhere between that of [<sup>177</sup>Lu]Lu-rhPSMA-7.3 and [<sup>177</sup>Lu]Lu-PSMA-617/PSMA-I&T. As demonstrated by Feurecker et al. (14), the remarkable tumor uptake of [<sup>177</sup>Lu]Lu-rhPSMA-7.3 found in our preclinical experiments (13) could also be observed in patients (effective dose of 6.4 ± 6.7 mGy/MBq for [<sup>177</sup>Lu]Lu-rhPSMA-7.3 vs. 2.6 ± 2.4 mGy/MBq for [<sup>177</sup>Lu]Lu-PSMA I&T). Thus, we are optimistic that we will be able to obtain a similarly improved tumor uptake in patients during the clinical assessment of [<sup>177</sup>Lu]Lu-rhPSMA-10.1 and thus tumor doses higher than those currently obtained with the state-of-the-art nonhybrid ligands (14).

Certainly there are also other effects determining different clearance kinetics of radiopharmaceuticals in mice and patients that must be considered—for example, species differences in drug binding to serum albumin (26) and differences in magnitude and binding affinities of the tracers to plasma proteins other than HSA, such as α-1-acid glycoprotein (27), transthyretin (28), or lipoproteins (29). Moreover, individual differences in uptake of PSMA ligands into the kidneys (30),

varying relative proportions of hepatobiliary to renal clearance, and effects of species differences between mice and humans must be considered. In summary, however, we are optimistic that the promising biodistribution profile of [<sup>177</sup>Lu]Lu-rhPSMA-10.1 observed in mice, together with its low AMW, will translate into improved tumor doses and tumor-to-kidney dose ratios of this isomer in patients.

## CONCLUSION

On the basis of this preclinical comparison, [<sup>177</sup>Lu]Lu-rhPSMA-10.1 seems to be a promising lead for the clinical development of an rhPSMA-targeted ligand for RLT. [<sup>177</sup>Lu]Lu-rhPSMA-10.1 could have the potential to outperform the *in vivo* characteristics of the currently developed state-of-the-art PSMA targeted radioligands [<sup>177</sup>Lu]Lu-PSMA-617 and [<sup>177</sup>Lu]Lu-PSMA-I&T in men. Clinical studies are required to demonstrate whether our newly introduced additional preclinical selection criterion, the AMW, could be a valuable parameter for the future development of further therapeutic radiopharmaceuticals with optimally adjusted clearance kinetics.

## DISCLOSURE

Hans-Jürgen Wester, Alexander Wurzer, Jan-Philip Kunert, Sebastian Fischer, and Veronika Felber are listed as inventors in patent applications for some types of therapeutic rhPSMA. Hans-Jürgen Wester receives funding from the SFB 824 (Deutsche Forschungsgemeinschaft, Bonn, Germany, Sonderforschungsbereich 824, project B11 and Z). Hans-Jürgen Wester is a founder and shareholder of, and a scientific advisor for, Scintomics GmbH, Fuerstenfeldbruck, Germany. Wolfgang Weber is a consultant for Blue Earth Diagnostics Ltd. No other potential conflict of interest relevant to this article was reported.

## ACKNOWLEDGMENT

We thank Catriona Turnbull for carefully proofreading the manuscript.

## KEY POINTS

**QUESTION:** Which <sup>177</sup>Lu-labeled rhPSMA ligand shows the best characteristics for RLT of prostate cancer?

**PERTINENT FINDINGS:** In preclinical experiments, [<sup>177</sup>Lu]Lu-rhPSMA-10.1 demonstrated fast clearance kinetics from healthy tissues while preserving high tumor uptake.

**IMPLICATIONS FOR PATIENT CARE:** Preclinical data indicate more favorable pharmacokinetics for [<sup>177</sup>Lu]Lu-rhPSMA-10.1 than for [<sup>177</sup>Lu]Lu-PSMA-617 and [<sup>177</sup>Lu]Lu-PSMA-I&T for RLT, a finding that has to be investigated in prospective clinical studies.

## REFERENCES

1. Benešová M, Schafer M, Bauder-Wust U, et al. Preclinical evaluation of a tailor-made DOTA-conjugated PSMA inhibitor with optimized linker moiety for imaging and endoradiotherapy of prostate cancer. *J Nucl Med*. 2015;56:914–920.
2. Weineisen M, Schottelius M, Simecek J, et al. <sup>68</sup>Ga- and <sup>177</sup>Lu-labeled PSMA I&T: optimization of a PSMA-targeted theranostic concept and first proof-of-concept human studies. *J Nucl Med*. 2015;56:1169–1176.
3. Heck MM, Tauber R, Schwaiger S, et al. Treatment outcome, toxicity, and predictive factors for radioligand therapy with <sup>177</sup>Lu-PSMA-I&T in metastatic castration-resistant prostate cancer. *Eur Urol*. 2019;75:920–926.

4. Hofman MS, Violet J, Hicks RJ, et al. [<sup>177</sup>Lu]-PSMA-617 radionuclide treatment in patients with metastatic castration-resistant prostate cancer (LuPSMA trial): a single-centre, single-arm, phase 2 study. *Lancet Oncol*. 2018;19:825–833.
5. Kratochwil C, Fendler WP, Eiber M, et al. EANM procedure guidelines for radionuclide therapy with <sup>177</sup>Lu-labelled PSMA-ligands (<sup>177</sup>Lu-PSMA-RLT). *Eur J Nucl Med Mol Imaging*. 2019;46:2536–2544.
6. Morris MJ, Bono JSD, Chi KN, et al. Phase III study of lutetium-177-PSMA-617 in patients with metastatic castration-resistant prostate cancer (VISION) [abstract]. *J Clin Oncol*. 2021;39(suppl):LBA4.
7. Kulkarni HR, Singh A, Schuchardt C, et al. PSMA-based radioligand therapy for metastatic castration-resistant prostate cancer: the Bad Berka experience since 2013. *J Nucl Med*. 2016;57(suppl 3):97S–104S.
8. Wurzer A, Di Carlo D, Schmidt A, et al. Radiohybrid ligands: a novel tracer concept exemplified by <sup>18</sup>F- or <sup>68</sup>Ga-labeled rhPSMA inhibitors. *J Nucl Med*. 2020;61:735–742.
9. Kroenke M, Wurzer A, Schwamborn K, et al. Histologically confirmed diagnostic efficacy of <sup>18</sup>F-rhPSMA-7 PET for N-staging of patients with primary high-risk prostate cancer. *J Nucl Med*. 2020;61:710–715.
10. Eiber M, Kroenke M, Wurzer A, et al. <sup>18</sup>F-rhPSMA-7 PET for the detection of biochemical recurrence of prostate cancer after radical prostatectomy. *J Nucl Med*. 2020;61:696–701.
11. Oh SW, Wurzer A, Teoh EJ, et al. Quantitative and qualitative analyses of biodistribution and PET image quality of a novel radiohybrid PSMA, <sup>18</sup>F-rhPSMA-7, in patients with prostate cancer. *J Nucl Med*. 2020;61:702–709.
12. Wurzer A, Parzinger M, Konrad M, et al. Preclinical comparison of four [<sup>18</sup>F, <sup>nat</sup>Ga]rhPSMA-7 isomers: influence of the stereoconfiguration on pharmacokinetics. *EJNMMI Res*. 2020;10:149.
13. Yusufi N, Wurzer A, Herz M, et al. Comparative preclinical biodistribution, dosimetry, and endoradiotherapy in metastatic castration-resistant prostate cancer using <sup>19</sup>F/<sup>166</sup>Lu-rhPSMA-7.3 and <sup>177</sup>Lu-PSMA I&T. *J Nucl Med*. 2021;62:1106–1111.
14. Feuerecker B, Chantadisai M, Allmann A, et al. Pretherapeutic comparative dosimetry of <sup>177</sup>Lu-rhPSMA-7.3 and <sup>177</sup>Lu-PSMA I&T in patients with metastatic castration-resistant prostate cancer. *J Nucl Med*. 2022;63:833–839.
15. Wadas TJ, Wong EH, Weisman GR, Anderson CJ. Coordinating radiometals of copper, gallium, indium, yttrium, and zirconium for PET and SPECT imaging of disease. *Chem Rev*. 2010;110:2858–2902.
16. Umbricht CA, Benešová M, Schmid RM, et al. <sup>44</sup>Sc-PSMA-617 for radiotheragnostics in tandem with <sup>177</sup>Lu-PSMA-617: preclinical investigations in comparison with <sup>68</sup>Ga-PSMA-11 and <sup>68</sup>Ga-PSMA-617. *EJNMMI Res*. 2017;7:9.
17. Wirtz M, Schmidt A, Schottelius M, et al. Synthesis and in vitro and in vivo evaluation of urea-based PSMA inhibitors with increased lipophilicity. *EJNMMI Res*. 2018;8:84.
18. Yordanova A, Becker A, Eppard E, et al. The impact of repeated cycles of radioligand therapy using [<sup>177</sup>Lu]Lu-PSMA-617 on renal function in patients with hormone refractory metastatic prostate cancer. *Eur J Nucl Med Mol Imaging*. 2017;44:1473–1479.
19. Oh SW, Wurzer A, Yusufi N, et al. Preclinical dosimetry and human biodistribution of <sup>18</sup>F-rhPSMA-7 and <sup>18</sup>F-rhPSMA-7.3 [abstract]. *J Nucl Med*. 2019;60(suppl 1):1635.
20. Wester HJ, Schottelius M. PSMA-targeted radiopharmaceuticals for imaging and therapy. *Semin Nucl Med*. 2019;49:302–312.
21. Delker A, Fendler WP, Kratochwil C, et al. Dosimetry for <sup>177</sup>Lu-DKFZ-PSMA-617: a new radiopharmaceutical for the treatment of metastatic prostate cancer. *Eur J Nucl Med Mol Imaging*. 2016;43:42–51.
22. Kabasakal L, Toklu T, Yeyin N, et al. Lu-177-PSMA-617 prostate-specific membrane antigen inhibitor therapy in patients with castration-resistant prostate cancer: stability, bio-distribution and dosimetry. *Mol Imaging Radionucl Ther*. 2017;26:62–68.
23. Violet J, Jackson P, Ferdinandus J, et al. Dosimetry of <sup>177</sup>Lu-PSMA-617 in metastatic castration-resistant prostate cancer: correlations between pretherapeutic imaging and whole-body tumor dosimetry with treatment outcomes. *J Nucl Med*. 2019;60:517–523.
24. Okamoto S, Thieme A, Allmann J, et al. Radiation dosimetry for <sup>177</sup>Lu-PSMA I&T in metastatic castration-resistant prostate cancer: absorbed dose in normal organs and tumor lesions. *J Nucl Med*. 2017;58:445–450.
25. Norden AG, Lapsley M, Lee PJ, et al. Glomerular protein sieving and implications for renal failure in Fanconi syndrome. *Kidney Int*. 2001;60:1885–1892.
26. Colclough N, Ruston L, Wood JM, MacFaul PA. Species differences in drug plasma protein binding. *MedChemComm*. 2014;5:963–967.
27. Smith SA, Waters NJ. Pharmacokinetic and pharmacodynamic considerations for drugs binding to alpha-1-acid glycoprotein. *Pharm Res*. 2018;36:30.
28. Buxbaum JN, Reixach N. Transthyretin: the servant of many masters. *Cell Mol Life Sci*. 2009;66:3095–3101.
29. Wasan KM, Brocks DR, Lee SD, Sachs-Barrable K, Thornton SJ. Impact of lipoproteins on the biological activity and disposition of hydrophobic drugs: implications for drug discovery. *Nat Rev Drug Discov*. 2008;7:84–99.
30. Begum NJ, Thieme A, Eberhardt N, et al. The effect of total tumor volume on the biologically effective dose to tumor and kidneys for <sup>177</sup>Lu-labeled PSMA peptides. *J Nucl Med*. 2018;59:929–933.

## General Information

Analytical and preparative high-performance liquid chromatography (HPLC) was performed using Shimadzu gradient systems (Neufahrn, Germany) equipped with an SPD-20A UV/Vis detector. The columns for analytical (MultoKrom 100C18, 150×4.6 mm, 5 μm), radio-analytical (Multospher 100RP18, 125×4.6 mm, 5 μm) and preparative (MultoKrom 100C18, 250×20 mm, 5 μm) HPLC were purchased from CS Chromatographie Service (Langerwehe, Germany). Eluents for all HPLC operations were water (solvent A) and acetonitrile with 2 vol.% water (solvent B), both containing 0.1 vol.% trifluoroacetic acid (TFA). Radioactivity was detected via a HERM LB 500 NaI detector (Berthold Technologies, Bad Wildbad, Germany). Radio-thin layer chromatography (TLC) was carried out with a Scan-RAM detector (LabLogic Systems, Sheffield, United Kingdom). Electrospray ionization-mass spectra were acquired on an expression<sup>L</sup> CMS (Advion, Harlow, UK).

## Synthesis of PSMA Ligands

The uncomplexed radiohybrid ligands rhPSMA-7.1, -7.2, -7.3 and -7.4 were prepared by applying a mixed solid phase/solution phase synthetic strategy, according to the literature protocols (1). rhPSMA-10.1 and -10.2 were obtained in analogy to the rhPSMA-7 isomers, by substitution of the DOTA-GA chelator with DOTA. PSMA I&T was prepared according to the published procedure (2) and PSMA-617 was purchased from MedChemExpress LLC (Monmouth Junction, USA).

For complexation with non-radioactive lutetium for *in vitro* studies, a 2 mM solution of the PSMA inhibitor (1.0 eq.) in DMSO was combined with a 20 mM aqueous solution of LuCl<sub>3</sub> (2.5 eq.) and heated to 95°C for 30 min. Analytical data of the Lu-chelated PSMA ligands are summarized in the supporting information.

## Analytical data of Lu-complexed PSMA inhibitors:

**Lu-rhPSMA-7.1:** RP-HPLC (10 to 70% B in 15 min):  $t_R = 9.7$  min,  $K' = 3.85$ . Calculated monoisotopic mass (C<sub>63</sub>H<sub>96</sub>FLuN<sub>12</sub>O<sub>25</sub>Si): 1642.6; found:  $m/z = 1643.5$  [M+H]<sup>+</sup>, 822.5 [M+2H]<sup>2+</sup>.

**Lu-rhPSMA-7.2:** RP-HPLC (10 to 70% B in 15 min):  $t_R = 9.4$  min,  $K' = 3.70$ . Calculated monoisotopic mass (C<sub>63</sub>H<sub>96</sub>FLuN<sub>12</sub>O<sub>25</sub>Si): 1642.6; found:  $m/z = 1642.9$  [M+H]<sup>+</sup>, 822.0 [M+2H]<sup>2+</sup>.

**Lu-rhPSMA-7.3:** RP-HPLC (10 to 70% B in 15 min):  $t_R = 9.6$  min,  $K' = 3.80$ . Calculated monoisotopic mass (C<sub>63</sub>H<sub>96</sub>FLuN<sub>12</sub>O<sub>25</sub>Si): 1642.6; found:  $m/z = 1643.4$  [M+H]<sup>+</sup>, 822.3 [M+2H]<sup>2+</sup>.

**Lu-rhPSMA-7.4:** RP-HPLC (10 to 70% B in 15 min):  $t_R = 9.6$  min,  $K' = 3.80$ . Calculated monoisotopic mass (C<sub>63</sub>H<sub>96</sub>FLuN<sub>12</sub>O<sub>25</sub>Si): 1642.6; found:  $m/z = 1643.0$  [M+H]<sup>+</sup>, 822.3 [M+2H]<sup>2+</sup>.

**Lu-rhPSMA-10.1:** RP-HPLC (10 to 70% B in 15 min):  $t_R = 9.9$  min,  $K' = 3.95$ . Calculated monoisotopic mass ( $C_{60}H_{92}FLuN_{12}O_{23}Si$ ): 1570.6; found:  $m/z = 1571.8 [M+H]^+$ ,  $786.2 [M+2H]^{2+}$ .

**Lu-rhPSMA-10.2:** RP-HPLC (10 to 70% B in 15 min):  $t_R = 9.6$  min,  $K' = 3.80$ . Calculated monoisotopic mass ( $C_{60}H_{92}FLuN_{12}O_{23}Si$ ): 1570.6; found:  $m/z = 1571.9 [M+H]^+$ ,  $786.6 [M+2H]^{2+}$ .

**Lu-PSMA-I&T:** RP-HPLC (10 to 70% B in 15 min):  $t_R = 7.2$  min,  $K' = 3.32$ . Calculated monoisotopic mass ( $C_{63}H_{89}ILuN_{11}O_{23}$ ): 1669.5; found:  $m/z = 1670.5 [M+H]^+$ ,  $1113.8 [2M+3H]^{3+}$ .

**Lu-PSMA-617:** RP-HPLC (10 to 70% B in 15 min):  $t_R = 6.5$  min,  $K' = 2.82$ . Calculated monoisotopic mass ( $C_{49}H_{68}LuN_9O_{16}$ ): 1213.4; found:  $m/z = 1213.6 [M+H]^+$ ,  $607.5 [M+2H]^{2+}$ .

**Supplemental Table 1:** Radiochemical purity (RCP) of  $^{177}Lu$ -labeled rhPSMA isomers, determined by radio-TLC before lipophilicity studies, using either the citrate buffer system (0.1 M sodium citrate buffer on iTLC-SG chromatography paper) or acetate buffer system (1.0 M  $NH_4OAc$ /DMF buffer (1/1; v/v) on TLC Silica gel 60 F254 plates).

$[^{177}Lu]Lu-$	<b>citrate-TLC RCP</b>	<b>acetate-TLC RCP</b>
rhPSMA-7.1	99.5%	99.7%
rhPSMA-7.2	99.8%	99.8%
rhPSMA-7.3	99.8%	99.9%
rhPSMA-7.4	99.8%	99.8%
rhPSMA-10.1	99.8%	99.8%
rhPSMA-10.2	99.7%	99.7%

**Supplemental Table 2:** Binding affinities ( $IC_{50}$  [nM], 1 h, 4°C) of Lu-rhPSMA-7.1 to -7.4 (n=3), Lu-rhPSMA-10.1, -10.2 (n=3) and the references Lu-PSMA-617 and Lu-PSMA-I&T (n=3); PSMA-mediated internalization of [ $^{177}\text{Lu}$ ]Lu-rhPSMA-7.1 to -7.4 (n=3), [ $^{177}\text{Lu}$ ]Lu-rhPSMA-10.1, -10.2 (n=3) and the references [ $^{177}\text{Lu}$ ]Lu-PSMA-617 and [ $^{177}\text{Lu}$ ]Lu-PSMA I&T (n=3) by LNCaP cells (1 h, 37°C) as a percentage of the reference ligand ([ $^{125}\text{I}$ ]IBA)KuE); Lipophilicity of [ $^{177}\text{Lu}$ ]Lu-rhPSMA-7.1 to -7.4 (n=6), [ $^{177}\text{Lu}$ ]Lu-rhPSMA-10.1, -10.2 (n=6) and the references [ $^{177}\text{Lu}$ ]Lu-PSMA-617 and [ $^{177}\text{Lu}$ ]Lu-PSMA I&T (n=6), expressed as partition coefficient ( $\log D_{7.4}$ ) using the *n*-octanol/PBS (pH 7.4) distribution system ; Apparent molecular weight ( $MW_{\text{app}}$ ) of [ $^{177}\text{Lu}$ ]Lu-rhPSMA-7.1 to -7.4, [ $^{177}\text{Lu}$ ]Lu-rhPSMA-10.1, -10.2 and the references [ $^{177}\text{Lu}$ ]Lu-PSMA-617 and [ $^{177}\text{Lu}$ ]Lu-PSMA I&T, as determined by human serum albumin mediated size exclusion chromatography (AMSEC).

Compound	[ $^{177}\text{Lu}$ ]Lu-rhPSMA-7.1	[ $^{177}\text{Lu}$ ]Lu-rhPSMA-7.2	[ $^{177}\text{Lu}$ ]Lu-rhPSMA-7.3	[ $^{177}\text{Lu}$ ]Lu-rhPSMA-7.4	[ $^{177}\text{Lu}$ ]Lu-rhPSMA-	[ $^{177}\text{Lu}$ ]Lu-rhPSMA-	[ $^{177}\text{Lu}$ ]Lu-PSMA-617	[ $^{177}\text{Lu}$ ]Lu-PSMA I&T
$IC_{50}$ [nM]	3.11 ± 0.64	2.88 ± 1.06	3.29 ± 1.00	3.06 ± 1.51	2.76 ± 0.51	3.61 ± 0.59	3.27 ± 0.19	4.17 ± 0.78
Internalization [%IBA-KuE]	137.4 ± 5.8	197.3 ± 15.0	184.4 ± 11.8	190.4 ± 10.5	177.4 ± 14.6	205.6 ± 8.3	203.2 ± 10.1	145.4 ± 13.8
$\log D_{7.4}$	-4.27 ± 0.24	-4.25 ± 0.29	-4.12 ± 0.11	-4.10 ± 0.14	-3.78 ± 0.06	-3.83 ± 0.10	-4.1 ± 0.1	-4.1 ± 0.1
$MW_{\text{app}}$ [kDa]	26.3	31.7	30.4	35.7	25.1	21.8	13.7	5.3

**Supplemental Table 3:** Biodistribution of [<sup>177</sup>Lu]Lu-rhPSMA-7.1 to -7.4 at 24 h p.i. in male LNCaP tumor-bearing SCID mice. Data are expressed as a percentage of the injected dose per gram (% ID/g), mean ± standard deviation (SD; n=4).

uptake in % ID/g	[ <sup>177</sup> Lu]Lu- rhPSMA-7.1 24 h p.i., n = 4		[ <sup>177</sup> Lu]Lu- rhPSMA-7.2 24 h p.i., n = 4		[ <sup>177</sup> Lu]Lu- rhPSMA-7.3 24 h p.i., n = 4		[ <sup>177</sup> Lu]Lu- rhPSMA-7.4 24 h p.i., n = 4	
	mean	SD	mean	SD	mean	SD	mean	SD
<b>blood</b>	<b>0.0023</b>	<b>0.0006</b>	<b>0.0090</b>	<b>0.0015</b>	<b>0.0032</b>	<b>0.0007</b>	<b>0.0052</b>	<b>0.0026</b>
heart	0.036	0.009	0.032	0.005	0.031	0.009	0.032	0.006
lung	0.050	0.006	0.049	0.009	0.049	0.011	0.056	0.014
<b>liver</b>	<b>0.28</b>	<b>0.06</b>	<b>0.24</b>	<b>0.06</b>	<b>0.22</b>	<b>0.04</b>	<b>0.16</b>	<b>0.03</b>
spleen	0.24	0.04	0.79	0.13	0.73	0.23	0.72	0.29
pancreas	0.019	0.003	0.076	0.071	0.025	0.005	0.027	0.006
stomach	0.071	0.018	0.246	0.236	0.059	0.028	0.068	0.029
intestine	0.15	0.05	0.34	0.31	0.13	0.08	0.15	0.07
<b>kidney</b>	<b>4.10</b>	<b>0.81</b>	<b>19.04</b>	<b>4.45</b>	<b>9.82</b>	<b>2.74</b>	<b>15.66</b>	<b>8.92</b>
adrenals	0.12	0.04	0.61	0.13	0.56	0.22	0.34	0.18
muscle	0.011	0.001	0.010	0.002	0.009	0.003	0.010	0.003
bone	0.030	0.009	0.034	0.008	0.048	0.010	0.023	0.009
<b>tumor</b>	<b>12.40</b>	<b>1.27</b>	<b>12.73</b>	<b>2.76</b>	<b>11.63</b>	<b>2.24</b>	<b>12.56</b>	<b>3.52</b>
parotid gl.	0.083	0.020	0.114	0.030	0.131	0.042	0.111	0.057
submand. gl.	0.051	0.004	0.072	0.005	0.056	0.010	0.075	0.019

**Supplemental Table 4:** Biodistribution of [<sup>177</sup>Lu]Lu-rhPSMA-10.1, -10.2 and the references [<sup>177</sup>Lu]Lu-PSMA-617 and [<sup>177</sup>Lu]Lu-PSMA I&T at 24 h p.i. in male LNCaP tumor-bearing SCID mice. Data are expressed as a percentage of the injected dose per gram (% ID/g), mean ± standard deviation (SD; n=4-5). Values of [<sup>177</sup>Lu]Lu-PSMA I&T were taken from a previously published study by our group (3). N.d. not determined.

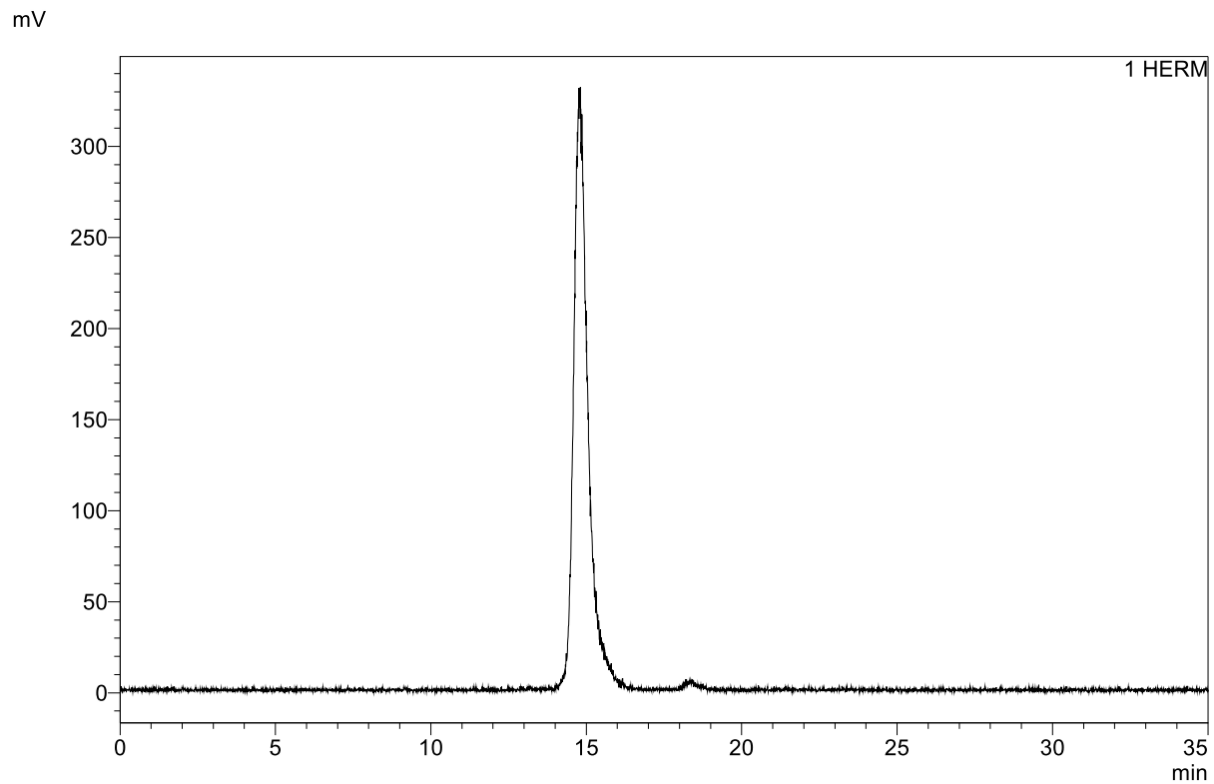
uptake in % ID/g	[ <sup>177</sup> Lu]Lu- rhPSMA-10.1 24 h p.i., n = 5		[ <sup>177</sup> Lu]Lu- rhPSMA-10.2 24 h p.i., n = 4		[ <sup>177</sup> Lu]Lu- PSMA-617 24 h p.i., n = 4		[ <sup>177</sup> Lu]Lu- PSMA-I&T 24 h p.i., n = 4	
	mean	SD	mean	SD	mean	SD	mean	SD
<b>blood</b>	<b>0.0009</b>	<b>0.0001</b>	<b>0.0022</b>	<b>0.0008</b>	<b>0.0056</b>	<b>0.0026</b>	<b>0.0118</b>	<b>0.0064</b>
heart	0.017	0.001	0.020	0.004	0.012	0.004	0.049	0.034
lung	0.032	0.004	0.036	0.007	0.039	0.013	0.158	0.029
<b>liver</b>	<b>0.18</b>	<b>0.06</b>	<b>0.15</b>	<b>0.05</b>	<b>0.12</b>	<b>0.06</b>	<b>0.05</b>	<b>0.01</b>
spleen	0.17	0.03	0.53	0.26	0.08	0.01	1.94	1.01
pancreas	0.013	0.002	0.021	0.002	0.011	0.004	0.048	0.029
stomach	0.056	0.014	0.104	0.069	0.020	0.003	0.048	0.021
intestine	0.11	0.05	0.24	0.13	0.12	0.08	0.12	0.06
<b>kidney</b>	<b>1.97</b>	<b>0.78</b>	<b>8.09</b>	<b>1.68</b>	<b>1.44</b>	<b>0.42</b>	<b>34.66</b>	<b>17.20</b>
adrenals	0.06	0.04	0.41	0.17	0.19	0.07	1.06	0.24
muscle	0.003	0.002	0.007	0.002	0.009	0.002	0.010	0.004
bone	0.022	0.008	0.020	0.008	0.027	0.017	0.014	0.004
<b>tumor</b>	<b>9.82</b>	<b>0.30</b>	<b>10.45</b>	<b>3.25</b>	<b>7.46</b>	<b>0.90</b>	<b>4.06</b>	<b>1.12</b>
parotid gl.	0.041	0.009	0.100	0.017	n.d.	n.d.	n.d.	n.d.
submand. gl.	0.037	0.007	0.046	0.009	n.d.	n.d.	n.d.	n.d.

**Supplemental Table 5:** Tumor-to-organ ratios of [<sup>177</sup>Lu]Lu-rhPSMA-7.1 to -7.4 at 24 h p.i. in male LNCaP tumor-bearing SCID mice. Mean ± standard deviation (SD; n=4). Tumor-to-organ ratios were calculated from individual mice and mean values were determined.

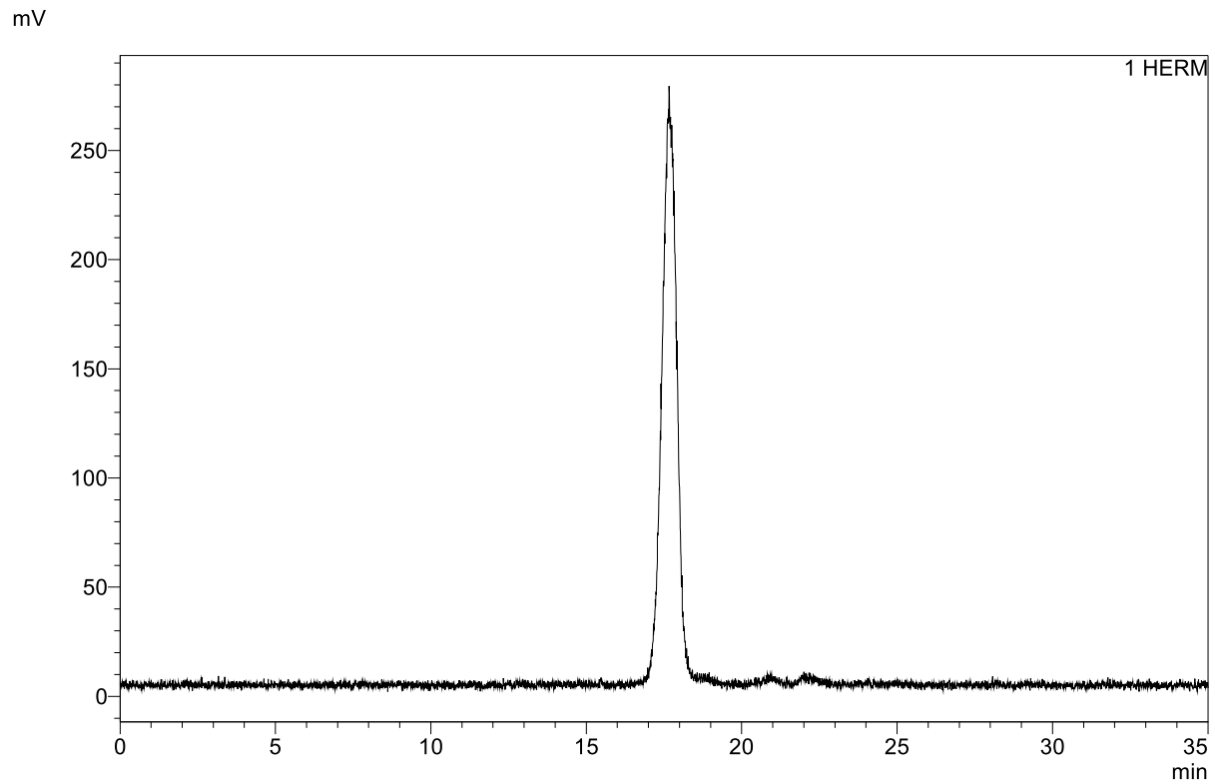
tumor-to-organ ratio	<b>[<sup>177</sup>Lu]Lu-rhPSMA-7.1</b> 24 h p.i., n = 4		<b>[<sup>177</sup>Lu]Lu-rhPSMA-7.2</b> 24 h p.i., n = 4		<b>[<sup>177</sup>Lu]Lu-rhPSMA-7.3</b> 24 h p.i., n = 4		<b>[<sup>177</sup>Lu]Lu-rhPSMA-7.4</b> 24 h p.i., n = 4	
	mean	SD	mean	SD	mean	SD	mean	SD
<b>blood</b>	<b>5971</b>	<b>2358</b>	<b>1460</b>	<b>495</b>	<b>3843</b>	<b>1145</b>	<b>2570</b>	<b>820</b>
heart	368	122	409	125	394	82	387	81
lung	252	53	275	113	239	24	234	87
<b>liver</b>	<b>47</b>	<b>13</b>	<b>54</b>	<b>12</b>	<b>54</b>	<b>2</b>	<b>78</b>	<b>13</b>
spleen	54	13	16	3	17	3	19	4
pancreas	671	211	285	170	487	133	489	180
stomach	191	70	187	210	262	177	228	135
intestine	95	40	150	211	129	86	104	55
<b>kidney</b>	<b>3.2</b>	<b>0.9</b>	<b>0.7</b>	<b>0.2</b>	<b>1.2</b>	<b>0.3</b>	<b>1.0</b>	<b>0.5</b>
adrenals	119	54	21	1	23	7	43	14
muscle	1167	214	1453	623	1454	601	1269	92
bone	453	190	384	66	264	111	616	309
parotid gl.	163	69	112	14	93	21	99	13
submand. gl.	244	43	177	40	207	27	169	33

**Supplemental Table 6:** Tumor-to-organ ratios [<sup>177</sup>Lu]Lu-rhPSMA-10.1, -10.2 and the references [<sup>177</sup>Lu]Lu-PSMA-617 and [<sup>177</sup>Lu]Lu-PSMA I&T at 24 h p.i. in male LNCaP tumor-bearing SCID mice. Mean ± standard deviation (SD; n=4-5). Values of [<sup>177</sup>Lu]PSMA I&T were taken from a previously published study by our group (3). Tumor-to-organ ratios were calculated from individual mice and mean values were determined.

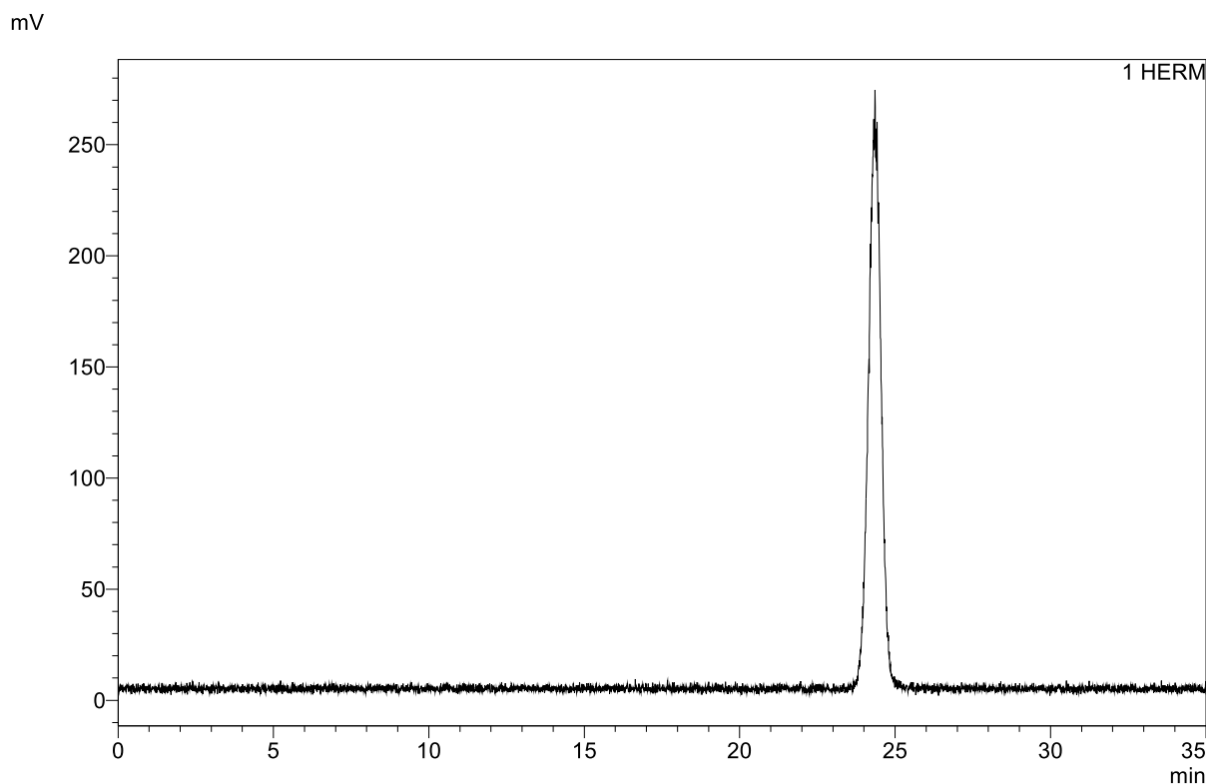
tumor-to-organ ratio	<b>[<sup>177</sup>Lu]Lu-rhPSMA-10.1</b> 24 h p.i., n = 5		<b>[<sup>177</sup>Lu]Lu-rhPSMA-10.2</b> 24 h p.i., n = 4		<b>[<sup>177</sup>Lu]Lu-PSMA-617</b> 24 h p.i., n = 4		<b>[<sup>177</sup>Lu]Lu-PSMA-I&amp;T</b> 24 h p.i., n = 4	
	mean	SD	mean	SD	mean	SD	mean	SD
<b>blood</b>	<b>11498</b>	<b>1953</b>	<b>6125</b>	<b>4185</b>	<b>1424</b>	<b>455</b>	<b>408</b>	<b>209</b>
heart	568	52	585	321	704	270	128	77
lung	313	33	295	100	210	74	26	9
<b>liver</b>	<b>57</b>	<b>13</b>	<b>69</b>	<b>17</b>	<b>91</b>	<b>73</b>	<b>86</b>	<b>31</b>
spleen	58	11	27	19	93	22	3.0	2.0
pancreas	774	189	511	198	799	293	144	115
stomach	187	47	221	231	376	65	105	60
intestine	115	75	111	162	90	50	49	33
<b>kidney</b>	<b>5.7</b>	<b>2.0</b>	<b>1.4</b>	<b>0.6</b>	<b>5.9</b>	<b>3.0</b>	<b>0.15</b>	<b>0.08</b>
adrenals	171	111	33	22	44	15	4.1	1.5
muscle	2441	373	1798	792	855	279	496	242
bone	595	462	589	280	472	378	315	144
parotid gl.	250	64	107	37	n.d.	n.d.	n.d.	n.d.
submand. gl.	275	49	223	45	n.d.	n.d.	n.d.	n.d.



**Supplemental Figure 1:** Exemplary radio-chromatogram of [ $^{177}\text{Lu}$ ]Lu-rhPSMA-7.3 in the AMSEC experiment. The retention time of 14.8 min measured in this particular experiment correlates with an AMW of 30.3 kDa (AMW of  $30.4 \pm 0.5$  kDa (mean  $\pm$  SD) for  $n = 10$  independent measurements).



**Supplemental Figure 2:** Radio-chromatogram of [ $^{177}\text{Lu}$ ]Lu-PSMA-617 in the AMSEC experiment. The retention time of 17.7 min measured in this particular experiment correlates with an AMW of 13.7 kDa.



**Supplemental Figure 3:** Radio-chromatogram of [ $^{18}\text{F}$ ]fluoride in the AMSEC experiment. Due to the absence of interaction of fluoride with HSA, [ $^{18}\text{F}$ ]fluoride is eluted after 24.4 min, as expected for a small inorganic ion, and the corresponding AMW of 2.1 kDa lies below the fractionation range of the gel filtration column (70 – 3 kDa).

## References

1. Wurzer A, Parzinger M, Konrad M, et al. Preclinical comparison of four [(18)F, (nat)Ga]rhPSMA-7 isomers: influence of the stereoconfiguration on pharmacokinetics. *EJNMMI Res.* 2020;10:149.
2. Weineisen M, Schottelius M, Simecek J, et al.  $^{68}\text{Ga}$ - and  $^{177}\text{Lu}$ -Labeled PSMA I&T: Optimization of a PSMA-Targeted Theranostic Concept and First Proof-of-Concept Human Studies. *J Nucl Med.* 2015;56:1169-1176.
3. Wirtz M, Schmidt A, Schottelius M, et al. Synthesis and in vitro and in vivo evaluation of urea-based PSMA inhibitors with increased lipophilicity. *EJNMMI Res.* 2018;8:84.

**6.2.2. *Pharmaceuticals – Albumin-Mediated Size Exclusion Chromatography: The Apparent Molecular Weight of PSMA Radioligands as Novel Parameter to Estimate Their Blood Clearance Kinetics***

The peer-reviewed article “*Albumin-Mediated Size Exclusion Chromatography: The Apparent Molecular Weight of PSMA Radioligands as Novel Parameter to Estimate Their Blood Clearance Kinetics*” was published in *Pharmaceuticals* under an open access Creative Commons Attribution 4.0 International License (CC BY 4.0). The copyright is retained by the authors and the published work may be quoted, reused or redistributed in any medium or format provided that the original version is properly cited.

For additional information see the publisher’s copyright policy (<https://www.mdpi.com/authors/rights>) and CC BY 4.0 conditions (<https://creativecommons.org/licenses/by/4.0/>).

Please turn to the next page for the reprint of the original publication and the supplementary material.

## Article

# Albumin-Mediated Size Exclusion Chromatography: The Apparent Molecular Weight of PSMA Radioligands as Novel Parameter to Estimate Their Blood Clearance Kinetics

Jan-Philip Kunert , Sebastian Fischer, Alexander Wurzer and Hans-Jürgen Wester

Chair of Pharmaceutical Radiochemistry, TUM Department of Chemistry, Technical University of Munich (TUM), 85748 Garching, Germany

\* Correspondence: jan-philip.kunert@tum.de; Tel.: +49-89-289-12203

**Abstract:** A meticulously adjusted pharmacokinetic profile and especially fine-tuned blood clearance kinetics are key characteristics of therapeutic radiopharmaceuticals. We, therefore, aimed to develop a method that allowed the estimation of blood clearance kinetics *in vitro*. For this purpose,  $^{177}\text{Lu}$ -labeled PSMA radioligands were subjected to a SEC column with human serum albumin (HSA) dissolved in a mobile phase. The HSA-mediated retention time of each PSMA ligand generated by this novel ‘albumin-mediated size exclusion chromatography’ (AMSEC) was converted to a ligand-specific apparent molecular weight ( $\text{MW}_{\text{app}}$ ), and a normalization accounting for unspecific interactions between individual radioligands and the SEC column matrix was applied. The resulting normalized  $\text{MW}_{\text{app, norm.}}$  could serve to estimate the blood clearance of renally excreted radioligands by means of their influence on the highly size-selective process of glomerular filtration (GF). Based on the correlation between MW and the glomerular sieving coefficients (GSCs) of a set of plasma proteins,  $\text{GSC}_{\text{calc}}$  values were calculated to assess the relative differences in the expected GF/blood clearance kinetics *in vivo* and to select lead candidates among the evaluated radioligands. Significant differences in the  $\text{MW}_{\text{app, norm.}}$  and  $\text{GSC}_{\text{calc}}$  values, even for stereoisomers, were found, indicating that AMSEC might be a valuable and high-resolution tool for the preclinical selection of therapeutic lead compounds for clinical translation.

**Keywords:** albumin; plasma protein binding; blood clearance; pharmacokinetics; size exclusion chromatography; radioligand therapy; prostate cancer; PSMA; rhPSMA



**Citation:** Kunert, J.-P.; Fischer, S.; Wurzer, A.; Wester, H.-J. Albumin-Mediated Size Exclusion Chromatography: The Apparent Molecular Weight of PSMA Radioligands as Novel Parameter to Estimate Their Blood Clearance Kinetics. *Pharmaceuticals* **2022**, *15*, 1161. <https://doi.org/10.3390/ph15091161>

Academic Editors: Martina Benešová and Gábor Bakos

Received: 11 August 2022

Accepted: 14 September 2022

Published: 19 September 2022

**Publisher’s Note:** MDPI stays neutral with regard to jurisdictional claims in published maps and institutional affiliations.



**Copyright:** © 2022 by the authors. Licensee MDPI, Basel, Switzerland. This article is an open access article distributed under the terms and conditions of the Creative Commons Attribution (CC BY) license (<https://creativecommons.org/licenses/by/4.0/>).

## 1. Introduction

The contribution of nuclear medicine to the clinical management of cancer patients has been on a constant rise throughout the last years [1]. In addition to established diagnostic applications guiding clinical decision making, such as positron emission tomography (PET) [2,3] or single-photon emission computed tomography (SPECT) [4,5], targeted radioligand therapy (RLT) has evolved into an important tool in the treatment of oncological diseases and is still growing in its everyday clinical relevance [6–8]. Pioneered by [ $^{177}\text{Lu}$ ]Lu-DOTA-TATE [9] (Lutathera<sup>®</sup>) and fueled by its regulatory approval for the treatment of neuroendocrine tumors by the FDA in early 2018 [10], intensive preclinical and clinical research toward novel targeted radiotherapeutics for oncologic targets, such as prostate-specific membrane antigen (PSMA) [11,12], human epidermal growth factor receptor 2 (HER2) [13,14], gastrin-releasing peptide receptor (GRPR) [15,16] and cholecystokinin-2-receptor (CCK2R) [17,18], among others, has been undertaken. The growing patient population suffering from prostate cancer and the resulting clinical demand have especially driven the development of PSMA-targeted radioligands [19–21]. As a result, [ $^{177}\text{Lu}$ ]Lu-PSMA-617 (Pluvicto<sup>TM</sup>) was recently approved as a first-in-class PSMA-targeted radiopharmaceutical for the RLT of metastatic castration-resistant prostate cancer (mCRPC) [22]. Further developments in radiotracer design and the clinical application of PSMA-targeted RLT in

earlier stages of prostate cancer are eagerly awaited to increase the therapeutic options for oncologists and the possible benefit for patients in the near future.

In the development of new PSMA radiotherapeutics, various preclinical *in vitro* parameters are conventionally assessed to identify lead candidates for clinical translation [23]. Among these parameters, PSMA affinity, as well as uptake and internalization in PSMA-positive cells, are determined to analyze the target binding properties of a radioligand, while lipophilicity is usually assessed to avoid hepatobiliary and to foster renal excretion. In this context, extensive work on the modulation of albumin binding has been carried out with the aim to exploit a depot effect for leveraging increased tumor uptake [24–27].

However, the optimization of the therapeutic efficacy of a radioligand more than anything requires a meticulously adjusted pharmacokinetic profile [28]. Compared to diagnostic tracers, a slightly slower excretion of therapeutic radioligands is needed to support high tumor uptake, yet excretion must occur fast enough to avoid excessive off-target radiation toxicity [29–31]. Despite their undeniable value in preclinical development, the aforementioned *in vitro* parameters are not suitable to assess, predict, or fine-tune such delicate pharmacokinetic requirements. In contrast, a parameter that governs the complex synergy of tumor delivery and excretion from healthy tissue is the blood clearance kinetics of a radioligand. All relevant pharmacokinetic effects between the site of injection and the tumor cell membrane are influenced by and integrally summarized within the blood clearance kinetics of a ligand. The preclinical assessment of this parameter is, therefore, of utmost importance to select suitable lead compounds for clinical translation and to develop next-generation radiopharmaceuticals with improved therapeutic efficacy.

Therapeutic radioligands are generally designed to be excreted via the renal pathway [29,32]. Consequently, clearance from the blood pool predominantly occurs via glomerular filtration (GF) [33]. According to the kidney's physiological function, GF is highly size-selective and high-molecular-weight proteins (such as human serum albumin, HSA) are almost quantitatively retained in the blood plasma, while low-molecular-weight compounds (e.g., drugs) are readily filtered [34–36]. Therefore, the rate of a compound's GF and, thus, its clearance from the blood pool can be assumed to be highly dependent on its molecular weight (MW). The availability of a compound for GF, however, is influenced by its binding to plasma proteins, as a small molecule complexed to a high-molecular-weight plasma protein (e.g., HSA) evades GF, resulting in a prolonged circulatory half-life. Assuming metabolic stability, the interplay between plasma protein binding and MW-dependent GF can, thus, be considered the key element shaping the blood clearance kinetics of a renally excreted radioligand.

Several methods to determine the plasma protein binding of drugs have been described in the literature, among them ultrafiltration (UF) [37], different chromatographic procedures [38–40], spectroscopic methods [41,42] and even *in silico* studies on molecular docking and molecular dynamics [43,44]. In the context of radiopharmaceuticals, UF upon incubation in fresh human plasma [45–47] or in solutions of HSA [48,49], as well as high-performance affinity chromatography (HPAC) with HSA-modified HPLC columns [26,50,51], represent the most-established approaches that have been applied in the development of diverse PSMA-targeted radioligands. Both methods offer attractive features, such as short analysis times and the possibility of screening-like procedures in HPAC or incubation conditions closely mimicking the *in vivo* situation before analysis via UF. However, the informative value of these methods remains limited to the mere quantification of a drug's protein-bound fraction [27,45–47,50] or its affinity toward a plasma protein, such as HSA [26,48,51]. The actual need in developing optimized therapeutic radioligands, however, lies in the assessment and interpretation of different renal clearance kinetics of albumin-complexed drugs, especially for those drugs that have very similar plasma protein affinities, plasma protein bindings, and molecular weights, such as PSMA ligands. As the mere ratio of protein binding or the plasma protein affinity of a drug determined by UF or HPAC are insufficient to draw conclusions on their respective quantitative effect on the drug's renal clearance kinetics, these established methods are not suitable to meet the aforementioned need.

With respect to these considerations, we aim to develop a method based on size exclusion chromatography (SEC) that not only allows to merely determine the binding of radioligands to HSA but also to possibly deduce conclusions on radioligand blood clearance kinetics. The general feasibility of assessing protein–drug interactions using SEC has been exemplified in the literature by the Hummel–Dreyer method [52]. In this method, a protein is injected onto a size exclusion column equilibrated with a buffered solution of a drug. The depletion of drug concentration caused by protein–drug complexation generates a trough in the UV elution profile observed at the cut-off volume of the chromatogram. Based on the size of the trough, the extent of drug binding to the protein can be determined (Figure 1A). Inspired by the Hummel–Dreyer method and with the aim to account for specific requirements when evaluating radioligands, we developed a novel methodology named albumin-mediated size exclusion chromatography (AMSEC). When compared to the Hummel–Dreyer method, AMSEC works in a reversed fashion: a radioligand is injected onto a size exclusion column equilibrated with a buffered solution of HSA to assess the binding interaction between HSA and the radioligand (Figure 1B).

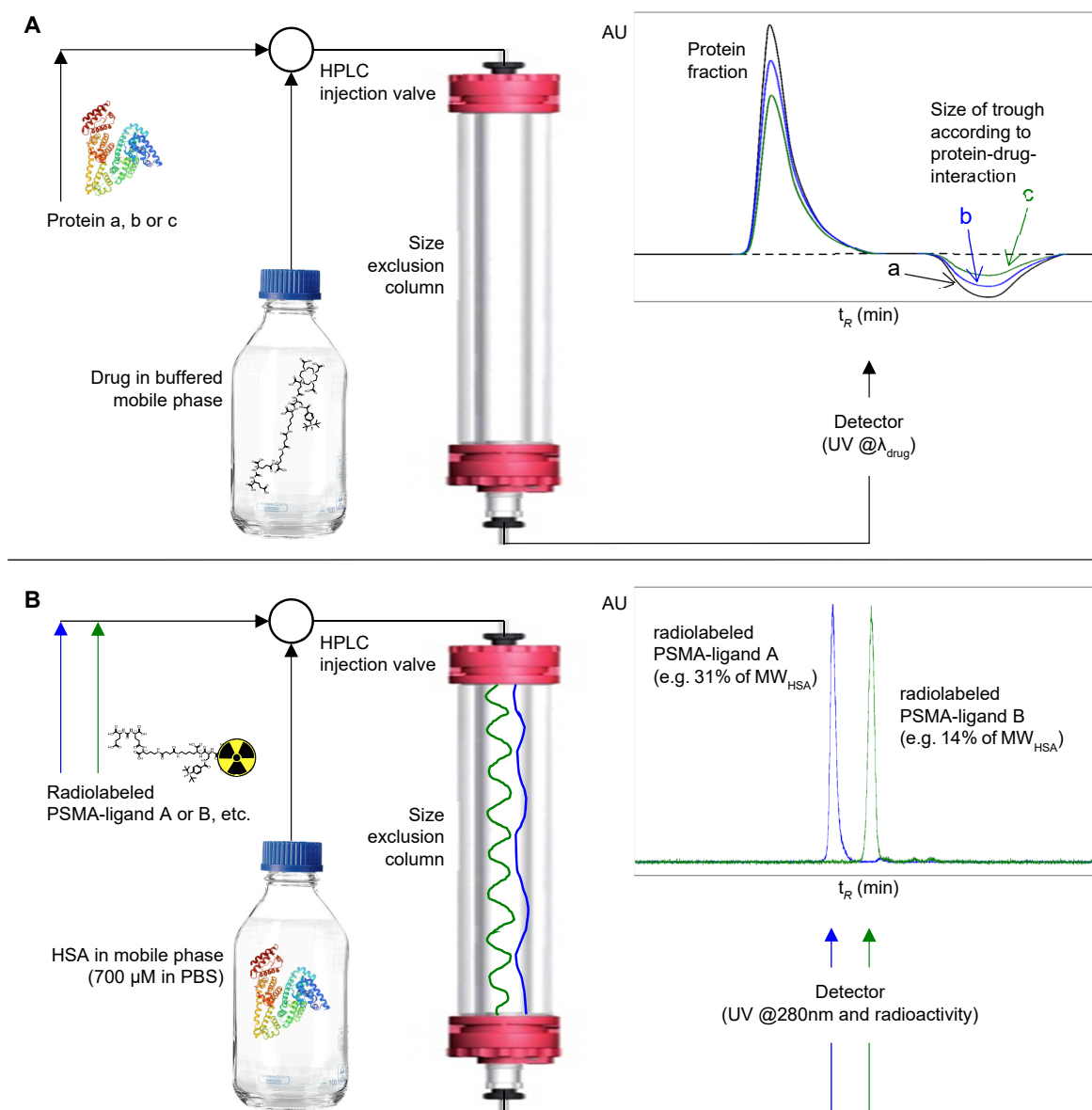


**Figure 1.** (A) Experimental setup of the Hummel–Dreyer method. This method was introduced 1962 to investigate the binding of a drug to proteins. For this purpose, a protein is injected onto a size ex-

clusion column equilibrated with a buffered solution of a drug. After injection, drug molecules from the mobile phase are complexed to the injected protein until equilibrium is reached. The troughs (a, b, c) observed at the cut-off volume in the UV elution profile correspond to the different amounts of drug complexed by the different injected protein samples, thus representing a depleted concentration of the drug at the low-molecular-weight fraction, while the protein fraction shows a stronger signal (protein and complexed drug). (B) Experimental setup of the newly developed albumin-mediated size exclusion chromatography (AMSEC). Radiolabeled PSMA ligands are injected onto a size exclusion column equilibrated with a buffered solution of human serum albumin (HSA, physiological concentration of  $\sim 700 \mu\text{M}$  in PBS; pH 7.4). Throughout the chromatographic run, the radioligand binds to and dissociates from HSA in a transient manner. The observed retention time of a radioligand is the result of the mean time the ligand is complexed by HSA, which in turn depends on the strength of the drug–albumin interaction. Thus, an apparent molecular weight ( $MW_{\text{app}}$ ) higher than its actual molecular weight (MW) but below the MW of HSA can be assigned to each radioligand.

The aim of this study is to present the development of AMSEC as a novel approach to estimate blood clearance kinetics, to show the method's basic feasibility as exemplified by the evaluation of  $^{177}\text{Lu}$ -labeled PSMA radioligands, and to discuss the potential contribution of AMSEC in the future preclinical development of therapeutic radioligands with optimized pharmacokinetics for RLT.

## 2. Results and Discussion

Several considerations of physiological, methodological, and practical nature guided the conceptualization of the AMSEC method. Because of the aforementioned impact of MW on glomerular sieving [34–36], we wanted to create an experimental setting capable of producing MW-related data. Therefore, size exclusion chromatography was chosen as the basic technique to assess the interaction between  $^{177}\text{Lu}$ -labeled PSMA radioligands and HSA. The latter protein represents one of several human plasma proteins that play an important role in the binding of endo- and exogenous ligands [53–55]. As HSA is by far the most abundant human plasma protein [56] and its role and function have been intensively studied [54,56,57], we identified this particular protein as the best-suited candidate to evaluate this new method. In contrast to the Hummel–Dreyer method, we decided to apply HSA in the mobile phase rather than to inject a probe of the protein [52]. This holds the distinct advantage that a variety of different PSMA radioligands can be analyzed in a screening-like fashion using the same protein-containing mobile phase and sensitive radioactivity detection for data acquisition (Figure 1B). Furthermore, the mobile phase was composed of HSA at a physiological concentration ( $700 \mu\text{M}$  [53]) in phosphate-buffered saline (PBS; pH 7.4), mimicking physiological pH and HSA concentration in blood. Thus, upon the injection of a PSMA radioligand into the HPLC system, HSA and the radioligand interact in solution state and in a flowing, blood-like environment complying with fundamental aspects of the actual *in vivo* situation.

Despite these thoughtful considerations in the conceptual design of AMSEC, it was initially unclear how the resulting elution profiles would look like and whether valid and quantitative interpretation in terms of the albumin binding and blood clearance of PSMA radioligands would be feasible. The SEC approach provides the necessary conditions for HSA-complexed radioligands and uncomplexed radioligands to behave differently according to the species' MWs. However, whether single or multiple radiopeaks (e.g., HSA-complexed or uncomplexed radioligands) and, potentially, tailing or fronting of peaks would be observed could not be judged with certainty in advance, as these features of an elution profile are inherently influenced by the binding kinetics and, especially, the lifespan of an HSA–radioligand complex. Dissociation constants ( $K_d$ ) in the micromolar range were reported for lipophilic, halogen-, and alkyl-substituted aromatic HSA-binding motifs [58,59]. Theoretically, lifespans of a few milliseconds up to several minutes could arise from these affinities, depending on the rate of dissociation ( $k_{\text{off}}$ ) [60]. The radiohybrid (rh) PSMA ligands and further PSMA-binding model compounds (MCs) evaluated in

this study contain a lipophilic silicon-fluoride acceptor (SiFA) or a positively charged SiFA (SiFAlin) moiety as an albumin-binding motif [61–63]. As neither the  $K_d$  nor the lifespan of HSA complexes with SiFA- or SiFAlin-bearing rhPSMA ligands have been investigated so far, our expectations toward the outcome of the first AMSEC experiments were unprejudiced.

To our delightful surprise, the injection of  $^{177}\text{Lu}$ -labeled rhPSMA-7.3 onto the SEC column equilibrated with 700  $\mu\text{M}$  HSA in PBS resulted in a sharp and single radiopeak (Figure 2A). This observation indicated fast binding kinetics ( $k_{\text{on}}/k_{\text{off}}$ ) between HSA and the radioligand. Therefore, within the AMSEC experiment, the transient HSA–radioligand complex might be regarded as a single species. Interestingly, the observed retention time of rhPSMA-7.3 ( $t_{R,AMSEC}$ , 14.722 min) was closer to the retention time of HSA ( $t_{R,HSA}$ , 11.791 min) than to the retention time of acetone ( $t_{R,acetone}$ , 24.809 min, corresponding to the cut-off elution volume), both determined in conventional SEC runs without HSA (Figure 2A). Due to its actual MW (~1.6 kDa) beneath the column fractionation range (70–3 kDa), rhPSMA-7.3 should be eluted in the cut-off volume (like acetone) in the absence of HSA.

We, therefore, concluded that the reduced retention time of rhPSMA-7.3 observed in the AMSEC experiment ( $t_{R,AMSEC}$ ) arises from the transient binding of rhPSMA-7.3 to HSA during the passage through the column bed. Whenever rhPSMA-7.3 is complexed to HSA, passage through the column bed occurs rapidly according to the high MW of the HSA–radioligand complex ( $MW_{HSA} = 66.5$  kDa [56]), whereas slow elution according to the ligands' low actual MW occurs whenever uncomplexed. Consequently, the albumin-mediated retention time  $t_{R,AMSEC}$  observed in the AMSEC run is governed by a ligand's binding interaction with HSA.

In analogy to the results obtained for rhPSMA-7.3, evaluation of the remaining three isomers of rhPSMA-7, as well as rhPSMA-10.1, rhPSMA-10.2, PSMA-617, and PSMA-I&T, also revealed sharp, single radiopeaks and an individual  $t_{R,AMSEC}$  for each radioligand (Figure 2B). These findings are of particular interest as, by means of column calibration, an apparent molecular weight ( $MW_{\text{app}}$ ) can be calculated from the ligand-specific  $t_{R,AMSEC}$ . Such a  $MW_{\text{app}}$  is higher than the radioligand's actual, physical MW and arises from transient binding to HSA. With respect to GF, the  $MW_{\text{app}}$  might be understood as a "biologically effective" MW of the radioligand that describes the relation between albumin binding and the reduced rate of GF, which is commonly observed for albumin-bound drugs. We, thus, hypothesized that, in terms of GF in vivo, the radioligands might pharmacokinetically behave according to their  $MW_{\text{app}}$  rather than their actual MW. Because of the quantitative correlation between MW and glomerular sieving coefficients (GSCs) [64], the  $MW_{\text{app}}$  determined by AMSEC could be used to estimate the GF and, thus, the blood clearance of PSMA radioligands.

Within this study,  $MW_{\text{app}}$  determined directly from experimentally acquired retention times  $t_{R,AMSEC}$  (corrected according to Section 3.3) are referred to as raw apparent MW ( $MW_{\text{app,raw}}$ , Figure 2C,D and Table 1).

As shown in Figure 2C and Table 1,  $MW_{\text{app,raw}}$  ranging from 5.4 kDa for PSMA-I&T to 36.0 kDa for rhPSMA-7.4 were determined. These values corresponded to a wide range, between 18% and nearly 120% of the value determined for rhPSMA-7.3 (Figure 2D). The latter radioligand served as an internal standard and was assessed whenever AMSEC studies were carried out ( $n = 14$ ). The resulting mean value for  $MW_{\text{app,raw}}$  of 30.6 kDa and the low standard deviation of 0.5 kDa showed the high reproducibility of the method. Bearing in mind that the analyzed rhPSMA isomers are structurally highly similar, it constituted a stunning finding that the  $MW_{\text{app,raw}}$  of, e.g., rhPSMA-7.1 and rhPSMA-7.2, diverged by 20%, even though both isomers structurally differ in only a single stereocenter (chemical structures of  $^{177}\text{Lu}$ -labeled rhPSMA compounds, PSMA-617, and PSMA-I&T are provided in the Supplementary Materials, Figures S1–S8). This impressive resolution of AMSEC allowing differentiation even between stereoisomers provides an important basis for a possible contribution to the preclinical selection of promising PSMA radioligands.

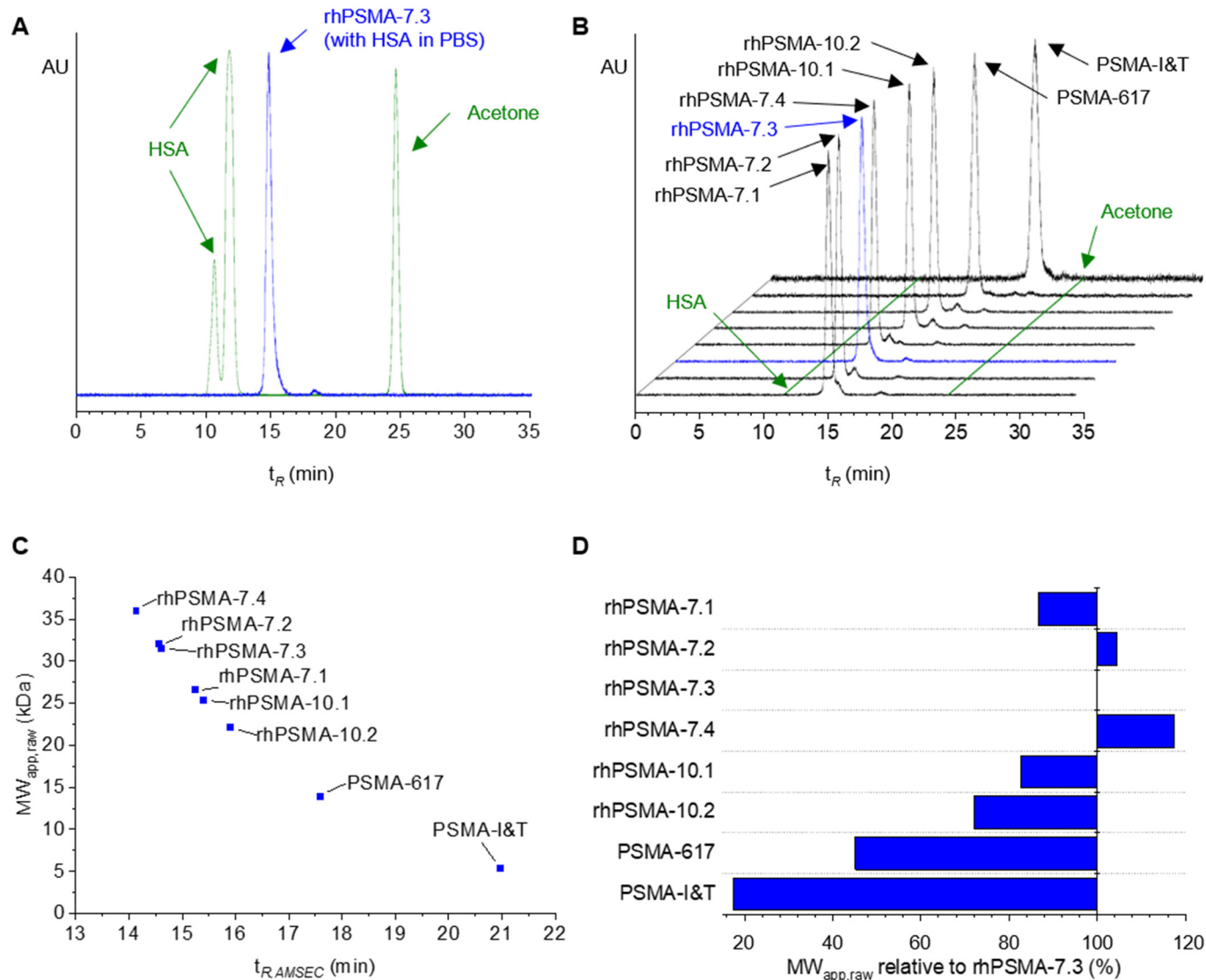


**Figure 2.** (A) Elution profile of rhPSMA-7.3 (blue) in AMSEC experiments (mobile phase of 700  $\mu$ M HSA in PBS). Elution in the cut-off volume of the column similar to acetone would be expected due to the actual MW of rhPSMA-7.3. Transient binding of rhPSMA-7.3 to HSA during the chromatographic procedure leads to an albumin-mediated reduction in the retention time ( $t_{R,AMSEC}$ ) according to the ligand's HSA-binding strength. The UV peak of HSA indicates the shortest theoretical retention time obtainable for  $t_{R,AMSEC}$  (in the case of continuous HSA-binding, the dominant peak corresponds to the monomeric mass of HSA, and the respective retention time of 11.791 min was used for all calculations). (B) Elution profiles of rhPSMA-7.3 (blue line) and rhPSMA-7.1, -7.2, -7.4, rhPSMA-10.1, rhPSMA-10.2, PSMA-617, and PSMA-I&T (black lines) in AMSEC experiments. Retention times of HSA and acetone as references are indicated as green lines. (C)  $t_{R,AMSEC}$  of radioligands plotted against the corresponding raw apparent molecular weight ( $MW_{app,raw}$ ).  $t_{R,AMSEC}$  of 14.1–21.0 min led to  $MW_{app,raw}$  between 36.0–5.4 kDa. (D)  $MW_{app,raw}$  of all ligands in percentage of the  $MW_{app,raw}$  of rhPSMA-7.3 (100%). Observed  $MW_{app,raw}$  ranged from approximately 18% for PSMA-I&T to almost 120% for rhPSMA-7.4.

However, if we critically assess the validity of the determined  $MW_{app,raw}$ , it becomes apparent that the interpretation of the results presented so far is based on the following hypothesis: the comparability of  $MW_{app,raw}$  between different radioligands is only given if the retention times on the SEC column in the absence of HSA are identical for all the radioligands. In this case, any differences observed in  $t_{R,AMSEC}$  among the radioligands

would exclusively arise from the ligand-specific interaction with HSA. This uniform retention time in the absence of HSA is furthermore expected to correspond to the cut-off volume, as indicated by the retention time of acetone ( $t_{R,acetone}$ ), as the actual MWs of all the radioligands (~1.6 kDa) lies below the column fractionation range (70–3 kDa). In this case, any excess of determined  $MW_{app,raw}$  over the actual MW of a radioligand would solely arise from its interaction with HSA in the AMSEC experiment, and the absolute values of  $MW_{app,raw}$  would, thus, be precise and meaningful in relation to GF.

**Table 1.** Retention times of rhPSMA radioligands, PSMA-617, and PSMA-I&T in AMSEC runs ( $t_{R,AMSEC}$ ) and corresponding raw apparent molecular weights ( $MW_{app,raw}$ ).

Radioligand	$t_{R,AMSEC}$ <sup>1</sup> (min)	$MW_{app,raw}$ (kDa) <sup>2</sup>
rhPSMA-7.1	15.240	26.5
rhPSMA-7.2	14.564	32.0
rhPSMA-7.3	14.722 <sup>3</sup>	30.6 <sup>3</sup>
rhPSMA-7.4	14.143	36.0
rhPSMA10.1	15.410	25.3
rhPSMA-10.2	15.908	22.0
PSMA-617	17.586	13.8
PSMA-I&T	20.983	5.4

<sup>1</sup> Retention times are corrected for the offset between UV-vis and radio-detector and are normalized to the elution behavior of the respective compound on gel filtration column 1 (for detailed information, see Equations (S1) and (S2) and Table S1 in the Supplementary Materials). <sup>2</sup>  $MW_{app,raw}$  corresponds to apparent molecular weights previously reported by Wurzer et al. [62]. Minor discrepancy in reported values (<1%) results from refined calibration calculations and correction for the offset between UV-vis and radio-detector in the present study (see Section 3.3). <sup>3</sup> Data presented for rhPSMA-7.3 are taken from an exemplary experiment. The mean  $MW_{app,raw}$  for rhPSMA-7.3 was  $30.6 \pm 0.5$  kDa ( $n = 14$ ).

To validate this hypothesis, blank runs (PBS pH 7.4 as mobile phase) of the radioligands on the SEC column were performed. The resulting retention times were termed  $t_{R,blank}$  and represent the ligand-specific retention time that would correspond to 0% HSA binding in the AMSEC experiment. Interestingly, a first finding was that rhPSMA-7.3 showed a  $t_{R,blank}$  significantly shorter than  $t_{R,acetone}$ , mathematically corresponding to a MW of 6.0 kDa (Figure 3A). We concluded that unspecific electrostatic interactions between the highly negatively charged radioligand and the agarose/dextran-based matrix of the superdex column are present and lead to an elution prior to the expected cut-off volume [65,66]. Consequently, apart from the radioligand's binding to HSA in the AMSEC run, the unspecific interactions with the column matrix contribute to the determined  $MW_{app,raw}$ , thus hampering its informative value. In a similar fashion, all other evaluated radioligands also showed shorter  $t_{R,blank}$  than  $t_{R,acetone}$  values (see Table S1). Furthermore, slightly different  $t_{R,blank}$  between 20.4 min and 22.3 min were observed for the evaluated radioligands (see Table S1). Hence, slightly different windows of retention times represented the whole spectrum, between 100% ( $t_{R,HSA}$ ) and 0% HSA binding (individual  $t_{R,blank}$ ), for each radioligand, thus compromising the quantitative comparability of the obtained  $MW_{app,raw}$ . To address these limitations, a normalization of the experimentally obtained  $t_{R,AMSEC}$  was required that would account for ligand-specific interactions with the column matrix and, furthermore, provide a common window of retention times representing 100% to 0% HSA binding that is valid for the determination of the  $MW_{app}$  values of all the radioligands.

Such normalization was found to be feasible by means of mathematical transformations that require a radioligand's retention time in the AMSEC run ( $t_{R,AMSEC}$ ) and its retention time in the blank run ( $t_{R,blank}$ ), as well as the retention times of HSA ( $t_{R,HSA}$ ) and acetone ( $t_{R,acetone}$ ) in conventional SEC runs in PBS (pH 7.4). The approach and mathematical implementation are described as follows.

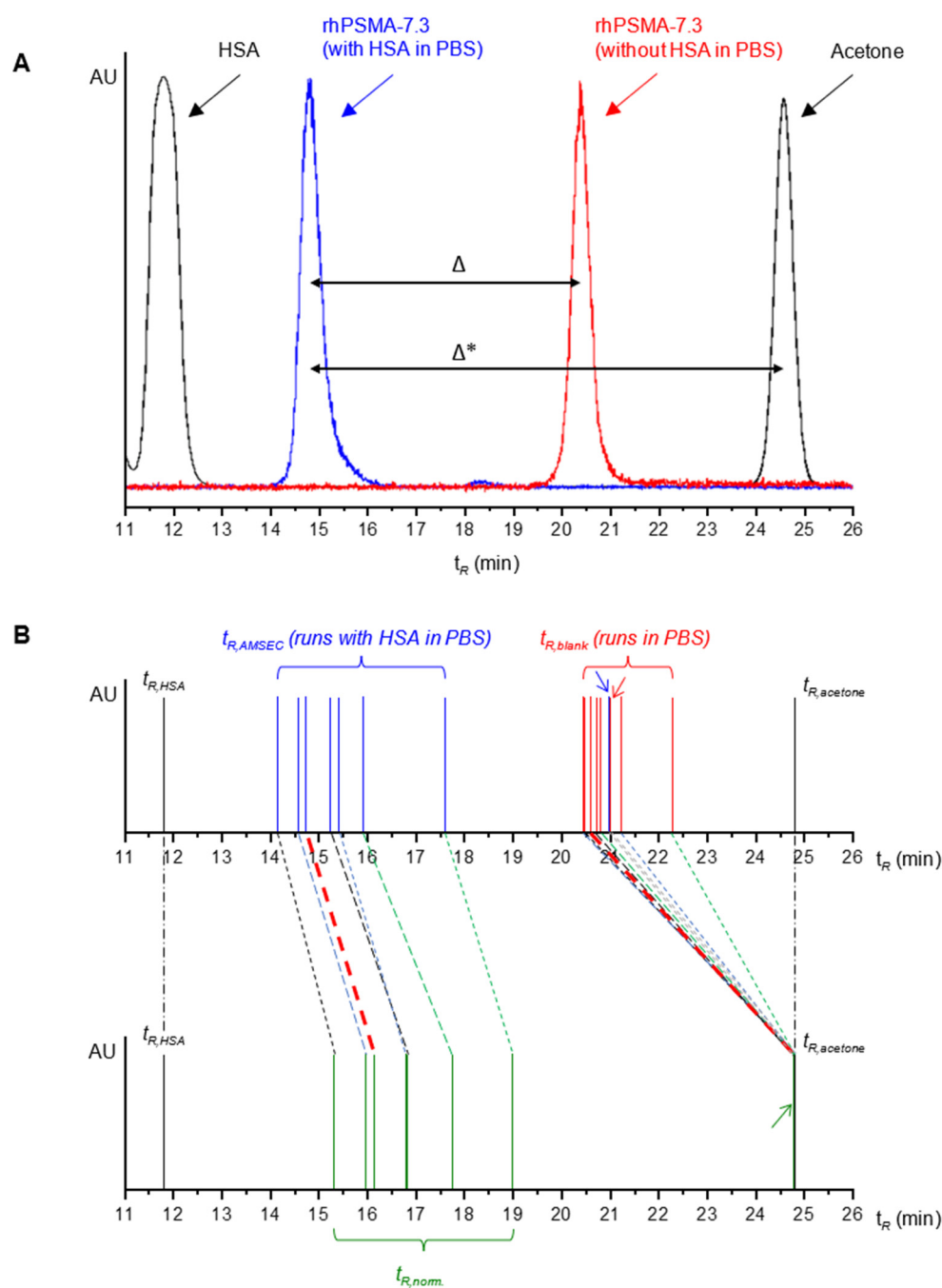


**Figure 3.** (A) The elution profile of the blank run (red) of rhPSMA-7.3 (in PBS without HSA) showed a significantly shorter retention time ( $t_R$ ) than for acetone, probably due to unspecific electrostatic interactions of the radioligand with the column matrix. The actual albumin-mediated reduction in  $t_R$  ( $\Delta$ ) was, therefore, smaller than initially expected ( $\Delta^*$ ). (B) Graphical depiction of normalization of  $t_{R,AMSEC}$  that was carried out to correct for unspecific interaction with the column matrix. Within the  $t_R$  window between HSA ( $t_{R,HSA}$ , 100% HSA binding) and acetone ( $t_{R,acetone}$ , 0% HSA binding), normalized  $t_R$  ( $t_{R,norm.}$ ) were obtained by the proportional dilatation of  $t_{R,AMSEC}$  (ligand-specific HSA binding) and  $t_{R,blank}$  (0% HSA binding) to the extent that all  $t_{R,blank}$  values became equal to  $t_{R,acetone}$ . For the purpose of better readability, the blue, red, and green arrows indicate the  $t_{R,AMSEC}$ ,  $t_{R,blank}$ , and  $t_{R,norm.}$  of PSMA-I&T, respectively.

During the AMSEC run, the radioligand is present on the column either in an HSA-complexed or a free, uncomplexed state. Accordingly, at every timepoint, the radioligand moves across the column bed either with the elution velocity of HSA or with the elution

velocity of the unbound, free radioligand. As these elution velocities refer to the same column dimensions and are reciprocally proportional to the retention times, the experimental unit of retention time can be used to describe the following correlations.

The retention time of a radioligand in the AMSEC run ( $t_{R,AMSEC}$ ) can be expressed as the following linear combination:

$$t_{R,AMSEC} = k \cdot t_{R,HSA} + (1 - k) \cdot t_{R,blank}, \quad (1)$$

where the retention factor  $k \in [0;1]$  is the fraction of time the radioligand is complexed to HSA during the AMSEC run. Solving Equation (1) for the retention factor  $k$  gives the following correlation:

$$k = \frac{|t_{R,AMSEC} - t_{R,blank}|}{|t_{R,HSA} - t_{R,blank}|}. \quad (2)$$

The term  $|t_{R,AMSEC} - t_{R,blank}|$  in the numerator of Equation (2) represents the shift of the drug's radiopeak that is observed in the AMSEC run by HSA complexation compared to the blank run. The bigger the shift, the stronger the interaction (and the extent of binding) between a radioligand and HSA. The term  $|t_{R,HSA} - t_{R,blank}|$  in the denominator describes the window of retention times between 100% ( $t_{R,HSA}$ ) and 0% HSA binding ( $t_{R,blank}$ ) for such shifts. Theoretically, the radiopeak of a particular radioligand in the AMSEC run is observed within this window. Thus, the denominator in Equation (2) describes the base reference to comparably quantify the extent of binding expressed by the numerator. According to these correlations, a radioligand with a retention factor of, e.g.,  $k = 0.5$ , would exhibit a  $t_{R,AMSEC}$  exactly in the middle between  $t_{R,HSA}$  and  $t_{R,blank}$ . The retention factor  $k$  is dimensionless and independent of ligand-specific interactions with the column matrix. It is, thus, a quantitative and ligand-specific parameter for HSA binding that allows for the comparison of the HSA binding between different compounds.

In Equation (2) the ligand-specific retention time  $t_{R,blank}$  represents 0% HSA binding. As stated earlier, a common point of reference equaling 0% HSA binding for all radioligands is required to determine MWs that are quantitatively comparable. Acetone was chosen as this reference, as this small molecule does not exhibit any unspecific interactions with the agarose/dextran-matrix of superdex columns and is eluted within the cut-off volume of the column. The latter was theoretically also expected for the radioligands evaluated herein, as their actual MW lies beneath the fractionation range of the column. The implementation of  $t_{R,acetone}$  into Equation (2) gives the following equation:

$$k = \frac{|t_{R,norm.} - t_{R,acetone}|}{|t_{R,HSA} - t_{R,acetone}|}, \quad (3)$$

with the normalized retention time  $t_{R,norm.}$  replacing  $t_{R,AMSEC}$ . The normalized retention time  $t_{R,norm.}$  is the virtual retention time of a radioligand that, within the newly defined window of 100% ( $t_{R,HSA}$ ) to 0% HSA binding ( $t_{R,acetone}$ ), results in the same retention factor  $k$  determined in Equation (2). According to Equation (3),  $t_{R,norm.}$  is defined as follows:

$$t_{R,norm.} = k \cdot t_{R,HSA} + (1 - k) \cdot t_{R,acetone}. \quad (4)$$

Combining Equations (2) and (4),  $t_{R,norm.}$  can finally be determined from solely experimental input factors as follows:

$$t_{R,norm.} = \frac{|t_{R,AMSEC} - t_{R,blank}|}{|t_{R,HSA} - t_{R,blank}|} \cdot t_{R,HSA} + \left(1 - \frac{|t_{R,AMSEC} - t_{R,blank}|}{|t_{R,HSA} - t_{R,blank}|}\right) \cdot t_{R,acetone}. \quad (5)$$

Consistent with the comparability of  $k$ ,  $t_{R,norm.}$  is also comparable among different radioligands and can be used to calculate a normalized apparent MW ( $MW_{app,norm.}$ ) by means of column calibration. The corresponding data of the aforementioned rhPSMA

compounds, PSMA-617, PSMA-I&T, and ten further model compounds (MC-1 to MC-10) are presented in Table 2 ( $t_{R,AMSEC}$  and  $MW_{app,raw}$  of MC-1 to MC-10 are provided in Table S2).

**Table 2.** Retention factors  $k$ , normalized retention times ( $t_{R,norm.}$ ), normalized apparent molecular weights ( $MW_{app,norm.}$ ), and calculated glomerular sieving coefficients ( $GSC_{calc}$ ) of rhPSMA radioligands, PSMA-617, PSMA-I&T, and model compounds (MCs) 1 to 10.

Radioligand	Retention Factor $k$	$t_{R,norm.}$ (min)	$MW_{app,norm.}$ (kDa)	$GSC_{calc}$
rhPSMA-7.1	0.613	16.824	17.1	0.655
rhPSMA-7.2	0.680	15.962	21.7	0.344
rhPSMA-7.3	0.667 <sup>1</sup>	16.125 <sup>1</sup>	20.7 <sup>1</sup>	0.408
rhPSMA-7.4	0.729	15.316	26.0	0.138
rhPSMA10.1	0.616	16.789	17.2	0.644
rhPSMA-10.2	0.543	17.736	13.2	0.846
PSMA-617	0.447	18.988	9.4	0.942
PSMA-I&T	0.001	24.792	1.9	0.992
MC-1	0.848	13.773	39.9	0.003
MC-2	0.798	14.414	33.3	0.020
MC-3	0.764	14.862	29.4	0.057
MC-4	0.747	15.081	27.7	0.089
MC-5	0.747	15.083	27.7	0.090
MC-6	0.658	16.248	20.0	0.454
MC-7	0.593	17.086	15.9	0.726
MC-8	0.540	17.781	13.1	0.852
MC-9	0.424	19.293	8.6	0.953
MC-10	0.194	22.287	3.7	0.987

<sup>1</sup> Presented data for rhPSMA-7.3 were taken from an exemplary experiment. Mean retention factor  $k$  was  $0.667 \pm 0.06$  ( $n = 14$ ), and mean  $MW_{app,norm.}$  was  $20.7 \pm 0.5$  kDa ( $n = 14$ ).

In addition to the mathematical derivation, the presented normalization can also be understood in a geometrical way when the peaks of HSA ( $t_{R,HSA}$ , 100% binding), the radiopeak in the AMSEC run ( $t_{R,AMSEC}$ , ligand-specific binding to HSA), and the radiopeak in the blank run ( $t_{R,blank}$ , no HSA in mobile phase, thus 0% HSA-specific binding) are thought of as one peak profile. The described mathematical transformations correspond to a proportional dilatation of that peak profile to the extent that the shifted  $t_{R,blank}$  values become equal to  $t_{R,acetone}$ , the new uniform point of reference for 0% HSA binding, while  $t_{R,HSA}$  is kept unaltered (see Figure 3B).

As the normalization provides both a correction of the ligand-specific interactions with the column matrix and a common window of retention times between 100% and 0% HSA binding, the obtained  $MW_{app,norm.}$  are comparable among the different radioligands and the increase in  $MW_{app,norm.}$  compared to the actual MW of a radioligand is solely HSA-mediated. We, therefore, consider  $MW_{app,norm.}$  to be the valid and informative parameter that can be obtained by applying AMSEC in the preclinical development of PSMA radioligands.

Only the above-described normalization of the AMSEC data on the binding of radioligands to HSA provides MW-related data with the unique advantage that conclusions related to the MW-dependent physiological process of GF might be drawn, allowing for the estimation of the relative blood clearance kinetics of different radioligands.

Apart from rhPSMA compounds, PSMA-617, and PSMA-I&T, ten further model compounds (MC-1 to MC-10, including SiFA- and SiFAlin-bearing PSMA ligands) were evaluated using AMSEC to show the broad range of  $MW_{app,norm.}$  values that could be obtained for structurally different compounds.  $MW_{app,norm.}$  values from 1.9 kDa to 39.9 kDa were observed, which corresponds to a range of 9% to 192% of the  $MW_{app,norm.}$  determined for rhPSMA-7.3 (Figure 4A,B). As already stated in the context of  $MW_{app,raw}$ , distinct differences even between stereoisomers were also found for  $MW_{app,norm.}$ . For example, a 27% higher value was found for rhPSMA-7.2 than for rhPSMA-7.1 (21.7 vs. 17.1 kDa,

respectively), and even a 30% higher value was found for rhPSMA-10.1 than for rhPSMA-10.2 (17.2 vs. 13.2 kDa, respectively). These findings suggest an impressive resolution of AMSEC, which might be of considerable value, especially for the diligent structure optimization of a therapeutic lead compound.

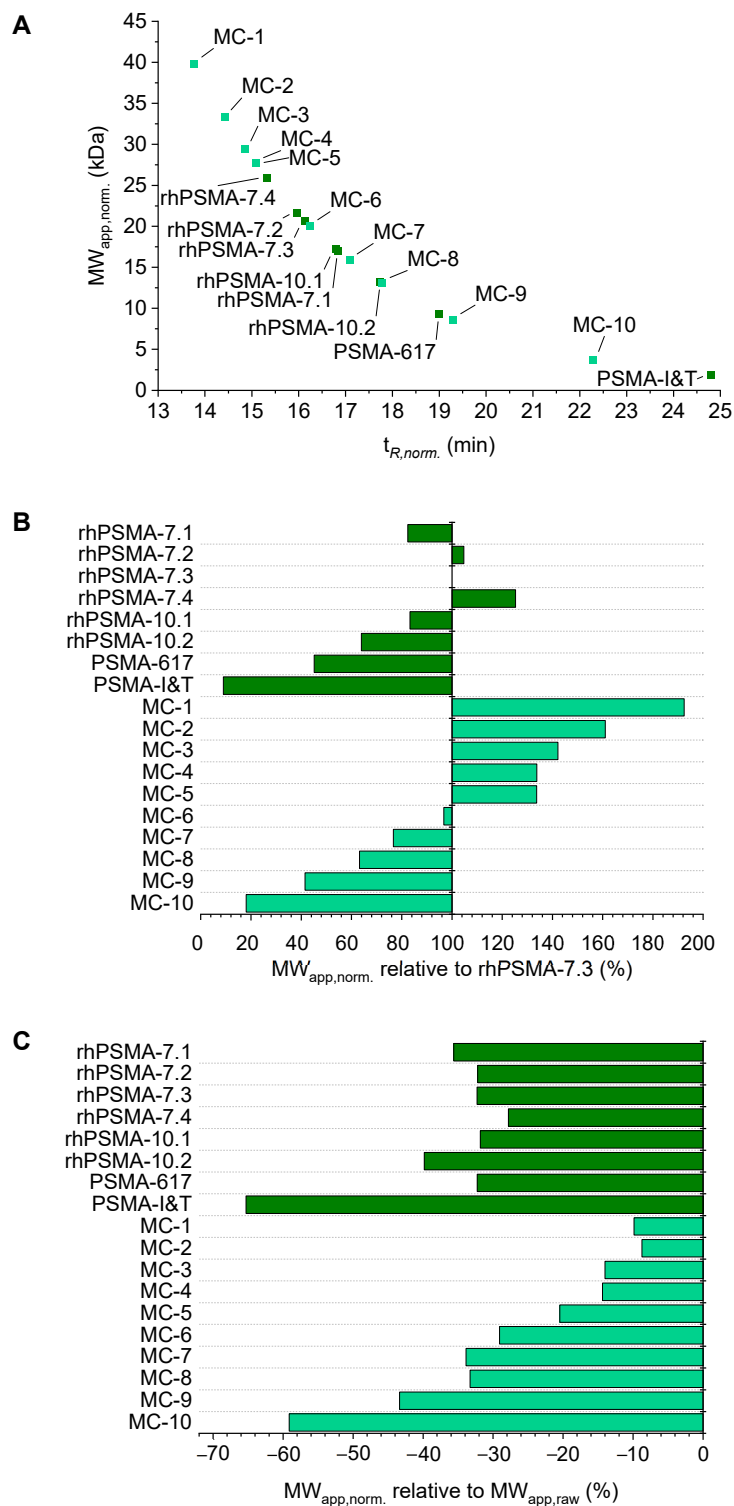


**Figure 4.** (A) Correlation between  $t_{R, norm.}$  of radioligands and the corresponding normalized apparent molecular weight ( $MW_{app, norm.}$ ).  $t_{R, norm.}$  of 13.8–24.8 min corresponded to  $MW_{app, norm.}$  between

39.9–1.9 kDa. (B)  $MW_{app, norm.}$  of all ligands in percentage of the  $MW_{app, norm.}$  of rhPSMA-7.3 (100%). Observed  $MW_{app, norm.}$  ranged from approximately 10% to almost 190% of the  $MW_{app, norm.}$  of rhPSMA-7.3. (C) Relative reduction in  $MW_{app, norm.}$  compared to their corresponding  $MW_{app, raw}$ . The extent of the effect of the normalization was dependent on the molecular structure of the radioligand and ranged between  $-10\%$  and  $-65\%$  for the compounds presented in this work.

Within the set of acquired data, however, the single lowest  $MW_{app, norm.}$  of 1.9 kDa determined for PSMA-I&T needs to be treated with caution. In contrast to all the other radioligands, the evaluation of PSMA-I&T yielded nearly identical  $t_{R, AMSEC}$  and  $t_{R, blank}$  (20.983 min and 20.995 min, respectively) leading to a disproportionately low retention factor  $k$  of only 0.0013. Consequently, a high  $t_{R, norm.}$  of 24.792 min comparable to  $t_{R, acetone}$  was determined, resulting in a suspiciously low  $MW_{app, norm.}$  for PSMA-I&T. This apparent lack of interaction between HSA and PSMA-I&T seems unreliable, as an albumin-binding capacity was reported for PSMA-I&T [67]. Apart from electrostatic interactions, the delayed elution of analytes bearing (multiple) aromatic residues caused by attractive hydrophobic interactions with crosslinked polysaccharide-based SEC gels (e.g., superdex and sephadex) has been reported by several groups [68–70]. PSMA-I&T bears a patch of two hydrophobic aromatic amino acids, namely phenylalanine and halogenated 3-iodo-tyrosine. We hypothesized that this unique structural feature might lead to a complex interplay of electrostatic and hydrophobic interactions for this particular derivative, possibly leading to an underestimation of its  $MW_{app, raw}$  and  $MW_{app, norm.}$ . Thus, AMSEC data for PSMA-I&T might presumably be compromised by these hydrophobic interactions and, therefore, valid comparability with the data obtained for the remaining radioligands might not be given for PSMA-I&T.

Since the normalization eliminated contributions to  $MW_{app, raw}$  caused by ligand-specific interactions, presumably electrostatic interactions with the column matrix, it was not surprising that values for  $MW_{app, norm.}$  were smaller than the respective  $MW_{app, raw}$  values. It is noteworthy, however, that the relative effect of the normalization on  $MW_{app, raw}$  was very different for the radioligands. As shown in Figure 4C, normalization resulted in  $MW_{app, norm.}$  values reduced by only about 10% (MC-1 and MC-2) to around 60% (PSMA-I&T and MC-10) of the original  $MW_{app, raw}$ . Among the rhPSMA compounds and PSMA-617, the influence of the normalization was comparable (approximately 30% to 40% reduction). There seems to be a trend of diminished influence of the normalization for radioligands with high  $MW_{app, raw}$  values. This phenomenon can be explained by the fact that the aforementioned electrostatic interactions between radioligands and the column matrix only occur when a radioligand is not complexed to HSA. As radioligands with high HSA binding are mainly complexed to the protein (reflected in high retention factors  $k$ ), the influence of the electrostatic interactions on  $MW_{app, raw}$  is accordingly smaller and the  $MW_{app, norm.}$ , hence, deviates to a lesser extent from  $MW_{app, raw}$  than for radioligands with weaker HSA binding (e.g., significantly lower  $MW_{app, raw}$ ).

Regarding the pharmacokinetically relevant conclusions that might be drawn from the determined  $MW_{app, norm.}$ , it is important to bear in mind that the correlation between MW and GSC and, thus, GF is not linear but shows a sigmoidal curve. Therefore, when comparing the  $MW_{app, norm.}$  of different radioligands, not only their relative difference but also the absolute values of  $MW_{app, norm.}$  are of importance. To gain a more intuitive understanding of how a certain  $MW_{app, norm.}$  might influence blood clearance by means of GF, we used a sigmoidal fit of the MWs and glomerular sieving coefficients (GSCs) of 12 human plasma proteins (Figure 5, data reported by Norden et al. [64]) to determine calculated GSCs ( $GSC_{calc}$ ) from  $MW_{app, norm.}$ . These  $GSC_{calc}$  determined for all the PSMA radioligands (Table 2, Figure 5) inherently account for the exponential nature of the relationship between their albumin-mediated  $MW_{app, norm.}$  and MW-dependent GF and could, therefore, be a useful parameter to estimate differences in blood clearance by means of GF. The GSC is defined as the ratio of a compound's concentration in the glomerular filtrate to that in the blood [64]; thus, a GSC of 1 represents unhindered filtration through the

capillary membrane in the glomerulus, while a lower GSC corresponds to a restricted filtration and, thus, a prolonged circulatory half-life. Interestingly, the determined  $GSC_{calc}$  values for the evaluated PSMA radioligands covered a wide range, from values above 0.95 (PSMA-I&T, MC-9, and MC-10), which correlates to mostly unhindered GF, to values below 0.05 (MC-1 and MC-2), which should be associated with high blood retention. The  $GSC_{calc}$  of rhPSMA-compounds were more moderate, yet they varied significantly among each other (0.138 to 0.846), even in the subgroup of the isomers of rhPSMA-7. As an example, a  $GSC_{calc}$  of 0.408 was determined for rhPSMA-7.3, while an almost three-fold smaller  $GSC_{calc}$  of 0.138 was determined for rhPSMA-7.4. Accordingly, if we assume GF to be the only contribution of renally induced blood clearance, a three-fold decelerated blood clearance should be expected for rhPSMA-7.4 compared to rhPSMA-7.3. This would constitute a dramatic physiological effect that, in its extent, could not be predicted only based on subtle differences in molecular structure and other conventionally determined in vitro parameters. We, therefore, believe that the  $MW_{app, norm.}$  and  $GSC_{calc}$  obtained by AMSEC could be important parameters that, already at the preclinical stage of development, could help in the selection of promising therapeutic radioligands with pharmacokinetic profiles suitable for patient application.

Regarding the current state of the art in the RLT of mCRPC, recently approved  $^{177}\text{Lu}$ -labeled PSMA-617 is considered the gold standard, and rapid, bi-phasic blood clearance was reported for this radioligand [71]. In the past years, considerable efforts have been made by various groups to develop derivatives of PSMA-617 with improved therapeutic efficacy via the incorporation of a dedicated albumin-binding entity [24–26]. Preclinical therapy studies in mice of, e.g.,  $^{177}\text{Lu}$ -labeled EB-PSMA-617 and PSMA-ALB-56, have shown superior therapeutic efficacy compared to PSMA-617 [24,25] and have raised hopes for a similar performance in patients. Lamentably, increased blood retention in patients resulted not only in increased tumor dose but also in disproportionately higher doses to most healthy tissues, among them bone marrow and kidneys, two potentially dose-limiting organs in PSMA-targeted RLT [72,73]. Consequently, the resulting inferior therapeutic efficacy indicates that the blood clearance of these novel radiotherapeutics might already be too slow. An inpatient dosimetry comparison between  $^{177}\text{Lu}$ -labeled radioligands rhPSMA-7.3 and PSMA-I&T (an established PSMA ligand for RLT with similar pharmacokinetics as PSMA-617 [74]) showed a 2.4-fold higher tumor dose for rhPSMA-7.3 [75]. However, nearly identically increased doses to kidneys and bone marrow resulted in an overall similar therapeutic efficacy of both radioligands. Once more, these findings could not keep promises made by preclinical therapy studies that had indicated a higher therapeutic efficacy for rhPSMA-7.3 than for PSMA-I&T [76], which once again underlines the so far unmet need of valid preclinical indicators for a pharmacokinetic profile yielding improved therapeutic efficacy in patients.

Considering the aforementioned clinical data, it might be suggested that the sweet spot of albumin binding and, thus, the narrow window of optimal blood clearance for improved therapeutic efficacy may actually lie between rhPSMA-7.3 and PSMA-617. In that light, rhPSMA-10.1 might be an attractive candidate for RLT of mCRPC. In a recent preclinical study in mice, rhPSMA-10.1 revealed fast blood clearance and improved tumor-to-background ratios in a head-to-head comparison with four isomers of rhPSMA-7 and rhPSMA-10.2 [62]. Furthermore, our study determined a  $MW_{app, norm.}$  of 17.2 kDa and a  $GSC_{calc}$  of 0.644 for rhPSMA-10.1. Thus, rhPSMA-10.1 could possibly exploit this interesting window of blood clearance kinetics between rhPSMA-7.3 ( $MW_{app, norm.}$ : 20.7 kDa;  $GSC_{calc}$ : 0.408) and PSMA-617 ( $MW_{app, norm.}$ : 9.4 kDa;  $GSC_{calc}$ : 0.942). However, clinical data are needed to verify this assumption, and a currently initiated, integrated phase 1 and 2 study with  $^{177}\text{Lu}$ -labeled rhPSMA-10.1 ([clinicalTrial.gov](https://clinicaltrials.gov/ct2/show/study/NCT05413850) identifier: NCT05413850) will hopefully shed light on that question.

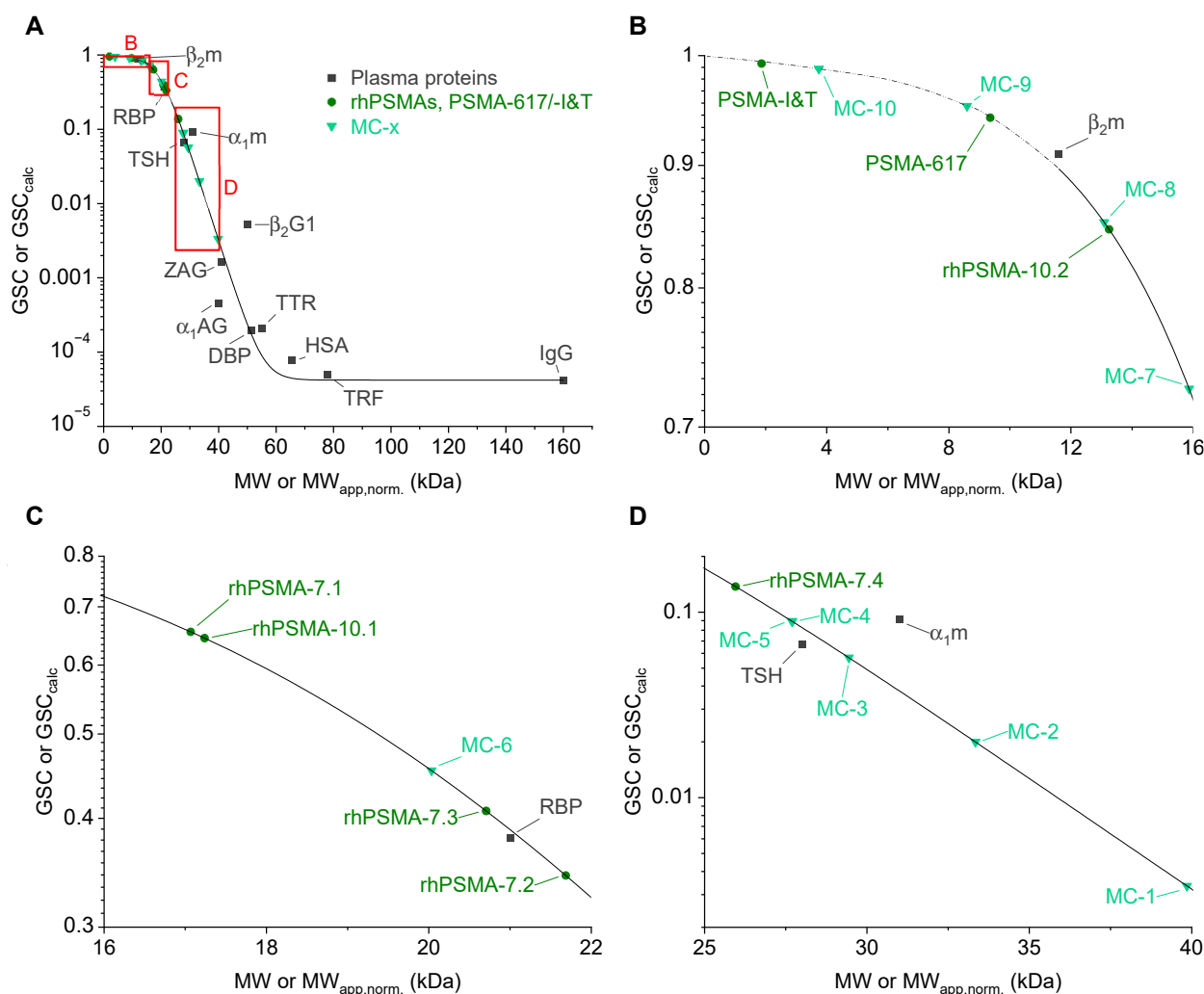


**Figure 5.** (A) Correlation between molecular weights (MWs) of plasma proteins and their glomerular sieving coefficients (GSCs, data from Norden et al. [64]).  $\alpha_1$ AG:  $\alpha_1$ -acid glycoprotein;  $\alpha_1$ m:  $\alpha_1$ -microglobulin; HSA: human serum albumin;  $\beta_2$ G1:  $\beta_2$ -glycoprotein I;  $\beta_2$ m:  $\beta_2$ -microglobulin; DBP: vitamin-D-binding protein; IgG: immunoglobulin G; RBP: retinol-binding protein; TRF: transferrin; TSH: thyroid-stimulating hormone; TTR: transthyretin; ZAG: zinc- $\alpha_2$ -globulin. MW<sub>app,norm.</sub> of PSMA radioligands were plotted against their respective calculated GSCs (GSC<sub>calc.</sub>). Panels (B–D) show different zoom-ins on PSMA radioligands, as depicted with red squares in panel (A). The extrapolation (dotted line) of the sigmoidal fit of GSC against MW in panel (B) was eye-fitted.

Regarding the limitations of the newly developed AMSEC method, it needs to be stated that the mobile phase composition did not account for the influence of plasma proteins other than HSA (e.g., alpha-1-acid glycoprotein [55,56]) on the pharmacokinetics of the evaluated radioligands. As discussed earlier, HSA is the most abundant human plasma protein and, next to its dominant role in the binding of exogenous compounds, HSA also meets the practical requirement of commercial availability in decent quantities. While a further refinement of the mobile phase in AMSEC, e.g., by supplementation with other relevant human plasma proteins, exceeds the scope of this study, it might be a worthwhile approach for future research.

The feasibility of a normalization accounting for the unspecific, presumably electrostatic interactions of PSMA ligands with the agarose/dextran-based column matrix was an important finding of the present study. However, the aforementioned inconclusive results obtained for PSMA-I&T presumably caused by hydrophobic interactions that were (among the evaluated radioligands) seemingly unique to this particular compound emphasize the

complexibility of possible interactions between peptidic ligands and gel filtration matrices. Therefore, more detailed studies evaluating the interactions between a superdex matrix and peptidic radioligands are necessary to elucidate this explicit case. A broader understanding of the unspecific interactions between radioligands and column resin would, furthermore, help to ascertain whether further series of peptidic radioligands other than PSMA show largely deviating, group- (or better structure-) specific interactions with a superdex matrix. Thus, it remains to be investigated with a variety of other peptidic radioligands to various targets whether comparable HSA binding also results in comparable  $MW_{app,norm.}$  values and, thus, comparable  $GSC_{calc}$  or whether  $MW_{app,norm.}$  primarily allows only for the differentiation of relative GF rates within a group of structurally highly similar ligands.

Another limitation constitutes the fact that HSA is a biologic product and batches might vary according to the origin of the plasma samples that were used in production. For example, results obtained in this study could not be adequately reproduced with HSA of another supplier. To examine the influences of different batches of HSA on the obtained data, however, exceeds the scope of this study and remains to be investigated.

Finally, in order to generally assess the validity of data generated by AMSEC for the estimation of blood clearance kinetics, clinical data of the evaluated PSMA radioligands in patients are necessary. To date, most of the available data describe the dosimetry and biodistribution of PSMA-617, and data on blood clearance (e.g., time–activity curves) are reported for the latter [71,77,78] and some other PSMA radioligands [72,73,79]. However, applied protocols to determine blood clearance kinetics vary among different studies (e.g., serial blood sampling [71,73,79] vs. image-based approaches [72] and varying or unmentioned parameters for the fitting of time–activity curves [73,77,79]), thus hampering comparability of the reported results. Furthermore, direct inter- or inpatient comparisons of the blood clearance of PSMA radioligands evaluated herein (e.g., rhPSMA-7.3 vs. PSMA-617 or rhPSMA-7.3 vs. rhPSMA-10.1) are currently lacking. Consequently, even though relative trends, e.g., slower blood clearance of rhPSMA-7.3 compared to PSMA-617, can be deduced from data reported in different comparative studies, the current state of our knowledge does not yet allow for a valid correlation of  $MW_{app,norm.}$  and  $GSC_{calc}$  obtained in our study. However, ongoing research and clinical studies, e.g., on rhPSMA-10.1 (NCT05413850), will provide more data in the future and, thus, will help to validate and interpret parameters such as  $MW_{app,norm.}$  and  $GSC_{calc}$  with more accuracy. Furthermore, AMSEC studies of other PSMA radioligands with reported clinical data could help sharpen our understanding of the actual correlation between  $MW_{app,norm.}$  and blood clearance kinetics in vivo.

In summary, the newly developed AMSEC method allows for the determination of HSA-mediated  $MW_{app,norm.}$  values of PSMA radioligands. High reproducibility was observed, and the resolution of differences in  $MW_{app,norm.}$  values, even among stereoisomeric radioligands, was feasible. The novel parameter of  $MW_{app,norm.}$  could serve as a valuable tool in the preclinical development of predominantly renally excreted therapeutic PSMA radioligands, as blood clearance by means of GF is a highly MW-dependent physiological process. According to the correlation between MW and glomerular sieving, we thus suggest the determination of  $GSC_{calc}$  from  $MW_{app,norm.}$  as a means to assess different blood clearance kinetics of PSMA radioligands in vitro. However, a broader availability of comparable clinical data on the pharmacokinetics of the radioligands evaluated herein is needed to validate and specify the predictive values of  $MW_{app,norm.}$  and  $GSC_{calc}$ .

### 3. Materials and Methods

#### 3.1. Instrumentation and Software

A high-performance liquid chromatography (HPLC) gradient system from Shimadzu (Neufahrn, Germany) equipped with LC20-AD gradient pumps and a SIL-20A HT autosampler was used for all chromatographic experiments. Detection of UV signals was carried out using an SPD-20A UV-vis detector, and radioactivity was detected with a HERM LB 500 NaI detector (Berthold Technologies, Bad Wildbad, Germany). Chromatograms were analyzed using LabSolutions software from Shimadzu. The readout of radio thin-layer

chromatography (radio-TLC) for quality control of radiolabelings was carried out using a Scan-RAM detector and Laura software (LabLogic Systems, Sheffield, UK). Microsoft excel (Redmond, WA, USA) was used for all calculative evaluations. OriginPro software (v9.7) from OriginLab (Northampton, MA, USA) was used for sigmoidal curve fitting.

### 3.2. Preparation of $^{177}\text{Lu}$ -Labeled PSMA Radioligands

The four isomers of uncomplexed rhPSMA-7 (7.1 to 7.4) and the two isomers of uncomplexed rhPSMA-10 (10.1 and 10.2) were synthesized as described earlier [62]. Compounds MC-1 to MC-9 represent PSMA-SiFA compounds, and compound MC-10 represents a PSMA-SiFalin compound. PSMA-617 was supplied by MedChemExpress LLC (Monmouth Junction, NJ, USA), and PSMA-I&T was prepared according to the published procedure [80].

Radiolabeling with no-carrier-added [ $^{177}\text{Lu}$ ]LuCl<sub>3</sub> (specific activity > 3000 GBq/mg at the time of radiolabeling, 740 MBq/mL, 0.04 M HCl, ITM, Garching, Germany) was carried out according to a previously established procedure [62] with molar activities of 10–20 GBq/μmol. Quality control of radiolabelings was performed using either analytical reversed-phase (RP) HPLC or radio-TLC. For analytical RP-HPLC, the HPLC-system described above was equipped with an RP column (MultoKrom 100C18, 150 × 4.6 mm, 5 μm; Multospher 100RP18, 125 × 4.6 mm, 5 μm; CS Chromatographie Service, Langerwehe, Germany), and linear gradients of water (solvent A, + 0.1% TFA, *v/v*) and acetonitrile (solvent B, +2% water, +0.1% TFA, *v/v*) were applied. Quality control via radio-TLC was performed using 1.0 M NH<sub>4</sub>OAc/DMF (1/1, *v/v*) on TLC silica gel 60 F<sub>254</sub> plates (Merck Millipore, Burlington, VT, USA) or 0.1 M sodium citrate buffer on iTLC-SG chromatography paper (Agilent, Santa Clara, CA, USA). Radioligands were used for experiments if the radio chemical purity (RCP) was > 95%.

All data presented in this work were obtained with the  $^{177}\text{Lu}$ -labeled species of PSMA ligands. For ease of readability, the lutetium complex is omitted in the designation of all radioligands in running text, figures, and tables (e.g., “rhPSMA-7.3” instead of “[ $^{177}\text{Lu}$ ]Lu-rhPSMA-7.3” or “MC-1” instead of “[ $^{177}\text{Lu}$ ]Lu-MC-1”).

### 3.3. AMSEC Experiments

All size exclusion chromatographic (SEC) experiments were carried out using the above-mentioned HPLC system equipped with a Superdex 75 Increase 10/300 GL gel filtration size exclusion column (fractionation range 70–3 kDa, GE Healthcare, Uppsala, Sweden). Eluents at room temperature, a constant flow rate of 0.8 mL/min, and an acquisition time of 35 min were generally applied. The column was calibrated as recommended by the manufacturer using a commercially available set of proteins (Gel Filtration LMW Calibration Kit, GE Healthcare, Buckinghamshire, UK). Retention times of calibration proteins and calculated calibration parameters are given in the Supplementary Materials (Table S3). UV signal detection occurred at 280 nm.

All retention times of radio signals were corrected for the offset between the UV-vis detector and radio-detector ( $\Delta t = 0.084$  min). Throughout the development of the AMSEC method, three gel filtration columns of the same type were used for experiments (most data were acquired using column 1). As calculations were based on absolute empirical retention times that inherently differed slightly from column to column, all retention times determined on column 2 and column 3 were mathematically converted to an equivalent retention time on column 1 using the columns' calibration parameters. A detailed description of these calculations is provided in the Supplementary Materials. A tabular summary of corrected retention times for all compounds is given in Table S1.

All numerical retention times explicitly given in running text or tables and plotted in diagrams are already corrected for the offset between UV-vis and radio-detector and, if initially determined on columns 2 or 3, converted to the equivalent retention time on column 1 (for detailed information, see Equations (S1) and (S2) and Table S1 in the Supplementary Materials).

### 3.3.1. Determination of Raw Apparent Molecular Weight ( $MW_{app,raw}$ )

AMSEC runs were executed with a solution of HSA (Biowest, Nuaille, France) in PBS (pH 7.4) at physiological concentration (700  $\mu$ M) as a mobile phase. Upon injection of approximately 1.0 MBq (5–10  $\mu$ L) of a radioligand, the elution profile was monitored via radioactivity detection, and the retention times of observed radiopeaks ( $t_{R,AMSEC}$ ) were determined via semi-automated peak integration. By means of calibration, retention times were translated into a ligand-specific raw apparent molecular weight ( $MW_{app,raw}$ ) as a parameter to assess the extent of HSA binding (for calculation, see Equation (S6) in the Supplementary Materials). rhPSMA-7.3 served as an internal standard during AMSEC studies and was co-evaluated whenever new data were collected to assess the reproducibility of the method ( $n = 14$ ).

For reference purposes, conventional SEC runs of HSA (100  $\mu$ L, 3 mg/mL) and acetone (100  $\mu$ L, 2% in PBS pH 7.4) with PBS (pH 7.4) as a mobile phase were executed. The retention time of HSA ( $t_{R,HSA}$ ) corresponded to the maximal  $MW_{app,raw}$ , theoretically observable in AMSEC runs in the case of continuous binding of a radioligand to HSA (equivalent to 100% HSA binding). The retention time of acetone ( $t_{R,acetone}$ ) served as a reference for a ligand with no interaction with HSA in AMSEC runs (equivalent to 0% HSA binding) and an actual physical molecular weight below the column fractionation range (this was the case for all investigated radioligands).

### 3.3.2. Determination of Normalized Apparent Molecular Weight ( $MW_{app,norm.}$ )

$MW_{app,raw}$  values determined as described in Section 3.3.1. were normalized in order to account for ligand-specific influences on experimentally determined retention times and to establish quantitative comparability of the obtained  $MW_{app,norm.}$  values. The normalization was based on a SEC run (referred to as blank run) of a radioligand executed in analogy to the AMSEC run but using PBS (pH 7.4) without HSA as a mobile phase. The determined retention time  $t_{R,blank}$ , together with the retention time  $t_{R,AMSEC}$  from the AMSEC run,  $t_{R,HSA}$ , and  $t_{R,acetone}$  determined in Section 3.3.1, were used to calculate a normalized retention time  $t_{R,norm.}$  for every radioligand (for formulae and details on the calculation, see Section 2. Results and Discussion). The  $MW_{app,norm.}$  values were subsequently calculated from  $t_{R,norm.}$  by means of column calibration (an exemplary calculation is provided within Equation (S3) in the Supplementary Materials).

### 3.4. Determination of Calculated Glomerular Sieving Coefficients ( $GSC_{calc}$ )

A sigmoidal fit of molecular weights (MWs, in kDa) and corresponding glomerular sieving coefficients (GSCs) of 12 human plasma proteins (data taken from Norden et al. [64]) was executed using OriginPro software. A dose-response model based on Equation (6) was applied:

$$GSC = A1 + \frac{A2 - A1}{1 + 10^{(LOGx0 - MW) \cdot p}} \quad (6)$$

The values of bottom asymptote A1 and top asymptote A2 were set to  $4.2 \cdot 10^{-5}$  (GSC of IgG, data taken from Norden et al. [64]) and 1 (equaling complete sieving), respectively. Curve fitting gave the center parameter  $LOGx0 = 19.36833$  and the Hill slope  $p = -0.12108$ .  $GSC_{calc}$  values were calculated via implementation of fitting parameters and the experimentally determined  $MW_{app,norm.}$  in Equation (6).

## 4. Conclusions

In conclusion, AMSEC might offer the unique possibility to gain insight into human blood clearance kinetics, a fundamental aspect in the pharmacokinetics of radioligands already in vitro at the preclinical stage. If clinical data confirm this novel preclinical approach, AMSEC could furthermore contribute to continually ameliorated animal protection, as preclinical in vivo experiments (e.g., in rodents, with anyway limited transferability to humans) could be reduced to pre-selected compounds that exhibit favorable  $MW_{app,norm.}$  and  $GSC_{calc}$  values. Thus, the implementation of AMSEC into the preclinical develop-

ment process could help to further refine the identification of therapeutic lead compounds for clinical translation with suitable blood clearance kinetics in patients, hopefully fostering the development of next-generation (PSMA) radioligands for RLT with improved therapeutic efficacy.

**Supplementary Materials:** The following supporting information can be downloaded at: <https://www.mdpi.com/article/10.3390/ph15091161/s1>, Table S1: Experimental retention times of AMSEC runs ( $t_{R,AMSEC}$  raw) and blank runs ( $t_{R,blank}$  raw), as well as corrected retention times converted to column 1 ( $t_{R,AMSEC}$  C1 and  $t_{R,blank}$  C1) of HSA, acetone, and all radioligands. Retention times of radiosignals are additionally corrected for the offset between UV-vis detector and radio-detector ( $t_{R,AMSEC}$  C1 + OC and  $t_{R,blank}$  C1 + OC). C1: column 1; OC: offset-corrected; n.a.: not applicable; Table S2: Retention times of model compounds (MCs) 1 to 10 in AMSEC runs ( $t_{R,AMSEC}$ ) and corresponding raw apparent molecular weights ( $MW_{app,raw}$ ); Table S3: Retention times of Blue Dextran 2000 (BD) and the calibration proteins conalbumin (CO, 75 kDa), ovalbumin (OV, 44 kDa), carbonic anhydrase (CA, 29 kDa), ribonuclease (RN, 13.7 kDa), and aprotinin (AP, 6.5 kDa) on superdex 75 increase columns 1, 2, and 3 (PBS pH 7.4 as mobile phase). *a* and *b*: calibration parameters; Cn: column *n*;  $V_e$ : elution volume;  $V_0$ : column void volume;  $R^2$ : coefficient of determination of column calibration; Figure S1: Chemical structure of  $^{177}\text{Lu}$ -labeled rhPSMA-7.1 ((*R*)-configured diaminopropionic acid branching unit and (*R*)-configured DOTAGA chelator); Figure S2: Chemical structure of  $^{177}\text{Lu}$ -labeled rhPSMA-7.2 ((*S*)-configured diaminopropionic acid branching unit and (*R*)-configured DOTAGA chelator); Figure S3: Chemical structure of  $^{177}\text{Lu}$ -labeled rhPSMA-7.3 ((*R*)-configured diaminopropionic acid branching unit and (*S*)-configured DOTAGA chelator); Figure S4: Chemical structure of  $^{177}\text{Lu}$ -labeled rhPSMA-7.4 ((*S*)-configured diaminopropionic acid branching unit and (*S*)-configured DOTAGA chelator); Figure S5: Chemical structure of  $^{177}\text{Lu}$ -labeled rhPSMA-10.1 ((*R*)-configured diaminopropionic acid branching unit and DOTA chelator); Figure S6: Chemical structure of  $^{177}\text{Lu}$ -labeled rhPSMA-10.2 ((*S*)-configured diaminopropionic acid branching unit and DOTA chelator); Figure S7: Chemical structure of  $^{177}\text{Lu}$ -labeled PSMA-617; Figure S8: Chemical structure of  $^{177}\text{Lu}$ -labeled PSMA-I&T.

**Author Contributions:** Conceptualization, J.-P.K. and H.-J.W.; methodology, J.-P.K. and H.-J.W.; validation, J.-P.K. and S.F.; formal analysis, J.-P.K.; investigation, J.-P.K., S.F. and A.W.; resources, J.-P.K., S.F. and A.W.; data curation, J.-P.K. and S.F.; writing—original draft preparation, J.-P.K.; writing—review and editing, S.F., A.W. and H.-J.W.; visualization, J.-P.K.; supervision, H.-J.W.; project administration, J.-P.K.; funding acquisition, H.-J.W. All authors have read and agreed to the published version of the manuscript.

**Funding:** This research was funded by the Deutsche Forschungsgemeinschaft (DFG, German Research Foundation, Project Number SFB 824, Project B11 and Z01). The APC was funded by the TUM Publishing Fund.

**Institutional Review Board Statement:** Not applicable.

**Informed Consent Statement:** Not applicable.

**Data Availability Statement:** Data is contained within the article and Supplementary Material.

**Acknowledgments:** The authors thank Harald Bothe (Cytiva Europe GmbH) for his kind and helpful scientific support.

**Conflicts of Interest:** A.W., H.J.W., J.P.K., and S.F. are listed as inventors in patent applications for some therapeutic rhPSMA. HJW is a founder and shareholder of Scintomics GmbH, Munich, Germany. No other potential conflict of interest relevant to this article exist. The funders had no role in the design of the study; in the collection, analyses, or interpretation of data; in the writing of the manuscript; or in the decision to publish the results.

## References

1. Weber, W.A.; Czernin, J.; Anderson, C.J.; Badawi, R.D.; Barthel, H.; Bengel, F.; Bodei, L.; Buvat, I.; DiCarli, M.; Graham, M.M.; et al. The Future of Nuclear Medicine, Molecular Imaging, and Theranostics. *J. Nucl. Med.* **2020**, *61*, 263S–272S. [[CrossRef](#)] [[PubMed](#)]
2. Kantorova, I.; Lipska, L.; Belohlavek, O.; Visokai, V.; Trubac, M.; Schneiderova, M. Routine  $^{18}\text{F}$ -FDG PET preoperative staging of colorectal cancer: Comparison with conventional staging and its impact on treatment decision making. *J. Nucl. Med.* **2003**, *44*, 1784–1788. [[PubMed](#)]

3. Grubmuller, B.; Baltzer, P.; D'Andrea, D.; Korn, S.; Haug, A.R.; Hacker, M.; Grubmuller, K.H.; Goldner, G.M.; Wadsak, W.; Pfaff, S.; et al.  $^{68}\text{Ga}$ -PSMA 11 ligand PET imaging in patients with biochemical recurrence after radical prostatectomy—Diagnostic performance and impact on therapeutic decision-making. *Eur. J. Nucl. Med. Mol. Imaging* **2018**, *45*, 235–242. [[CrossRef](#)] [[PubMed](#)]
4. Castaldi, P.; Rufini, V.; Treglia, G.; Bruno, I.; Perotti, G.; Stifano, G.; Barbaro, B.; Giordano, A. Impact of  $^{111}\text{In}$ -DTPA-octreotide SPECT/CT fusion images in the management of neuroendocrine tumours. *Radiol. Med.* **2008**, *113*, 1056–1067. [[CrossRef](#)]
5. Dittmann, H.; Kaltenbach, S.; Weissinger, M.; Fiz, F.; Martus, P.; Pritzkow, M.; Kupferschlaeger, J.; la Fougere, C. The Prognostic Value of Quantitative Bone SPECT/CT Before  $^{223}\text{Ra}$  Treatment in Metastatic Castration-Resistant Prostate Cancer. *J. Nucl. Med.* **2021**, *62*, 48–54. [[CrossRef](#)]
6. Kratochwil, C.; Fendler, W.P.; Eiber, M.; Baum, R.; Bozkurt, M.F.; Czernin, J.; Delgado Bolton, R.C.; Ezziddin, S.; Forrer, F.; Hicks, R.J.; et al. EANM procedure guidelines for radionuclide therapy with  $^{177}\text{Lu}$ -labelled PSMA-ligands ( $^{177}\text{Lu}$ -PSMA-RLT). *Eur. J. Nucl. Med. Mol. Imaging* **2019**, *46*, 2536–2544. [[CrossRef](#)]
7. Herrmann, K.; Giovanella, L.; Santos, A.; Gear, J.; Kiratli, P.O.; Kurth, J.; Denis-Bacelar, A.M.; Hustinx, R.; Patt, M.; Wahl, R.L.; et al. Joint EANM, SNMMI and IAEA enabling guide: How to set up a theranostics centre. *Eur. J. Nucl. Med. Mol. Imaging* **2022**, *49*, 2300–2309. [[CrossRef](#)]
8. Nicolas, G.P.; Morgenstern, A.; Schottelius, M.; Fani, M. New Developments in Peptide Receptor Radionuclide Therapy. *J. Nucl. Med.* **2018**, *60*, 167–171. [[CrossRef](#)]
9. Kwekkeboom, D.J.; Bakker, W.H.; Kooij, P.P.; Konijnenberg, M.W.; Srinivasan, A.; Erion, J.L.; Schmidt, M.A.; Bugaj, J.L.; de Jong, M.; Krenning, E.P. [ $^{177}\text{Lu}$ -DOTA $^{\circ}$ , Tyr $^3$ ]octreotate: Comparison with [ $^{111}\text{In}$ -DTPA $^{\circ}$ ]octreotide in patients. *Eur. J. Nucl. Med.* **2001**, *28*, 1319–1325. [[CrossRef](#)]
10. Hennrich, U.; Kopka, K. Lutathera $^{\circ}$ : The First FDA- and EMA-Approved Radiopharmaceutical for Peptide Receptor Radionuclide Therapy. *Pharmaceuticals* **2019**, *12*, 114. [[CrossRef](#)]
11. Benesova, M.; Schafer, M.; Bauder-Wust, U.; Afshar-Oromieh, A.; Kratochwil, C.; Mier, W.; Haberkorn, U.; Kopka, K.; Eder, M. Preclinical Evaluation of a Tailor-Made DOTA-Conjugated PSMA Inhibitor with Optimized Linker Moiety for Imaging and Endoradiotherapy of Prostate Cancer. *J. Nucl. Med.* **2015**, *56*, 914–920. [[CrossRef](#)] [[PubMed](#)]
12. Zacherl, M.J.; Gildehaus, F.J.; Mittlmeier, L.; Boning, G.; Gosewisch, A.; Wenter, V.; Unterrainer, M.; Schmidt-Hegemann, N.; Belka, C.; Kretschmer, A.; et al. First Clinical Results for PSMA-Targeted alpha-Therapy Using  $^{225}\text{Ac}$ -PSMA-I&T in Advanced-mCRPC Patients. *J. Nucl. Med.* **2021**, *62*, 669–674. [[CrossRef](#)] [[PubMed](#)]
13. Wickstroem, K.; Karlsson, J.; Ellingsen, C.; Cruciani, V.; Kristian, A.; Hagemann, U.B.; Bjerke, R.M.; Ryan, O.B.; Linden, L.; Mumberg, D.; et al. Synergistic Effect of a HER2 Targeted Thorium-227 Conjugate in Combination with Olaparib in a BRCA2 Deficient Xenograft Model. *Pharmaceuticals* **2019**, *12*, 155. [[CrossRef](#)] [[PubMed](#)]
14. Sorensen, J.; Sandberg, D.; Sandstrom, M.; Wennborg, A.; Feldwisch, J.; Tolmachev, V.; Astrom, G.; Lubberink, M.; Garske-Roman, U.; Carlsson, J.; et al. First-in-human molecular imaging of HER2 expression in breast cancer metastases using the  $^{111}\text{In}$ -ABY-025 affibody molecule. *J. Nucl. Med.* **2014**, *55*, 730–735. [[CrossRef](#)] [[PubMed](#)]
15. Kurth, J.; Krause, B.J.; Schwarzenbock, S.M.; Bergner, C.; Hakenberg, O.W.; Heuschkel, M. First-in-human dosimetry of gastrin-releasing peptide receptor antagonist [ $^{177}\text{Lu}$ ]Lu-RM2: A radiopharmaceutical for the treatment of metastatic castration-resistant prostate cancer. *Eur. J. Nucl. Med. Mol. Imaging* **2020**, *47*, 123–135. [[CrossRef](#)]
16. Guenther, T.; Deiser, S.; Felber, V.; Beck, R.; Wester, H.J. Substitution of L-Trp by alpha-methyl-L-Trp in  $^{177}\text{Lu}$ -RM2 results in  $^{177}\text{Lu}$ -AMTG, a high affinity GRPR ligand with improved in vivo stability. *J. Nucl. Med.* **2022**. [[CrossRef](#)]
17. Rottenburger, C.; Nicolas, G.P.; McDougall, L.; Kaul, F.; Cachovan, M.; Vija, A.H.; Schibli, R.; Geistlich, S.; Schumann, A.; Rau, T.; et al. Cholecystokinin 2 Receptor Agonist  $^{177}\text{Lu}$ -PP-F11N for Radionuclide Therapy of Medullary Thyroid Carcinoma: Results of the Lumed Phase 0a Study. *J. Nucl. Med.* **2020**, *61*, 520–526. [[CrossRef](#)]
18. Klingler, M.; Summer, D.; Rangger, C.; Haubner, R.; Foster, J.; Sosabowski, J.; Decristoforo, C.; Virgolini, I.; von Guggenberg, E. DOTA-MGS5, a New Cholecystokinin-2 Receptor-Targeting Peptide Analog with an Optimized Targeting Profile for Theranostic Use. *J. Nucl. Med.* **2019**, *60*, 1010–1016. [[CrossRef](#)]
19. Banerjee, S.R.; Kumar, V.; Lisok, A.; Chen, J.; Minn, I.; Brummet, M.; Boinapally, S.; Cole, M.; Ngen, E.; Wharram, B.; et al.  $^{177}\text{Lu}$ -labeled low-molecular-weight agents for PSMA-targeted radiopharmaceutical therapy. *Eur. J. Nucl. Med. Mol. Imaging* **2019**, *46*, 2545–2557. [[CrossRef](#)]
20. Dos Santos, J.C.; Schafer, M.; Bauder-Wust, U.; Lehnert, W.; Leotta, K.; Morgenstern, A.; Kopka, K.; Haberkorn, U.; Mier, W.; Kratochwil, C. Development and dosimetry of  $^{203}\text{Pb}$ / $^{212}\text{Pb}$ -labelled PSMA ligands: Bringing “the lead” into PSMA-targeted alpha therapy? *Eur. J. Nucl. Med. Mol. Imaging* **2019**, *46*, 1081–1091. [[CrossRef](#)]
21. Sartor, O.; de Bono, J.; Chi, K.N.; Fizazi, K.; Herrmann, K.; Rahbar, K.; Tagawa, S.T.; Nordquist, L.T.; Vaishampayan, N.; El-Haddad, G.; et al. Lutetium-177-PSMA-617 for Metastatic Castration-Resistant Prostate Cancer. *N. Engl. J. Med.* **2021**, *385*, 1091–1103. [[CrossRef](#)] [[PubMed](#)]
22. FDA Approves Pluvicto for Metastatic Castration-Resistant Prostate Cancer. Available online: <https://www.fda.gov/drugs/resources-information-approved-drugs/fda-approves-pluvicto-metastatic-castration-resistant-prostate-cancer> (accessed on 8 July 2022).
23. Kopka, K.; Benesova, M.; Barinka, C.; Haberkorn, U.; Babich, J. Glu-Ureido-Based Inhibitors of Prostate-Specific Membrane Antigen: Lessons Learned During the Development of a Novel Class of Low-Molecular-Weight Theranostic Radiotracers. *J. Nucl. Med.* **2017**, *58*, 17S–26S. [[CrossRef](#)] [[PubMed](#)]

24. Wang, Z.; Tian, R.; Niu, G.; Ma, Y.; Lang, L.; Szajek, L.P.; Kiesewetter, D.O.; Jacobson, O.; Chen, X. Single Low-Dose Injection of Evans Blue Modified PSMA-617 Radioligand Therapy Eliminates Prostate-Specific Membrane Antigen Positive Tumors. *Bioconjug. Chem.* **2018**, *29*, 3213–3221. [[CrossRef](#)]
25. Umbricht, C.A.; Benesova, M.; Schibli, R.; Muller, C. Preclinical Development of Novel PSMA-Targeting Radioligands: Modulation of Albumin-Binding Properties to Improve Prostate Cancer Therapy. *Mol. Pharm.* **2018**, *15*, 2297–2306. [[CrossRef](#)] [[PubMed](#)]
26. Kelly, J.M.; Amor-Coarasa, A.; Ponnala, S.; Nikolopoulou, A.; Williams, C., Jr.; DiMagno, S.G.; Babich, J.W. Albumin-Binding PSMA Ligands: Implications for Expanding the Therapeutic Window. *J. Nucl. Med.* **2019**, *60*, 656–663. [[CrossRef](#)] [[PubMed](#)]
27. Deberle, L.M.; Benesova, M.; Umbricht, C.A.; Borgna, F.; Buchler, M.; Zhernosekov, K.; Schibli, R.; Muller, C. Development of a new class of PSMA radioligands comprising ibuprofen as an albumin-binding entity. *Theranostics* **2020**, *10*, 1678–1693. [[CrossRef](#)] [[PubMed](#)]
28. Lau, J.; Jacobson, O.; Niu, G.; Lin, K.S.; Benard, F.; Chen, X. Bench to Bedside: Albumin Binders for Improved Cancer Radioligand Therapies. *Bioconjug. Chem.* **2019**, *30*, 487–502. [[CrossRef](#)]
29. Yordanova, A.; Becker, A.; Eppard, E.; Kurpig, S.; Fisang, C.; Feldmann, G.; Essler, M.; Ahmadzadehfar, H. The impact of repeated cycles of radioligand therapy using [<sup>177</sup>Lu]Lu-PSMA-617 on renal function in patients with hormone refractory metastatic prostate cancer. *Eur. J. Nucl. Med. Mol. Imaging* **2017**, *44*, 1473–1479. [[CrossRef](#)]
30. Kashyap, R.; Jackson, P.; Hofman, M.S.; Eu, P.; Beaugard, J.M.; Zannino, D.; Hicks, R.J. Rapid blood clearance and lack of long-term renal toxicity of <sup>177</sup>Lu-DOTATATE enables shortening of renoprotective amino acid infusion. *Eur. J. Nucl. Med. Mol. Imaging* **2013**, *40*, 1853–1860. [[CrossRef](#)]
31. Langbein, T.; Chausse, G.; Baum, R.P. Salivary Gland Toxicity of PSMA Radioligand Therapy: Relevance and Preventive Strategies. *J. Nucl. Med.* **2018**, *59*, 1172–1173. [[CrossRef](#)]
32. Van Binnebeek, S.; Baete, K.; Terwinghe, C.; Vanbilloen, B.; Haustermans, K.; Mortelmans, L.; Borbath, I.; Van Cutsem, E.; Verslype, C.; Mottaghy, F.M.; et al. Significant impact of transient deterioration of renal function on dosimetry in PRRT. *Ann. Nucl. Med.* **2013**, *27*, 74–77. [[CrossRef](#)]
33. Tucker, G.T. Measurement of the renal clearance of drugs. *Br. J. Clin. Pharmacol.* **1981**, *12*, 761–770. [[CrossRef](#)]
34. Jarad, G.; Miner, J.H. Update on the glomerular filtration barrier. *Curr. Opin. Nephrol. Hypertens.* **2009**, *18*, 226–232. [[CrossRef](#)]
35. Chang, R.L.; Deen, W.M.; Robertson, C.R.; Bennett, C.M.; Glassock, R.J.; Brenner, B.M.; Troy, J.L.; Ueki, I.F.; Rasmussen, B. Permeability of the glomerular capillary wall. Studies of experimental glomerulonephritis in the rat using neutral dextran. *J. Clin. Investig.* **1976**, *57*, 1272–1286. [[CrossRef](#)]
36. Tencer, J.; Frick, I.M.; Oquist, B.W.; Alm, P.; Rippe, B. Size-selectivity of the glomerular barrier to high molecular weight proteins: Upper size limitations of shunt pathways. *Kidney Int.* **1998**, *53*, 709–715. [[CrossRef](#)]
37. Toma, C.-M.; Imre, S.; Vari, C.-E.; Muntean, D.-L.; Tero-Vescan, A. Ultrafiltration Method for Plasma Protein Binding Studies and Its Limitations. *Processes* **2021**, *9*, 382. [[CrossRef](#)]
38. Hage, D.S. High-performance affinity chromatography: A powerful tool for studying serum protein binding. *J. Chromatogr. B* **2002**, *768*, 3–30. [[CrossRef](#)]
39. Shibukawa, A.; Kuroda, Y.; Nakagawa, T. High-performance frontal analysis for drug-protein binding study. *J. Pharm. Biomed. Anal.* **1999**, *18*, 1047–1055. [[CrossRef](#)]
40. Clarke, W.; Chowdhuri, A.R.; Hage, D.S. Analysis of free drug fractions by ultrafast immunoaffinity chromatography. *Anal. Chem.* **2001**, *73*, 2157–2164. [[CrossRef](#)]
41. Varlan, A.; Hillebrand, M. Bovine and human serum albumin interactions with 3-carboxyphenoxathiin studied by fluorescence and circular dichroism spectroscopy. *Molecules* **2010**, *15*, 3905–3919. [[CrossRef](#)]
42. Ascoli, G.; Bertucci, C.; Salvadori, P. Stereospecific and competitive binding of drugs to human serum albumin: A difference circular dichroism approach. *J. Pharm. Sci.* **1995**, *84*, 737–741. [[CrossRef](#)]
43. Rehman, M.T.; Shamsi, H.; Khan, A.U. Insight into the binding mechanism of imipenem to human serum albumin by spectroscopic and computational approaches. *Mol. Pharm.* **2014**, *11*, 1785–1797. [[CrossRef](#)]
44. Jana, S.; Dalapati, S.; Ghosh, S.; Guchhait, N. Binding interaction between plasma protein bovine serum albumin and flexible charge transfer fluorophore: A spectroscopic study in combination with molecular docking and molecular dynamics simulation. *J. Photochem. Photobiol.* **2012**, *231*, 19–27. [[CrossRef](#)]
45. Benesova, M.; Umbricht, C.A.; Schibli, R.; Muller, C. Albumin-Binding PSMA Ligands: Optimization of the Tissue Distribution Profile. *Mol. Pharm.* **2018**, *15*, 934–946. [[CrossRef](#)]
46. Wester, H.J.; Willoch, F.; Tolle, T.R.; Munz, F.; Herz, M.; Oye, I.; Schadrack, J.; Schwaiger, M.; Bartenstein, P. 6-O-(2-[<sup>18</sup>F]fluoroethyl)-6-O-desmethyldiprenorphine ([<sup>18</sup>F]DPN): Synthesis, biologic evaluation, and comparison with [<sup>11</sup>C]DPN in humans. *J. Nucl. Med.* **2000**, *41*, 1279–1286.
47. Muller, C.; Struthers, H.; Winiger, C.; Zhernosekov, K.; Schibli, R. DOTA conjugate with an albumin-binding entity enables the first folic acid-targeted <sup>177</sup>Lu-radionuclide tumor therapy in mice. *J. Nucl. Med.* **2013**, *54*, 124–131. [[CrossRef](#)]
48. Muller, C.; Farkas, R.; Borgna, F.; Schmid, R.M.; Benesova, M.; Schibli, R. Synthesis, Radiolabeling, and Characterization of Plasma Protein-Binding Ligands: Potential Tools for Modulation of the Pharmacokinetic Properties of (Radio)Pharmaceuticals. *Bioconjug. Chem.* **2017**, *28*, 2372–2383. [[CrossRef](#)]

49. Borgna, F.; Deberle, L.M.; Busslinger, S.D.; Tschan, V.J.; Walde, L.M.; Becker, A.E.; Schibli, R.; Muller, C. Preclinical Investigations to Explore the Difference between the Diastereomers [ $^{177}\text{Lu}$ ]Lu-SibuDAB and [ $^{177}\text{Lu}$ ]Lu-RibuDAB toward Prostate Cancer Therapy. *Mol. Pharm.* **2022**, *19*, 2105–2114. [[CrossRef](#)]
50. Schottelius, M.; Wurzer, A.; Wissmiller, K.; Beck, R.; Koch, M.; Gorpas, D.; Notni, J.; Buckle, T.; van Oosterom, M.N.; Steiger, K.; et al. Synthesis and Preclinical Characterization of the PSMA-Targeted Hybrid Tracer PSMA-I&F for Nuclear and Fluorescence Imaging of Prostate Cancer. *J. Nucl. Med.* **2019**, *60*, 71–78. [[CrossRef](#)]
51. Kelly, J.M.; Jeitner, T.M.; Ponnala, S.; Williams, C., Jr.; Nikolopoulou, A.; DiMagno, S.G.; Babich, J.W. A Trifunctional Theranostic Ligand Targeting Fibroblast Activation Protein-alpha (FAPalpha). *Mol. Imaging Biol.* **2021**, *23*, 686–696. [[CrossRef](#)]
52. Hummel, J.P.; Dreyer, W.J. Measurement of protein-binding phenomena by gel filtration. *Biochim. Biophys. Acta* **1962**, *63*, 530–532. [[CrossRef](#)]
53. Tozer, T.N.; Rowland, M. *Introduction to Pharmacokinetics and Pharmacodynamics—The Quantitative Basis of Drug Therapy*, 1st ed.; Lippincott Williams & Wilkins: Baltimore, MD, USA, 2006; p. 84.
54. Fasano, M.; Curry, S.; Terreno, E.; Galliano, M.; Fanali, G.; Narciso, P.; Notari, S.; Ascenzi, P. The extraordinary ligand binding properties of human serum albumin. *IUBMB Life* **2005**, *57*, 787–796. [[CrossRef](#)]
55. Smith, S.A.; Waters, N.J. Pharmacokinetic and Pharmacodynamic Considerations for Drugs Binding to Alpha-1-Acid Glycoprotein. *Pharm. Res.* **2018**, *36*, 30. [[CrossRef](#)]
56. Bteich, M. An overview of albumin and alpha-1-acid glycoprotein main characteristics: Highlighting the roles of amino acids in binding kinetics and molecular interactions. *Heliyon* **2019**, *5*, e02879. [[CrossRef](#)]
57. Ghuman, J.; Zunszain, P.A.; Petitpas, I.; Bhattacharya, A.A.; Otagiri, M.; Curry, S. Structural basis of the drug-binding specificity of human serum albumin. *J. Mol. Biol.* **2005**, *353*, 38–52. [[CrossRef](#)]
58. Dumelin, C.E.; Trussel, S.; Buller, F.; Trachsel, E.; Bootz, F.; Zhang, Y.; Mannocci, L.; Beck, S.C.; Drumea-Mirancea, M.; Seeliger, M.W.; et al. A portable albumin binder from a DNA-encoded chemical library. *Angew. Chem. Int. Ed. Engl.* **2008**, *47*, 3196–3201. [[CrossRef](#)]
59. Kelly, J.M.; Amor-Coarasa, A.; Nikolopoulou, A.; Wustemann, T.; Barelli, P.; Kim, D.; Williams, C., Jr.; Zheng, X.; Bi, C.; Hu, B.; et al. Dual-Target Binding Ligands with Modulated Pharmacokinetics for Endoradiotherapy of Prostate Cancer. *J. Nucl. Med.* **2017**, *58*, 1442–1449. [[CrossRef](#)]
60. Corzo, J. Time, the forgotten dimension of ligand binding teaching. *Biochem. Mol. Biol. Educ.* **2006**, *34*, 413–416. [[CrossRef](#)]
61. Iovkova, L.; Wangler, B.; Schirmmayer, E.; Schirmmayer, R.; Quandt, G.; Boening, G.; Schurmann, M.; Jurkschat, K. para-Functionalized aryl-di-tert-butylfluorosilanes as potential labeling synthons for  $^{18}\text{F}$  radiopharmaceuticals. *Chemistry* **2009**, *15*, 2140–2147. [[CrossRef](#)]
62. Wurzer, A.; Kunert, J.P.; Fischer, S.; Felber, V.; Beck, R.; De Rose, F.; D'Alessandria, C.; Weber, W.A.; Wester, H.J. Synthesis and Preclinical Evaluation of  $^{177}\text{Lu}$ -labeled Radiohybrid PSMA Ligands (rhPSMAs) for Endoradiotherapy of Prostate Cancer. *J. Nucl. Med.* **2022**, *63*. [[CrossRef](#)]
63. Gower-Fry, L.; Kronemann, T.; Dorian, A.; Pu, Y.; Jaworski, C.; Wangler, C.; Bartenstein, P.; Beyer, L.; Lindner, S.; Jurkschat, K.; et al. Recent Advances in the Clinical Translation of Silicon Fluoride Acceptor (SiFA) (18)F-Radiopharmaceuticals. *Pharmaceuticals* **2021**, *14*, 701. [[CrossRef](#)]
64. Norden, A.G.; Lapsley, M.; Lee, P.J.; Pusey, C.D.; Scheinman, S.J.; Tam, F.W.; Thakker, R.V.; Unwin, R.J.; Wrong, O. Glomerular protein sieving and implications for renal failure in Fanconi syndrome. *Kidney Int.* **2001**, *60*, 1885–1892. [[CrossRef](#)]
65. Fatin-Rouge, N.; Milon, A.; Buffle, J. Diffusion and Partitioning of Solutes in Agarose Hydrogels: The Relative Influence of Electrostatic and Specific Interactions. *J. Phys. Chem. B* **2003**, *107*, 12126–12137. [[CrossRef](#)]
66. Wang, Y.; Ding, S.; Gong, M.; Xu, S.; Xu, W.; Zhang, C. Diffusion characteristics of agarose hydrogel used in diffusive gradients in thin films for measurements of cations and anions. *Anal. Chim. Acta* **2016**, *945*, 47–56. [[CrossRef](#)]
67. Schmidt, A.; Wirtz, M.; Farber, S.F.; Osl, T.; Beck, R.; Schottelius, M.; Schwaiger, M.; Wester, H.J. Effect of Carbohydration on the Theranostic Tracer PSMA I&T. *ACS Omega* **2018**, *3*, 8278–8287. [[CrossRef](#)]
68. Joyce, J.G.; Cook, J.C.; Przysiecki, C.T.; Lehman, E.D. Chromatographic separation of low-molecular-mass recombinant proteins and peptides on Superdex 30 prep grade. *J. Chromatogr. B Biomed. Appl.* **1994**, *662*, 325–334. [[CrossRef](#)]
69. Bretthauer, R.K.; Golichowski, A.M. Adsorption chromatography of phenylalanine peptides on Sephadex. *Biochim. Biophys. Acta BBA Nucleic Acids Protein Synth.* **1967**, *155*, 549–557. [[CrossRef](#)]
70. Aird, S.D. Chromatographic behavior of Bothrops erythromelas phospholipase and other venom constituents on Superdex 75. *Prep. Biochem. Biotechnol.* **2004**, *34*, 345–364. [[CrossRef](#)]
71. Kratochwil, C.; Giesel, F.L.; Stefanova, M.; Benesova, M.; Bronzel, M.; Afshar-Oromieh, A.; Mier, W.; Eder, M.; Kopka, K.; Haberkorn, U. PSMA-Targeted Radionuclide Therapy of Metastatic Castration-Resistant Prostate Cancer with  $^{177}\text{Lu}$ -Labeled PSMA-617. *J. Nucl. Med.* **2016**, *57*, 1170–1176. [[CrossRef](#)]
72. Zang, J.; Fan, X.; Wang, H.; Liu, Q.; Wang, J.; Li, H.; Li, F.; Jacobson, O.; Niu, G.; Zhu, Z.; et al. First-in-human study of  $^{177}\text{Lu}$ -EB-PSMA-617 in patients with metastatic castration-resistant prostate cancer. *Eur. J. Nucl. Med. Mol. Imaging* **2019**, *46*, 148–158. [[CrossRef](#)]
73. Kramer, V.; Fernandez, R.; Lehnert, W.; Jimenez-Franco, L.D.; Soza-Ried, C.; Eppard, E.; Ceballos, M.; Meckel, M.; Benesova, M.; Umbricht, C.A.; et al. Biodistribution and dosimetry of a single dose of albumin-binding ligand [ $^{177}\text{Lu}$ ]Lu-PSMA-ALB-56 in patients with mCRPC. *Eur. J. Nucl. Med. Mol. Imaging* **2020**, *48*, 893–903. [[CrossRef](#)] [[PubMed](#)]

74. Kulkarni, H.R.; Singh, A.; Schuchardt, C.; Niepsch, K.; Sayeg, M.; Leshch, Y.; Wester, H.J.; Baum, R.P. PSMA-Based Radioligand Therapy for Metastatic Castration-Resistant Prostate Cancer: The Bad Berka Experience Since 2013. *J. Nucl. Med.* **2016**, *57*, 97S–104S. [[CrossRef](#)] [[PubMed](#)]
75. Feuerecker, B.; Chantadisai, M.; Allmann, A.; Tauber, R.; Allmann, J.; Steinhelfer, L.; Rauscher, I.; Wurzer, A.; Wester, H.J.; Weber, W.A.; et al. Pretherapeutic Comparative Dosimetry of  $^{177}\text{Lu}$ -rhPSMA-7.3 and  $^{177}\text{Lu}$ -PSMA I&T in Patients with Metastatic Castration-Resistant Prostate Cancer. *J. Nucl. Med.* **2022**, *63*, 833–839. [[CrossRef](#)] [[PubMed](#)]
76. Yusufi, N.; Wurzer, A.; Herz, M.; D'Alessandria, C.; Feuerecker, B.; Weber, W.; Wester, H.J.; Nekolla, S.; Eiber, M. Comparative Preclinical Biodistribution, Dosimetry, and Endoradiotherapy in Metastatic Castration-Resistant Prostate Cancer Using  $^{19}\text{F}/^{177}\text{Lu}$ -rhPSMA-7.3 and  $^{177}\text{Lu}$ -PSMA I&T. *J. Nucl. Med.* **2021**, *62*, 1106–1111. [[CrossRef](#)]
77. Delker, A.; Fendler, W.P.; Kratochwil, C.; Brunegraf, A.; Gosewisch, A.; Gildehaus, F.J.; Tritschler, S.; Stief, C.G.; Kopka, K.; Haberkorn, U.; et al. Dosimetry for  $^{177}\text{Lu}$ -DKFZ-PSMA-617: A new radiopharmaceutical for the treatment of metastatic prostate cancer. *Eur. J. Nucl. Med. Mol. Imaging* **2016**, *43*, 42–51. [[CrossRef](#)]
78. Kabasakal, L.; Toklu, T.; Yeyin, N.; Demirci, E.; Abuqbeith, M.; Ocak, M.; Aygun, A.; Karayel, E.; Pehlivanoglu, H.; Alan Selcuk, N. Lu-177-PSMA-617 Prostate-Specific Membrane Antigen Inhibitor Therapy in Patients with Castration-Resistant Prostate Cancer: Stability, Bio-distribution and Dosimetry. *Mol. Imaging Radionucl. Ther.* **2017**, *26*, 62–68. [[CrossRef](#)]
79. Baum, R.P.; Kulkarni, H.R.; Schuchardt, C.; Singh, A.; Wirtz, M.; Wiessalla, S.; Schottelius, M.; Mueller, D.; Klette, I.; Wester, H.J.  $^{177}\text{Lu}$ -Labeled Prostate-Specific Membrane Antigen Radioligand Therapy of Metastatic Castration-Resistant Prostate Cancer: Safety and Efficacy. *J. Nucl. Med.* **2016**, *57*, 1006–1013. [[CrossRef](#)]
80. Weineisen, M.; Schottelius, M.; Simecek, J.; Baum, R.P.; Yildiz, A.; Beykan, S.; Kulkarni, H.R.; Lassmann, M.; Klette, I.; Eiber, M.; et al.  $^{68}\text{Ga}$ - and  $^{177}\text{Lu}$ -Labeled PSMA I&T: Optimization of a PSMA-Targeted Theranostic Concept and First Proof-of-Concept Human Studies. *J. Nucl. Med.* **2015**, *56*, 1169–1176. [[CrossRef](#)]

## Supplementary Material

# Albumin-Mediated Size Exclusion Chromatography: The Apparent Molecular Weight of PSMA Radioligands as Novel Parameter to Estimate Their Blood Clearance Kinetics

Jan-Philip Kunert <sup>1,\*</sup>, Sebastian Fischer <sup>1</sup>, Alexander Wurzer <sup>1</sup> and Hans-Jürgen Wester <sup>1</sup>

<sup>1</sup> Technical University of Munich (TUM), Germany; TUM Department of Chemistry, Chair of Pharmaceutical Radiochemistry

\* Correspondence: jan-philip.kunert@tum.de; Tel.: +49.89.289.12203

### Calculation of corrected retention times and exemplary calculation of normalized apparent molecular weight ( $MW_{app, norm.}$ )

Throughout the development of the AMSEC method, three gel filtration columns of the same type (Superdex 75 Increase 10/300 GL gel filtration size exclusion column, fractionation range 70 – 3 kDa, GE Healthcare, Uppsala, Sweden) were used. The different columns gave slightly different retention times for the same probes, as exemplified by one of the calibration proteins, carbonic anhydrase (MW: 29 kDa), which showed retention times of 14.914 min, 14.352 min and 14.500 min, respectively. Calculations for the normalization of raw apparent molecular weights ( $MW_{app, raw}$ ) were performed with the input of absolute retention times. Data acquired on different columns were combined in normalization calculations. Therefore, experimentally determined retention times of chromatographic runs performed on column 2 (three AMSEC-runs of rhPSMA-7.3) and column 3 (one AMSEC-runs of rhPSMA-7.3 and blank-runs) had to be converted to equivalent retention times on column 1 by means of the calibration parameters of the three columns, as described in the following.

Due to the calibration of each column, the calculated MW of the same probe was assumed to be identical when determined on two columns (see Equation S1). Equating the calculation of the probe's MW on e.g. column 1 ( $C_1$ ; calibration parameters  $a_{C_1}$ ,  $b_{C_1}$  and  $V_{0,C_1}$ ) and column n (e.g. 2 and 3;  $C_n$ ; calibration parameters  $a_{C_n}$ ,  $b_{C_n}$  and  $V_{0,C_n}$ ), gives the following correlation (the formula for the calculation of MW is explained in the context of Table S3, see below):

$$MW = e^{\frac{0.8 \cdot t_{R,C_1} - V_{0,C_1} - b_{C_1}}{24 - V_{0,C_1} - a_{C_1}}} = e^{\frac{0.8 \cdot t_{R,C_n} - V_{0,C_n} - b_{C_n}}{24 - V_{0,C_n} - a_{C_n}}} \quad (S1)$$

The transformation of Equation S1 gives the retention time of column 1 ( $t_{R,C_1}$ ) as follows

$$t_{R,C_1} = 1.25 \cdot \left\{ \left[ \left( \frac{a_{C_1}}{a_{C_2}} \cdot \left( \frac{0.8 \cdot t_{R,C_2} - V_{0,C_2} - b_{C_2}}{24 - V_{0,C_2}} \right) + b_{C_1} \right) \cdot (24 - V_{0,C_1}) + V_{0,C_1} \right] \right\} \quad (S2)$$

Thus for a probe analyzed on column 2, an equivalent retention time on column 1 ( $t_{R,C_1}$ ) can be calculated with Equation S2 using no other input than the experimentally determined retention time on column 2 ( $t_{R,C_2}$ ) and the calibration parameters  $a$ ,  $b$  and  $V_0$  of both columns.

Experimentally detected retention times as well as retention times obtained from stepwise corrections for all the compounds are summarized in Table S1.

As an example, the calculation of the  $MW_{app, norm.}$  of rhPSMA-7.1 was carried out as follows:

$$MW_{app} = e^{\frac{0.8 \cdot t_{R, norm.} - V_{0,C1} - b_{C1}}{24 - V_{0,C1} - a_{C1}}} = e^{\frac{0.8 \cdot 16.824 - 8.02880 - 2.09685}{24 - 8.02880 - 0.18028}} = 17067 [Da] \quad (S3)$$

**Table S1.** Experimental retention times of AMSEC-runs ( $t_{R,AMSEC}$  raw) and blank-runs ( $t_{R,blank}$  raw) as well as corrected retention times converted to column 1 ( $t_{R,AMSEC}$  C1 and  $t_{R,blank}$  C1) of HSA, acetone and all radioligands. Retention times of radiosignals are additionally corrected for the offset between UV-vis-detector and radio-detector ( $t_{R,AMSEC}$  C1 + OC and  $t_{R,blank}$  C1 + OC). C1: column 1; OC: offset-corrected; n.a.: not applicable.

compound	column AMSEC	$t_{R,AMSEC}$ (min)			column blank	$t_{R,blank}$ (min)		
		raw	C1	C1 + OC <sup>1</sup>		raw	C1	C1 + OC
HSA	-	-	-	-	1	11.791	11.791	n.a.
acetone	-	-	-	-	3	24.596	24.809	n.a.
rhPSMA-7.1	1	15.324	15.324	15.240	3	20.509	20.795	20.711
rhPSMA-7.2	1	14.648	14.648	14.564	3	20.238	20.529	20.445
rhPSMA-7.3 <sup>2</sup>	1	14.806	14.806	14.722	3	20.391	20.679	20.595
rhPSMA-7.4	1	14.227	14.227	14.143	3	20.271	20.561	20.477
rhPSMA-10.1	1	15.494	15.494	15.410	3	21.025	21.302	21.218
rhPSMA-10.2	1	15.992	15.992	15.908	3	20.605	20.889	20.805
PSMA-617	1	17.670	17.670	17.586	3	22.100	22.357	22.273
PSMA-I&T	1	21.067	21.067	20.983	3	20.798	21.079	20.995
MC-1	1	13.483	13.483	13.399	3	22.183	22.439	22.355
MC-2	1	14.170	14.170	14.086	3	23.022	23.263	23.179
MC-3	1	14.402	14.402	14.318	3	22.335	22.588	22.504
MC-4	1	14.607	14.607	14.523	3	22.433	22.684	22.600
MC-5	1	14.343	14.343	14.259	3	21.363	21.634	21.550
MC-6	1	15.096	15.096	15.012	3	21.006	21.283	21.199
MC-7	1	15.682	15.682	15.598	3	20.956	21.234	21.150
MC-8	1	16.408	16.408	16.324	3	21.458	21.727	21.643
MC-9	1	17.332	17.332	17.248	3	21.068	21.344	21.260
MC-10	1	19.151	19.151	19.067	3	20.615	20.899	20.815

<sup>1</sup>  $t_{R,AMSEC}$  as given in Table 1 and Table S2. <sup>2</sup> Data presented for rhPSMA-7.3 are taken from an exemplary experiment.

**Table S2.** Retention times of model compounds (MC) 1 to 10 in AMSEC-runs ( $t_{R,AMSEC}$ ) and corresponding raw apparent molecular weights ( $MW_{app,raw}$ ).

radioligand	$t_{R,AMSEC}^1$ (min)	$MW_{app,raw}$ (kDa)
MC-1	13.399	44.2
MC-2	14.086	36.5
MC-3	14.318	34.2
MC-4	14.523	32.4
MC-5	14.259	34.8
MC-6	15.012	28.2
MC-7	15.598	24.0
MC-8	16.324	19.6
MC-9	17.248	15.2
MC-10	19.067	9.2

<sup>1</sup> retention times are already corrected for the offset between UV-vis- and radio-detector and normalized to column 1 as described above.

**Table S3.** Retention times of Blue Dextran 2000 (BD) and the calibration proteins conalbumin (CO, 75 kDa), ovalbumin (OV, 44 kDa), carbonic anhydrase (CA, 29 kDa), ribonuclease (RN, 13.7 kDa) and aprotinin (AP, 6.5 kDa) on superdex 75 increase columns 1, 2, and 3 (PBS pH 7.4 as mobile phase). *a* and *b*: calibration parameters; Cn: column n;  $V_e$ : elution volume;  $V_0$ : column void volume;  $R^2$ : coefficient of determination of column calibration.

parameter	column 1	column 2	column 3
$t_R$ (BD) (min)	10.036	9.657	9.676
$t_R$ (CO) (min)	11.861	11.337	11.431
$t_R$ (OV) (min)	13.036	12.491	12.607
$t_R$ (CA) (min)	14.914	14.352	14.500
$t_R$ (RN) (min)	17.399	16.891	17.031
$t_R$ (AP) (min)	20.533	20.091	20.264
$V_{0,Cn}$ (mL)	8.0288	7.7256	7.7408
$V_e$ (CO) (mL)	9.4888	9.0696	9.1448
$V_e$ (OV) (mL)	10.4288	9.9928	10.0856
$V_e$ (CA) (mL)	11.9312	11.4816	11.6000
$V_e$ (RN) (mL)	13.9192	13.5128	13.6248
$V_e$ (AP) (mL)	16.4264	16.0728	16.2112
$a_{Cn}$	-0.18028	-0.17873	-0.18032
$b_{Cn}$	2.09685	2.06926	2.09130
$R^2_{Cn}$ (%)	99.2	99.1	99.1

Calibration parameters were determined as recommended by the manufacturer of Gel Filtration LMW Calibration Kits (GE Healthcare, Buckinghamshire, United Kingdom). In brief, the partition coefficient  $K_{av}$  was defined as:

$$K_{av} = \frac{V_e - V_0}{V_c - V_0} \quad (S4)$$

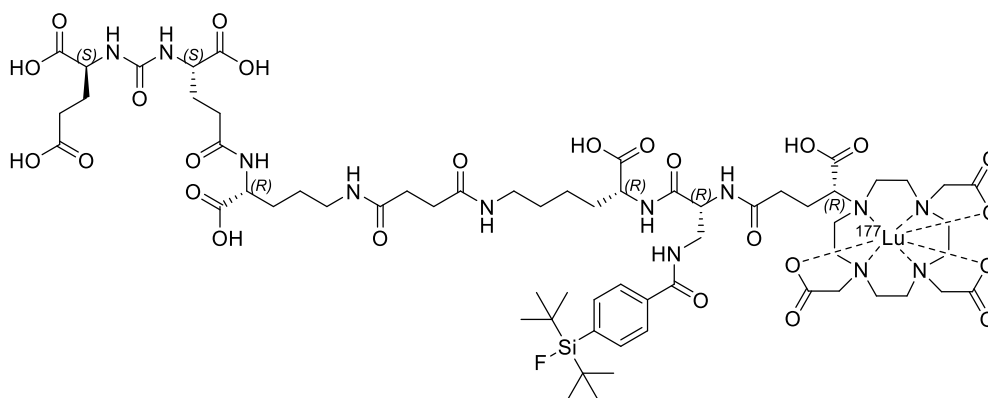
where  $V_e$  is the elution volume,  $V_0$  is the column void volume, and  $V_c$  is the geometric column volume of 24 mL.  $K_{av}$  is semi-logarithmically plotted against MW, and the resulting linear calibration curve gives the calibration parameters *a* and *b* according to the following equation:

$$K_{av} = a \cdot \ln(MW) + b . \quad (S5)$$

According to Equation S5, MW can be calculated from  $K_{av}$  and the calibration parameters  $a$  and  $b$  (Equation S6).  $K_{av}$  can be described according to Equation S4 wherein  $V_e$  is defined as the product of solvent flow (0.8 mL/min) with the retention time  $t_R$  resulting in Equation S6:

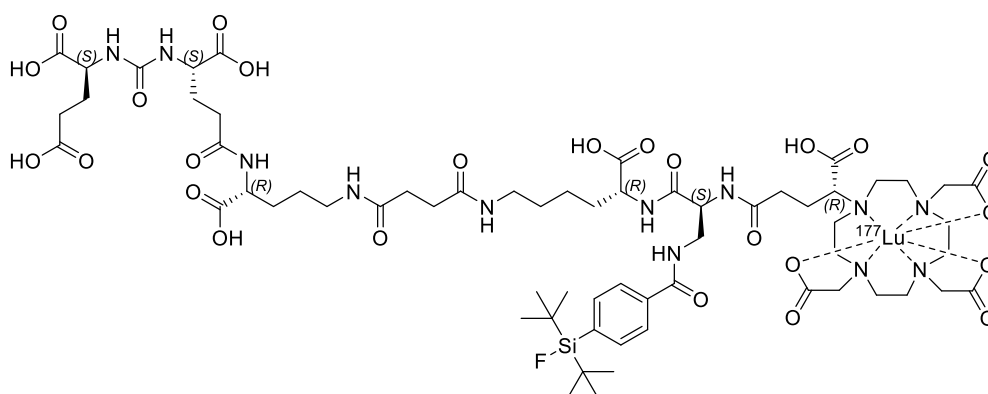
$$MW = e^{\frac{K_{av}-b}{a}} = e^{\frac{\frac{V_e-V_0}{V_c-V_0}-b}{a}} = e^{\frac{0.8 \cdot t_R - V_0 - b}{24 - V_0 - a}} . \quad (S6)$$

### Chemical structures of $^{177}\text{Lu}$ -labeled rhPSMA compounds and $^{177}\text{Lu}$ -labeled references PSMA-617 and PSMA-I&T



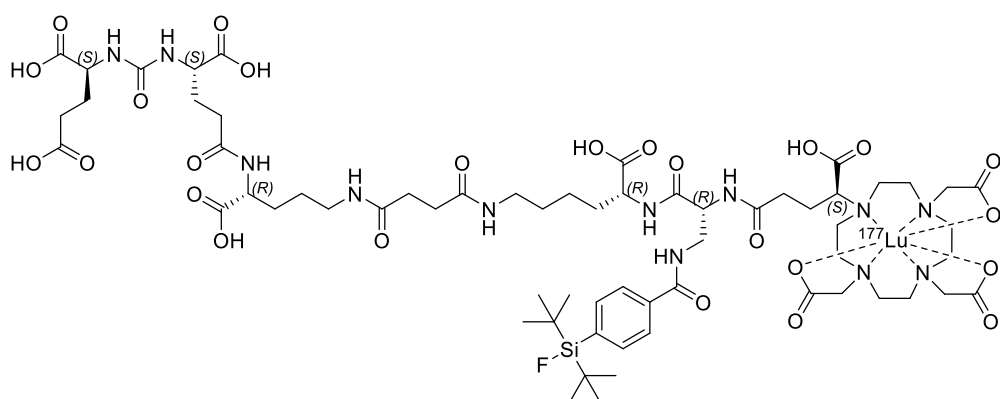
Chemical Formula:  $\text{C}_{63}\text{H}_{96}\text{F}^{177}\text{LuN}_{12}\text{O}_{25}\text{Si}$   
Molecular Weight: 1645,55

**Figure S1:** Chemical structure of  $^{177}\text{Lu}$ -labeled rhPSMA-7.1 ((*R*)-configured diaminopropionic acid branching unit and (*R*)-configured DOTAGA chelator).



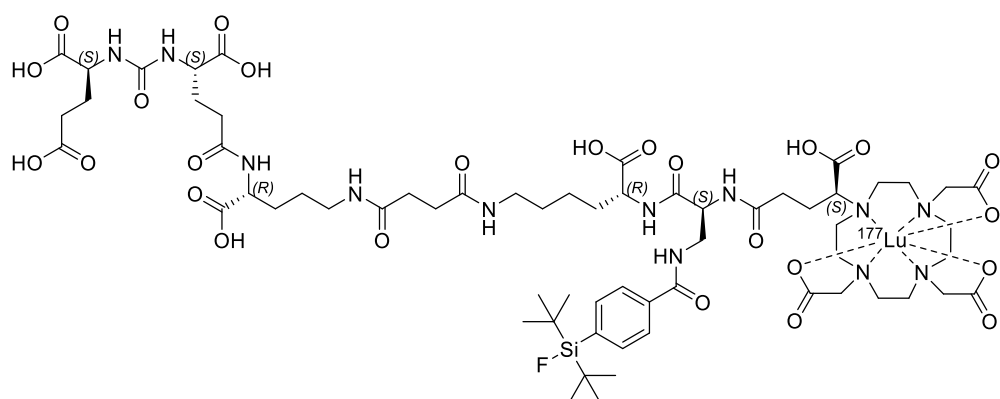
Chemical Formula:  $\text{C}_{63}\text{H}_{96}\text{F}^{177}\text{LuN}_{12}\text{O}_{25}\text{Si}$   
Molecular Weight: 1645,55

**Figure S2:** Chemical structure of  $^{177}\text{Lu}$ -labeled rhPSMA-7.2 ((*S*)-configured diaminopropionic acid branching unit and (*R*)-configured DOTAGA chelator).



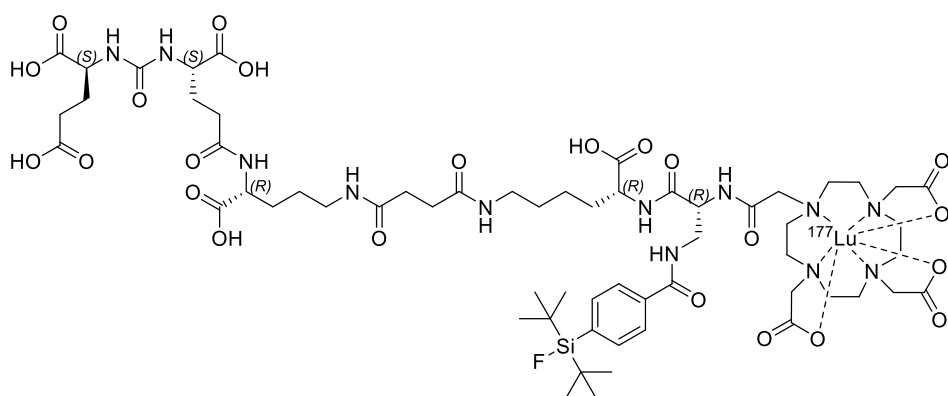
Chemical Formula:  $C_{63}H_{96}F^{177}LuN_{12}O_{25}Si$   
Molecular Weight: 1645,55

**Figure S3:** Chemical structure of  $^{177}Lu$ -labeled rhPSMA-7.3 ((*R*)-configured diaminopropionic acid branching unit and (*S*)-configured DOTAGA chelator).



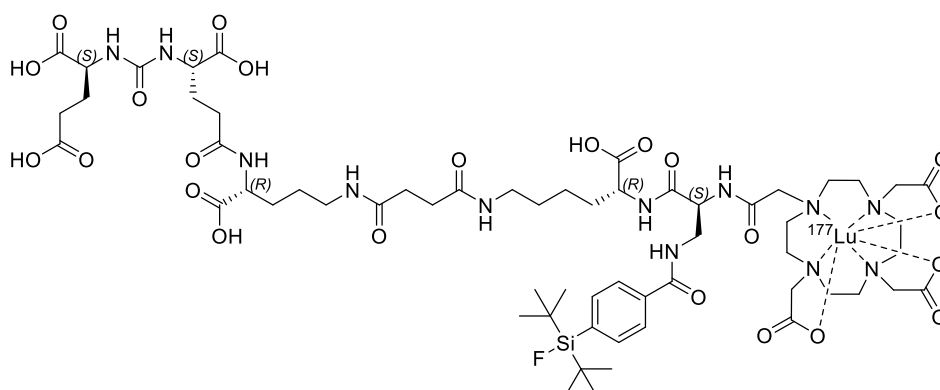
Chemical Formula:  $C_{63}H_{96}F^{177}LuN_{12}O_{25}Si$   
Molecular Weight: 1645,55

**Figure S4:** Chemical structure of  $^{177}Lu$ -labeled rhPSMA-7.4 ((*S*)-configured diaminopropionic acid branching unit and (*S*)-configured DOTAGA chelator).



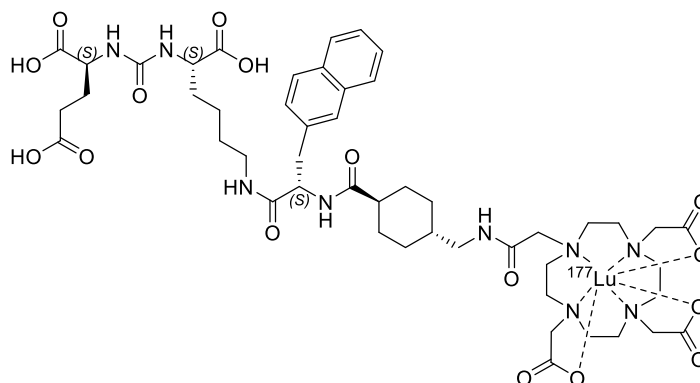
Chemical Formula:  $C_{60}H_{92}F^{177}LuN_{12}O_{23}Si$   
Molecular Weight: 1573,48

**Figure S5:** Chemical structure of  $^{177}\text{Lu}$ -labeled rhPSMA-10.1 ((*R*)-configured diaminopropionic acid branching unit and DOTA chelator).



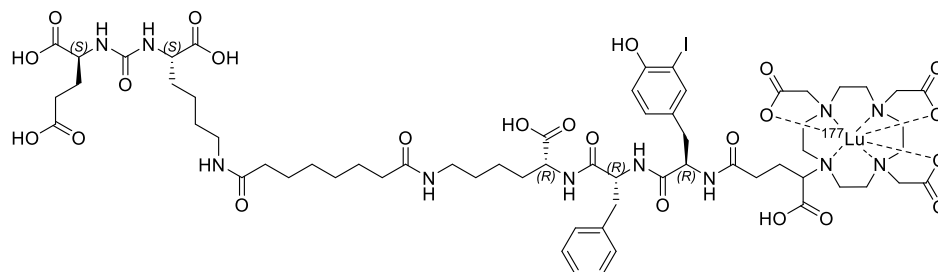
Chemical Formula:  $\text{C}_{60}\text{H}_{92}\text{F}^{177}\text{LuN}_{12}\text{O}_{23}\text{Si}$   
Molecular Weight: 1573,48

**Figure S6:** Chemical structure of  $^{177}\text{Lu}$ -labeled rhPSMA-10.2 ((*S*)-configured diaminopropionic acid branching unit and DOTA chelator).



Chemical Formula:  $\text{C}_{49}\text{H}_{68}^{177}\text{LuN}_9\text{O}_{16}$   
Molecular Weight: 1216,07

**Figure S7:** Chemical structure of  $^{177}\text{Lu}$ -labeled PSMA-617.



Chemical Formula:  $\text{C}_{63}\text{H}_{89}^{177}\text{LuN}_{11}\text{O}_{23}$   
Molecular Weight: 1672,31

**Figure S8:** Chemical structure of  $^{177}\text{Lu}$ -labeled PSMA-I&T.

Chemical structures of MC1-10 have not yet been disclosed.

**6.2.3. EJNMMI Research – Synthesis and Preclinical Evaluation of Novel <sup>99m</sup>Tc-labeled PSMA Ligands for Radioguided Surgery of Prostate Cancer**

The peer-reviewed article “*Synthesis and Preclinical Evaluation of Novel <sup>99m</sup>Tc-labeled PSMA Ligands for Radioguided Surgery of Prostate Cancer*” is licensed under a Creative Commons Attribution 4.0 International License, which permits use, sharing, adaptation, distribution and reproduction in any medium or format, as long as you give appropriate credit to the original author(s) and the source, provide a link to the Creative Commons license, and indicate if changes were made. The images or other third party material in this article are included in the article's Creative Commons license, unless indicated otherwise in a credit line to the material. If material is not included in the article's Creative Commons license and your intended use is not permitted by statutory regulation or exceeds the permitted use, you will need to obtain permission directly from the copyright holder.

To view a copy of this license, visit <http://creativecommons.org/licenses/by/4.0/>.

Please turn to the next page for the reprint of the original publication and the supplementary material.

ORIGINAL RESEARCH

Open Access



# Synthesis and preclinical evaluation of novel $^{99m}\text{Tc}$ -labeled PSMA ligands for radioguided surgery of prostate cancer

Jan-Philip Kunert<sup>\*</sup>, Max Müller, Thomas Günther, León Stopper, Nicole Urtz-Urban, Roswitha Beck and Hans-Jürgen Wester

## Abstract

**Background:** Radioguided surgery (RGS) has recently emerged as a valuable new tool in the management of recurrent prostate cancer (PCa). After preoperative injection of a  $^{99m}\text{Tc}$ -labeled prostate-specific membrane antigen (PSMA) inhibitor, radioguided intraoperative identification and resection of lesions is facilitated by means of suitable  $\gamma$ -probes. First clinical experiences show the feasibility of RGS and suggest superiority over conventional lymph node dissection in recurrent PCa. However, commonly used [ $^{99m}\text{Tc}$ ]Tc-PSMA-I&S exhibits slow whole-body clearance, thus hampering optimal tumor-to-background ratios (TBR) during surgery. We therefore aimed to develop novel  $^{99m}\text{Tc}$ -labeled, PSMA-targeted radioligands with optimized pharmacokinetic profile to increase TBR at the time of surgery.

**Methods:** Three  $^{99m}\text{Tc}$ -labeled N4-PSMA ligands were preclinically evaluated and compared to [ $^{99m}\text{Tc}$ ]Tc-PSMA-I&S. PSMA affinity ( $\text{IC}_{50}$ ) and internalization were determined on LNCaP cells. Lipophilicity was assessed by means of the distribution coefficient  $\log D_{7.4}$  and an ultrafiltration method was used to determine binding to human plasma proteins. Biodistribution studies and static  $\mu\text{SPECT/CT}$ -imaging were performed at 6 h p.i. on LNCaP tumor-bearing CB17-SCID mice.

**Results:** The novel N4-PSMA tracers were readily labeled with [ $^{99m}\text{Tc}$ ]TcO<sub>4</sub><sup>-</sup> with RCP > 95%. Comparable and high PSMA affinity was observed for all [ $^{99m}\text{Tc}$ ]Tc-N4-PSMA-ligands. The ligands showed variable binding to human plasma and medium to low lipophilicity ( $\log D_{7.4}$  – 2.6 to – 3.4), both consistently decreased compared to [ $^{99m}\text{Tc}$ ]Tc-PSMA-I&S. Biodistribution studies revealed comparable tumor uptake among all [ $^{99m}\text{Tc}$ ]Tc-N4-PSMA-ligands and [ $^{99m}\text{Tc}$ ]Tc-PSMA-I&S, while clearance from most organs was superior for the novel tracers. Accordingly, increased TBR were achieved. [ $^{99m}\text{Tc}$ ]Tc-N4-PSMA-12 showed higher TBR than [ $^{99m}\text{Tc}$ ]Tc-PSMA-I&S for blood and all evaluated tissue. In addition, a procedure suitable for routine clinical production of [ $^{99m}\text{Tc}$ ]Tc-N4-PSMA-12 was established. Labeling with  $553 \pm 187$  MBq was achieved with RCP of  $98.5 \pm 0.6\%$  ( $n = 10$ ).

**Conclusion:** High tumor accumulation and favorable clearance from blood and non-target tissue make [ $^{99m}\text{Tc}$ ]Tc-N4-PSMA-12 an attractive tracer for RGS, possibly superior to currently established [ $^{99m}\text{Tc}$ ]Tc-PSMA-I&S. Its GMP-production according to a method presented here and first clinical investigations with this novel radioligand is highly recommended.

**Keywords:** Technetium-99m, PSMA, Radioguided surgery, Prostate cancer

## Introduction

Throughout the last decade, radiopharmaceuticals targeting prostate-specific membrane antigen (PSMA) have become an integral part in clinical management

\*Correspondence: jan-philip.kunert@tum.de

Chair of Pharmaceutical Radiochemistry, Department of Chemistry, Technical University of Munich (TUM), Walther-Meißner-Str 3, 85748 Garching, Germany

of prostate cancer (PCa) [1, 2]. Almost in parallel with the clinical success of diagnostic tracers such as [ $^{68}\text{Ga}$ ]Ga-PSMA-11 [3] and [ $^{18}\text{F}$ ]DCFPyL [4] for positron emission tomography (PET) or [ $^{99\text{m}}\text{Tc}$ ]Tc-MIP-1404 [5] for single-photon emission computed tomography (SPECT) imaging, several therapeutic compounds entered the stage, among them  $^{177}\text{Lu}$ -labeled PSMA-I&T and PSMA-617 [6, 7]. In addition, several distinct therapeutic approaches have found their way into preclinical and clinical research, among them long-acting albumin-binding PSMA-ligands [8, 9], targeted alpha therapy [10] or so-called tandem therapy combining [ $^{225}\text{Ac}$ ]Ac- and [ $^{177}\text{Lu}$ ]Lu-PSMA-617 [11]. The recent approval of [ $^{177}\text{Lu}$ ]Lu-PSMA-617 (Pluvicto<sup>TM</sup>, Novartis) for RLT of metastatic castration-resistant PCa (mCRPC) represents a milestone for nuclear medicine, broadens the armamentarium of oncologists, and might pave the way for further approved targeted therapeutic radiopharmaceuticals.

Radioguided surgery (RGS) is another therapeutic intervention successfully harnessing the potential of radioactive PSMA-targeted probes [12]. Patients with early biochemical recurrence after radical prostatectomy that show only regional pelvic lymph node metastases (LNM) in PSMA-PET imaging can benefit from radioguided salvage lymph node dissection (sLND) to delay disease progression and future systemic treatment [13]. In contrast to conventional sLND, a  $\gamma$ -emitting PSMA-targeted radioligand is intravenously injected up to 24 h prior to surgery. With the help of a  $\gamma$ -probe, localization and resection of metastatic lymph nodes are facilitated during surgery, which is especially useful in the case of small or atypically localized lesions. Furthermore, resected tissue can be identified instantly by ex vivo  $\gamma$ -probe measurements to confirm the successful removal of tumor-infested tissue. After initial proof-of-concept with [ $^{111}\text{In}$ ]In-PSMA-I&T [14], PSMA-RGS has been carried out with [ $^{99\text{m}}\text{Tc}$ ]Tc-PSMA-I&S [15], owing to its similar performance in vivo and more favorable radiation properties, the more common allowance to work with  $^{99\text{m}}\text{Tc}$ -tracers in surgery rooms, lower costs and higher availability of [ $^{99\text{m}}\text{Tc}$ ]TcO<sub>4</sub><sup>-</sup> compared to [ $^{111}\text{In}$ ]InCl<sub>3</sub>. A recent study with 121 patients by Horn et al. described the successful removal of preoperatively identified lesions in 99% of patients and a complete biochemical response in 66% of patients [16], which confirms results reported earlier by Maurer et al. for a smaller group of patients [13]. In the latter study, even additional lesions not previously detected on PSMA-PET could be removed, which highlights the potential of RGS for sLND [13]. However, prospective clinical trials such as the TRACE study (NCT03857113) are required to accurately assess the

long-term outcome and added benefit of RGS for PCa patients.

Whether conventional or radioguided, the main limitation of sLND procedures is constituted in the incomplete resection of metastatic lesions. Even though state-of-the-art PSMA radio-guidance using [ $^{99\text{m}}\text{Tc}$ ]Tc-PSMA-I&S showed superior short-term efficacy in terms of biochemical response in a prospective study by Knipper et al. [17], the still insufficient sensitivity with regard to micro-metastatic lesions seems to be a major reason for recurrent disease [13, 18]. Technological developments like robot-assisted laparoscopic surgery implying drop-in or click-on  $\gamma$ -probes [19] and more differentiated criteria for patient selection [20] can certainly move the application forward. However, on a radiopharmaceutical level we identified a pending need of improvement, namely a radiotracer providing higher contrast and lower background signal than currently applied [ $^{99\text{m}}\text{Tc}$ ]Tc-PSMA-I&S. Its comparably slow whole-body clearance and partial hepatobiliary excretion is caused by high plasma protein binding (PPB) of 94% and reduced hydrophilicity compared to DOTA-based PSMA-radiochelated tracers [15]. As a result, unspecific background signal hampers both contrast in early SPECT-imaging and accurate detection during surgery [21, 22]. Thus, often [ $^{99\text{m}}\text{Tc}$ ]Tc-PSMA-I&S is not used to reliably identify LNMs in situ during surgery, but rather to confirm PSMA-positivity of resected tissue ex vivo. However, technically a more accurate lesion detection even in the surgical field should be feasible if TBR are sufficiently high, and thus, even smaller lesions might become detectable with an appropriately performing radiotracer. In spite of the known limitations of [ $^{99\text{m}}\text{Tc}$ ]Tc-PSMA-I&S, to our knowledge, no dedicated optimization of a  $^{99\text{m}}\text{Tc}$ -labeled PSMA-ligand intended for RGS application has been performed so far.

To address this medical need, we developed a novel series of  $^{99\text{m}}\text{Tc}$ -labeled PSMA-targeted radioligands for RGS aiming for an improved pharmacokinetic behavior. The optimized ligand structure was conceptually designed and comprises a common PSMA-inhibitor motif derived from highly potent radiohybrid PSMA diagnostics [23] and therapeutics [24], a tetraamine (N4) chelator for reliable complexation of technetium-99m, and a variable amino acid for the modulation of pharmacokinetic properties of the peptide (Fig. 1). Such rational and iterative modifications constitute the core of radiopharmaceutical structure development and a multitude of studies have brought forth interesting PSMA radioligands for manifold applications using that approach [25–27]. As we aimed for differential (and primarily reduced) lipophilicity and plasma protein binding of the novel ligands, D-glutamate (D-Glu;

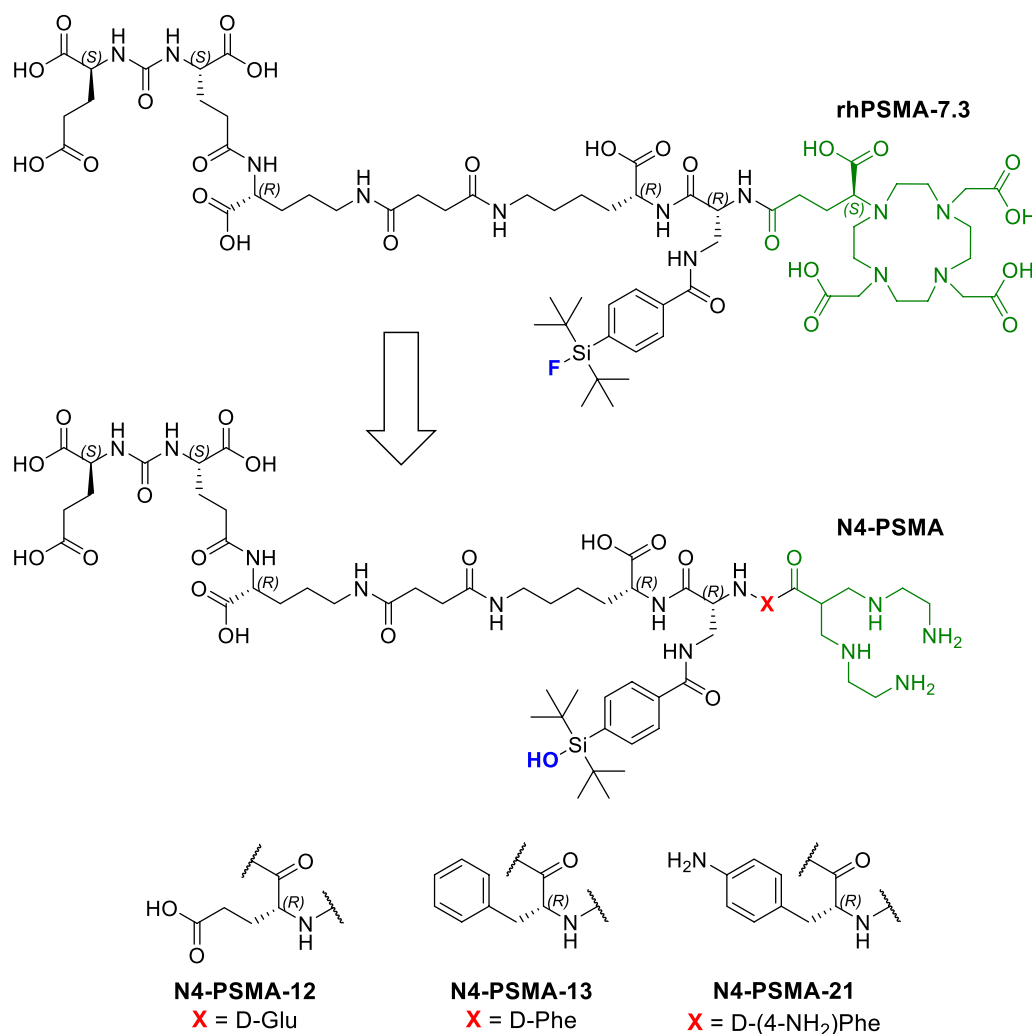


**Fig. 1** Molecular structures of the novel N4-PSMA ligands were derived from rhPSMA-7.3 by substitution of (S)-DOTAGA with a tetraamine (N4) chelator for complexation of technetium-99m (indicated in green) and incorporation of a less lipophilic, hydrolyzed derivative of the silicon fluoride acceptor-moiety (indicated in blue). A variable amino acid (X, red) is introduced in N4-PSMA-12, N4-PSMA-13 and N4-PSMA-21 to modulate their pharmacokinetic properties

negatively charged), D-phenylalanine (D-Phe; aromatic, uncharged), and 4-amino-D-phenylalanine (D-(4-NH<sub>2</sub>)Phe; aromatic, positively charged) were used as variable amino acids to introduce different charges and optional aromatic moieties.

In this study, we report the comparative preclinical evaluation of three <sup>99m</sup>Tc-labeled N4-PSMA ligands in vitro and in vivo. All experiments were performed in comparison with [<sup>99m</sup>Tc]Tc-PSMA-I&S, the current clinical standard for PSMA-targeted RGS. In preparation of first clinical studies, we furthermore established a labeling procedure of the most promising

derivative at patient scale that should be suited for routine clinical radioligand production.

## Materials and methods

Further general information and a detailed description of ligand synthesis are provided in Additional file 1.

## Radiolabeling

<sup>99m</sup>Tc-Labeling of N4-PSMA ligands was carried out by addition of 1 nmol peptide precursor (0.5 mM in DMSO) to a mixture of 0.05 M Na<sub>2</sub>HPO<sub>4</sub> (12.5 μL, in Tracepur<sup>®</sup>-water, pH 9.25) and 0.1 M disodium citrate sesquihydrate (1.5 μL, in Tracepur<sup>®</sup>-water) in saline. After addition of

a freshly prepared solution of  $\text{SnCl}_2$  (2.5  $\mu\text{L}$ , 1 mg/mL in ethanol),  $^{99\text{m}}\text{Tc}[\text{TcO}_4^-]$  (40 MBq/nmol) in saline was added and the labeling solution (final volume 250  $\mu\text{L}$ ) was heated to 95 °C for 15 min. Subsequently, 10  $\mu\text{L}$  of 1 M sodium ascorbate (in PBS) was added and quality control was performed using radio-TLC and radio-RP-HPLC (UV-detection at 220 nm). A slightly modified protocol for radiolabeling at patient scale and labeling of PSMA-I&S are described in Additional file 1.

#### Lipophilicity and binding to human plasma

The lipophilicity of  $^{99\text{m}}\text{Tc}$ -labeled PSMA ligands, expressed as distribution coefficient ( $\log D_{7.4}$ ), was determined using the shake-flask method. A solution of approximately 1 MBq of radioligand in 1 mL of a 1:1 mixture of PBS (pH=7.4) and *n*-octanol ( $n=8$ ) was vortexed vigorously for 3 min. After centrifugation at 9000 rpm for 5 min aliquots of both phases (200  $\mu\text{L}$  *n*-octanol, 50  $\mu\text{L}$  PBS) were collected and the activity was quantified in a  $\gamma$ -counter.  $\log D_{7.4}$  values were calculated as decadic logarithm of the activity concentration ratio between the *n*-octanol phase and the aqueous phase. Data are given as mean  $\pm$  standard deviation (SD).

Binding to human plasma was determined by incubation of radioligands in human plasma (2 nM concentration, 37 °C for 30 min) and subsequent ultrafiltration (250  $\mu\text{L}$  aliquots, 3200 rpm, 40 min) in Centrifree® ultrafiltration devices (Merck Millipore, Cork, Ireland). The fraction bound to human plasma proteins was calculated as the ratio of unfiltered activity and the total activity in the ultrafiltration device. Measurements were performed in three independent experiments, each with two replicates ( $n=6$ , data are given as mean  $\pm$  SD). All values were corrected for non-specific binding (control experiments in PBS).

#### Determinations of affinities ( $\text{IC}_{50}$ ) and internalization studies

Competitive binding studies were carried out in analogy to a previously reported procedure [28]. As a modification the non-radiolabeled standard competitor (((*S*)-1-carboxy-5-(4-(iodo)benzamido)pentyl) carbamoyl)-*L*-glutamic acid (IBA-KuE) was applied in increasing concentrations ( $10^{-5}$ – $10^{-11}$  M/well,  $n=3$  each) whereas the novel PSMA-binding compounds of interest were applied as  $^{99\text{m}}\text{Tc}$ -labeled radioligands (0.2 nM/well). In this inversed experimental approach, higher values correspond to higher affinities and are referred to as inverse  $\text{IC}_{50}$ . Poly-L-lysine coated 24-well plates were used ( $n=3$ ). Data are given as mean  $\pm$  SD. To determine the cellular uptake of the  $^{99\text{m}}\text{Tc}$ -labeled PSMA ligands into LNCaP cells by means of PSMA-mediated internalization at 1 h, a previously reported protocol was

applied with assay concentrations of 1.0 nM and 0.2 nM for  $^{99\text{m}}\text{Tc}$ -labeled PSMA ligands and the reference compound [ $^{125}\text{I}$ ]IBA-KuE, respectively [28]. Data are corrected for non-specific binding and normalized to the specific internalization of the reference. Results are given as mean  $\pm$  SD.

#### In vivo experiments

All animal experiments were conducted in accordance with general animal welfare regulations in Germany (German animal protection act, in the edition of the announcement, dated May 18th, 2006, as amended by Article 280 of June 19th 2020, approval no. ROB-55.2-1-2532.Vet\_02-18-109 by the General Administration of Upper Bavaria) and the institutional guidelines for the care and use of animals. Male CB17-SCID mice were purchased from Charles River (Sulzfeld, Germany) and arrived at the in-house animal facility to acclimate at least 1 week before the start of the experiment. Tumor xenografts were established by subcutaneous inoculation of LNCaP cells (approx.  $2 \times 10^7$  cells in 200  $\mu\text{L}$  of a 1:1 mixture of Cultrex BME (R&D Systems, Minneapolis, United States) and DMEM/Ham's F-12) onto the right shoulder of 6–8 weeks old male CB17-SCID mice. The animals were used for experiments when tumors had grown to a size of 5–10 mm in diameter. Criteria for the exclusion of animals from the experiment were weight loss higher than 20%, tumor size above 1.5  $\text{cm}^3$ , ulceration of the tumor, respiratory distress or change of behavior. These criteria did not apply to any mouse. Neither randomisation nor blinding was applied in the allocation of the experiments. Quarterly health monitoring was performed according to the FELASA recommendations.

#### Biodistribution studies

The  $^{99\text{m}}\text{Tc}$ -labeled radioligands ( $2.7 \pm 0.7$  MBq,  $82 \pm 20$  pmol) were injected into a lateral tail vein of LNCaP-tumor bearing mice ( $n=4-5$ ) under isoflurane anesthesia. Animals were sacrificed at 6 h post injection (p.i.) by carbon dioxide inhalation and blood withdrawal via cardiac puncture. Blood and tissues of interest were collected, weighed and the activity measured in a  $\gamma$ -counter. Radioligand uptake is given in percent of the injected dose per gram of tissue (% ID/g) and results are presented as mean  $\pm$  SD. Further details on the analysis of biodistribution data are provided in Additional file 1: Fig. S1.

#### $\mu\text{SPECT/CT}$ imaging

Static imaging of sacrificed animals was performed on a VECTOr4 small-animal SPECT/PET/CT/OI scanner from MILabs (Utrecht, Netherlands) directly after blood collection with an acquisition time of 45 min using an

HE-GP-RM collimator and a step-wise multiplanar bed movement via MILabs acquisition software (v11.00 and v12.26). Imaging data were reconstructed using MILabs-Reconstruction software (v12.00) and image analysis was performed with PMOD4.0 (PMOD technologies LLC, Zurich, Switzerland). Animals were subjected to biodistribution studies after imaging.

### Data analysis

Acquired data were statistically analyzed performing a one-way analysis of variances (ANOVA) followed by a Tukey's multiple comparison post-test using Origin-Pro software (version 9.7) from OriginLab Corporation (Northampton, United States). Pairwise statistical comparisons were performed applying the two-sample student's *t*-test in Microsoft Excel (Redmond, United States). Acquired *P* values of <0.05 were considered statistically significant.

## Results

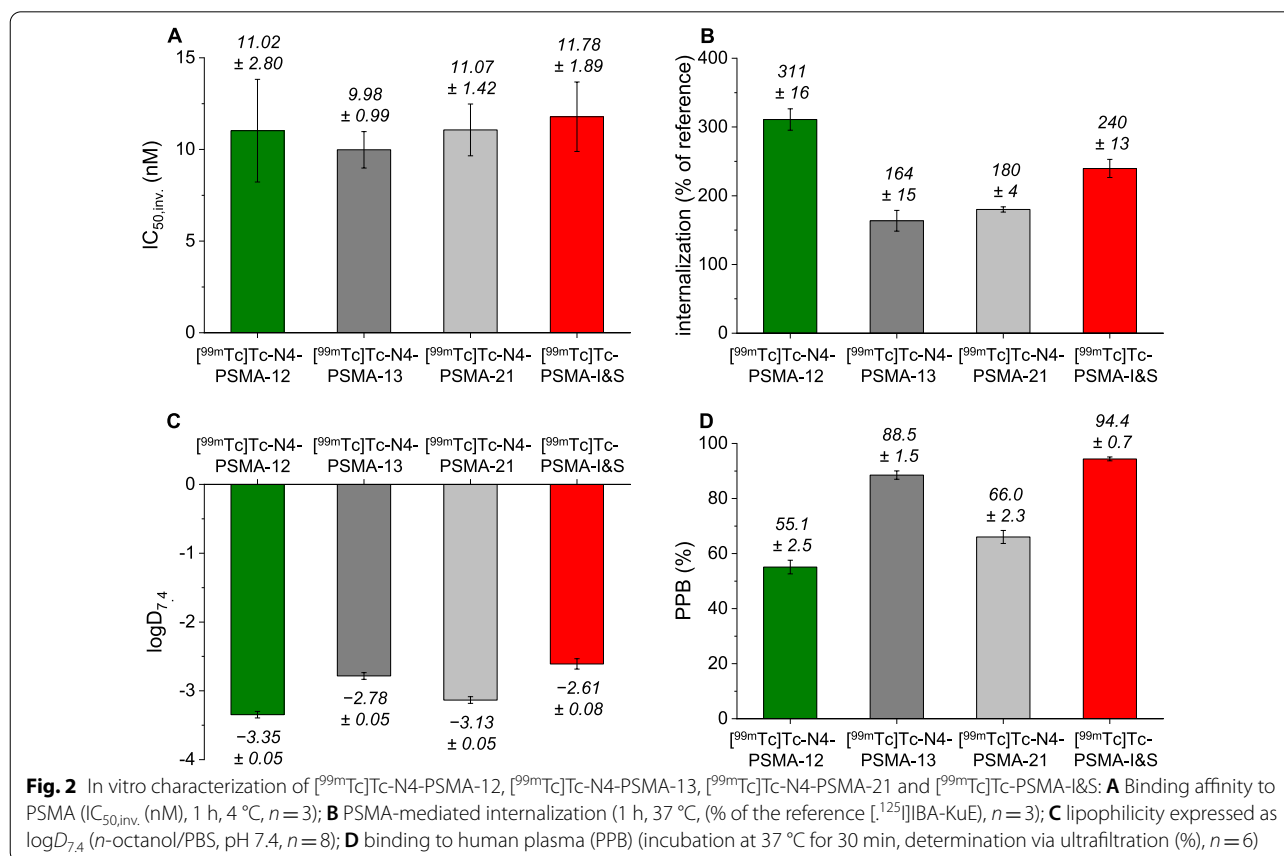
### Synthesis and radiolabeling

The novel PSMA ligands were synthesized using a mixed solution/solid phase synthetic approach and obtained with chemical purity of >98% in yields of 29%, 25% and

21%, respectively. Compound identity was confirmed by mass spectrometry. Radiolabeling with  $[^{99m}\text{Tc}]\text{TcO}_4^-$  resulted in radiochemical purities (RCP) of >95% as determined by radio-TLC and radio-*RP*-HPLC. Up-scaling of the reported labeling protocol for patient-scale production of  $[^{99m}\text{Tc}]\text{Tc-N4-PSMA-12}$  was found to be feasible, however proportionally reduced amounts of stannous chloride were applied to prevent the formation of colloidal technetium-species. Under consideration of requirements of a clinical workflow for routine radiosynthesis, labeling of N4-PSMA-12 (20  $\mu\text{g}$ , 15 nmol) with activities of 194–810 MBq ( $553 \pm 187$  MBq, mean  $\pm$  SD,  $n=10$ ) reproducibly yielded the desired radioligand with a RCP of  $98.5 \pm 0.6\%$  (range, 97.6–99.2%,  $n=10$ ). Detailed information on single radiolabelings is provided in Additional file 1: Table S1.

### In Vitro Characterization

Results of the in vitro characterization of  $[^{99m}\text{Tc}]\text{Tc}$ -labeled N4-PSMA ligands and the reference  $[^{99m}\text{Tc}]\text{Tc-PSMA-I\&S}$  are summarized in Fig. 2 and Additional file 1: Table S2. PSMA affinity was assessed via determination of the inverse  $\text{IC}_{50}$  ( $\text{IC}_{50,\text{inv}}$ ). Irrespective of the variable amino acid, all radioligands



showed high PSMA affinity displayed by low nanomolar  $IC_{50,inv}$  values (range, 10.0–11.8 nM) with no statistically significant difference ( $P > 0.66$ ). In contrast, PSMA mediated internalization, expressed as percentage of the reference compound [ $^{125}I$ ]IBA-KuE, was significantly influenced by the variable amino acid. [ $^{99m}Tc$ ]Tc-N4-PSMA-12 ( $311 \pm 16\%$ ) exhibited 1.3-fold higher internalization than [ $^{99m}Tc$ ]Tc-PSMA-I&S ( $240 \pm 13\%$ ), and an even 1.9- and 1.7-fold higher value than [ $^{99m}Tc$ ]Tc-N4-PSMA-13 ( $164 \pm 15\%$ ) and [ $^{99m}Tc$ ]Tc-N4-PSMA-21 ( $180 \pm 4\%$ ), respectively. In comparison with [ $^{99m}Tc$ ]Tc-PSMA-I&S, all novel [ $^{99m}Tc$ ]Tc-N4-PSMA compounds showed increased hydrophilicity, expressed by the distribution coefficient ( $\log D_{7.4}$ ). Within the group of N4-bearing radioligands, highest lipophilicity was observed for [ $^{99m}Tc$ ]Tc-N4-PSMA-13 ( $\log D_{7.4} = -2.78 \pm 0.05$ ), comprising an aromatic D-Phe residue, followed by [ $^{99m}Tc$ ]Tc-N4-PSMA-21 ( $\log D_{7.4} = -3.13 \pm 0.05$ , D-(4-NH<sub>2</sub>)-Phe) and [ $^{99m}Tc$ ]Tc-N4-PSMA-12 ( $\log D_{7.4} = -3.35 \pm 0.05$ , D-Glu). Compared to [ $^{99m}Tc$ ]Tc-PSMA-I&S, binding to human plasma was significantly reduced for all [ $^{99m}Tc$ ]Tc-N4-PSMA tracers (94.4% vs 55.1–88.5%), and followed the same trend as described for lipophilicity. Thus, the highest hydrophilicity ( $\log D_{7.4} = -3.35 \pm 0.05$ ) and lowest binding to human plasma proteins ( $55.1 \pm 2.5\%$ ) was both

found for [ $^{99m}Tc$ ]Tc-N4-PSMA-12 ( $P < 0.001$  for both parameters).

### In vivo characterization

#### Biodistribution studies

Comparative biodistribution studies in LNCaP tumor-bearing mice at 6 h p.i. were performed for all four radiotracers (Fig. 3, Additional file 1: Table S3).

Among the three N4-bearing radioligands, a similar distribution profile with high uptake in the tumor (11.0–13.0% ID/g), varying but moderate activity levels in the kidneys and efficient clearance from blood and background tissue was observed (see also  $\mu$ SPECT/CT-scans in Fig. 4). [ $^{99m}Tc$ ]Tc-N4-PSMA-12 showed slightly higher kidney retention ( $12.3 \pm 8.0\%$  ID/g) than [ $^{99m}Tc$ ]Tc-N4-PSMA-13 and [ $^{99m}Tc$ ]Tc-N4-PSMA-21 ( $6.6 \pm 4.8\%$  ID/g and  $4.6 \pm 1.4\%$  ID/g, respectively) which was, however, not statistically significant ( $P > 0.81$ ). In clear contrast to the N4-PSMA radioligands, very high activity retention in the kidney was found for [ $^{99m}Tc$ ]Tc-PSMA-I&S ( $191 \pm 26\%$  ID/g, >15-fold higher than that of [ $^{99m}Tc$ ]Tc-N4-PSMA-12). Significantly higher activity retention after injection of [ $^{99m}Tc$ ]Tc-PSMA-I&S at 6 h p.i. was also present in several other organs such as lungs, spleen, adrenals and parotid gland ( $P < 0.001$  each). The higher activity uptake of [ $^{99m}Tc$ ]Tc-PSMA-I&S in tumors, however, was less pronounced ( $15.6 \pm 2.8\%$  ID/g). The

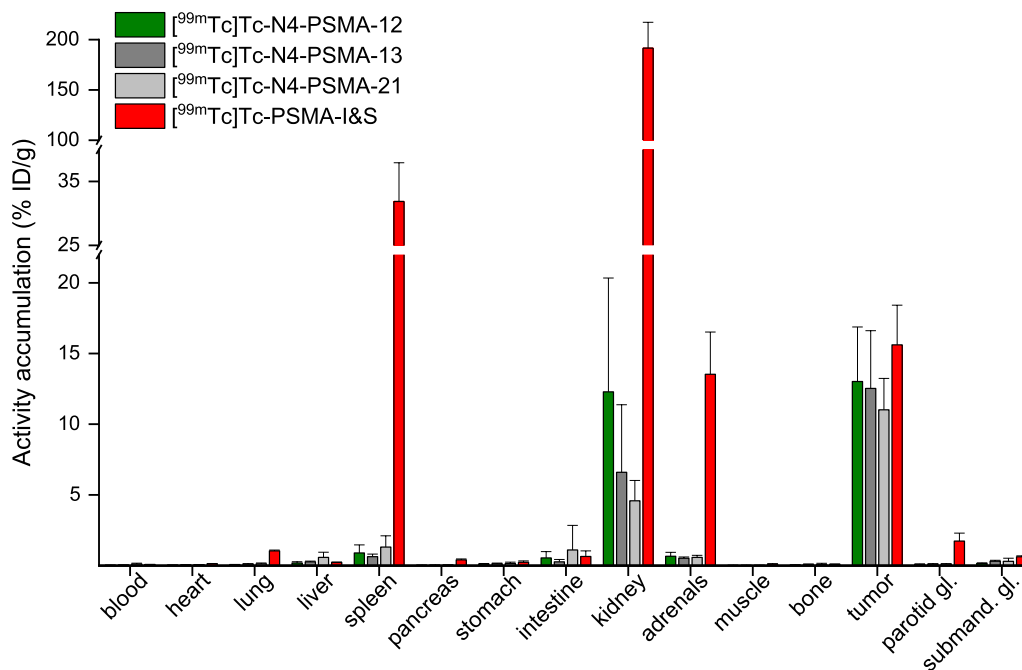


**Fig. 3** Ex vivo biodistribution data of  $^{99m}Tc$ -labeled N4-PSMA derivatives and [ $^{99m}Tc$ ]Tc-PSMA-I&S at 6 h p.i. in male LNCaP tumor-bearing CB17-SCID mice. Data are expressed as a percentage of the injected dose per gram (% ID/g), mean  $\pm$  standard deviation ( $n = 4-5$ ). gl.: gland; submand.: submandibular

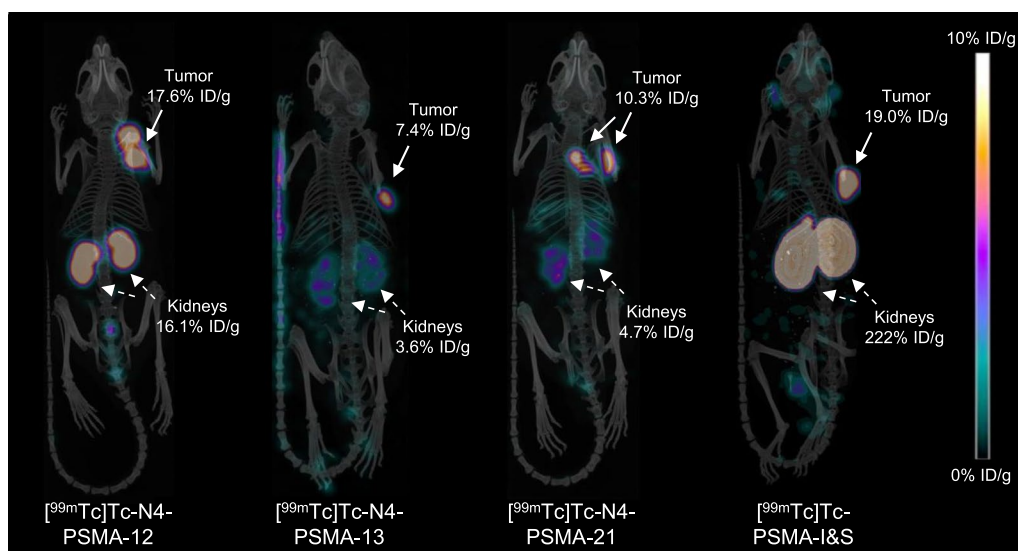


**Fig. 4** Static  $\mu$ SPECT/CT images (maximum intensity projections) of  $^{99m}\text{Tc}$ -labeled N4-PSMA-derivatives and [ $^{99m}\text{Tc}$ ]Tc-PSMA-I&S in LNCaP tumor-bearing mice. Animals were sacrificed at 6 h p.i. and imaged directly after blood collection for 45 min on a VECToR4 small-animal SPECT/PET/OI/CT. Tracer uptake in tumor and kidneys (in percent of the injected dose/gram, (% ID/g)) was determined from subsequent biodistribution studies

corresponding differences to the novel N4-PSMA radioligands were not statistically significant ( $P > 0.27$ ). Efficient activity clearance from the blood pool was observed for all radioligands. The lowest blood activity level at 6 h p.i. was found for [ $^{99m}\text{Tc}$ ]Tc-N4-PSMA-12 ( $0.0200 \pm 0.0044\%$  ID/g), which correlates with its low  $\log D_{7.4}$  and low PPB. Blood activity levels of [ $^{99m}\text{Tc}$ ]Tc-N4-PSMA-13, [ $^{99m}\text{Tc}$ ]Tc-N4-PSMA-21 and [ $^{99m}\text{Tc}$ ]Tc-PSMA-I&S were increased by 1.6-, 5.4- and 3.6-fold, respectively, as compared to [ $^{99m}\text{Tc}$ ]Tc-N4-PSMA-12.

#### Tumor-to-background ratios (TBR)

As depicted in Fig. 5, [ $^{99m}\text{Tc}$ ]Tc-N4-PSMA-12 showed the highest TBR among all radioligands throughout the majority of organs. It is noteworthy, that in direct comparison with [ $^{99m}\text{Tc}$ ]Tc-PSMA-I&S, [ $^{99m}\text{Tc}$ ]Tc-N4-PSMA-12 showed increased TBR for every analyzed organ and blood, thus demonstrating its notably superior clearance properties. In particular, a threefold T/blood-ratio ( $658 \pm 147$  vs  $219 \pm 62$ ) and an even 20-fold T/kidney-ratio ( $1.64 \pm 1.29$  vs  $0.08 \pm 0.01$ ) represent important advances towards optimized pharmacokinetics. Although less pronounced, improvements were also found for the TBR of [ $^{99m}\text{Tc}$ ]Tc-N4-PSMA-13 and [ $^{99m}\text{Tc}$ ]Tc-N4-PSMA-21. A tabular overview of TBR is provided in Additional file 1: Table S4.

#### Discussion

With the N4-PSMA ligand design we aimed to create a versatile structural platform that ensures high PSMA affinity and reliable complexation of technetium-99m while also allowing for flexible modifications to adjust the pharmacokinetic profile of the entire ligand. To reach this goal we followed our expertise acquired in the development of theranostic rhPSMA ligands, where the combination of an EuE binding motif and a SiFA-moiety addressing the remote arene binding site has led to a series of highly potent PSMA tracers for imaging and therapy [23, 24]. To retain high affinity, while ensuring low lipophilicity of the new tracers, a less lipophilic SiOH-moiety (formally a hydrolyzed SiFA) was preferred. For complexation of technetium-99m a tetraamine (N4) chelator was chosen, as this chelating system exhibits excellent in vivo stability and confers high hydrophilicity to peptidic radioligands [29, 30]. A further advantage over  $\text{N}_3\text{S}$ -based chelating systems such as mercaptoacetyltriserine is the absence of chemically reactive thiol-groups which might limit the shelf-life of radioligand precursors, an oftentimes neglected aspect in early radioligand development. Finally, the incorporation of a variable amino acid afforded three novel ligands with distinct properties in vitro and in vivo.

Slow whole-body clearance and in part hepatobiliary excretion of [ $^{99m}\text{Tc}$ ]Tc-PSMA-I&S is assumed to be caused by high PPB and increased lipophilicity compared to other PSMA-addressing radiometal chelates [15]. Therefore, a main focus in the design of the novel

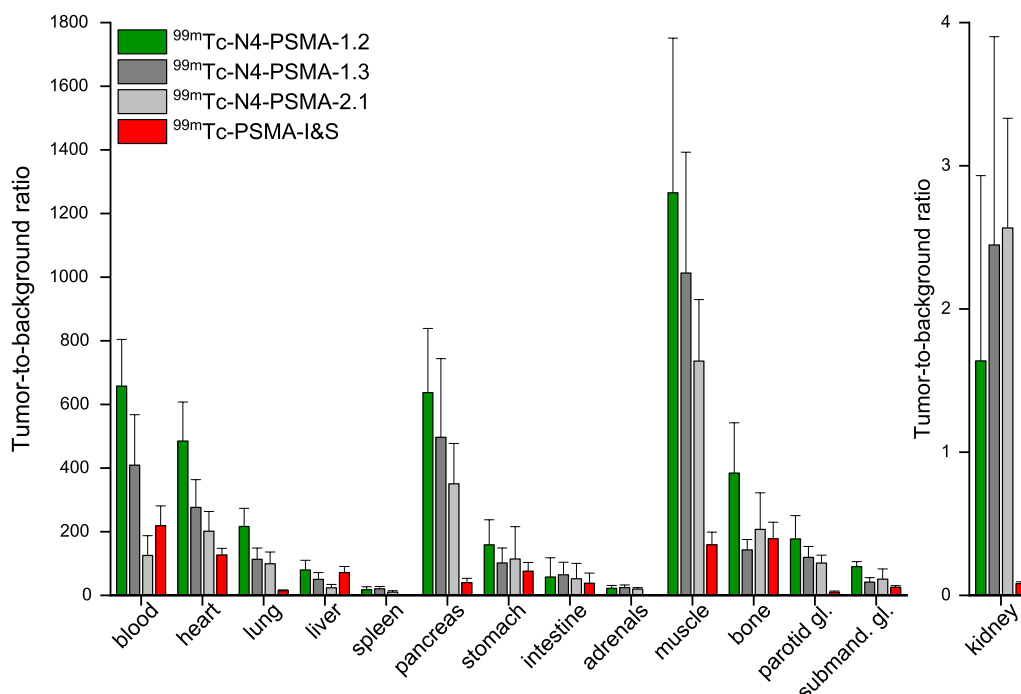


**Fig. 5** Tumor-to-background ratios (TBR) of  $^{99m}\text{Tc}$ -labeled N4-PSMA compounds and [ $^{99m}\text{Tc}$ ]Tc-PSMA-I&S at 6 h p.i. in male LNCaP tumor-bearing CB17-SCID mice. Data are given as mean  $\pm$  standard deviation ( $n=4-5$ ). Mean values were determined from TBR calculated for individual animals. gl.: gland; submand.: submandibular

ligands was set on reduced lipophilicity and PPB. Fortunately, these objectives were met by all three N4-PSMA compounds. As expected, the intrinsic lipophilicity of the variable amino acid ( $\log P$ : Phe > (4-NH<sub>2</sub>)-Phe > Glu) [31] translated into similar trends for lipophilicity and PPB of the corresponding radioligands ( $\log D_{7.4}$  and PPB: [ $^{99m}\text{Tc}$ ]Tc-PSMA-I&S > [ $^{99m}\text{Tc}$ ]Tc-N4-PSMA-13 > [ $^{99m}\text{Tc}$ ]Tc-N4-PSMA-21 > [ $^{99m}\text{Tc}$ ]Tc-N4-PSMA-12). Especially [ $^{99m}\text{Tc}$ ]Tc-N4-PSMA-12 combines a favorable lipophilicity, comparable to diagnostic rhPSMA compounds [23], and a PPB that is significantly lower than for [ $^{99m}\text{Tc}$ ]Tc-PSMA-I&S, [ $^{68}\text{Ga}$ ]Ga/[ $^{177}\text{Lu}$ ]Lu-PSMA-I&F [32] or [ $^{99m}\text{Tc}$ ]Tc-EuK-(SO<sub>3</sub>)Cy5-mas<sub>3</sub> [25] (all ligands developed for PSMA-guided surgery) and comparable to fast-clearing [ $^{177}\text{Lu}$ ]Lu-PSMA-617 [33]. In agreement with many prior studies [25–27], these findings underline how the pharmacokinetically relevant properties of a radioligand can be shaped in a rational fashion by thoughtful structural modifications.

Even though [ $^{99m}\text{Tc}$ ]Tc-PSMA-I&S showed favorable dosimetry in patients [21] and application in RGS suggests superiority over conventional salvage surgery [17], we have to admit that [ $^{99m}\text{Tc}$ ]Tc-PSMA-I&S is not yet the optimal radioligand for RGS. This is exemplified by a study among 31 patients by Maurer et al. who reported successful resection of all lesions detected on

prior PSMA-PET and even additional lesions as small as 3 mm [13]. However, the same study revealed that in 12 of 86 resected tissue specimens that were classified PSMA-negative according to  $\gamma$ -probe measurements, histochemical analysis discovered previously unidentified metastatic lesions.

The obvious need for higher sensitivity in RGS is, from a radiopharmaceutical perspective, a need for an optimized radioactive probe providing higher TBR during surgery. Thus, to assess TBR of our novel  $^{99m}\text{Tc}$ -labeled N4-PSMA ligands, biodistribution studies at 6 h p.i. were performed. This rather long distribution time comes with the limitation of scarce comparability with literature, where mostly time-points of 1 h or 4 h were investigated. However, RGS is performed around 20–24 h p.i. in patients [13, 19, 36] and, based on the rule of thumb of approximately fourfold faster metabolism in mice compared to men, we chose a distribution time of 6 h to simulate TBR at the time of surgery as accurately as possible. In that context, our preclinical findings on the in vivo performance of [ $^{99m}\text{Tc}$ ]Tc-N4-PSMA ligands represent a remarkable development. While similar high uptake in LNCaP-xenografts was observed at 6 h p.i., the clearance of the novel ligands from most background tissue was significantly improved compared to [ $^{99m}\text{Tc}$ ]Tc-PSMA-I&S. In addition, drastically and favorably reduced kidney

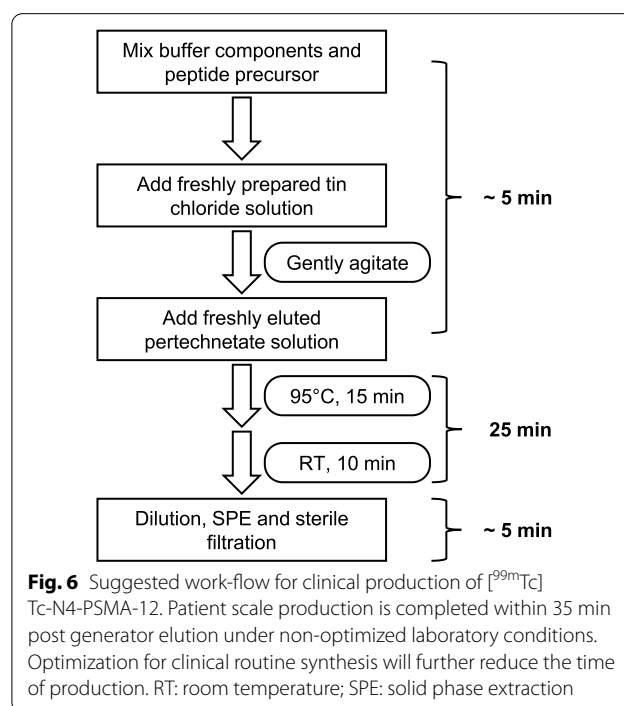
retention compared to [ $^{99m}\text{Tc}$ ]Tc-PSMA-I&S was found to be a common feature of the new ligands, which can probably be attributed to their shared molecular scaffold derived from rhPSMA-compounds [23, 24], while being pronounced by the use of the hydrolyzed SiFA moiety. This finding is of particular interest, as high renal activity accumulation may interfere with accurate lesion detection during RGS [36]. Nevertheless, clinical studies are necessary to validate whether our preclinical findings also apply to the human situation. To an even greater extend, incomplete clearance of [ $^{99m}\text{Tc}$ ]Tc-PSMA-I&S from the blood pool and thus a suboptimal T/blood-ratio can affect the accuracy of RGS [15]. In this regard, the 3.6-fold decreased blood activity at 6 h p.i. represents another distinct advantage of [ $^{99m}\text{Tc}$ ]Tc-N4-PSMA-12 and emphasizes the positive influence of the negatively charged amino acid D-Glu towards accelerated clearance kinetics. Compared to [ $^{99m}\text{Tc}$ ]Tc-N4-PSMA-12, slightly higher uptake in blood and several background organs such as heart, lung, liver, parotid gland and submandibular gland were observed for [ $^{99m}\text{Tc}$ ]Tc-N4-PSMA-13 and [ $^{99m}\text{Tc}$ ]Tc-N4-PSMA-21, which can be attributed to the incorporation of the aromatic amino acids D-Phe and D-(4-NH<sub>2</sub>)Phe conferring higher lipophilicity and plasma protein binding to these compounds. A further possible limitation of [ $^{99m}\text{Tc}$ ]Tc-PSMA-I&S is background activity in the bowel hampering the detection of lesions with low signal strength during surgery. In this regard, when completely ignoring the significantly improved T/kidney ratio of [ $^{99m}\text{Tc}$ ]Tc-N4-PSMA-12 and when taking into account only the hepatic and intestinal uptake of [ $^{99m}\text{Tc}$ ]Tc-PSMA-I&S and [ $^{99m}\text{Tc}$ ]Tc-N4-PSMA-12 (no statistically significant difference observed,  $P > 0.19$  and  $P > 0.36$ , respectively), we would expect at least similar performance of [ $^{99m}\text{Tc}$ ]Tc-PSMA-I&S and [ $^{99m}\text{Tc}$ ]Tc-N4-PSMA-12 in men. Beyond that, the finding that TBR of blood and all analyzed organs (see Fig. 5) obtained with [ $^{99m}\text{Tc}$ ]Tc-N4-PSMA-12 are higher than that of [ $^{99m}\text{Tc}$ ]Tc-PSMA-I&S clearly demonstrates the superior pharmacokinetic profile of that radioligand. Finally, as the only apparent advantage of [ $^{99m}\text{Tc}$ ]Tc-N4-PSMA-13 and [ $^{99m}\text{Tc}$ ]Tc-N4-PSMA-21 over [ $^{99m}\text{Tc}$ ]Tc-N4-PSMA-12, namely a slightly decreased kidney retention, was not statistically significant ( $P > 0.81$ ), and based on the aforementioned superior overall pharmacokinetic profile of [ $^{99m}\text{Tc}$ ]Tc-N4-PSMA-12, the latter was identified as most promising compound.

Besides [ $^{99m}\text{Tc}$ ]Tc-PSMA-I&S, the feasibility of PSMA-targeted RGS using [ $^{99m}\text{Tc}$ ]Tc-MIP-1404, a tracer originally developed for SPECT-imaging, was recently described in a small cohort of nine patients [34]. In a pre-clinical evaluation by Hillier et al. this tracer had shown a tissue distribution profile at 4 h p.i. which is highly

similar to our data for [ $^{99m}\text{Tc}$ ]Tc-N4-PSMA-12 (see Additional file 1: Fig. S2) [37]. Surprisingly and in contrast to the pharmacokinetics observed in mice, biodistribution studies in patients revealed high hepatic uptake and delayed clearance for [ $^{99m}\text{Tc}$ ]Tc-MIP-1404 [35] indicating limited transferability of preclinical data to the human situation for this radioligand. Consistent with the similar patient dosimetry reported for [ $^{99m}\text{Tc}$ ]Tc-PSMA-I&S and [ $^{99m}\text{Tc}$ ]Tc-MIP-1404 [21, 35], the latter yielded comparable results in the recent RGS study [34]. This example underlines not only the need for an optimized radioactive probe in PSMA-targeted RGS but also that, ultimately, clinical studies will be needed to assess whether the promising performance of [ $^{99m}\text{Tc}$ ]Tc-N4-PSMA-12 in mice will also translate into improved outcomes of RGS in patients.

To facilitate future clinical translation, we developed a protocol for GMP-production of [ $^{99m}\text{Tc}$ ]Tc-N4-PSMA-12 (see Fig. 6). As the simple, reliable, one-step process complies with basic nuclear medicine infrastructure and established clinical workflows and procedures, it provides an important basis for widespread availability of [ $^{99m}\text{Tc}$ ]Tc-N4-PSMA-12 and may contribute to minimize the logistic hurdle for a first clinical application.

In summary, the rational design, development and comparative preclinical evaluation of three novel  $^{99m}\text{Tc}$ -labeled PSMA inhibitors resulted in the identification of [ $^{99m}\text{Tc}$ ]Tc-N4-PSMA-12 as lead candidate. Compared to [ $^{99m}\text{Tc}$ ]Tc-PSMA-I&S, this novel radioligand showed



a significantly improved pharmacokinetic profile, 3.6-fold reduced blood activity, 15-fold decreased kidney activity and improved TBR for blood and all organs. Furthermore, a clinically suited radiolabeling process is suggested rendering [<sup>99m</sup>Tc]Tc-N4-PSMA-12 a highly attractive candidate for clinical application in RGS.

## Conclusion

Based on the promising data presented in this pre-clinical work, a first clinical study with [<sup>99m</sup>Tc]Tc-N4-PSMA-12 is highly warranted. It can be expected that this tracer has the potential to overcome current limitations obtained with [<sup>99m</sup>Tc]Tc-PSMA-I&S and thus might pave the way towards a broader future use of PSMA-targeted RGS in the therapy of patients with biochemical recurrent PCa.

## Abbreviations

HPLC: High performance liquid chromatography; IBA-KuE: (((S)-1-Carboxy-5-(4-(iodo)benzamido)pentyl)carbamoyl)-L-glutamic acid; LNM: Lymph node metastases; mCRPC: Metastatic castration resistant prostate cancer; N4: Tetraamine/6-carboxy-1,4,8,11-tetraazaundecane; PBS: Phosphate buffered saline; PCa: Prostate cancer; PET: Positron emission tomography; PPB: Plasma protein binding; PSMA: Prostate-specific membrane antigen; RCP: Radiochemical purity; RGS: Radioguided surgery; RP: Reversed phase; SD: Standard deviation; SIFA: Silicon fluoride acceptor; sLND: Sentinel lymph node dissection; SPECT: Single photon emission computed tomography; TBR: Tumor-to-background ratio; TLC: Thin layer chromatography; UV: Ultra-violet.

## Supplementary Information

The online version contains supplementary material available at <https://doi.org/10.1186/s13550-022-00942-7>.

**Additional file 1.** Supplementary information.

## Acknowledgements

Not applicable.

## Author contributions

JPK, MM, TG and LS synthesized and analyzed synthetic building blocks and the precursor ligands. JPK and MM performed radiolabelings, cell studies and in vitro studies. JPK and TG optimized radiolabeling towards a clinically suited labeling procedure. NUU and RB established the practical legal framework for the animal experiments and coordinated and supervised the in vivo studies. JPK, NUU and RB carried out animal experiments including tumor cell inoculation, biodistribution studies and imaging studies. JPK interpreted data, carried out statistical analysis and contributed significantly in writing this manuscript. HJW initiated and designed the study, interpreted data and contributed in writing this manuscript. All authors read, drafted and approved the final manuscript.

## Funding

Open Access funding enabled and organized by Projekt DEAL. HJW receives funding from the SFB 824 (Deutsche Forschungsgemeinschaft, Bonn, Germany, Sonderforschungsbereich 824, Project B11 and Z01).

## Availability of data and materials

The datasets used and analyzed during the current study are available from the corresponding author on reasonable request.

## Declarations

### Ethics approval and consent to participate

All animal experiments were conducted in accordance with general animal welfare regulations in Germany (German animal protection act, in the edition of the announcement, dated May 18th, 2006, as amended by Article 280 of June 19th 2020, approval no. ROB-55.2-1-2532.Vet\_02-18-109 by the General Administration of Upper Bavaria) and the institutional guidelines for the care and use of animals. The study was carried out in compliance with the ARRIVE guidelines. This article does not contain any studies with human participants.

### Consent for publication

Not applicable.

### Competing interests

JPK and HJW are listed as inventors in patent applications for some silicon-containing PSMA compounds. HJW receives funding from the SFB 824 (Deutsche Forschungsgemeinschaft, Bonn, Germany, Sonderforschungsbereich 824, Project B11 and Z01). HJW is founder and shareholder of Scintomics GmbH, Fuerstenfeldbruck, Germany. No other potential conflicts of interest relevant to this article exist.

Received: 28 July 2022 Accepted: 15 October 2022

Published online: 16 January 2023

## References

- Gillesen S, Attard G, Beer TM, Beltran H, Bjartell A, Bossi A, et al. Management of patients with advanced prostate cancer: report of the advanced prostate cancer consensus conference 2019. *Eur Urol*. 2020;77:508–47. <https://doi.org/10.1016/j.eururo.2020.01.012>.
- Lawhn-Heath C, Salavati A, Behr SC, Rowe SP, Calais J, Fendler WP, et al. Prostate-specific membrane antigen PET in prostate cancer. *Radiology*. 2021;299:248–60. <https://doi.org/10.1148/radiol.2021202771>.
- Afshar-Oromieh A, Haberkorn U, Schlemmer HP, Fenchel M, Eder M, Eisenhut M, et al. Comparison of PET/CT and PET/MRI hybrid systems using a <sup>68</sup>Ga-labelled PSMA ligand for the diagnosis of recurrent prostate cancer: initial experience. *Eur J Nucl Med Mol Imaging*. 2014;41:887–97. <https://doi.org/10.1007/s00259-013-2660-z>.
- Rowe SP, Macura KJ, Mena E, Blackford AL, Nadal R, Antonarakis ES, et al. PSMA-based [<sup>18</sup>F]DCFPyL PET/CT is superior to conventional imaging for lesion detection in patients with metastatic prostate cancer. *Mol Imaging Biol*. 2016;18:411–9. <https://doi.org/10.1007/s11307-016-0957-6>.
- Schmidkonz C, Hollweg C, Beck M, Reinfelder J, Goetz TI, Sanders JC, et al. <sup>99m</sup>Tc-MIP-1404-SPECT/CT for the detection of PSMA-positive lesions in 225 patients with biochemical recurrence of prostate cancer. *Prostate*. 2018;78:54–63. <https://doi.org/10.1002/pros.23444>.
- Weineisen M, Schottelius M, Simecek J, Baum RP, Yildiz A, Beykan S, et al. <sup>68</sup>Ga- and <sup>177</sup>Lu-labeled PSMA I&T: optimization of a PSMA-targeted theranostic concept and first proof-of-concept human studies. *J Nucl Med*. 2015;56:1169–76. <https://doi.org/10.2967/jnumed.115.158550>.
- Benesova M, Schafer M, Bauder-Wust U, Afshar-Oromieh A, Kratochwil C, Mier W, et al. Preclinical evaluation of a tailor-made DOTA-conjugated PSMA inhibitor with optimized linker moiety for imaging and endoradiotherapy of prostate cancer. *J Nucl Med*. 2015;56:914–20. <https://doi.org/10.2967/jnumed.114.147413>.
- Zang J, Fan X, Wang H, Liu Q, Wang J, Li H, et al. First-in-human study of <sup>177</sup>Lu-EB-PSMA-617 in patients with metastatic castration-resistant prostate cancer. *Eur J Nucl Med Mol Imaging*. 2019;46:148–58. <https://doi.org/10.1007/s00259-018-4096-y>.
- Kramer V, Fernandez R, Lehnert W, Jimenez-Franco LD, Soza-Ried C, Eppard E, et al. Biodistribution and dosimetry of a single dose of albumin-binding ligand [<sup>177</sup>Lu]Lu-PSMA-ALB-56 in patients with mCRPC. *Eur J Nucl Med Mol Imaging*. 2021;48:893–903. <https://doi.org/10.1007/s00259-020-05022-3>.
- Kratochwil C, Haberkorn U, Giesel FL. <sup>225</sup>Ac-PSMA-617 for therapy of prostate cancer. *Semin Nucl Med*. 2020;50:133–40. <https://doi.org/10.1053/j.semnuclmed.2020.02.004>.

11. Khreish F, Ebert N, Ries M, Maus S, Rosar F, Bohnenberger H, et al.  $^{225}\text{Ac}$ -PSMA-617/ $^{177}\text{Lu}$ -PSMA-617 tandem therapy of metastatic castration-resistant prostate cancer: pilot experience. *Eur J Nucl Med Mol Imaging*. 2020;47:721–8. <https://doi.org/10.1007/s00259-019-04612-0>.
12. Maurer T, Graefen M, van der Poel H, Hamdy F, Briganti A, Eiber M, et al. Prostate-specific membrane antigen-guided surgery. *J Nucl Med*. 2020;61:6–12. <https://doi.org/10.2967/jnumed.119.232330>.
13. Maurer T, Robu S, Schottelius M, Schwamborn K, Rauscher I, van den Berg NS, et al.  $^{99\text{mTc}}$ Technetium-based prostate-specific membrane antigen-radioguided surgery in recurrent prostate cancer. *Eur Urol*. 2019;75:659–66. <https://doi.org/10.1016/j.eururo.2018.03.013>.
14. Schottelius M, Wirtz M, Eiber M, Maurer T, Wester HJ. [ $^{111}\text{In}$ ]PSMA-I&T: expanding the spectrum of PSMA-I&T applications towards SPECT and radioguided surgery. *EJNMMI Res*. 2015;5:68. <https://doi.org/10.1186/s13550-015-0147-6>.
15. Robu S, Schottelius M, Eiber M, Maurer T, Gschwend J, Schwaiger M, et al. Preclinical evaluation and first patient application of  $^{99\text{mTc}}$ -PSMA-I&S for SPECT imaging and radioguided surgery in prostate cancer. *J Nucl Med*. 2017;58:235–42. <https://doi.org/10.2967/jnumed.116.178939>.
16. Horn T, Kronke M, Rauscher I, Haller B, Robu S, Wester HJ, et al. Single lesion on prostate-specific membrane antigen-ligand positron emission tomography and low prostate-specific antigen are prognostic factors for a favorable biochemical response to prostate-specific membrane antigen-targeted radioguided surgery in recurrent prostate cancer. *Eur Urol*. 2019;76:517–23. <https://doi.org/10.1016/j.eururo.2019.03.045>.
17. Knipper S, Tilki D, Mansholt J, Berliner C, Bernreuther C, Steuber T, et al. Metastases-yield and prostate-specific antigen kinetics following salvage lymph node dissection for prostate cancer: a comparison between conventional surgical approach and prostate-specific membrane antigen-radioguided surgery. *Eur Urol Focus*. 2019;5:50–3. <https://doi.org/10.1016/j.euf.2018.09.014>.
18. Rauscher I, Horn T, Eiber M, Gschwend JE, Maurer T. Novel technology of molecular radio-guidance for lymph node dissection in recurrent prostate cancer by PSMA-ligands. *World J Urol*. 2018;36:603–8. <https://doi.org/10.1007/s00345-018-2200-3>.
19. de Barros HA, van Oosterom MN, Donswijk ML, Hendriks J, Vis AN, Maurer T, et al. Robot-assisted prostate-specific membrane antigen-radioguided salvage surgery in recurrent prostate cancer using a DROP-IN gamma probe: the first prospective feasibility study. *Eur Urol*. 2022;82:97–105. <https://doi.org/10.1016/j.eururo.2022.03.002>.
20. Fossati N, Suardi N, Gandaglia G, Bravi CA, Soligo M, Karnes RJ, et al. Identifying the optimal candidate for salvage lymph node dissection for nodal recurrence of prostate cancer: results from a large multi-institutional analysis. *Eur Urol*. 2019;75:176–83. <https://doi.org/10.1016/j.eururo.2018.09.009>.
21. Urban S, Meyer C, Dahlbom M, Farkas I, Sipka G, Besenyi Z, et al. Radiation dosimetry of  $^{99\text{mTc}}$ -PSMA I&S: a single-center prospective study. *J Nucl Med*. 2021;62:1075–81. <https://doi.org/10.2967/jnumed.120.253476>.
22. Werner P, Neumann C, Eiber M, Wester HJ, Schottelius M. [ $^{99\text{mTc}}$ ] Tc-PSMA-I&S-SPECT/CT: experience in prostate cancer imaging in an outpatient center. *EJNMMI Res*. 2020;10:45. <https://doi.org/10.1186/s13550-020-00635-z>.
23. Wurzer A, Di Carlo D, Schmidt A, Beck R, Eiber M, Schwaiger M, et al. Radiohybrid ligands: a novel tracer concept exemplified by  $^{18}\text{F}$ - or  $^{68}\text{Ga}$ -labeled rhPSMA inhibitors. *J Nucl Med*. 2020;61:735–42. <https://doi.org/10.2967/jnumed.119.234922>.
24. Wurzer A, Kunert JP, Fischer S, Felber V, Beck R, De Rose F, et al. Synthesis and preclinical evaluation of  $^{177}\text{Lu}$ -labeled radiohybrid PSMA ligands (rhPSMAs) for endoradiotherapy of prostate cancer. *J Nucl Med*. 2022. <https://doi.org/10.2967/jnumed.121.263371>.
25. Hensbergen AW, Buckle T, van Willigen DM, Schottelius M, Welling MM, van der Wijk FA, et al. Hybrid tracers based on cyanine backbones targeting prostate-specific membrane antigen: tuning pharmacokinetic properties and exploring dye-protein interaction. *J Nucl Med*. 2020;61:234–41. <https://doi.org/10.2967/jnumed.119.233064>.
26. Eder AC, Schafer M, Schmidt J, Bauder-Wust U, Roscher M, Leotta K, et al. Rational linker design to accelerate excretion and reduce background uptake of peptidomimetic PSMA-targeting hybrid molecules. *J Nucl Med*. 2021;62:1461–7. <https://doi.org/10.2967/jnumed.120.248443>.
27. Wurzer A, Parzinger M, Konrad M, Beck R, Gunther T, Felber V, et al. Preclinical comparison of four [ $^{18}\text{F}$ ,  $^{68}\text{Ga}$ ]rhPSMA-7 isomers: influence of the stereoconfiguration on pharmacokinetics. *EJNMMI Res*. 2020;10:149. <https://doi.org/10.1186/s13550-020-00740-z>.
28. Weineisen M, Simecek J, Schottelius M, Schwaiger M, Wester HJ. Synthesis and preclinical evaluation of DOTAGA-conjugated PSMA ligands for functional imaging and endoradiotherapy of prostate cancer. *EJNMMI Res*. 2014;4:63. <https://doi.org/10.1186/s13550-014-0063-1>.
29. Abiraj K, Ursillo S, Tamma ML, Rylova SN, Waser B, Constable EC, et al. The tetraamine chelator outperforms HYNIC in a new technetium-99m-labelled somatostatin receptor 2 antagonist. *EJNMMI Res*. 2018;8:75. <https://doi.org/10.1186/s13550-018-0428-y>.
30. Fani M, Weingaertner V, Kolenc Peitl P, Mansi R, Gaonkar RH, Garnuszek P, et al. Selection of the first  $^{99\text{mTc}}$ -labelled somatostatin subtype 2 antagonist for clinical translation-preclinical assessment of two optimized candidates. *Pharmaceuticals*. 2020;14:19. <https://doi.org/10.3390/ph14010019> (Basel).
31. Kubyskhin V. Experimental lipophilicity scale for coded and noncoded amino acid residues. *Org Biomol Chem*. 2021;19:7031–40. <https://doi.org/10.1039/d1ob01213d>.
32. Schottelius M, Wurzer A, Wissmiller K, Beck R, Koch M, Gorpas D, et al. Synthesis and preclinical characterization of the PSMA-targeted hybrid tracer PSMA-I&F for nuclear and fluorescence imaging of prostate cancer. *J Nucl Med*. 2019;60:71–8. <https://doi.org/10.2967/jnumed.118.212720>.
33. Benesova M, Umbricht CA, Schibli R, Muller C. Albumin-binding PSMA ligands: optimization of the tissue distribution profile. *Mol Pharm*. 2018;15:934–46. <https://doi.org/10.1021/acs.molpharmaceut.7b00877>.
34. Koehler D, Sauer M, Klutmann S, Apostolova I, Lehnert W, Budaus L, et al. Feasibility of  $^{99\text{mTc}}$ -MIP-1404 for SPECT/CT imaging and subsequent PSMA-radioguided surgery in early biochemical recurrent prostate cancer: a case series of 9 patients. *J Nucl Med*. 2022. <https://doi.org/10.2967/jnumed.122.263892>.
35. Vallabhajosula S, Nikolopoulou A, Babich JW, Osborne JR, Tagawa ST, Lipai I, et al.  $^{99\text{mTc}}$ -labeled small-molecule inhibitors of prostate-specific membrane antigen: pharmacokinetics and biodistribution studies in healthy subjects and patients with metastatic prostate cancer. *J Nucl Med*. 2014;55:1791–8. <https://doi.org/10.2967/jnumed.114.140426>.
36. Mix M, Schultze-Seemann W, von Buren M, Sigle A, Omrane MA, Grabbert MT, et al.  $^{99\text{mTc}}$ -labelled PSMA ligand for radio-guided surgery in nodal metastatic prostate cancer: proof of principle. *EJNMMI Res*. 2021;11:22. <https://doi.org/10.1186/s13550-021-00762-1>.
37. Hillier SM, Maresca KP, Lu G, Merkin RD, Marquis JC, Zimmerman CN, et al.  $^{99\text{mTc}}$ -labeled small-molecule inhibitors of prostate-specific membrane antigen for molecular imaging of prostate cancer. *J Nucl Med*. 2013;54:1369–76. <https://doi.org/10.2967/jnumed.112.116624>.

## Publisher's Note

Springer Nature remains neutral with regard to jurisdictional claims in published maps and institutional affiliations.

**Submit your manuscript to a SpringerOpen® journal and benefit from:**

- Convenient online submission
- Rigorous peer review
- Open access: articles freely available online
- High visibility within the field
- Retaining the copyright to your article

Submit your next manuscript at ► [springeropen.com](https://www.springeropen.com)

# Synthesis and Preclinical Evaluation of Novel $^{99m}\text{Tc}$ -labeled PSMA Ligands for Radioguided Surgery of Prostate Cancer

## ----- Supplementary Information -----

Jan-Philip Kunert, Max Müller, Thomas Günther, León Stopper, Nicole Urtz-Urban, Roswitha Beck  
and Hans-Jürgen Wester

Technical University of Munich (TUM), Germany; TUM Department of Chemistry, Chair of  
Pharmaceutical Radiochemistry, Garching, Germany.

### Corresponding author:

Jan-Philip Kunert, M.Sc.

Phone: +49.89.289.12203

Fax: +49.89.289.12204

Email: [jan-philip.kunert@tum.de](mailto:jan-philip.kunert@tum.de)

Technical University of Munich,

Chair of Pharmaceutical Radiochemistry,

Walther-Meißner-Str. 3

85748 Garching

GERMANY

## General Information

Protected amino acids for peptide synthesis were purchased from Carbolution (St. Ingbert, Germany) and Iris Biotech (Marktredwitz, Germany). The 2-Chlorotrityl chloride polystyrene (TCP) resin was obtained from Sigma-Aldrich (Steinheim, Germany). Solvents and all other organic and inorganic reagents were purchased from Alfa Aesar (Karlsruhe, Germany), Fluorochem (Hadfield, United Kingdom), Sigma-Aldrich (Steinheim, Germany) or VWR (Darmstadt, Germany) and used without further purification. Radioactive [ $^{99m}\text{Tc}$ ]TcO $_4^-$  was obtained from a Ultra-Technekow FM 2 (15 - 43.00 GBq) generator (Curium, Petten, Netherlands).

Solid phase peptide synthesis (SPPS) was carried out manually in syringe reactors for peptide synthesis (Carl Roth, Karlsruhe, Germany) using a MX-RD-Pro syringe shaker from SCILOGEX (Rocky Hill, United States). Analytical and preparative reversed-phase high-performance liquid chromatography (RP-HPLC) was performed using Shimadzu gradient systems (Shimadzu, Neufahrn, Germany) each equipped with a SPD-20A UV/Vis-detector (detection at  $\lambda = 220$  nm) and LC-20AD solvent pumps. Eluents for all chromatographic procedures were water (solvent A, 0.1% TFA (v/v)) and acetonitrile (solvent B, 0.1% TFA (v/v), 2% or 5% water (v/v) in analytical or preparative procedures, respectively). For analytical measurements a MultoKrom 100-5 C18 column (150 mm x 4.6 mm, CS Chromatographie-Service, Langerwehe, Germany) was used at a constant flow rate of 1 mL/min. Preparative RP-HPLC was performed on a MultoKrom 100-5 C18 column (250 mm x 20 mm, CS Chromatographie-Service) applying a constant flow rate of 10 mL/min. Reversed-phase high performance flash chromatography (RP-HPFC) was performed on an SP HPFC system with SNAP cartridges (KP-C18-HS, 12 g) from Biotage (Charlottesville, United States) applying water (solvent A, 0.1% TFA (v/v)) and acetonitrile (solvent B, 0.1% TFA (v/v)) as eluents. Electrospray ionization (ESI) mass spectra and atmospheric pressure chemical ionization (APCI) mass spectra for compound characterization were acquired on an expression<sup>L</sup> CMS mass spectrometer from Advion (Harlow, United Kingdom).  $^1\text{H}$ -NMR-spectra were acquired on an AVHD 400 from Bruker (Billerica, United States) at 300 K. Chemical shifts ( $\delta$ ) are given in parts per million (ppm), spectra are calibrated to the residual  $^1\text{H}$  solvent signal of DMSO- $d_6$  at 2.50 ppm and signal multiplicities are described as: s = singlet, m = multiplet.

Analytical and preparative radio RP-HPLC was performed on a Shimadzu system equivalent as stated above and additionally equipped with a SIL-20A HAT autosampler using a MultoKrom 100-5 C18 column (125 mm x 4.6 mm) from CS Chromatographie-Service at a constant flow rate of 1 mL/min. A HERM LB 500 NaI scintillation detector (Berthold Technologies, Bad Wildbad, Germany) was connected to the outlet of the UV-photometer for the detection of radioactivity. Radio thin layer chromatography (TLC) was performed on iTLC-SG stripes (Agilent Technologies, Waldbronn, Germany) using butanone or NH $_4$ OAc (1 M in water) with DMF (1/1 (v/v)) as mobile phase for quantification of free [ $^{99m}\text{Tc}$ ]TcO $_4^-$  or colloidal technetium-99m, respectively. Radio-TLC stripes were analyzed using a Scan-RAM Radio-TLC detector from LabLogic Systems (Sheffield, United Kingdom).

Activity quantification of radioactive probes was carried out using a 2480 WIZARD<sup>2</sup> automatic gamma counter (PerkinElmer, Waltham, United States).

Centrifuges used for the determination of lipophilicity and binding to human plasma were a HERAEUS Pico 17 and a HERAEUS Megafuge 16R, respectively (Thermo Scientific, Osterode, Germany).

### Solution state synthesis of building blocks for SPPS

*(tBu)<sub>2</sub>EuE(tBu)*:

The *tert*-butyl protected Glu-urea-Glu binding motive was synthesized in analogy to the synthesis of *tert*-butyl protected Lys-urea-Glu reported in literature [1, 2].

*4-(Di-tert-butylhydroxysilyl)benzoic acid (SiOH-BA)*:

4-(Di-*tert*-butylhydroxysilyl)benzoic acid (SiOH-BA) was obtained by hydrolysis of 4-(Di-*tert*-butylfluorosilyl)benzoic acid (SiFA-BA). The latter was synthesized according to a published procedure [3]. To a stirring solution of SiFA-BA (114 mg, 403  $\mu$ mol, 1.0 eq.) in DMF (4 mL) a solution of KOH (113 mg, 2013  $\mu$ mol, 5.0 eq.) in TP-water (1 mL) was added at room temperature and stirred for 1 h. The solution was acidified (pH 4-5) by addition of 2.013 mL 1 M HCl<sub>(aq)</sub> and extracted with diethyl ether (5x 5 mL). The combined organic phases were dried over MgSO<sub>4</sub> and solvents were evaporated *in vacuo*. Residual DMF was removed via lyophilization to obtain the product as colorless, amorphous solid (96%).

*RP*-HPLC (50-100% B in 15 min):  $t_R = 5.8$  min,  $K' = 2.90$ . Calculated monoisotopic mass (C<sub>15</sub>H<sub>24</sub>O<sub>3</sub>Si): 280.2; found:  $m/z$  (APCI) = 279.0 [M-H]<sup>-</sup>.

*N,N',N'',N'''-Tetrakis(tert-butyloxycarbonyl)-6-carboxy-1,4,8,11-tetraazaundecane ((tBu)<sub>4</sub>N<sub>4</sub>)*:

*N*-Boc-ethylenediamine (4.0 eq.) was slowly added to a solution of 3-bromo-2-(bromomethyl)propionic acid (1.0 eq.) in THF (25 mL/mmol) and stirred for 24 h at room temperature. The solvent was removed *in vacuo* and the crude residue dissolved in acetone/H<sub>2</sub>O (1/1 (v/v), 25 mL/mmol). The solution was cooled to 0°C and triethylamine (3.0 eq.) was added. After 5 min di-*tert*-butyl dicarbonate (4.0 eq.) was added and the stirring mixture was left to warm up to room temperature within 15 h. Solvents were removed *in vacuo*, the raw product was purified via *RP*-HPFC (35-71% B in 15min) and the desired product was obtained as colorless, amorphous solid.

ESI-MS: calculated monoisotopic mass (C<sub>28</sub>H<sub>52</sub>N<sub>4</sub>O<sub>10</sub>): 604.4; found:  $m/z$  (ESI) = 605.5 [M+H]<sup>+</sup>.

<sup>1</sup>H-NMR (400 MHz, DMSO-*d*<sub>6</sub>)  $\delta = 7.17$ -6.19 (m, 2H, NH), 3.28-3.17 (m, 6H, CH<sub>2</sub>), 3.10-2.95 (m, 6H, CH<sub>2</sub>), 2.94-2.90 (m, 1H, CH), 1.38 (s, 18H, CH<sub>3</sub>), 1.36 (s, 18H, CH<sub>3</sub>).

## Synthesis of PSMA ligands

Chemical synthesis of novel N4-bearing PSMA-ligands was carried out via Fmoc-based standard solid phase peptide synthesis (SPPS). Reference compound PSMA-I&S was synthesized as described earlier [4]. Purity of all labeling precursors was determined via *RP*-HPLC (UV-detection at 220 nm) and was >98% in all cases.

*General procedures (GP) for solid phase peptide synthesis:*

All synthetic steps were carried out in a syringe reactor for peptide synthesis at room temperature. After each coupling or deprotection step, the resin was thoroughly washed with DMF (5 mL/g resin) six or eight times, respectively.

*TCP-resin loading (GP1):* The amino acid (2.0 eq.) and DIPEA (3.75 eq.) are dissolved in DMF (5 mL/g resin) and added to the TCP resin. After 2.5 h, methanol (2 mL/g resin) is added for capping of remaining trityl chloride groups. Subsequently, the resin is washed thoroughly with DMF (6x 5 mL/g resin), DCM (3x 5 mL/g resin) and methanol (3x 5 mL/g resin) and dried *in vacuo*. The loading  $l$  of the amino acid is determined by the equation

$$l \left[ \frac{\text{mmol}}{\text{g}} \right] = \frac{(m_2 - m_1) \cdot 1000}{(M_{AA} - M_{HCl}) \cdot m_2}$$

with  $m_1$  = mass of unloaded resin [g],  $m_2$  = mass of loaded resin [g],  $M_{AA}$  = molecular weight of amino acid [g/mol] and  $M_{HCl}$  = molecular weight of HCl [g/mol].

*On-resin amide bond formation (GP2):* For the conjugation of Fmoc-protected amino acids and other building blocks, their carboxylic acid functionality is preactivated by addition of TBTU (2.0 eq.), HOAt (2.0 eq.) and DIPEA (6.0 eq.) in DMF. After 5 min the solution is added to the resin and left to react for 2.5 h (differing coupling times are mentioned in the synthesis protocol). Coupling of Fmoc-*D*-Dap(Dde)-OH is performed with 2,4,6-trimethylpyridine (6.7 eq.) as base instead of DIPEA to prevent racemization.

*On-resin Fmoc-deprotection (GP3):* Deprotection of Fmoc-protecting groups is achieved by addition of 20% piperidine in DMF (8 mL/g resin) for 5 min and subsequently for 15 min.

*N4-PSMA ligands:*

Fmoc-*D*-Orn(Dde)-OH was loaded to the TCP resin as first building block according to GP1, and after subsequent Fmoc cleavage (GP3), (*t*BuO)EuE(*O**t*Bu)<sub>2</sub> was conjugated for 4.5 h (GP2). Deprotection of Dde was carried out using a solution of 2% hydrazine monohydrate in DMF (5 mL/g resin) for 20 min. Subsequently, a solution of succinic anhydride (7 eq.) and DIPEA (7 eq.) in DMF was added and left to react for 2.5 h. The resin bound carboxylate was then preactivated by addition of TBTU (2.0 eq.), HOAt

(2.0 eq.) and DIPEA (6.0 eq.) in DMF for 30 min and Fmoc-*D*-Lys-OtBu (2.0 eq.) in DMF was added for conjugation for 2.5 h. Subsequent Fmoc deprotection (GP3) was followed by conjugation of Fmoc-*D*-Dap(Dde)-OH (GP2). Orthogonal deprotection of Dde was carried out using hydroxylamine hydrochloride (1.26 g/g resin) and imidazole (0.92 g/g resin) in a mixture of DMF (1 mL/g resin) and NMP (5 mL/g resin) for 3.5 h. Subsequently, SiOH-BA was conjugated (GP2) and the remaining Fmoc protecting group was cleaved according to GP3. In the following step, either Fmoc-*D*-Glu(OtBu)-OH (in N4-PSMA-12), Fmoc-*D*-Phe-OH (in N4-PSMA-13) or Fmoc-*D*-Phe(4-NHBoc)-OH (in N4-PSMA-21) was coupled according to GP2. After subsequent Fmoc-deprotection (GP3), the *tert*-butyl protected N4-chelator was conjugated according to GP2. Cleavage from the resin and simultaneous deprotection of the ligand was performed in TFA (+2.5% TIPS, +2.5% H<sub>2</sub>O) for 1 h. After purification by semipreparative *RP*-HPLC, N4-PSMA-12, N4-PSMA-13 and N4-PSMA-21 were obtained as colorless, amorphous solids in yields of 29%, 25% and 21%, respectively (yields refer to the amount of substance of resin-bound Fmoc-*D*-Orn(Dde) at the start of solid phase synthesis).

N4-PSMA-12: *RP*-HPLC (10-60% B in 15 min):  $t_R = 9.3$  min,  $K' = 3.72$ . Calculated monoisotopic mass (C<sub>57</sub>H<sub>95</sub>N<sub>13</sub>O<sub>21</sub>Si): 1325.7; found:  $m/z$  (ESI) = 1326.5 [M+H]<sup>+</sup>, 664.0 [M+2H]<sup>2+</sup>.

N4-PSMA-13: *RP*-HPLC (10-60% B in 15 min):  $t_R = 10.2$  min,  $K' = 4.08$ . Calculated monoisotopic mass (C<sub>61</sub>H<sub>97</sub>N<sub>13</sub>O<sub>19</sub>Si): 1343.7; found:  $m/z$  (ESI) = 1344.4 [M+H]<sup>+</sup>, 673.0 [M+2H]<sup>2+</sup>.

N4-PSMA-21: *RP*-HPLC (10-60% B in 15 min):  $t_R = 9.0$  min,  $K' = 3.60$ . Calculated monoisotopic mass (C<sub>61</sub>H<sub>98</sub>N<sub>14</sub>O<sub>19</sub>Si): 1358.7; found:  $m/z$  (ESI) = 1359.7 [M+H]<sup>+</sup>, 680.5 [M+2H]<sup>2+</sup>.

#### *IBA-KuE:*

For the synthesis of IBA-KuE, the protected binding motive (OtBu)KuE(OtBu)<sub>2</sub> was synthesized as previously described [1]. 4-iodo-benzoic acid (6.1 mg, 24.6 μmol, 1.2 eq.) was preactivated by addition of TBTU (7.9 mg, 24.6 μmol, 1.2 eq.), HOAt (3.3 mg, 24.6 μmol, 1.2 eq.) and DIPEA (12.9 μL, 73.8 μmol, 3.6 eq.) in DMF (1 mL). After 5 min of pre-activation at room temperature, (OtBu)KuE(OtBu)<sub>2</sub> (10.0 mg, 20.5 μmol, 1.0 eq.) in DMF (2 mL) was added and the solution was stirred overnight (21 h) at room temperature. The solvent was evaporated and upon addition of TFA (+2.5% TIPS, +2.5% H<sub>2</sub>O) the solution was stirred for 1 h. TFA was evaporated and the crude product dissolved in DMF. After purification by semi-preparative *RP*-HPLC (30-45% B in 20 min) the product was obtained as colorless, amorphous solid (48%).

*RP*-HPLC (20-40% B in 20 min):  $t_R = 11.0$  min,  $K' = 7.68$ . Calculated monoisotopic mass (C<sub>19</sub>H<sub>24</sub>IN<sub>3</sub>O<sub>8</sub>): 549.1; found:  $m/z$  (ESI) = 550.2 [M+H]<sup>+</sup>.

### **Radiosynthesis of [<sup>99m</sup>Tc]Tc-N4-PSMA-12 at patient scale**

In a 10 mL glass vial, 15 nmol N4-PSMA-12 (20 µg, 0.5 mM in DMSO) were added to a mixture of 0.05 M Na<sub>2</sub>HPO<sub>4</sub> (250 µL, in TP-water, pH 9.25) and 0.1 M disodium citrate sesquihydrate (30 µL, in TP-water) in saline. After addition of a freshly prepared solution of SnCl<sub>2</sub> (10 µL, 1 mg/mL in ethanol), [<sup>99m</sup>Tc]TcO<sub>4</sub><sup>-</sup> in saline was added and the labeling solution (final volume 2-5 mL) was heated to 95°C for 15 min. The labeling solution was left to cool for 10 min and, subsequently, quality control was performed using radio-TLC and radio-*RP*-HPLC.

### **Radiosynthesis of [<sup>99m</sup>Tc]Tc-PSMA-I&S**

Labeling of PSMA-I&S was carried out using 2 nmol of peptide precursor in a kit formulation as described by Robu et al [4]. After addition of [<sup>99m</sup>Tc]TcO<sub>4</sub><sup>-</sup> (40 MBq/nmol) in 500 µL saline the solution was heated to 95°C for 20 min. Subsequently, 10 µL of 1 M sodium ascorbate (PBS) was added and quality control was performed using radio-TLC and radio-*RP*-HPLC.

### **Radioiodination of [<sup>125</sup>I]IBA-KuE**

The synthesis of the protected stannyl-precursor, radioiodination and deprotection yielding [<sup>125</sup>I]IBA-KuE was carried out as previously described [1]. Purification of the crude labelling product was performed using preparative radio-*RP*-HPLC with a gradient of 20-40% B in 20 min.

### **Analytical data of PSMA inhibitors labeled with technetium-99m or iodine-125**

[<sup>99m</sup>Tc]Tc-N4-PSMA-12: radio-*RP*-HPLC (10-70% B in 15 min): t<sub>R</sub> = 9.1 min, K' = 6.36.

[<sup>99m</sup>Tc]Tc-N4-PSMA-13: radio-*RP*-HPLC (10-70% B in 15 min): t<sub>R</sub> = 10.0 min, K' = 6.98.

[<sup>99m</sup>Tc]Tc-N4-PSMA-21: radio-*RP*-HPLC (10-70% B in 15 min): t<sub>R</sub> = 8.6 min, K' = 5.99.

[<sup>99m</sup>Tc]Tc-PSMA-I&S: radio-*RP*-HPLC (10-70% B in 15 min): t<sub>R</sub> = 8.2 min, K' = 5.76.

[<sup>125</sup>I]IBA-KuE: radio-*RP*-HPLC (20-40% B in 20 min): t<sub>R</sub> = 11.0 min, K' = 7.68.

**Supplementary Table 1:** Detailed data on  $^{99m}\text{Tc}$ -labeling of N4-PSMA-12 at patient scale. The volume of the labeling solution (V), the applied activity (A) as well as the amount of free  $^{99m}\text{Tc}[\text{TcO}_4^-]$  and colloidal technetium-99m, as determined via radio-TLC, and the resulting radio chemical purity (RCP) are given for single labeling experiments. Mean values and standard deviation (SD,  $n = 10$ ) are given for the whole data set.

entry	V [mL]	A [MBq]	Free $^{99m}\text{Tc}[\text{TcO}_4^-]$ [%]	Colloidal Tc-99m [%]	RCP [%]
1	5.00	194	0.21	0.85	98.94
2	5.00	810	0.40	0.44	99.16
3	5.00	542	0.24	2.21	97.55
4	5.00	502	0.17	1.98	97.85
5	5.00	760	0.30	1.78	97.92
6	3.18	634	0.23	1.12	98.65
7	2.66	470	0.23	1.02	98.75
8	3.02	388	0.31	0.64	99.05
9	2.00	727	0.97	0.73	98.30
10	4.00	501	0.28	1.31	98.41
<b>mean</b>	<b>3.99</b>	<b>553</b>	<b>0.33</b>	<b>1.21</b>	<b>98.46</b>
<b>SD</b>	<b>1.18</b>	<b>187</b>	<b>0.23</b>	<b>0.60</b>	<b>0.55</b>

**Supplementary Table 2:** Lipophilicity of the three novel  $^{99m}\text{Tc}$ -labeled N4-PSMA compounds and  $^{99m}\text{Tc}$ -labeled PSMA-I&S expressed as partition coefficient ( $\log D_{7.4}$ ) using the *n*-octanol/PBS (pH 7.4) distribution system ( $n = 8$ ), binding affinity towards PSMA (inverse  $\text{IC}_{50}$  (nM), 1 h, 4°C,  $n = 3$ ), PSMA-mediated internalization by LNCaP cells (1 h, 37°C,  $n = 3$ ) as a percentage of the radiolabeled reference ( $^{125}\text{I}$ IBA)KuE) and plasma protein binding (PPB, determined by a ultrafiltration method,  $n = 6$ ) of  $^{99m}\text{Tc}$ -labeled N4-PSMA compounds and  $^{99m}\text{Tc}[\text{Tc}]\text{PSMA-I&S}$ .

compound	$^{99m}\text{Tc}[\text{Tc}]\text{-N4-PSMA-12}$	$^{99m}\text{Tc}[\text{Tc}]\text{-N4-PSMA-13}$	$^{99m}\text{Tc}[\text{Tc}]\text{-N4-PSMA-21}$	$^{99m}\text{Tc}[\text{Tc}]\text{-PSMA-I&S}$
$\log D_{7.4}$	$-3.35 \pm 0.05$	$-2.78 \pm 0.05$	$-3.13 \pm 0.05$	$-2.61 \pm 0.08$
$\text{IC}_{50, \text{inv.}}$ (nM)	$11.02 \pm 2.80$	$9.98 \pm 0.99$	$11.07 \pm 1.42$	$11.78 \pm 1.89$
internalization (% IBA-KuE)	$311 \pm 16$	$164 \pm 15$	$180 \pm 4$	$240 \pm 13$
PPB (%)	$55.1 \pm 2.5$	$88.5 \pm 1.5$	$66.0 \pm 2.3$	$94.4 \pm 0.7$

**Supplementary Table 3:** Numeric data of the biodistribution of <sup>99m</sup>Tc-labeled N4-PSMA compounds and <sup>99m</sup>Tc-labeled PSMA-I&S at 6 h p.i. in male LNCaP tumor-bearing CB17-SCID mice. Data are expressed as percentage of the injected dose per gram (% ID/g), mean ± standard deviation (SD, n = 4-5).

uptake in % iD/g	<sup>99m</sup> Tc]Tc-N4-PSMA-12 (n = 5)		<sup>99m</sup> Tc]Tc-N4-PSMA-13 (n = 5)		<sup>99m</sup> Tc]Tc-N4-PSMA-21 (n = 4)		<sup>99m</sup> Tc]Tc-PSMA-I&S (n = 4)	
	mean	SD	mean	SD	mean	SD	mean	SD
blood	0.0200	0.0044	0.0320	0.0100	0.1074	0.0623	0.0728	0.0072
heart	0.0274	0.0083	0.0456	0.0090	0.0568	0.0128	0.1246	0.0252
lung	0.0613	0.0177	0.1108	0.0186	0.1250	0.0578	1.0378	0.0612
liver	0.1796	0.0890	0.2618	0.0556	0.5752	0.3652	0.2215	0.0234
spleen	0.8928	0.5700	0.6314	0.1819	1.3064	0.7969	31.8636	6.0507
pancreas	0.0206	0.0031	0.0270	0.0053	0.0335	0.0099	0.4040	0.0639
stomach	0.0988	0.0506	0.1348	0.0441	0.1458	0.0956	0.2306	0.1018
intestine	0.5391	0.4453	0.2661	0.1637	1.1034	1.7380	0.6415	0.3960
kidney	12.2924	8.0491	6.5974	4.7823	4.5811	1.4363	191.560	25.7140
adrenals	0.6570	0.2747	0.5170	0.0912	0.5759	0.1443	13.5354	2.9883
muscle	0.0110	0.0041	0.0127	0.0018	0.0153	0.0027	0.1020	0.0290
bone	0.0365	0.0136	0.0862	0.0139	0.0828	0.0778	0.0907	0.0157
tumor	13.0231	3.8549	12.5347	4.0835	11.0155	2.2227	15.6183	2.8033
parotid gland	0.0804	0.0339	0.1056	0.0262	0.1105	0.0199	1.7348	0.5573
submandibular gland	0.1450	0.0431	0.3069	0.0642	0.3009	0.2151	0.6196	0.0695

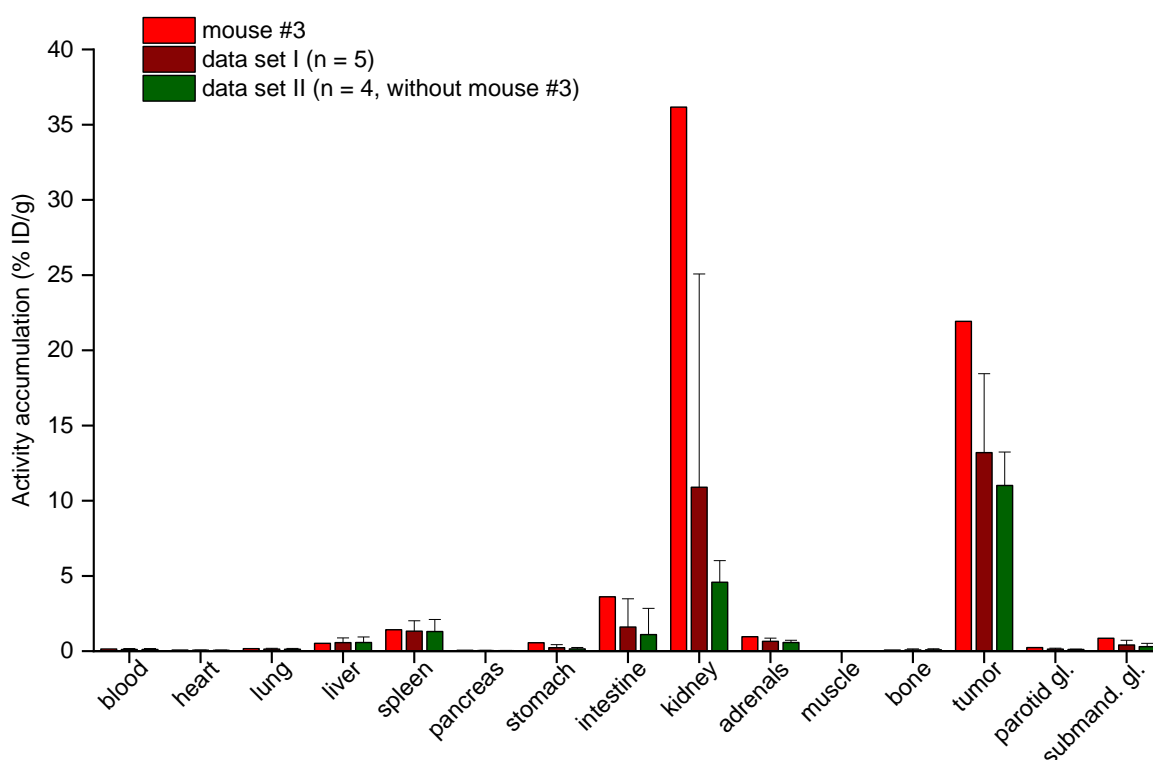
**Supplementary Table 4:** Tumor-to-background ratios of <sup>99m</sup>Tc-labeled N4-PSMA compounds and <sup>99m</sup>Tc-labeled PSMA-I&S at 6 h p.i. in male LNCaP tumor-bearing CB17-SCID mice. Data are given as mean ± standard deviation (SD, n = 4-5). Mean values were determined from tumor-to-organ ratios calculated for individual animals.

tumor-to-background ratio	<sup>99m</sup> Tc]Tc-N4-PSMA-12 (n = 5)		<sup>99m</sup> Tc]Tc-N4-PSMA-13 (n = 5)		<sup>99m</sup> Tc]Tc-N4-PSMA-21 (n = 4)		<sup>99m</sup> Tc]Tc-PSMA-I&S (n = 4)	
	mean	SD	mean	SD	mean	SD	mean	SD
blood	657.74	146.75	409.29	158.60	125.55	62.05	218.97	62.09
heart	484.90	122.64	276.38	87.34	201.50	62.05	127.22	20.53
lung	216.68	56.82	113.30	35.32	99.35	36.86	15.01	2.29
liver	79.92	30.33	50.17	21.50	23.75	10.51	71.64	19.02
spleen	17.89	9.02	20.57	7.45	10.32	4.39	0.49	0.06
pancreas	637.21	201.56	496.73	247.35	350.74	126.56	40.19	13.36
stomach	158.87	78.55	101.82	47.12	114.49	101.37	76.24	27.21
intestine	57.76	60.23	64.62	39.59	52.29	48.36	38.15	31.76
kidney	1.64	1.29	2.45	1.45	2.57	0.77	0.08	0.01
adrenals	22.15	9.04	24.50	8.36	19.85	4.82	1.24	0.52
muscle	1265.34	486.05	1013.12	379.65	736.44	193.04	159.28	39.53
bone	384.40	158.05	142.94	32.47	207.38	115.07	178.36	51.53
parotid gland	177.38	73.36	119.35	34.53	101.59	24.83	9.87	3.90
submandibular gland	90.45	15.58	41.60	14.26	50.80	32.33	25.44	5.00

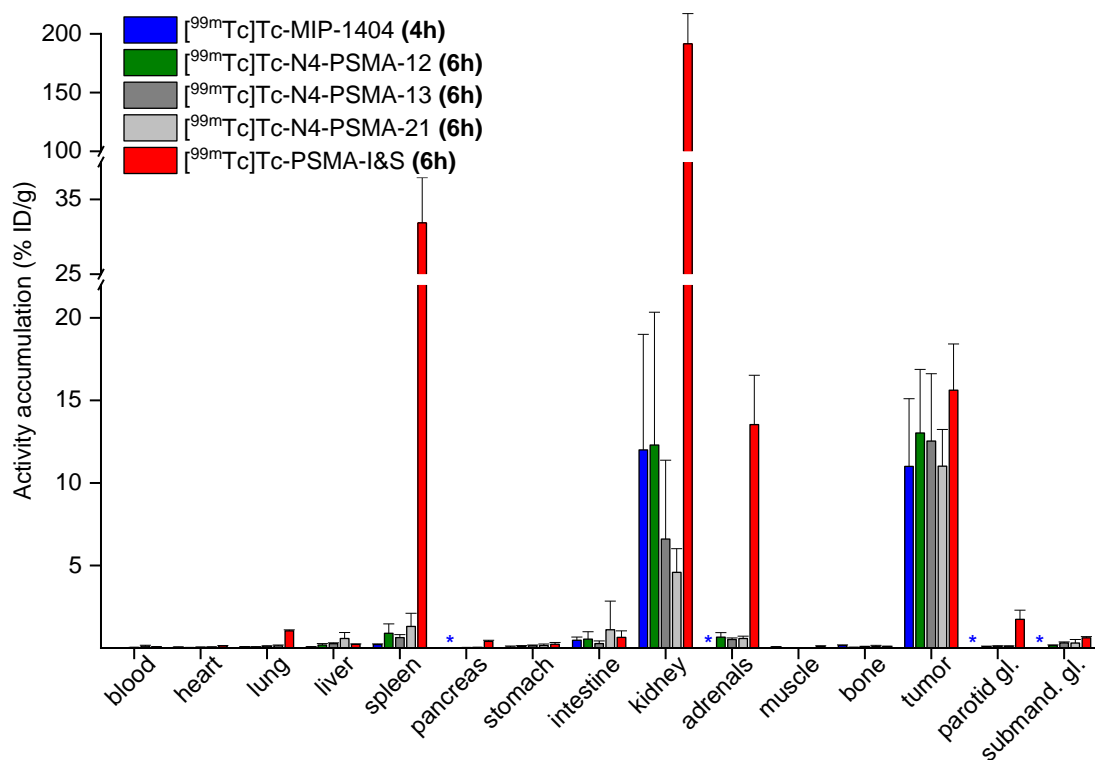
## Analysis of biodistribution data of [<sup>99m</sup>Tc]Tc-N4-PSMA-21

We report the following data in order to comply with the ARRIVE guidelines for the reporting of research involving animals. The biodistribution study of [<sup>99m</sup>Tc]Tc-N4-PSMA-21 was carried out with  $n = 5$  animals (“data set I”). All animals were healthy and did not show any signs of pain, distress or change in behavior throughout the experiment. However, as depicted in supplementary figure 1, gross deviations in the kidney uptake and elevated tumor uptake were observed for one particular animal (mouse #3) as compared to the other four animals. Kidney uptake of mouse #3 (36.17 %ID/g) exceeded the value obtained from the other four animals ( $4.58 \pm 1.44$  %ID/g, mean  $\pm$  SD) 7.9-fold or by more than 20 standard deviations. In addition, tumor uptake of mouse #3 (21.92 %ID/g) exceeded the value obtained from the other four animals ( $11.02 \pm 2.22$  %ID/g, mean  $\pm$  SD) 2.0-fold or by more than 4 standard deviations. Due to the uncertainty, whether these huge deviations arise from an experimental error or might be related to strongly deviating metabolic processes e.g. abnormal kidney function in mouse #3, the study primarily presents and discusses the data set based on the other four animals ( $n = 4$ , “data set II”).

A thorough evaluation and comparison was, however, also carried out including mouse #3. For both, “data set I” ( $n = 5$ , including mouse #3) and “data set II” ( $n = 4$ , without mouse #3) kidney uptake of [<sup>99m</sup>Tc]Tc-N4-PSMA-21 was significantly reduced compared to [<sup>99m</sup>Tc]Tc-PSMA-I&S (both  $P < 0.001$ ) but not statistically different from other <sup>99m</sup>Tc-labeled N4-PSMA-ligands ( $P > 0.92$  and  $P > 0.81$  for “data set I” and “data set II”, respectively). Although mouse #3 also showed an elevated tumor uptake (see above), no statistically significant differences in tumor uptake among the <sup>99m</sup>Tc-labeled PSMA-ligands evaluated herein were found, regardless whether “data set I” ( $P > 0.69$ ) or “data set II” ( $P > 0.27$ ) was compared to the biodistribution data of the other radioligands.



**Supplementary Figure 1:** Biodistribution of [<sup>99m</sup>Tc]Tc-N4-PSMA-21 in a single mouse #3 (red) showing drastically increased kidney uptake and elevated tumor uptake as compared to the other four animals depicted by “data set II” (dark green,  $n = 4$ , without mouse #3). “Data set I” (dark red,  $n = 5$ , including mouse #3) represents the biodistribution of [<sup>99m</sup>Tc]Tc-N4-PSMA-21 including all animals. Data are expressed as percentage of the injected dose per gram (% ID/g), mean  $\pm$  standard deviation.



**Supplementary Figure 2:** Comparison of ex vivo biodistribution data of <sup>99m</sup>Tc-labeled MIP-1404 at 4 h p.i. in male LNCaP tumor-bearing NCr-*nu/nu* mice with ex vivo biodistribution data of the three novel <sup>99m</sup>Tc-labeled N4-PSMA compounds and <sup>99m</sup>Tc-labeled PSMA-I&S at 6 h p.i. in male LNCaP tumor-bearing CB17-SCID mice. Data are expressed as percentage of the injected dose per gram (% ID/g), mean ± standard deviation (n = 4-5). Organs for which no data on [<sup>99m</sup>Tc]Tc-MIP-1404 were available in literature are indicated with an asterisk. Biodistribution data of [<sup>99m</sup>Tc]Tc-MIP-1404 were originally published in *JNM* (Hillier et al. <sup>99m</sup>Tc-Labeled Small-Molecule Inhibitors of Prostate-Specific Membrane Antigen for Molecular Imaging of Prostate Cancer. *J Nucl Med.* 2013;54:1369-76. ©SNMMI)

## References

1. Weineisen M, Simecek J, Schottelius M, Schwaiger M, Wester HJ. Synthesis and preclinical evaluation of DOTAGA-conjugated PSMA ligands for functional imaging and endoradiotherapy of prostate cancer. *EJNMMI Res.* 2014;4:63. doi:10.1186/s13550-014-0063-1.
2. Robu S, Schmidt A, Eiber M, Schottelius M, Gunther T, Hooshyar Yousefi B, et al. Synthesis and preclinical evaluation of novel <sup>18</sup>F-labeled Glu-urea-Glu-based PSMA inhibitors for prostate cancer imaging: a comparison with <sup>18</sup>F-DCFpyl and <sup>18</sup>F-PSMA-1007. *EJNMMI Res.* 2018;8:30. doi:10.1186/s13550-018-0382-8.
3. Iovkova L, Wangler B, Schirmacher E, Schirmacher R, Quandt G, Boening G, et al. para-Functionalized aryl-di-tert-butylfluorosilanes as potential labeling synthons for <sup>18</sup>F radiopharmaceuticals. *Chemistry.* 2009;15:2140-7. doi:10.1002/chem.200802266.
4. Robu S, Schottelius M, Eiber M, Maurer T, Gschwend J, Schwaiger M, et al. Preclinical Evaluation and First Patient Application of <sup>99m</sup>Tc-PSMA-I&S for SPECT Imaging and Radioguided Surgery in Prostate Cancer. *J Nucl Med.* 2017;58:235-42. doi:10.2967/jnumed.116.178939.

### **6.3. Eidesstattliche Erklärung**

Ich, Jan-Philip Kunert, erkläre an Eides statt, dass ich die bei der promotionsführenden Einrichtung TUM School of Natural Sciences der TUM zur Promotionsprüfung vorgelegte Arbeit mit dem Titel

#### **Development and Evaluation of Therapeutic PSMA-Binding Radiopharmaceuticals with Optimized Pharmacokinetics**

unter der Anleitung und Betreuung durch Herr Prof. Dr. Hans-Jürgen Wester ohne sonstige Hilfe erstellt und bei der Abfassung nur die gemäß § 7 Abs. 6 und 7 angegebenen Hilfsmittel benutzt habe.

Ich habe keine Organisation eingeschaltet, die gegen Entgelt Betreuerinnen und Betreuer für die Anfertigung von Dissertationen sucht, oder die mir obliegenden Pflichten hinsichtlich der Prüfungsleistungen für mich ganz oder teilweise erledigt.

Ich habe die Dissertation in dieser oder ähnlicher Form in keinem anderen Prüfungsverfahren als Prüfungsleistung vorgelegt.

Teile der Dissertation wurden in den Zeitschriften *The Journal of Nuclear Medicine*, *Pharmaceuticals* und *EJNMMI Research* veröffentlicht.

Ich habe den angestrebten Doktorgrad noch nicht erworben und bin nicht in einem früheren Promotionsverfahren für den angestrebten Doktorgrad endgültig gescheitert.

Ich habe keine Kenntnis über ein strafrechtliches Ermittlungsverfahren in Bezug auf wissenschaftsbezogene Straftaten gegen mich oder eine rechtskräftige strafrechtliche Verurteilung mit Wissenschaftsbezug.

Die öffentlich zugängliche Promotionsordnung sowie die Richtlinien zur Sicherung guter wissenschaftlicher Praxis und für den Umgang mit wissenschaftlichem Fehlverhalten der TUM sind mir bekannt, insbesondere habe ich die Bedeutung von § 27 PromO (Nichtigkeit der Promotion) und § 28 PromO (Entzug des Doktorgrades) zur Kenntnis genommen. Ich bin mir der Konsequenzen einer falschen Eidesstattlichen Erklärung bewusst.

Mit der Aufnahme meiner personenbezogenen Daten in die Alumni-Datei bei der TUM bin ich einverstanden.

---

Jan-Philip Kunert, Augsburg, 20.03.2023